frontiers | Research Topics

Genomic discoveries and pharmaceutical development in urologic tumors, volume II

Edited by
Lei Yin, Jialin Meng, Yin Sun, Xiaolei Sun and Huan Yang

Published in
Frontiers in Pharmacology
Frontiers in Oncology

ISSN 1664-8714
ISBN 978-2-8325-7416-4
DOI 10.3389/978-2-8325-7416-4

Generative AI statement
Any alternative text (Alt text) provided alongside figures in the articles in this ebook has been generated by Frontiers with the support of artificial intelligence and reasonable efforts have been made to ensure accuracy, including review by the authors wherever possible. If you identify any issues, please contact us.

About Frontiers

Frontiers is more than just an open access publisher of scholarly articles: it is a pioneering approach to the world of academia, radically improving the way scholarly research is managed. The grand vision of Frontiers is a world where all people have an equal opportunity to seek, share and generate knowledge. Frontiers provides immediate and permanent online open access to all its publications, but this alone is not enough to realize our grand goals.

Frontiers journal series

The Frontiers journal series is a multi-tier and interdisciplinary set of open-access, online journals, promising a paradigm shift from the current review, selection and dissemination processes in academic publishing. All Frontiers journals are driven by researchers for researchers; therefore, they constitute a service to the scholarly community. At the same time, the *Frontiers journal series* operates on a revolutionary invention, the tiered publishing system, initially addressing specific communities of scholars, and gradually climbing up to broader public understanding, thus serving the interests of the lay society, too.

Dedication to quality

Each Frontiers article is a landmark of the highest quality, thanks to genuinely collaborative interactions between authors and review editors, who include some of the world's best academicians. Research must be certified by peers before entering a stream of knowledge that may eventually reach the public - and shape society; therefore, Frontiers only applies the most rigorous and unbiased reviews. Frontiers revolutionizes research publishing by freely delivering the most outstanding research, evaluated with no bias from both the academic and social point of view. By applying the most advanced information technologies, Frontiers is catapulting scholarly publishing into a new generation.

What are Frontiers Research Topics?

Frontiers Research Topics are very popular trademarks of the *Frontiers journals series*: they are collections of at least ten articles, all centered on a particular subject. With their unique mix of varied contributions from Original Research to Review Articles, Frontiers Research Topics unify the most influential researchers, the latest key findings and historical advances in a hot research area.

Find out more on how to host your own Frontiers Research Topic or contribute to one as an author by contacting the Frontiers editorial office: frontiersin.org/about/contact

Genomic discoveries and pharmaceutical development in urologic tumors, volume II

Topic editors

Lei Yin — Shanghai Jiaotong University School of Medicine, China
Jialin Meng — University of Science and Technology of China, China
Yin Sun — University of Rochester Medical Center, United States
Xiaolei Sun — Zhongshan Hospital- Fudan University, China
Huan Yang — Huazhong University of Science and Technology, China

Citation

Yin, L., Meng, J., Sun, Y., Sun, X., Yang, H., eds. (2026). *Genomic discoveries and pharmaceutical development in urologic tumors, volume II*.
Lausanne: Frontiers Media SA. doi: 10.3389/978-2-8325-7416-4

Table of contents

frontiers | Frontiers in Pharmacology

TYPE Editorial
PUBLISHED 12 January 2026
DOI 10.3389/fphar.2025.1743378

OPEN ACCESS

EDITED AND REVIEWED BY
Olivier Feron,
Université catholique de Louvain, Belgium

*CORRESPONDENCE
Lei Yin,
yltale@126.com
Tao Zhang,
katanazt@126.com

RECEIVED 10 November 2025
ACCEPTED 23 December 2025
PUBLISHED 12 January 2026

CITATION
Li W, Meng J, Yang H, Zhang T and Yin L (2026) Editorial: Genomic discoveries and pharmaceutical development in urologic tumors - volume II.
Front. Pharmacol. 16:1743378.
doi: 10.3389/fphar.2025.1743378

Editorial: Genomic discoveries and pharmaceutical development in urologic tumors - volume II

Wenjia Li[1], Jialin Meng[2], Huan Yang[3], Tao Zhang[4]* and Lei Yin[5,6]*

[1]Department of Cardiovascular Medicine, Ruijin Hospital, Shanghai Jiao Tong University School of Medicine, Shanghai, China, [2]Department of Urology, The First Affiliated Hospital of Anhui Medical University, Anhui Province Key Laboratory of Genitourinary Diseases, Anhui Medical University, Hefei, China, [3]Department of Urology, Tongji Hospital, Tongji Medical College of Huazhong University of Science and Technology, Wuhan, China, [4]Department of Urology, Putuo People's Hospital, School of Medicine, Tongji University, Shanghai, China, [5]Department of Urology, Putuo People's Hospital, Tongji University, Shanghai, China, [6]Department of Urology, Shanghai Ninth People's Hospital, Shanghai Jiao Tong University School of Medicine, Shanghai, China

KEYWORDS

urologic tumors, cancer biomarkers, drug screen, drug repurposing, genomic sequence

Editorial on the Research Topic
Genomic discoveries and pharmaceutical development in urologic tumors - volume II

Introduction

Urologic malignancies remain a global health concern, with steadily rising incidence and mortality. According to recent epidemiological surveys, prostate cancer has become one of the most common cancers among men worldwide, while bladder and renal cancers continue to pose substantial diagnostic and therapeutic challenges (Albigès et al., 2024; Cicchetti et al., 2025; Kratzer et al., 2025; Leung et al., 2025). The genomic era has profoundly reshaped our understanding of these diseases, unveiling molecular drivers, therapeutic targets, and pathways of drug resistance that now guide personalized treatment strategies.

Building on the success of the first volume of "*Genomic Discoveries and Pharmaceutical Development in Urologic Tumors*", this second volume broadens the landscape from genetic discoveries to translational and pharmacologic development (Meng et al., 2024). Across ten contributions, investigators integrated genomics, pharmacology, and computational biology to explore novel mechanisms, prognostic signatures, and therapeutic opportunities in prostate, bladder, and renal cancers. Together, these studies form a coherent narrative that bridges mechanistic discovery and clinical translation—the central vision of this Research Topic.

Genomic and molecular insights in prostate cancer

Five studies in this volume focus on prostate cancer, reflecting its complex genomic and metabolic heterogeneity. Hua et al. investigated SUCLG2, a mitochondrial enzyme

associated with the tricarboxylic acid cycle, and found its dysregulation to predict poor prognosis and altered immune infiltration in prostate cancer. Their integration of single-cell RNA sequencing and metabolic pathway analysis highlighted the interplay between tumor metabolism and immune microenvironment, providing a promising metabolic biomarker for prognosis and therapeutic targeting. Wu et al. examined the emerging concept of cuproptosis, a copper-dependent cell-death mechanism, and its relationship with RNA-methylation regulators. By combining single-cell and bulk RNA-seq data, they identified distinct cuproptosis-related subtypes that correlate with immune infiltration and therapeutic response. This multi-omics strategy offers new insights into redox regulation and treatment stratification. Chitluri et al. revealed that inhibition of DPP4 downregulates FGF17 and PDGFRA, suppressing the PI3K/Akt signaling cascade and inducing apoptosis in prostate cancer cells. This work underscores the value of drug repurposing by connecting a clinically used enzyme inhibitor to a novel anti-tumor mechanism. Zhou et al. conducted a comprehensive analysis of lactylation-related genes, integrating single-cell RNA-seq, bulk transcriptomics, and machine learning. They delineated intratumoral heterogeneity in prostate cancer and proposed a lactylation-based prognostic signature that links metabolic reprogramming to tumor aggressiveness and immune escape. Finally, Wang et al. performed a pharmacoepidemiologic study using the WHO-VigiAccess database to characterize adverse-reaction profiles of three anti-prostate-cancer drugs. By combining real-world pharmacovigilance data and bibliometric trends, they provided valuable insights into safety surveillance and rational drug use.

Molecular mechanisms and therapeutic targeting in bladder cancer

Two articles address the molecular mechanisms and pharmacologic vulnerabilities of bladder cancer. Zhu et al. reported that miR-146b promotes bladder-cancer cell proliferation by targeting SMAD4 and activating the c-Myc/Cyclin D1 axis. This mechanistic dissection not only elucidates tumor-promoting pathways but also provides a rationale for RNA-based therapeutic strategies in high-grade urothelial carcinoma. Complementing this, Yuan et al. combined *in silico* screening, molecular docking, and cell-based assays to identify artesunate—a clinically available anti-malarial—as a multi-target agent that suppresses bladder-cancer growth through MAPK and PI3K/Akt modulation. This integration of computational pharmacology and experimental validation illustrates a productive route for drug repurposing guided by genomic and systems biology.

Renal tumors and clinical translational advances

Three studies focus on renal cell carcinoma (RCC), where targeted and immune therapies have dramatically transformed treatment paradigms. Li et al. provided a comparative analysis of adverse-event profiles for four multi-targeted tyrosine kinase inhibitors (TKIs) using global pharmacovigilance data. Their study not only identified distinct toxicity spectra for agents such as sunitinib and axitinib but also emphasized the importance of continuous real-world safety monitoring during the post-approval phase. Expanding on the clinical translation dimension, Cui et al. reported the real-world efficacy and safety of tislelizumab plus axitinib as first-line therapy for intermediate- and high-risk metastatic clear-cell RCC. Their data supported the synergistic potential of PD-1 blockade combined with anti-angiogenic therapy, reinforcing the paradigm that rational combination therapy informed by genomic and immune profiling can improve patient outcomes. In addition, Zheng et al. described a rare renal epithelioid neoplasm harboring EWSR1::CREB fusions. This case enriches the spectrum of EWSR1-associated tumors and reminds clinicians of the diagnostic value of next-generation sequencing for rare and morphologically ambiguous renal neoplasms.

In conclusion, *Genomic Discoveries and Pharmaceutical Development in Urologic Tumors–Volume II* continues the mission initiated in Volume I: to connect fundamental genomic discoveries with tangible pharmacologic and clinical applications. From metabolism-linked biomarkers in prostate cancer to repurposed therapeutics in bladder and renal cancers, the ten contributions herein exemplify the multidimensional progress defining modern uro-oncology.

Despite these advances, several key challenges remain. First, a deeper understanding of tumor evolution, clonal dynamics, and therapeutic resistance is required—ideally supported by single-cell and spatial multi-omics technologies. Second, translation from genomic discovery to clinical practice faces persistent obstacles, including patient selection, pharmacokinetic/pharmacodynamic variability, and real-world treatment effectiveness (Yin et al., 2020; Yin et al., 2023; Yoshihara et al., 2025). Third, the integration of immuno-oncology, metabolic reprogramming, and tumor microenvironment analysis into the genomic-driven drug-development pipeline remains an open frontier. Finally, artificial intelligence and big-data analytics will play an increasingly critical role in predicting drug responses, stratifying patients, and optimizing therapeutic combinations (Zou and Green, 2023). Looking forward, international collaboration across genomics, pharmacology, and clinical oncology will be indispensable for realizing the full promise of precision medicine in urologic tumors.

Author contributions

WL: Formal Analysis, Methodology, Writing – original draft. JM: Project administration, Supervision, Writing – original draft. HY: Formal Analysis, Project administration, Software, Writing – review and editing. TZ: Conceptualization, Resources, Supervision, Validation, Writing – review and editing. LY: Conceptualization, Project administration, Supervision, Writing – original draft, Writing – review and editing.

Funding

The author(s) declared that financial support was received for this work and/or its publication. This work was supported by the

National Natural Science Foundation of China (No. 82203698), the Sailing Program of Shanghai Science and Technology Commission (No. 22YF1425000), the Postdoctoral Research Start Up Foundation of Shanghai Ninth People's Hospital (No. 202501042).

Acknowledgements

We sincerely thank all contributing authors, reviewers, and the editorial team of *Frontiers in Pharmacology* for their efforts and dedication in bringing this Research Topic to fruition.

Conflict of interest

The author(s) declared that this work was conducted in the absence of any commercial or financial relationships that could be construed as a potential conflict of interest.

Generative AI statement

The author(s) declared that generative AI was not used in the creation of this manuscript.

Any alternative text (alt text) provided alongside figures in this article has been generated by Frontiers with the support of artificial intelligence and reasonable efforts have been made to ensure accuracy, including review by the authors wherever possible. If you identify any issues, please contact us.

Publisher's note

References

Albigès, L., Bellera, C., Branchoux, S., Arnaud, M., Gouverneur, A., Néré, S., et al. (2024). Real-world treatment patterns and effectiveness of patients with advanced renal cell carcinoma: a nationwide observational study. *Clin. Genitourinary Cancer* 22 (2), 295–304.e6. doi:10.1016/j.clgc.2023.11.012

Cicchetti, R., Amparore, D., Tamborino, F., Tătaru, O. S., Ferro, M., Digiacomo, A., et al. (2025). The use of artificial intelligence in urologic oncology: current insights and challenges. *Res. Reports Urology* 17, 293–308. doi:10.2147/RRU.S526184

Kratzer, T. B., Mazzitelli, N., Star, J., Dahut, W. L., Jemal, A., and Siegel, R. L. (2025). Prostate cancer statistics, 2025. *CA Cancer J. Clin.* 75 (6), 485–497. doi:10.3322/caac.70028

Leung, D. K., Wong, C. H., Ko, I. C., Siu, B. W., Liu, A. Q., Meng, H. Y., et al. (2025). Global trends in the incidence, mortality, and risk-attributable deaths for prostate, bladder, and kidney cancers: a systematic analysis from the global burden of disease study 2021. *Eur. Urology Oncology* S2588-9311 (25), 00133-6–1543. doi:10.1016/j.euo.2025.05.007

Meng, J., Yang, H., and Yin, L. (2024). Editorial: genomic discoveries and pharmaceutical development in urologic tumors. *Front. Pharmacology* 15, 1508979. doi:10.3389/fphar.2024.1508979

Yin, L., Li, W., Xu, A., Shi, H., Wang, K., Yang, H., et al. (2020). SH3BGRL2 inhibits growth and metastasis in clear cell renal cell carcinoma *via* activating hippo/TEAD1-Twist1 pathway. *EBioMedicine* 51, 102596. doi:10.1016/j.ebiom.2019.12.005

Yin, L., Li, W., Chen, X., Wang, R., Zhang, T., Meng, J., et al. (2023). HOOK1 inhibits the progression of renal cell carcinoma *via* TGF-β and TNFSF13B/VEGF-A axis. *Adv. Science* 10 (17), e2206955. doi:10.1002/advs.202206955

Yoshihara, K., Ito, K., Kimura, T., Yamamoto, Y., and Urabe, F. (2025). Single-cell RNA sequencing and spatial transcriptome analysis in bladder cancer: current status and future perspectives. *Bladder Cancer* 11 (1), 23523735251322017. doi:10.1177/23523735251322017

Zou, W., and Green, D. R. (2023). Beggars banquet: metabolism in the tumor immune microenvironment and cancer therapy. *Cell Metab.* 35 (7), 1101–1113. doi:10.1016/j.cmet.2023.06.003

frontiers | Frontiers in Pharmacology

TYPE Original Research
PUBLISHED 27 March 2025
DOI 10.3389/fphar.2025.1570661

OPEN ACCESS

EDITED BY
Lei Yin,
Shanghai Jiaotong University School of Medicine, China

REVIEWED BY
Jun Liu,
Dongguan Hospital of Guangzhou University of Chinese Medicine, China
Bo Wang,
Freiburg University Medical Center, Germany

*CORRESPONDENCE
Liwei Zhang,
medzlw@sina.com
Wei Wang,
wangw2005@zju.edu.cn
Feifei Wang,
wff@enzemed.com

†These authors have contributed equally to this work and share first authorship

RECEIVED 04 February 2025
ACCEPTED 17 March 2025
PUBLISHED 27 March 2025

CITATION
Wang J, You J, Huang W, Yuan C, Chen J, Wang F, Wang W and Zhang L (2025) The characteristics of adverse reactions of three anti-prostate cancer drugs based on Vigiaccess database and bibliometric analysis.
Front. Pharmacol. 16:1570661.
doi: 10.3389/fphar.2025.1570661

The characteristics of adverse reactions of three anti-prostate cancer drugs based on Vigiaccess database and bibliometric analysis

Jianqing Wang[1†], Jia You[2†], Weixing Huang[3,4†], Chiting Yuan[5], Jiangjie Chen[5], Feifei Wang[5*], Wei Wang[3*] and Liwei Zhang[5,6*]

[1]Nephrology department, Taizhou Hospital of Zhejiang Province, Zhejiang University School of Medicine, Taizhou, Zhejiang, China, [2]School of Integrative Medicine, Nanjing University of Chinese Medicine, Nanjing, China, [3]Department of Nursing, The First Affiliated Hospital, Zhejiang University School of Medicine, Hangzhou, Zhejiang, China, [4]Department of General surgery, Taizhou Hospital of Zhejiang Province, Zhejiang University School of Medicine, Taizhou, China, [5]Department of Orthopedics, Taizhou Hospital of Zhejiang Province, Zhejiang University School of Medicine, Taizhou, China, [6]Institute of Bone Metabolism, Taizhou Hospital of Zhejiang Province, Zhejiang University School of Medicine, Taizhou, China

Background: Androgen antagonists, including apalutamide, darolutamide, and enzalutamide, play a crucial role in the treatment of prostate cancer. This research evaluated the adverse drug reactions (ADRs) associated with the use of these androgen antagonists as reported by the World Health Organization (WHO). Additionally, it compared the adverse drug reaction (ADR) profiles of the three drugs to identify which one presents the lowest risk for individualized patient use.

Methods: This study employed a retrospective descriptive analysis design. We collected adverse event reports for three marketed androgen antagonists from WHO-VigiAccess and analyzed them in combination with a bibliometric analysis. We calculated the percentage of adverse reactions reported for each drug to compare the similarities and differences in adverse reactions among the three drugs.

Results: A total of 172,020 adverse events (AEs) associated with three androgen antagonists were reported in VigiAccess at the time of this study. Our findings show apalutamide causes the most endocrine disorders. Darolutamide has the highest rate of blood and lymphatic disorders, while enzalutamide causes the most nervous system disorders. The ten most common ADRs identified were fatigue, rash, death, hot flush, diarrhoea, asthenia, nausea, dizziness, arthralgia, and decreased appetite.

Conclusion: This study utilizes real data from WHO-VigiAccess, which offers valuable insights for clinical reference. On one hand, we confirm both existing and potential adverse effects associated with androgen antagonists. On the other hand, We analyzed the possible future research directions, thereby supporting the case for more scientific treatment.

KEYWORDS

prostate cancer, adverse drug reactions, WHO-vigiaccess, androgen antagonists, apalutamide, darolutamide, enzalutamide

Introduction

Androgens play a vital role in preserving typical male physiological functions and sexual differentiation, which is contained in the prostate gland (Werner and Holterhus, 2014). Furthermore, emerging evidence highlights their critical involvement in non-metastatic castration resistance to diseases such as prostate cancer. Androgens activate a series of signaling pathways by binding to androgen receptors, thereby affecting tumor growth (Mills, 2014). The activation of androgen signaling pathway promotes the growth of prostate cancer cells, while promoting tumor invasion and metastasis (Kim et al., 2022). Drugs that target androgen receptors have been used to inhibit the cancer-promoting effects of androgen signaling pathways. The SPARTAN, ARAMIS, and PROSPER studies demonstrated that androgen receptor inhibitors (apalutamide, darolutamide, enzalutamide) can extend metastasis-free survival and overall survival in nonmetastatic castration-resistant prostate cancer (nmCRPC) patients with a brief prostate-specific antigen (PSA) doubling time. These antiandrogen medications have been incorporated into clinical practice as a novel standard of care (Cattrini et al., 2022). For many years, patients with advanced prostate cancer were primarily treated with androgen deprivation therapy (ADT). However, patients with metastatic hormone-sensitive prostate cancer (mHSPC) who receive ADT only have a high risk of developing metastatic castration-resistant prostate cancer (mCRPC) (Xia et al., 2023). While androgen antagonists are generally well tolerated and clinically proven to be effective. For example, In a double-blind, phase 3 trial, androgen-deprivation therapy combined with apalutamide has been confirmed to prolong the survival of patients with metastatic and castration-sensitive prostate cancer without significant increase in adverse events (AEs) (Chi et al., 2019).

We searched the Drugs website (https://www.drugs.com/) to learn more about apalutamide, darolutamide, enzalutamide and their reported adverse reactions. The three drugs are oral androgen receptor inhibitors used to treat prostate cancer at different stages. Apalutamide is approved for nmCRPC and metastatic castration-sensitive disease (mCSPC) when combined with ADT. Darolutamide is indicated for nmCRPC and mHSPC alongside ADT or docetaxel, leveraging its unique structure to minimize central nervous system (CNS) penetration. Enzalutamide, a first-generation agent, is used for nmCRPC, mCRPC, and mHSPC with ADT. Enzalutamide is frequently associated with fatigue, hypertension, dizziness, and CNS-related issues, likely due to its ability to cross the blood-brain barrier. Apalutamide shares similar CNS risks but may also cause rash, hypothyroidism, and joint pain. Darolutamide, with limited CNS penetration, exhibits fewer neurological side effects but has been linked to fatigue, nausea, and elevated liver enzymes. All three agents may increase cardiovascular risks, though enzalutamide and apalutamide carry stronger warnings. Gastrointestinal disturbances are common across all, while enzalutamide and apalutamide are more often tied to seizures and thyroid dysfunction. Darolutamide's distinct profile may reduce drug interactions compared to the others. Despite stringent pre-marketing requirements, the actual safety of drugs still needs to be verified by analysis of a large amount of data, especially for biologics. Therefore, it is necessary to further study the adverse reactions of androgen antagonists.

WHO-VigiAccess is a free portal to the PIDM database, enabling access to safety reports of medicinal products received by the UMC. It was launched by the World Health Organization (WHO) in 2015 to provide public access to information in VigiBase, the WHO global database of reported potential side effects of medicinal products. These side effects, known technically as adverse drug reactions (ADRs) and adverse events following immunization (AEFIs), are reported by national pharmacovigilance centres or national drug regulatory authorities that are members of the WHO Programme for International Drug Monitoring (PIDM) (Watson et al., 2018; Habarugira and Figueras, 2021).

This study looked for three androgen antagonists approved by the WHO: apalutamide, darolutamide, enzalutamide with similar efficacy. The three drugs for the treatment of nmCRPC have been studied over the past decade. Clinicians often need to develop personalized treatment plans based on adverse drug reactions. This study conducted a comparative pharmacovigilance analysis to evaluate disproportionality in adverse drug reaction (ADR) profiles among three therapeutic agents, utilizing safety surveillance data from the WHO-VigiAccess global database.

Materials and methods

Data source

We use WHO-VigiAccess to retrieve all reported adverse events following the administration of androgen antagonists. The login URL is https://www.vigiaccess.org. Data were collected based on age groups, sex, report year, and continents through WHO-VigiAccess. Descriptive statistics were generated using Excel 2019. The classification of adverse events in WHO-VigiAccess is based on system organ class (SOC) and preferred terms (PTs) from the Medical Dictionary for Regulatory Activities (MedDRA). The MedDRA terms were derived from various sources, including the WHO Adverse Reaction Terminology (WHO-ART). Records for androgen antagonists were retrieved, and individual AEs were identified at the MedDRA SOC and PT levels to describe the spectrum of toxicities. A total of 27 items were categorized by SOC, and 20 items related to disease symptoms were selected for analysis (Brown et al., 1999). This study focused on the PTs, which are the level used in the publicly accessible VigiBase database via WHO-VigiAccess. We pay particular attention to serious adverse events, including treatment-interrupted events such as death, hospitalization and disability. It is important to note that due to strict data protection laws and agreements, individual case safety reports cannot be viewed in Vigiaccess. In order to carry out bibliometric analysis,we exported androgen antagonist-related literature from the Web of Science (WoS) database, constructed a co-occurrence network, performed cluster analysis, and ultimately conducted visualization processing.

Data extraction and mining

We use common names (apalutamide, darolutamide, enzalutamide) to identify related reports. In general, the drugs reported in WHO-VigiAccess fall into four categories: primary

suspect drugs, secondary suspect drugs, companion drugs, and interacting drugs. In the search results, we screened the reports with the target drug as the primary suspect drug and excluded duplicate reports and invalid reports. We performed a statistical analysis of the first suspect drug reports after screening. We first analyzed the clinical characteristics of these trials, including demographic characteristics (age, sex) and reporting characteristics (reporting year, region). Based on the MedDRA terminology system, we analyzed the distribution and characteristics of PTs within their respective SOC hierarchies. Severe consequences, meanwhile, were defined as death and hospitalization. After exporting the literature, we performed data deduplication, standardization, and completion to ensure data quality.

TABLE 1 Four major algorithms used for signal detection.

Algorithms	Calculation formulas	Criteria
ROR	$ROR=\frac{(a/c)}{(b/d)}=\frac{ad}{bc}$	95%CI>1
	$95\%CI=e^{\ln(ROR)\pm1.96\sqrt{(\frac{1}{a}+\frac{1}{b}+\frac{1}{c}+\frac{1}{d})}}$	
PRR	$PRR=\frac{a/(a+b)}{c/(c+d)}$	PRR≥2, 95%CI>1
	$95\%CI=e^{\ln(PRR)\pm1.96\sqrt{(\frac{1}{a}+\frac{1}{b}+\frac{1}{c}+\frac{1}{d})}}$	
BCPNN	$IC=\log_2\frac{a(a+b+c+d)}{(a+b)(a+c)}$	IC025>0
	$E(IC)=\log_2\frac{(a+\gamma11)(a+b+c+d+\alpha)(a+b+c+d+\beta)}{(a+b+c+d+\gamma)(a+b+\alpha1)(a+c+\beta1)}$	
EBGM	$EBGM=\frac{a(a+b+c+d)}{(a+c)(a+b)}$	EBGM05>2
	$95\%CI=e^{\ln(EBGM)\pm1.96\sqrt{(\frac{1}{a}+\frac{1}{b}+\frac{1}{c}+\frac{1}{d})}}$	

Statistical analysis

In this study, a retrospective descriptive approach was employed. The analysis involved comparing drugs based on the quantity and rate of ADR reports. At the same time, we used statistical methods such as reporting Odds ratio method (ROR) and Proportional Reporting ratio method (PRR) to mining the adverse event signal of the first suspected drug. The following approaches can be utilized to assess the degree of statistical correlation between a medication and an adverse reaction, which in turn can further substantiate the drug's status as the primary suspect. The Reporting Ratio technique gauges the intensity of the link between a drug and an adverse event by contrasting the incidence of a specific drug-adverse event pair with that of other drug-adverse event pairs (Rothman et al., 2004). The Proportional Reporting Ratio (PRR) method evaluates the link between a drug and an adverse event. It does this by computing the ratio of the target drug to the target adverse event, as well as the ratio of the non-target drug to the target adverse event (Evans et al., 2001). The Bayesian Confidence Propagation Neural Network (BCPNN) is a signal detection approach grounded in Bayesian statistical principles. It is utilized to analyze data within adverse drug reaction monitoring databases, aiming to pinpoint potential adverse drug reaction signals (Bate et al., 1998). In the BCPNN, Information Component (IC) is the core indicator used to measure the degree of association between a drug and an adverse reaction (Bate, 2007). Empirical Bayesian Geometric Mean (EBGM) is another signal detection method based on Bayesian methods, which assesses the association between drugs and adverse events by calculating the ratio between the number of reported drugs and adverse events and the number of expected reports (Noguchi et al., 2021). These methods have important application value in the detection of adverse drug reaction signals, and can help identify the potential association between drugs and adverse events, so as to improve the monitoring and evaluation of drug safety (Table 1).

Results

Description of the studied cases

Apalutamide and darolutamide were collected by WHO-VigiAccess from 2016 to 2024 for 11,452 and 2,269 adverse reaction reports, respectively. Enzalutamide had the highest number of adverse reactions reported, with 53,007 cases reported from 2012 to 2024. A total of 66,728 cases were reported for these three drugs (Table 2). In the 172,020 ADR reports concerning the three androgen antagonist drugs, there were 20,965 cases related to apalutamide, 5,236 cases to darolutamide, and 145,819 cases to enzalutamide. Except for 355 cases reported as female, all were male (Table 3). Excluding reports of unknown age, incidence increased with age group. Among the top five reporting countries, the Americas region has the highest incidence of adverse reactions, while Africa has the lowest (Figure 1).

Adverse drug reaction distribution and signal distribution of three androgen antagonists at SOC level

In this study, adverse reactions to three androgen antagonists included 27 SOCs, based on analysis of adverse event reports. Due to incomplete statistics of Pregnancy, puerperium and perinatal conditions, only 26 cases of SOC were actually analyzed. All three drugs had a high rate of general disorders and administration site conditions, as well as gastrointestinal disorders. These three drugs also showed a high incidence rate of skin and subcutaneous tissue disorders, with apalutamide (19.45%) having the highest rate. Enzalutamide had the highest rate of nervous system disorders (10.68%), while darolutamide had the highest rate of blood and lymphatic system disorders (2.16%). We found that apalutamide is the most likely to develop endocrine disorders (0.93%) (Table 3). The results of ADR signal detection were consistent with the incidence rate. Previous studies have shown that common endocrine adverse events associated with apalutamide include hypothyroidism, high blood pressure, and rashes (Pyrgidis et al., 2021). Darolutamide is more associated with hepatobiliary disorders, and enzalutamide has the strongest signal of product issues (Supplementary Table S1).

Distribution of adverse drug reactions of three androgen antagonists at PT level

We calculated the proportion of each adverse reaction by the number of ADR reports for the three drugs. At PT level, the common

TABLE 2 Number and distribution of ADR reports of three androgen antagonists.

	Apalutamide	Darolutamide	Enzalutamide
Number of ADR reports	11,452	2,269	53,007
Sex			
Female	35 (0.31%)	7 (0.31%)	313 (0.59%)
Male	10,751 (93.88%)	2,124 (93.61%)	51,764 (97.66%)
Unknown	666 (5.82%)	138 (6.08%)	930 (1.75%)
Age			
<18	3 (0.03%)	2 (0.09%)	7 (0.01%)
18–44	10 (0.09%)	3 (0.13%)	58 (0.11%)
45–64	722 (6.30%)	262 (11.55%)	4,091 (7.72%)
65–74	2,217 (19.36%)	495 (21.82%)	9,422 (17.78%)
≥75	3,624 (31.65%)	777 (34.24%)	17,308 (32.65%)
Unknown	4,876 (42.58%)	730 (32.17%)	22,121 (41.73%)
Top 5 reporting countries			
Africa	141 (1.23%)	0 (0.00%)	65 (0.12%)
Americas	5,932 (51.80%)	1,127 (49.67%)	42,759 (80.67%)
Asia	1,639 (14.31%)	368 (16.22%)	4,220 (7.96%)
Europe	3,724 (32.52%)	718 (31.64%)	5,648 (10.66%)
Oceania	16 (0.14%)	56 (2.47%)	315 (0.59%)
Reporting year			
Before 2017	3 (0.03%)	2 (0.09%)	14,551 (27.45%)
2017	4 (0.03%)	2 (0.09%)	8,209 (15.49%)
2018	75 (0.65%)	0 (0.00%)	10,471 (19.75%)
2019	844 (7.37%)	11 (0.48%)	7,789 (14.69%)
2020	1,091 (9.53%)	97 (4.28%)	2094 (3.95%)
2021	1,317 (11.50%)	242 (10.67%)	2,238 (4.22%)
2022	2,191 (19.13%)	336 (14.81%)	2,140 (4.04%)
2023	2,385 (20.83%)	580 (25.56%)	2,361 (4.45%)
2024	3,542 (30.93%)	999 (44.03%)	3,154 (5.95%)

ADRs in the three drugs are fatigue, rash, death, hot flush, diarrhoea, asthenia, nausea, dizziness, arthralgia and decreased appetite. The proportion of apalutamide-related rash was significantly higher than that of the other two androgen antagonists, while the proportion of fatigue related to darolutamide and enzalutamide was significantly higher than that of apalutamide (Table 4).

Serious AEs of three androgen antagonists drugs

Through WHO-VigiAccess, we were also able to identify major adverse events involving androgen antagonists, including death, hospitalization, and disability, with death accounting for the highest proportion. The reported number and rate of major adverse reactions were apalutamide(20,965, 4.94%), darolutamide (5236,2.85%) and enzalutamide (145,819,5.06%), respectively. All three androgen antagonists had a low likelihood of causing disability. Enzalutamide is the most likely to cause serious adverse reactions and has the greatest probability of leading to death (Figure 2).

The same and different points of common ADRs of three androgen antagonists

We compared and analyzed the similarities and differences of adverse reactions of three androgen antagonists. We found a total of

TABLE 3 ADR number and Incidence rate of SOCs of three androgen antagonists.

System organ classes	Apalutamide (N = 20,965)	Darolutamide (N = 5,236)	Enzalutamide (N = 145,819)
Blood and lymphatic system disorders	280 (1.34%)	113 (2.16%)	1,205 (0.83%)
Cardiac disorders	486 (2.32%)	119 (2.27%)	2,241 (1.54%)
Congenital, familial and genetic disorders	7 (0.03%)	1 (0.02%)	30 (0.02%)
Ear and labyrinth disorders	90 (0.43%)	22 (0.42%)	715 (0.49%)
Endocrine disorders	195 (0.93%)	5 (0.10%)	98 (0.07%)
Eye disorders	133 (0.63%)	55 (1.05%)	1,661 (1.14%)
Gastrointestinal disorders	1,328 (6.33%)	469 (8.96%)	14,604 (10.02%)
General disorders and administration site conditions	3,835 (18.29%)	992 (18.95%)	35,797 (24.55%)
Hepatobiliary disorders	103 (0.49%)	85 (1.62%)	461 (0.32%)
Immune system disorders	83 (0.40%)	19 (0.36%)	328 (0.23%)
Infections and infestations	586 (2.80%)	142 (2.71%)	4,007 (2.75%)
Injury, poisoning and procedural complications	1,443 (6.88%)	366 (6.99%)	10,731 (7.36%)
Investigations	1,482 (7.07%)	512 (9.78%)	10,219 (7.01%)
Metabolism and nutrition disorders	447 (2.13%)	111 (2.12%)	4,709 (3.23%)
Musculoskeletal and connective tissue disorders	973 (4.64%)	370 (7.07%)	10,467 (7.18%)
Neoplasms benign, malignant and unspecified (incl cysts and polyps)	604 (2.88%)	246 (4.70%)	7,216 (4.95%)
Nervous system disorders	1,495 (7.13%)	433 (8.27%)	15,569 (10.68%)
Psychiatric disorders	514 (2.45%)	147 (2.81%)	5,887 (4.04%)
Renal and urinary disorders	326 (1.56%)	127 (2.43%)	2,645 (1.81%)
Reproductive system and breast disorders	132 (0.63%)	57 (1.09%)	785 (0.54%)
Respiratory, thoracic and mediastinal disorders	574 (2.74%)	172 (3.29%)	4,407 (3.02%)
Skin and subcutaneous tissue disorders	4,078 (19.45%)	369 (7.05%)	4,196 (2.88%)
Social circumstances	40 (0.19%)	17 (0.33%)	356 (0.24%)
Surgical and medical procedures	594 (2.83%)	83 (1.59%)	1,208 (0.83%)
Vascular disorders	1,056 (5.04%)	199 (3.80%)	4,884 (3.35%)
Product issues	81 (0.39%)	5 (0.10%)	1,391 (0.95%)

162 identical adverse reaction signals at the PT level and categorized them by system organ classes. The top five system organ classes with the most adverse reaction signals are general disorders and administration site conditions, nervous system disorders, gastrointestinal disorders, musculoskeletal and connective tissue disorders, skin and subcutaneous tissue disorders (Table 5).

According to the statistical results of different adverse reactions of the three drugs, darolutamide had the most adverse reactions, while enzalutamide had the least (Figure 3). We found that apalutamide has adverse effects such as hypothyroidism and thyroid disorder, while darolutamide may cause hepatic cytolysis, hypertransaminasaemia and adverse reactions such as hepatitis. It further verified the conclusion that apalutamide is more likely to cause endocrine disorders and darolutamide is more likely to cause hepatobiliary disorders. At the same time, apalutamide had the most specific adverse reactions in skin and subcutaneous tissue disorders, which was consistent with the conclusion that apalutamide had the highest incidence of rash. It is worth mentioning that the specific adverse reactions of darolutamide in vascular disorders include deep vein thrombosis and orthostatic hypotension, suggesting its cardiovascular adverse reactions (Table 6).

The research trend of androgen antagonists based on bibliometric analysis

The bibliometric analysis revealed a consistent upward trend in the annual publication volume of androgen antagonists over the past decade, indicating intensified research focus and expanded therapeutic exploration in this field. Geographically, the majority of publications originated from the United States and select

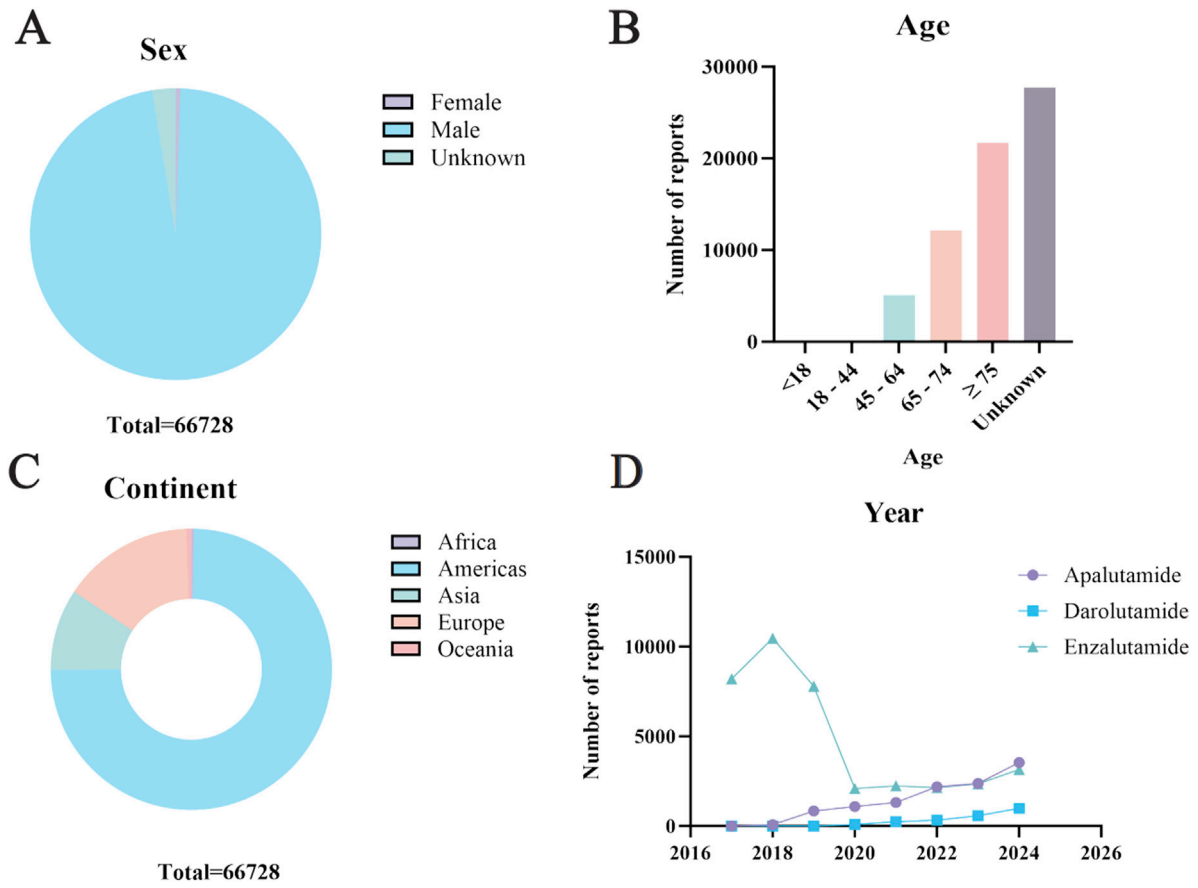

FIGURE 1
Characteristics of ADR reports of three androgen antagonists **(A)** Gender distribution of ADR report **(B)** Age distribution of ADR reports **(C)** Continent distribution of ADR reports **(D)** Trend of annual report volume.

European nations, aligning with Vigiaccess database findings that identified the highest rate of adverse event reports from the Americas. Discipline co-occurrence mapping demonstrated strong associations between Oncology and Cardiovascular Systems as well as Geriatrics & Gerontology, highlighting the critical need to address cardiovascular toxicity associated with androgen antagonist therapy and the unique therapeutic requirements of elderly cancer patients. Journal distribution analysis further underscored the predominance of oncology- and pharmacy-focused periodicals, reinforcing the central role of androgen antagonists in prostate cancer management. Keyword cluster analysis revealed significant attention to heart failure risk and its clinical management, emphasizing the cardiovascular toxicity profile as a critical safety consideration for these agents. Temporal keyword evolution mapping delineated the strong association between androgen receptor pathway inhibitors and therapeutic strategies such as abiraterone and antiandrogen therapy, consolidating prostate cancer treatment as the primary research trajectory (Figure 4).

Discussion

Apalutamide, darolutamide, and enzalutamide are next-generation androgen receptor signaling inhibitors (ARSIs) that target the androgen receptor (AR) pathway through distinct mechanisms, improving survival in nmCRPC. Apalutamide, a thiohydantoin derivative, inhibits AR nuclear translocation and DNA binding to androgen response elements (AREs), preventing transcriptional activation of androgen-dependent genes. Similarly, enzalutamide competitively antagonizes androgen binding to AR, blocks nuclear translocation, and disrupts AR-DNA interaction, thereby suppressing downstream signaling. Both agents exhibit no significant agonist activity but demonstrate central nervous system (CNS) penetration, contributing to seizure risk. In contrast, darolutamide, a structurally unique nonsteroidal AR antagonist with a polar pyrazole backbone, potently inhibits androgen binding while maintaining antagonistic efficacy even in AR-overexpressing cells. Its reduced blood-brain barrier penetration minimizes CNS-related adverse events. Pharmacokinetically, darolutamide undergoes CYP3A4-mediated metabolism with limited drug-drug interaction (DDI) potential, whereas apalutamide and enzalutamide act as strong CYP3A4 inducers, increasing DDI risks. While effective and generally tolerated, the mechanisms of action may raise safety concerns, highlighting the importance of studying their adverse effects and strengthening relevant management to improve therapeutic effect (Gasperoni et al., 2024).

TABLE 4 Top 20 ADRs of three androgen antagonists.

Apalutamide		Darolutamide		Enzalutamide	
ADR	Report rate %	ADR	Report rate %	ADR	Report rate %
Rash	9.93	Fatigue	6.26	Fatigue	6.34
Fatigue	4.25	Rash	2.46	Death	4.75
Death	4.17	Off label use	2.39	Malignant neoplasm progression	3.37
Hot flush	2.59	Death	2.23	Drug ineffective	2.63
Product dose omission issue	1.77	Asthenia	2.18	Prostatic specific antigen increased	2.53
Diarrhoea	1.72	Diarrhoea	1.83	Asthenia	2.48
Pruritus	1.47	Hot flush	1.83	Decreased appetite	2.09
Hypertension	1.46	Prostatic specific antigen increased	1.53	Nausea	2.06
Arthralgia	1.45	Pain in extremity	1.45	Hot flush	1.98
Asthenia	1.42	Nausea	1.43	Dizziness	1.86
Prostatic specific antigen increased	1.33	Dizziness	1.28	Diarrhoea	1.72
Dizziness	1.23	Arthralgia	1.20	Back pain	1.35
Off label use	1.18	Dyspnoea	1.15	Underdose	1.34
Fall	1.17	Decreased appetite	1.07	Arthralgia	1.22
Drug ineffective	1.06	Neuropathy peripheral	1.03	Constipation	1.05
Decreased appetite	1.01	Product dose omission issue	0.94	Headache	1.04
Nausea	0.94	Hormone-refractory prostate cancer	0.94	Weight decreased	1.03
Rash pruritic	0.88	Hypertension	0.90	Fall	1.02
Weight decreased	0.83	Prostate cancer	0.84	Pain	0.94
Interstitial lung disease	0.77	Peripheral swelling	0.78	Malaise	0.87

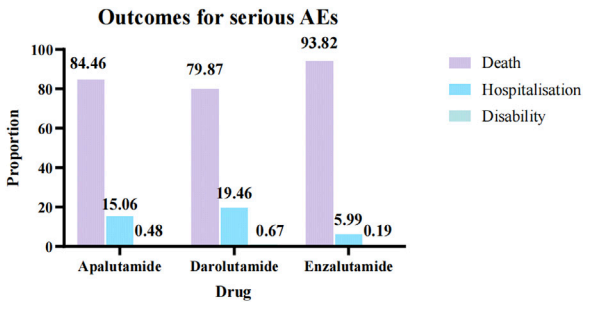

FIGURE 2
Serious AEs of three androgen antagonists drugs.

Our study comprehensively evaluated the adverse events associated with three androgen antagonists (apalutamide, darolutamide, enzalutamide). By analyzing data from WHO-VigiAccess, the study confirmed previous findings of adverse reactions on drug labels, including common ADRs such as rashes. In addition, adverse reactions not indicated on the label, including elevated prostate-specific antigens, were also found. These findings highlight in particular the need for drug surveillance. At the beginning of treatment, potential adverse effects should be identified and effectively managed.

In terms of the total number of adverse reactions reported, the number of adverse reactions reported by enzalutamide was much higher than that of apalutamide and darolutamide. However, this does not necessarily mean that enzalutamide has a higher rate of adverse reactions or is less safe, and may be attributed to the much higher use of enzalutamide than the other two drugs. The significantly higher incidence of adverse reactions in men than in women may be attributed to the fact that androgen antagonists are primarily used to treat male prostate cancer (Al-Salama, 2018). The number of adverse reactions increased with the increase of age group, which may be related to the decline of physical function and underlying diseases in the elderly (Gao et al., 2024). The decrease in the number of adverse reactions reported with enzalutamide from 2017 to date and the increase in apalutamide and darolutamide indicate a change in clinical use (Desai et al., 2021). In fact, the

TABLE 5 Same ADRs among three androgen antagonists.

System organ classes	ADRs	Signal N
General disorders and administration site conditions	Peripheral swelling, Gait inability, Pyrexia, Disease progression, Oedema, Chest discomfort, Swelling face, Chest pain, Asthenia, Adverse drug reaction, Drug ineffective, Drug intolerance, Gait disturbance, Death, General physical health deterioration, Oedema peripheral, Pain, Drug interaction, Condition aggravated, Chills, Malaise, Fatigue, Illness, Feeling hot, Feeling abnormal, Adverse event	25
Nervous system disorders	Taste disorder, Transient ischaemic attack, Dysgeusia, Somnolence, Loss of consciousness, Hypersomnia, Paraesthesia, Memory impairment, Ageusia, Dementia, Hypoaesthesia, Headache, Syncope, Neuropathy peripheral, Tremor, Cognitive disorder, Balance disorder, Cerebrovascular accident, Seizure, Dizziness, Lethargy	21
Gastrointestinal disorders	Abdominal distension, Vomiting, Diarrhoea, Abdominal discomfort, Dyspepsia, Abdominal pain upper, Dry mouth, Gastrooesophageal reflux disease, Gastrointestinal disorder, Nausea, Abdominal pain, Flatulence, Dysphagia, Constipation	14
Musculoskeletal and connective tissue disorders	Joint swelling, Arthralgia, Bone pain, Limb discomfort, Back pain, Mobility decreased, Muscle atrophy, Pain in extremity, Myalgia, Musculoskeletal pain, Muscle spasms, Muscular weakness, Arthritis	13
Skin and subcutaneous tissue disorders	Erythema, Urticaria, Alopecia, Dry skin, Night sweats, Rash pruritic, Pruritus, Skin exfoliation, Rash, Hyperhidrosis	10
Injury, poisoning and procedural complications	Product use in unapproved indication, Fracture, Off label use, Hip fracture, Incorrect dose administered, Fall, Wrong technique in product usage process, Inappropriate schedule of product administration, Product dose omission issue	9
Investigations	Weight decreased, Prostatic specific antigen increased, Blood glucose increased, Blood pressure decreased, Blood pressure increased, Heart rate increased, Weight increased, White blood cell count decreased, Haemoglobin decreased	9
Infections and infestations	Nasopharyngitis, Urinary tract infection, Pneumonia, Herpes zoster, Influenza, Infection, Sepsis, COVID-19	8
Renal and urinary disorders	Renal impairment, Acute kidney injury, Dysuria, Haematuria, Pollakiuria, Urinary retention, Nocturia, Renal failure	8
Psychiatric disorders	Insomnia, Hallucination, Anxiety, Depression, Eating disorder, Confusional state, Sleep disorder	7
Respiratory, thoracic and mediastinal disorders	Oropharyngeal pain, Dyspnoea, Pulmonary embolism, Interstitial lung disease, Epistaxis, Dyspnoea exertional, Cough	7
Cardiac disorders	Cardiac failure, Cardiac failure congestive, Cardiac disorder, Cardiac arrest, Myocardial infarction, Atrial fibrillation	6
Neoplasms benign, malignant and unspecified (incl cysts and polyps)	Metastases to bone, Hormone-refractory prostate cancer, Prostate cancer, Prostate cancer metastatic, Malignant neoplasm progression, Neoplasm malignant	6
Vascular disorders	Hot flush, Blood pressure fluctuation, Hypertension, Thrombosis, Hypotension	5
Blood and lymphatic system disorders	Neutropenia, Anaemia, Thrombocytopenia	3
Ear and labyrinth disorders	Tinnitus, Vertigo	2
Eye disorders	Visual impairment, Vision blurred	2
Metabolism and nutrition disorders	Dehydration, Decreased appetite	2
Reproductive system and breast disorders	Gynaecomastia, Erectile dysfunction	2
Hepatobiliary disorders	Hepatic function abnormal	1
Immune system disorders	Hypersensitivity	1
Surgical and medical procedures	Hospitalisation	1

AFFRIM trial found that men treated with enzalutamide reported higher rates of diarrhea, hot flashes, fatigue, high blood pressure, and a small percentage (0.6%) experienced seizures (Scher et al., 2012). Hypertension was a common adverse effect of enzalutamide in PREVAIL (Beer et al., 2014). A higher incidence of enzalutamide epilepsy was found in two subsequent phase 3 trials, ENZAMET and ARCHES (Davis et al., 2019; Armstrong et al., 2019). However, trials demonstrated that the adverse effects of apalutamide were milder, and adverse events such as dalloutamide seizures were less common (Rachner et al., 2018; Fizazi et al., 2019).

At the SOC level, the incidence of Skin and subcutaneous tissue disorders in apalutamide was much higher than that in darolutamide and enzalutamide. In one case report, four patients treated with apalutamide for castration-resistant prostate cancer

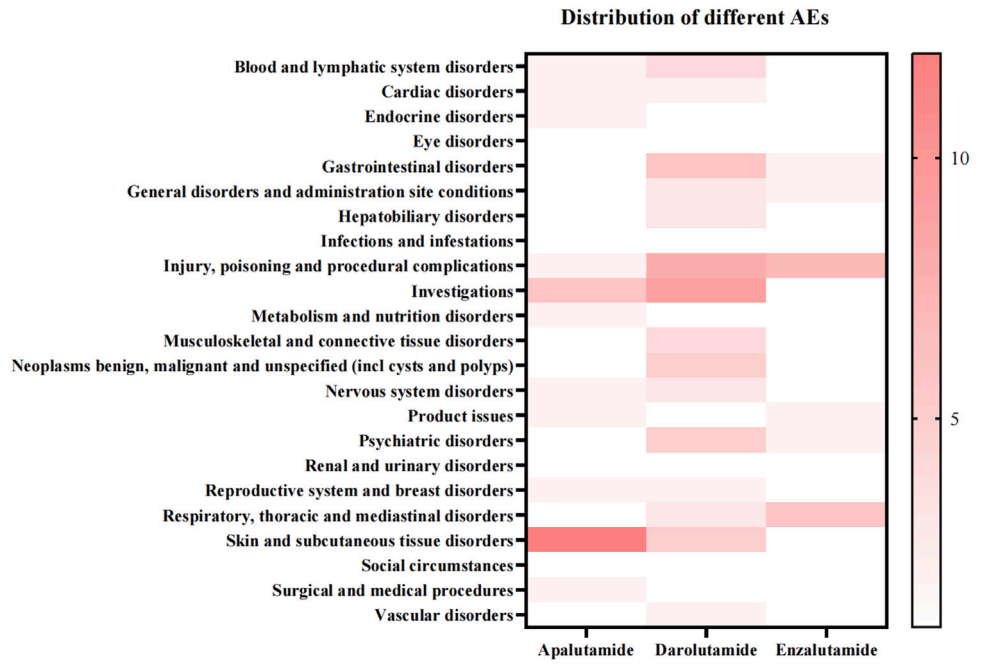

FIGURE 3
Distribution of different ADRs among three androgen antagonists.

developed severe and fatal drug eruptions including Stevens-Johnson syndrome and toxic epidermal necrolysis, with an average incubation period of 40 days. After discontinuation of apalutamide in all patients, three of them recovered (Wang et al., 2023). At the same time, apalutamide is more likely to cause heart and vessel disease. While enzalutamide had a higher incidence of nervous system disorders and psychiatric disorders than the other two drugs. Psychological adverse reactions may significantly affect patients. Such issues can impair both mental and physical wellbeing. They are often marked by feelings of low spirits, lack of energy, and sadness, which can further lead to sleep disturbances and a reduced ability to take pleasure in life (Cui, 2015). It is worth noting that clinical pharmacokinetic and pharmacodynamic analysis of darolutamide showed that darolutamide is over metabolized by oxidation and glucose-aldehyde acidification and excreted in urine and stool. Darolutamide should not be used in patients with moderate or severe renal or liver impairment (Podgoršek et al., 2023). The reason for the higher incidence of product issues with darolutamide may be attributed to its role as a substrate for P-gp and CYP3A4, as well as an inhibitor of breast cancer resistance protein (BCRP) and organic anion transporters (OATP1B1 and OATP1B3). This makes darolutamide prone to drug interactions when combined with other drugs, which can affect the metabolism and efficacy of the drug. Therefore, a thorough understanding of drug interactions is needed to optimize treatment outcomes and minimize adverse reactions (Bolek et al., 2024). At the PT level, the overall performance of darolutamide was relatively good in terms of adverse reactions, and the incidence of adverse reactions and serious adverse reactions was similar to enzalutamide, but the risk of treatment interruption due to adverse reactions was lower, and adverse reaction related mortality was slightly lower than enzalutamide. Apalutamide was slightly higher than the other two drugs in terms of risk of serious adverse reactions and treatment interruption.

The management of advanced prostate cancer with androgen antagonists (apalutamide, darolutamide, and enzalutamide) requires tailored strategies to mitigate their distinct adverse effect profiles. In view of the common situation of underlying diseases in the elderly, it is recommended to conduct a comprehensive assessment of liver and kidney function in elderly patients before medication. At the same time, consider the individual differences of the patient, such as body weight, to adjust the drug dose. When the elderly have basic diseases, try to reduce the variety of drugs and avoid unnecessary combination of drugs. The elderly are highly sensitive to the side effects of drugs, so the adverse reactions should be closely monitored and the medication regimen should be adjusted in time. Apalutamide, associated with endocrine disturbances and dermatologic reactions, necessitates regular monitoring of thyroid function, blood pressure, and skin evaluations, with dose interruption advised for severe cutaneous toxicity. Darolutamide is contraindicated in patients with hepatic impairment due to hepatotoxicity risks; baseline and bimonthly liver function tests are mandatory, and permanent discontinuation is recommended if hepatotoxicity develops. Enzalutamide, linked to neuropsychiatric AEs, warrants pre-treatment neurocognitive screening and periodic psychiatric assessments, with dose reduction or cessation for persistent symptoms. Prophylactic measures, such as photoprotection for dermatologic AEs and antiemetics for gastrointestinal toxicity, should be prioritized. Patient stratification by comorbidities and multidisciplinary collaboration are critical to optimizing safety.

Our research is based on the latest data from WHO-VigiAccess and is authoritative and timely. This study further analyzed the research trend of androgen antagonists through bibliometrics analysis, which has instructive significance. However, our study also has some limitations. First of all, there may be omissions or

TABLE 6 Different ADRs among three androgen antagonists.

ADR	Apalutamide	Darolutamide	Enzalutamide
Blood and lymphatic system disorders	Eosinophilia, Agranulocytosis	Myelosuppression, Disseminated intravascular coagulation, Cytopenia, Blood disorder	
Cardiac disorders	Myocardial ischaemia, Acute myocardial infarction	Cardiotoxicity, Bradycardia	
Endocrine disorders	Hypothyroidism, Thyroid disorder		
Eye disorders		Blindness	Cataract
Gastrointestinal disorders	Rectal haemorrhage	Faeces soft, Frequent bowel movements, Colitis, Faeces discoloured, Gastrointestinal motility disorder, Swollen tongue	Retching, Gastrointestinal haemorrhage
General disorders and administration site conditions	Therapeutic product effect decreased	Pre-existing condition improved, Feeling cold, Exercise tolerance decreased	Treatment failure, Influenza like illness
Hepatobiliary disorders		Hepatic cytolysis, Hypertransaminasaemia, Hepatitis	
Infections and infestations	Lower respiratory tract infection	*Escherichia* infection	
Injury, poisoning and procedural complications	Incorrect dosage administered, Intentional product use issue	Limb injury, Toxicity to various agents, Incorrect product administration duration, Multiple fractures, Product prescribing issue, Product dose omission in error, Accidental exposure to product, Nerve injury	Product storage error, Intentional product misuse, Overdose, Underdose, Circumstance or information capable of leading to medication error, Intentional dose omission, Foreign body in throat
Investigations	Glycosylated haemoglobin increased, Blood potassium increased, Blood triglycerides increased, Blood thyroid stimulating hormone increased, Laboratory test abnormal, Prostatic specific antigen decreased	Blood sodium decreased, Blood calcium decreased, Red blood cell count decreased, Transaminases increased, Blood bilirubin increased, Heart rate decreased, International normalised ratio increased, Blood potassium decreased, Blood testosterone decreased	Full blood count decreased
Metabolism and nutrition disorders	Hyperkalaemia, Hypercholesterolaemia	Increased appetite	Hypophagia
Musculoskeletal and connective tissue disorders	Osteoporosis	Rhabdomyolysis, Musculoskeletal discomfort, Musculoskeletal disorder, Groin pain	
Neoplasms benign, malignant and unspecified (incl cysts and polyps)	Lung neoplasm malignant	Bladder cancer, Neoplasm progression, Metastases to spine, Metastases to pelvis, Malignant melanoma	
Nervous system disorders	Sensory disturbance, Cerebral infarction	Head discomfort, Parkinson's disease, Motor dysfunction, Neuralgia, Presyncope	Dyskinesia
Product issues	Product label issue, Product packaging quantity issue		Product availability issue, Product physical issue
Psychiatric disorders		Poor quality sleep, Delirium, Apathy, Stress, Personality change	Disorientation, Restlessness
Renal and urinary disorders	Micturition urgency	Urinary tract disorder	
Reproductive system and breast disorders	Pelvic pain, Breast enlargement	Breast swelling, Breast pain	
Respiratory, thoracic and mediastinal disorders		Pulmonary hypertension, Lung disorder, Pneumonitis	Choking, Pleural effusion, Throat irritation, Chronic obstructive pulmonary disease, Rhinorrhoea, Productive cough
Skin and subcutaneous tissue disorders	Lichenoid keratosis, Skin toxicity, Drug reaction with eosinophilia and systemic symptoms, Erythema multiforme, Toxic epidermal necrolysis, Eczema, Dermatitis allergic, Stevens-johnson syndrome, Toxic skin eruption, Dermatitis, Skin reaction, Dermatitis exfoliative generalised	Haemorrhage subcutaneous, Skin atrophy, Palmar-plantar erythrodysaesthesia syndrome, Angioedema, Nail disorder	
Social circumstances		Bedridden	

(Continued on following page)

TABLE 6 (*Continued*) Different ADRs among three androgen antagonists.

ADR	Apalutamide	Darolutamide	Enzalutamide
Surgical and medical procedures	Therapy change, Surgery	Cardiac operation	
Vascular disorders		Deep vein thrombosis, Orthostatic hypotension	

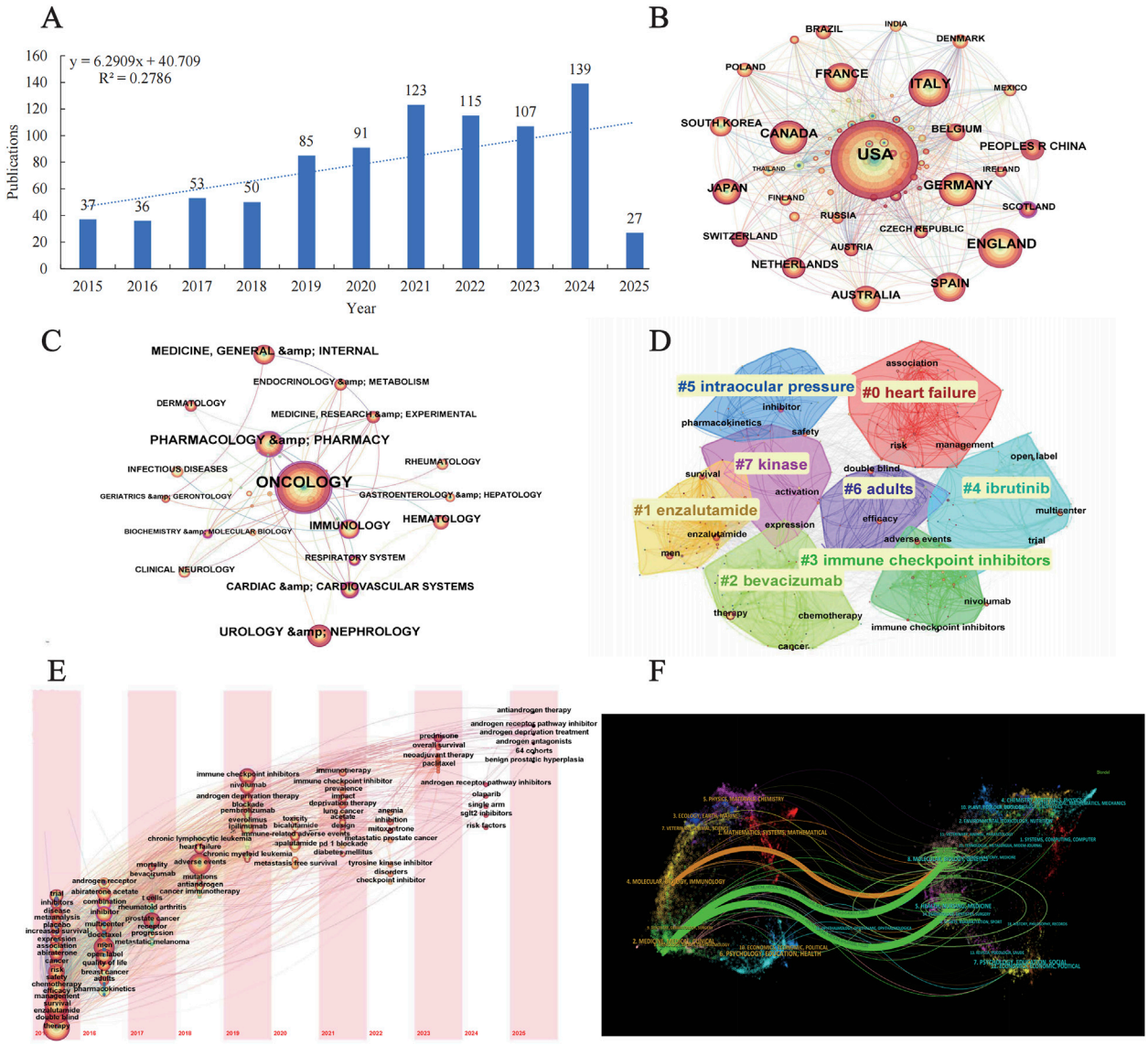

FIGURE 4
Bibliometric analysis **(A)** Annual publication trends **(B)** International collaboration networks **(C)** Keyword co-occurrence **(D)** Keyword clustering analysis **(E)** Keyword timezone map **(F)** Dual-map overlay of cross-disciplinary citation trajectories.

errors in adverse reactions reported in the WHO-VigiAccess. Meanwhile, most of the reports are from the Americas, which may be biased. Future studies should expand the sample size to improve the applicability of the conclusions. It is worth noting that there is no direct causal relationship between these adverse effects and androgen antagonists. Our research needs to be combined with the latest clinical trial results to guide more effective treatments. Recent studies have shown that patients treated with currently approved AR-targeted drugs develop resistance and relapse into castration-resistant prostate cancer (CRPC). In order to effectively inhibit reactivated AR signaling, new methods targeting AR should be actively explored. These new approaches include new small molecule inhibitors that target different domains of AR as well as drugs capable of degrading AR (Cole et al., 2024). Long-term studies are necessary to confirm potential adverse effects and develop personalized treatment.

Conclusion

Androgen antagonists are crucial in prostate cancer treatment but have reported over 170,000 AEs globally. AEs mainly involve skin and subcutaneous tissue disorders and gastrointestinal disorders. Comparative analysis shows apalutamide may cause endocrine issues, such as rashes and hypertension. Darolutamide has notable hepatobiliary AEs, including hepatotoxicity. Enzalutamide is linked to nervous and psychiatric disorders. Most AEs are mild, but severe ones can be fatal. Future research should focus on pharmacogenomics to identify genetic factors for severe reactions like hepatotoxicity. AI-driven natural language processing can mine unstructured clinical data. Integrative omics approaches (proteomics, metabolomics, immunophenotyping) could reveal biomarkers for early detection of hypersensitivity or resistance, guiding personalized androgen antagonist selection and preemptive AE management.

Data availability statement

The original contributions presented in the study are included in the article/Supplementary Material, further inquiries can be directed to the corresponding authors.

Author contributions

JW: Writing–original draft, Writing–review and editing. JY: Writing–original draft, Writing–review and editing. WH: Writing–original draft, Writing–review and editing. CY: Writing–original draft, Writing–review and editing. JC: Writing–original draft, Writing–review and editing. FW: Writing–original draft, Writing–review and editing. WW: Writing–original draft, Writing–review and editing. LZ: Writing–original draft, Writing–review and editing.

Funding

The author(s) declare that financial support was received for the research and/or publication of this article. This work was supported by the National Natural Science Foundation of China (82202738), Taizhou Social Development Science and Technology project (22ywa06), the Medical and Health Technology Program of Zhejiang Province (2023RC299, 2021KY1197, 2023KY667, and 2024KY976).

Acknowledgments

We sincerely appreciate the significant contributions made by all the authors towards this study, their invaluable efforts have been instrumental in its success.

Conflict of interest

The authors declare that the research was conducted in the absence of any commercial or financial relationships that could be construed as a potential conflict of interest.

Generative AI statement

The author(s) declare that no Generative AI was used in the creation of this manuscript.

Publisher's note

Supplementary material

The Supplementary Material for this article can be found online at: https://www.frontiersin.org/articles/10.3389/fphar.2025.1570661/full#supplementary-material

References

Al-Salama, Z. T. (2018). Apalutamide: first global approval. *Drugs* 78 (6), 699–705. doi:10.1007/s40265-018-0900-z

Armstrong, A. J., Szmulewitz, R. Z., Petrylak, D. P., Holzbeierlein, J., Villers, A., Azad, A., et al. (2019). ARCHES: a randomized, phase III study of androgen deprivation therapy with enzalutamide or placebo in men with metastatic hormone-sensitive prostate cancer. *J. Clin. Oncol.* 37 (32), 2974–2986. doi:10.1200/JCO.19.00799

Bate, A. (2007). Bayesian confidence propagation neural network. *Drug Saf.* 30 (7), 623–625. doi:10.2165/00002018-200730070-00011

Bate, A., Lindquist, M., Edwards, I. R., Olsson, S., Orre, R., Lansner, A., et al. (1998). A Bayesian neural network method for adverse drug reaction signal generation. *Eur. J. Clin. Pharmacol.* 54 (4), 315–321. doi:10.1007/s002280050466

Beer, T. M., Armstrong, A. J., Rathkopf, D. E., Loriot, Y., Sternberg, C. N., Higano, C. S., et al. (2014). Enzalutamide in metastatic prostate cancer before chemotherapy. *N. Engl. J. Med.* 371 (5), 424–433. doi:10.1056/NEJMoa1405095

Bolek, H., Yazgan, S. C., Yekedüz, E., Kaymakcalan, M. D., McKay, R. R., Gillessen, S., et al. (2024). Androgen receptor pathway inhibitors and drug-drug interactions in prostate cancer. *ESMO Open* 9 (11), 103736. doi:10.1016/j.esmoop.2024.103736

Brown, E. G., Wood, L., and Wood, S. (1999). The medical dictionary for regulatory activities (MedDRA). *Drug Saf.* 20 (2), 109–117. doi:10.2165/00002018-199920020-00002

Cattrini, C., Caffo, O., De Giorgi, U., Mennitto, A., Gennari, A., Olmos, D., et al. (2022). Apalutamide, darolutamide and enzalutamide for nonmetastatic castration-resistant prostate cancer (nmCRPC): a critical review. *Cancers (Basel)* 14 (7), 1792. doi:10.3390/cancers14071792

Chi, K. N., Agarwal, N., Bjartell, A., Chung, B. H., Pereira de Santana Gomes, A. J., Given, R., et al. (2019). Apalutamide for metastatic, castration-sensitive prostate cancer. *N. Engl. J. Med.* 381 (1), 13–24. doi:10.1056/NEJMoa1903307

Cole, R. N., Fang, Q., Matsuoka, K., and Wang, Z. (2024). Androgen receptor inhibitors in treating prostate cancer. *Asian J. Androl.* 27, 144–155. doi:10.4103/aja202494

Cui, R. (2015). Editorial: a systematic review of depression. *Curr. Neuropharmacol.* 13 (4), 480. doi:10.2174/1570159x1304150831123535

Davis, I. D., Martin, A. J., Stockler, M. R., Begbie, S., Chi, K. N., Chowdhury, S., et al. (2019). Enzalutamide with standard first-line therapy in metastatic prostate cancer. *N. Engl. J. Med.* 381 (2), 121–131. doi:10.1056/NEJMoa1903835

Desai, K., McManus, J. M., and Sharifi, N. (2021). Hormonal therapy for prostate cancer. *Endocr. Rev.* 42 (3), 354–373. doi:10.1210/endrev/bnab002

Evans, S. J., Waller, P. C., and Davis, S. (2001). Use of proportional reporting ratios (PRRs) for signal generation from spontaneous adverse drug reaction reports. *Pharmacoepidemiol Drug Saf.* 10 (6), 483–486. doi:10.1002/pds.677

Fizazi, K., Shore, N., Tammela, T. L., Ulys, A., Vjaters, E., Polyakov, S., et al. (2019). Darolutamide in nonmetastatic, castration-resistant prostate cancer. *N. Engl. J. Med.* 380 (13), 1235–1246. doi:10.1056/NEJMoa1815671

Gao, S., Sun, S., Sun, T., Lu, T., Ma, Y., Che, H., et al. (2024). Chronic diseases spectrum and multimorbidity in elderly inpatients based on a 12-year epidemiological survey in China. *BMC Public Health* 24 (1), 509. doi:10.1186/s12889-024-18006-x

Gasperoni, L., Giunta, E. F., Montanari, D., Masini, C., and De Giorgi, U. (2024). New-generation androgen receptor signaling inhibitors (ARSIs) in metastatic hormone-sensitive prostate cancer (mHSPC): pharmacokinetics, drug-drug interactions (DDIs), and clinical impact. *Expert Opin. Drug Metab. Toxicol.* 20 (6), 491–502. doi:10.1080/17425255.2024.2353749

Habarugira, J. M. V., and Figueras, A. (2021). Pharmacovigilance network as an additional tool for the surveillance of antimicrobial resistance. *Pharmacoepidemiol Drug Saf.* 30 (8), 1123–1131. doi:10.1002/pds.5249

Kim, W. K., Olson, A. W., Mi, J., Wang, J., Lee, D. H., Le, V., et al. (2022). Aberrant androgen action in prostatic progenitor cells induces oncogenesis and tumor development through IGF1 and Wnt axes. *Nat. Commun.* 13 (1), 4364. doi:10.1038/s41467-022-32119-0

Mills, I. G. (2014). Maintaining and reprogramming genomic androgen receptor activity in prostate cancer. *Nat. Rev. Cancer* 14 (3), 187–198. doi:10.1038/nrc3678

Noguchi, Y., Tachi, T., and Teramachi, H. (2021). Detection algorithms and attentive points of safety signal using spontaneous reporting systems as a clinical data source. *Brief. Bioinform* 22 (6), bbab347. doi:10.1093/bib/bbab347

Podgoršek, E., Mehra, N., van Oort, I. M., Somford, D. M., Boerrigter, E., and van Erp, N. P. (2023). Clinical pharmacokinetics and pharmacodynamics of the next generation androgen receptor inhibitor-darolutamide. *Clin. Pharmacokinet.* 62 (8), 1049–1061. doi:10.1007/s40262-023-01268-w

Pyrgidis, N., Vakalopoulos, I., and Sountoulides, P. (2021). Endocrine consequences of treatment with the new androgen receptor axis-targeted agents for advanced prostate cancer. *Horm. (Athens)* 20 (1), 73–84. doi:10.1007/s42000-020-00251-5

Rachner, T. D., Tsourdi, E., and Hofbauer, L. C. (2018). Apalutamide and metastasis-free survival in prostate cancer. *N. Engl. J. Med.* 378 (26), 2541–2542. doi:10.1056/NEJMc1806189

Rothman, K. J., Lanes, S., and Sacks, S. T. (2004). The reporting odds ratio and its advantages over the proportional reporting ratio. *Pharmacoepidemiol Drug Saf.* 13 (8), 519–523. doi:10.1002/pds.1001

Scher, H. I., Fizazi, K., Saad, F., Taplin, M. E., Sternberg, C. N., Miller, K., et al. (2012). Increased survival with enzalutamide in prostate cancer after chemotherapy. *N. Engl. J. Med.* 367 (13), 1187–1197. doi:10.1056/NEJMoa1207506

Wang, Q., Cao, H., Zhang, X., Wu, H., and Tang, Z. (2023). Case report: apalutamide-induced severe lethal cutaneous adverse effects in China. *Front. Immunol.* 14, 1291564. doi:10.3389/fimmu.2023.1291564

Watson, S., Chandler, R. E., Taavola, H., Härmark, L., Grundmark, B., Zekarias, A., et al. (2018). Safety concerns reported by patients identified in a collaborative signal detection workshop using VigiBase: results and reflections from lareb and uppsala monitoring centre. *Drug Saf.* 41 (2), 203–212. doi:10.1007/s40264-017-0594-2

Werner, R., and Holterhus, P. M. (2014). Androgen action. *Endocr. Dev.* 27, 28–40. doi:10.1159/000363610

Xia, Q. D., Zhang, S. H., Zeng, N., Lu, Y. C., Qin, B. L., and Wang, S. G. (2023). Novel androgen receptor inhibitors for metastatic hormone-sensitive prostate cancer: current application and future perspectives. *Biomed. Pharmacother.* 168, 115806. doi:10.1016/j.biopha.2023.115806

frontiers | Frontiers in Oncology

TYPE Original Research
PUBLISHED 28 March 2025
DOI 10.3389/fonc.2025.1565638

OPEN ACCESS

EDITED BY
Jialin Meng,
University of Science and Technology of China, China

REVIEWED BY
Amita Joshi,
Biobay Solutions, India
Dali K.,
Haramaya University, Ethiopia

*CORRESPONDENCE
Junlan Zhu
junlanzhu@zju.edu.cn
Jian Liu
liujianzy@zju.edu.cn
Weihua Liu
45103713@qq.com

†These authors have contributed equally to this work

RECEIVED 23 January 2025
ACCEPTED 03 March 2025
PUBLISHED 28 March 2025

CITATION
Zhu J, Zheng Z, Yin Z, Ding L, Li C, Wang X, Shu P, Zhou J, Liu W and Liu J (2025) MiR-146b overexpression promotes bladder cancer cell growth via the SMAD4/C-MYC/Cyclin D1 axis. *Front. Oncol.* 15:1565638. doi: 10.3389/fonc.2025.1565638

MiR-146b overexpression promotes bladder cancer cell growth via the SMAD4/C-MYC/Cyclin D1 axis

Junlan Zhu[1*†], Zhijian Zheng[2†], Zhangya Yin[1], Linchao Ding[3], Congya Li[1], Xuyao Wang[1], Peng Shu[1], Jun Zhou[4], Weihua Liu[4*] and Jian Liu[1*]

[1]Precision Medicine Laboratory, Beilun People's Hospital, Beilun Branch of the First Affiliated Hospital, School of Medicine, Zhejiang University, Ningbo, Zhejiang, China, [2]Department of Medical Oncology, Affiliated Jinhua Hospital, Zhejiang University School of Medicine, Jinhua, China, [3]Department of Scientific Research, Affiliated Jinhua Hospital, Zhejiang University School of Medicine, Jinhua, China, [4]Department of Urology, Beilun People's Hospital, Beilun Branch of the First Affiliated Hospital, School of Medicine, Zhejiang University, Ningbo, Zhejiang, China

MiR-146b has been identified as being overexpressed in human bladder cancer (BCa) and implicated in promoting cancer cell invasion. However, its specific involvement in BCa cell growth remains unclear. In this study, we demonstrate that the downregulation of miR-146b significantly suppresses tumorigenic growth of human BCa cells both *in vitro* and *in vivo* by inducing G0/G1 cell cycle arrest. Specifically, miR-146b inhibition resulted in a significant reduction in colony formation ($p < 0.05$) and anchorage-independent growth in both UMUC3 and T24T cells, as measured by soft agar assays, with three independent replicates for each experiment. Notably, Cyclin D1 protein plays a crucial role in miR-146b-induced BCa cell proliferation, as confirmed by Western blotting ($p < 0.05$), with each experiment performed in triplicate. Mechanistic investigations reveal that miR-146b reduces mothers against decapentaplegic homolog 4 (SMAD4) mRNA stability by directly binding to its 3′ untranslated region (3′-UTR), leading to decreased SMAD4 expression. This reduction in SMAD4 levels promotes cellular myelocytomatosis (C-MYC) transcription, which in turn enhances Cyclin D1 transcription, ultimately facilitating BCa cell proliferation. The findings unveil a novel regulatory axis involving SMAD4/C-MYC/Cyclin D1 in mediating the oncogenic role of miR-146b in BCa cells. Statistical significance was determined using Student's t-test, with p-values <0.05 considered significant. Together with its previously established function in BCa invasion, the results highlight the potential for developing miR-146b-based therapeutic strategies for treating human BCa patients.

KEYWORDS

MiR-146b, bladder cancer cell growth, SMAD4, C-MYC, Cyclin D1

1 Introduction

Bladder cancer (BCa) is the most common malignant tumor of the urinary system. The mortality rate of early-stage bladder cancer is not very high, but after lymphatic metastasis, most patients survive only approximately 2 years (1). Bladder cancer can be divided into two types, non-muscle-invasive bladder cancer (NMIBC) and muscle-invasive bladder cancer (MIBC) (2). NMIBC is treated by transurethral resection of bladder cancer, followed by intravesical treatment. However, up to two-thirds of the tumor patients will experience recurrence or progress to MIBC. For MIBC patients who have received radical cystectomy or systematic chemotherapy, the 5-year survival rate is still less than 60% (3). Thus, it is urgently needed to study the new biomarkers for the early detection and targeting of bladder cancer.

MicroRNAs (miRNAs), highly conserved small non-protein coding RNAs, participate in maintaining cell homeostasis by regulating gene expression (4). Proper regulation of miRNA expression is important because miRNAs influence almost every signaling pathway involved in cell proliferation, cell motility, and cell self-renewal (5). Deregulation of miRNA expression is observed in multiple tumors by playing the role of tumor suppressors or oncogenes (6). The oncogenic role of miR-146b has been identified in various malignancies, including cervical (7), colorectal (8), and prostate cancers (9). Our previous study also demonstrated that miR-146b was upregulated in human BCa tissues and cells. MiR-146b overexpression promoted the invasive ability of BCa cells by increasing *mmp2* mRNA transcription and protein expression (10). However, the mechanism underlying the roles of miR-146b regulating bladder cancer tumorigenic growth remains poorly understood. MiR-146b was chosen for this study due to its well-established role as an oncogenic microRNA in various cancers, including bladder cancer, where it has been shown to promote tumor invasion and progression. Previous studies have highlighted the upregulation of miR-146b in human bladder cancer tissues and its involvement in enhancing the invasive properties of bladder cancer cells by regulating matrix metalloproteinases (MMPs). Additionally, miR-146b has been implicated in the regulation of several critical cancer-related pathways, making it an attractive candidate for further exploration in the context of bladder cancer. While miR-146b holds great promise as a therapeutic target in bladder cancer, it is important to consider potential off-target effects and the challenges associated with targeting miRNAs. MiRNAs often regulate multiple genes involved in various biological processes, and their inhibition or overexpression can lead to unintended effects on non-target pathways. For example, miR-146b is known to interact with several target genes involved in inflammation, immunity, and other cancer-related pathways. As a result, therapies targeting miR-146b may have broader biological consequences that need to be carefully evaluated. Additionally, the delivery of miRNA-based therapies remains a significant challenge due to the need for efficient, specific, and safe delivery systems. Furthermore, there is a risk of immune system activation or off-target gene silencing due to the broad spectrum of miRNA–target interactions. Future studies should focus on optimizing the delivery mechanisms for miRNA-based therapies, minimizing off-target effects, and developing strategies to selectively modulate miR-146b expression in cancer cells. In addition to miR-146b, several other miRNAs have been shown to target key components of the SMAD4/C-MYC/Cyclin D1 axis. For example, the miR-17-92 cluster (11), including miR-17 and miR-20a, has been implicated in modulating the TGF-β signaling pathway by targeting SMAD2, SMAD4, and TGFBR2, contributing to cancer progression, and miR-26a (12) has been identified as a tumor suppressor in multiple cancers, including hepatocellular carcinoma, by directly targeting Cyclin D2 and Cyclin E2, leading to G1 phase cell cycle arrest. These miRNAs can regulate the SMAD4/C-MYC/Cyclin D1 axis through various mechanisms, influencing cell proliferation, invasion, and metastasis. While the role of miR-146b in bladder cancer remains under investigation, other miRNAs targeting this axis further highlight the potential of targeting miRNA pathways as a therapeutic strategy in cancer treatment.

Acting as the regulatory subunit of the cyclin-dependent kinases (CDKs), Cyclin D1 is sequentially expressed and integrates extracellular signals with the cell cycle machinery to drive cell cycle G1–S phase transition and cellular proliferation (13). The Cyclin D1 gene is regarded as the oncogene, the amplifications of which have been detected in cancers of various organs. Our group found that Cyclin D1 downregulation was responsible for the isorhapontigenin-induced anticancer effect on human bladder cancer cells (14). Transcriptional coordination of cellular myelocytomatosis (C-MYC) with Cyclin D1 was reported to accelerate tumor formation and make the tumor progress into a more aggressive phenotype (15). Moreover, acting as the upstream activator of Cyclin D1, C-MYC may elicit the transformation of cancer cells. Thus, targeting C-MYC and Cyclin D1 will be of great significance for the prevention and treatment of BCa. CDKs play a crucial role in regulating the cell cycle, particularly in driving the G1 to S phase transition, which is essential for cellular proliferation. These kinases are activated by cyclins, with Cyclin D1 being a key regulator of the G1 phase. Amplifications of the Cyclin D1 gene are commonly observed in cancers, where its upregulation drives unregulated cell growth. C-MYC, a transcription factor, acts as an upstream activator of Cyclin D1, promoting tumor progression by accelerating the cell cycle and enhancing cell proliferation. MiR-146b, an oncogenic microRNA, has been implicated in various malignancies, including bladder cancer, where it promotes tumor progression by regulating genes involved in cell invasion and matrix remodeling, such as MMP2. Additionally, miR-146b may influence Cyclin D1 and C-MYC expression, further contributing to the proliferative and invasive properties of cancer cells. Together, Cyclin D1, C-MYC, and miR-146b form an interconnected regulatory network that drives the rapid proliferation and progression of bladder cancer, making them potential targets for therapeutic intervention.

The SMAD4/C-MYC/Cyclin D1 axis plays a pivotal role in regulating key aspects of cancer biology, particularly in the context of cell cycle progression, proliferation, and tumor growth. SMAD4 is a key mediator of the TGF-β signaling pathway, which is traditionally known for its tumor-suppressive functions, including

the induction of cell cycle arrest and apoptosis in normal cells. However, in cancer, the loss or downregulation of SMAD4 can disrupt these processes, leading to uncontrolled cell proliferation. This disruption often results in the activation of downstream oncogenes, including C-MYC, which promotes the transcription of Cyclin D1, a critical regulator of the G1–S phase transition. Overexpression of Cyclin D1 is commonly observed in various cancers, where it accelerates cell cycle progression and contributes to tumorigenesis. The interplay between SMAD4, C-MYC, and Cyclin D1 thus forms an essential signaling network that governs the proliferative capacity of cancer cells. In this study, we propose that miR-146b-induced repression of SMAD4 leads to enhanced C-MYC expression and subsequent upregulation of Cyclin D1, facilitating the rapid growth and metastasis of bladder cancer cells. Understanding this axis not only offers insights into the molecular mechanisms underlying cancer progression but also presents potential therapeutic opportunities for targeting this pathway in cancer treatment.

BCa remains one of the most prevalent malignancies of the urinary system, characterized by a high recurrence rate and poor prognosis, particularly in muscle-invasive cases. Despite advancements in diagnostic and therapeutic strategies, the molecular mechanisms driving BCa progression remain insufficiently understood. MiRNAs, small non-coding RNAs, play a crucial role in regulating gene expression and are involved in various cellular processes including cell proliferation, invasion, and metastasis. MiR-146b has been identified as an oncogene in several cancers, including bladder cancer, where it is implicated in promoting cell invasion through the regulation of matrix metalloproteinases. However, its specific role in the regulation of BCa cell growth and tumorigenesis remains unclear. In this context, we explore the significance and therapeutic potential of miR-146b in bladder cancer. We will investigate the oncogenic role and the molecular mechanisms of miR-146b on human BCa cell proliferation and anchorage-independent growth. The objective of this study was to investigate the oncogenic role of miR-146b in bladder cancer cell growth and to explore the underlying molecular mechanisms. Specifically, we aimed to determine how miR-146b influences key cell cycle regulators, such as Cyclin D1, and the associated molecular pathways involving SMAD4, C-MYC, and Cyclin D1. By understanding these mechanisms, we seek to provide new insights into the regulatory networks that drive BCa cell proliferation, with the ultimate goal of identifying miR-146b as a potential therapeutic target for bladder cancer treatment.

2 Materials and methods

2.1 Plasmids, antibodies, and reagents

The aim of the experiment was to investigate the role of miR-146b inhibitor and its nonsense control in regulating various transcription factors and signaling pathways, particularly Cyclin D1, c-Myc, and SMAD4. The lentiviral constructs of miR-146b inhibitor and its nonsense control were constructed by GenePharma (Shanghai, China). The plasmid of the human Cyclin D1 promoter (from −1,407 to −167)-driven luciferase reporter was constructed with *Xho*I and *Hin*dIII using genomic DNA purified from UMUC3 cells based on the National Center for Biotechnology Information (NCBI) database. The plasmid of the human c-myc promoter (from −1,225 to −14)-driven luciferase reporter was constructed with *Xho*I and *Hin*dIII using genomic DNA purified from UMUC3 cells based on the NCBI database. The human mothers against decapentaplegic homolog 4 (smad4) 3′ untranslated region (3′-UTR) was cloned into the pMIR-report luciferase vector through the *Spe*I and *Hin*dIII sites. Smad4 3′-UTR point mutation was amplified from the WT template by overlap PCR using the following primers: forward, 5′-TTTAAAGGCAGAGAAGCCATCAAAGTTAATTCA-3′; reverse, 5′-TGAATTAACTTTGATGGCTTCTCTGCCTTTAAA-3′. The HA-tagged Cyclin D1 constitutively expressed plasmid and pT3EF1a-C-MYC plasmid were obtained from Addgene (Cambridge, MA, USA). The constructs of short hairpin RNA specifically targeting SMAD4 (shSMAD4) were purchased from Santa Cruz Biotechnology (Santa Cruz, CA, USA). All plasmids were prepared by the Plasmid Preparation/Extraction Maxi Kit from QIAGEN (Valencia, CA, USA). The antibodies specific against CDK4, CDK6, Cyclin D1, Cyclin E1, p27, HA, c-Jun, C-MYC, Elk1, ETS1, Sp1, SMAD4, GAPDH, and β-actin were bought from Cell Signaling Technology (Beverly, MA, USA). Actinomycin D (Act D) was bought from Calbiochem (Billerica, MA, USA).

2.2 Cell culture and transfection

The purpose of this experiment was to investigate the effects of specific gene modifications on human BCa cell lines T24T and UMUC3. The human BCa cell lines T24T and UMUC3 were used in the study. All cancer cell lines were subjected to DNA tests and authenticated before use for the studies. UMUC3 cells were maintained at 37°C in a 5% CO_2 incubator in Dulbecco's modified Eagle's medium (DMEM) (Gibco, Grand Island, NY, USA) supplemented with 10% fetal bovine serum (FBS) (Gibco, Grand Island, NY, USA). T24T cells were cultured with a 1:1 mixture of DMEM/Ham's F12 medium (Gibco, Grand Island, NY, USA) supplemented with 5% FBS. Stable transfections were performed with constructs using PolyJet DNA *In Vitro* Transfection Reagent (SignaGen Laboratories, Gaithersburg, MD, USA) according to the manufacturer's instructions, and stable transfectants were selected with puromycin (0.2–0.3 mg/mL) or hygromycin B (200–400 mg/mL) for 3 or 4 weeks according to the different antibiotic resistance plasmids transfected (16, 17). Although the cell lines and animal models used in this study are widely accepted as representative models for human bladder cancer, it is important to acknowledge their limitations. The UMUC3 and T24T human bladder cancer cell lines, while commonly used in bladder cancer research, may not fully recapitulate the heterogeneity of human tumors, particularly in terms of the tumor microenvironment and metastasis. Additionally, these cell lines are derived from advanced stages of bladder cancer, which

may not completely represent early-stage disease or the full spectrum of bladder cancer subtypes.

2.3 Protein expression analysis of BCa cells and transfectants

The aim of this experiment was to analyze the protein expression of specific targets in BCa cells and transfectants using Western blotting analysis. As previously described (10), BCa cells and the transfectants were seeded in six-well plates and cultured in a normal culture medium until 70%–80% confluence. The whole cell extracts were prepared and were then subjected to Western blotting analysis. The images were acquired by scanning with ChemiDoc™ MP Imaging System from Bio-Rad (Hercules, CA, USA).

2.4 Analysis of miR-146b and target gene expression in cultured cells

The aim of this experiment was to measure the expression levels of specific genes and miRNAs in BCa cells and transfectants using quantitative real-time PCR (qRT-PCR). First, the RNA was extracted from the cultured cells using TRIzol reagent (Invitrogen, Carlsbad, CA, USA). Reverse transcriptase was used to produce the first-strand complementary DNA (Aidlab, Beijing, China) according to the manufacturer's instructions. MiRNA real-time PCR Assay kit was used to detect the expression level of miR-146b (Aidlab, China). Furthermore, U6 was chosen to be the internal control. The primers used in this study were as follows: miR-146b (forward, 5′-TGA CCC ATC CTG GGC CTC AA-3′; reverse, 5′-CCA GTG GGC AAG ATG TGG GCC-3′), U6 (forward, 5′-CTC GCT TCG GCA GCA CA-3′; reverse, 5′-AAC GCT TCA CGA ATT TGC GT-3′), human Cyclin D1 (forward, 5′-GAGGTCTGCGAGGAACAGAAGTG-3′; reverse, 5′-GAGCGGGGATTGGAAATGAACTTC-3′), human C-MYC (forward, 5′-AAC ACA CAA CGT CTT GGA GC-3′; reverse, 5′-CCT TAC GCA CAA GAG TTC CG-3′), human SMAD4 (forward, 5′-ACA AGT AAT GAT GCC TGT CTG A-3′; reverse, 5′-CTC CCA TCC AAT GTT CTC TGT A-3′), and human GAPDH (forward, 5′-GAT GAT CTT GAG GCT GTT GTC-3′; reverse, 5′-CAG GGC TGC TTT TAA CTC TG-3′). The qRT-PCR analysis was carried out using the SYBR Green PCR kit (Qiagen, Santa Clarita, CA, USA) and the 7900HT Fast Real-time PCR system (Applied Biosystems, Carlsbad, CA, USA). The ΔΔCT value was used to calculate the relative expression of the indicated mRNA using gapdh as an endogenous control.

2.5 Luciferase assay

The aim of this experiment was to evaluate the luciferase activity of human Cyclin D1, c-myc promoters, and SMAD4 3′-UTR in BCa cells with different treatments. For the determination of human cyclin d1 promoter-driven luciferase activity and human c-myc promoter-driven luciferase activity, the indicated cells were each transiently co-transfected with pRL-TK, together with the related promoter-driven luciferase reporter. Twenty-four hours after transfection, luciferase activity was determined using the Luciferase Assay System Kit (Promega, Madison, WI, USA). For the determination of smad4 mRNA 3′-UTR activity, UMUC3 (nonsense) and UMUC3 (miR-146b inhibitor) cells were transiently transfected with pRL-TK together with smad4 mRNA 3′-UTR luciferase reporter. Twenty-four hours after transfection, luciferase activity was determined using the Luciferase Assay System Kit (Promega, Madison, WI, USA). The results were normalized by internal TK signal. All experiments were conducted in triplicate, and the results were expressed as mean ± standard error.

2.6 ChIP assay

The aim of this experiment was to investigate the binding of specific transcription factors to the human c-myc promoter using chromatin immunoprecipitation (ChIP) assay. ChIP assay was carried out as described in previous publications using reagents that were purchased from Millipore Technologies (Billerica, MA, USA) (18). To specifically amplify the region containing the putative responsive elements on the human c-myc promoter, PCR was performed with the following pair of primers: forward, 5′-GAG AAA TTG GGA ACT CCG TG-3′; reverse, 5′-CAA AGC AGC AGA TAC CGC CC-3′. The PCR products were separated on 2% agarose gels and stained with ethidium bromide; the images were then scanned using a UV light.

2.7 Cell proliferation analysis

The aim of this experiment was to assess the cell viability of BCa cells under different conditions using the CellTiter-Glo Luminescent Cell Viability Assay. Cell viability was determined by utilizing the CellTiter-Glo Luminescent Cell Viability Assay Kit (Promega, Madison, WI, USA) according to the manufacturer's instructions. Briefly, cells were plated in 96-well plates at a density of 5,000 cells per well and allowed to adhere overnight. The cell culture medium was replaced with 0.1% FBS DMEM, cultured for 12 h, then replaced with a normal medium, and cultured for another 1, 2, 3, or 4 days, and then 50 μL CellTiter-Glo assay reagent was added to each well. The contents were mixed on an orbital shaker for 2 minutes to induce cell lysis and then incubated at room temperature for 10 minutes to stabilize the luminescent signal. Results were read on a microplate luminometer LB 96V (Berthold GmbH & Co. KG, Bad Wildbad, Germany). Cell viability (%) was defined as the relative absorbance of treated samples versus that of the untreated control. All experiments were performed in 96-well plates for each experiment and repeated at least three times.

2.8 Cell cycle analysis

The aim of this experiment was to analyze the cell cycle distribution of BCa cells under different conditions using flow

cytometry with the BD Cycletest™ Plus DNA Reagent kit. The indicated cells (2×10^5) were cultured in each well of 6-well plates to 70%–80% confluence with normal culture medium. Following serum starvation for 12 h, the medium was replaced with 10% FBS DMEM for another 12 h. Then, the cells were treated with the BD Cycletest™ Plus DNA Reagent kit to treat the cultured cells (BD Biosciences, San Jose, CA, USA). First, the cell debris and fixation artifacts were gated out. Subsequently, the cell populations were quantified at the G0/G1, S, and G2/M phases using the ModFit software.

2.9 Anchorage-independent growth assay

The aim of this experiment was to assess the anchorage-independent growth of BCa cells by performing a soft agar colony formation assay. The 1×10^4 cells in 10% FBS Basal Medium Eagle (BME) containing 0.33% soft agar were seeded over the basal layer containing 0.5% agar containing 10% FBS BME in each well of 6-well plates. The plates were incubated in a 5% CO_2 incubator at 37°C for 3 weeks. Colonies were captured under a microscope, and only colonies with over 32 cells were counted. The results were presented as mean ± SD obtained from three independent experiments.

2.10 Xenograft model in nude mice *in vivo*

The aim of this experiment was to evaluate the *in vivo* tumorigenic potential of UMUC3 cells with miR-146b inhibitor or nonsense control in BALB/c athymic nude mice. BALB/c athymic nude mice (3–4 weeks old) were purchased from Vital River (Beijing, China). After 2-week acclimatization, the mice were randomly allocated into two groups (five in each group) and subcutaneously injected in the right side (lower back) with 0.1 mL UMUC3 (miR-146b inhibitor) and UMUC3 (nonsense) cells [in each case, 2×10^6 cells suspended in 100 µL phosphate-buffered saline (PBS)]. The sample size for the *in vivo* xenograft experiments was determined based on power calculations to ensure adequate statistical power for detecting significant differences in tumor growth between the experimental and control groups. A total of five mice per group (n = 5) were included, which is consistent with standard practices in similar studies involving xenograft tumor models. This sample size was selected to balance statistical power with ethical considerations and animal welfare. Tumor volumes and weights were measured weekly, and differences between groups were analyzed for statistical significance. After 4–5 weeks, the mice were sacrificed, and any tumor present was surgically removed, imaged, and weighed. The study for the animals was approved by the Experimental Animal Welfare and Ethics Committee of Affiliated Jinhua Hospital, Zhejiang University School of Medicine (Approval No. AL-JHYY202345). While athymic nude mice are useful for xenograft studies, they lack a fully functional immune system, which limits the ability to assess the role of immune responses in cancer progression and treatment. Future studies using primary bladder cancer samples, patient-derived xenografts (PDXs), or genetically engineered mouse models (GEMMs) could provide more accurate representations of tumor biology and therapeutic responses. Despite these limitations, the models used in this study are well-established tools that provide valuable insights into the molecular mechanisms driving bladder cancer growth and progression.

2.11 Statistical analysis

Statistical analysis was performed using the Prism 5.0 software (GraphPad Software, San Diego, CA, USA). All data were presented as the means of triplicate assays ± SD. Student's t-test was employed to determine the significance of differences between various groups. The differences were considered significant at $p < 0.05$.

3 Result

3.1 MiR-146b overexpression promoted human BCa tumorigenic growth both *in vitro* and *in vivo*

Our recent study has discovered that miR-146b is highly expressed in human BCa tissues and cells, which plays a promotion role in BCa cell invasion by upregulating MMP2 protein expression (10). To evaluate the biological role of miR-146b in regulating BCa cell proliferation and tumorigenic growth, the inhibitor constructs of miR-146b were stably transfected into UMUC3 and T24T human BCa cells ($p < 0.05$), respectively (Figures 1A, B). Colony formation assay results showed that miR-146b inhibition decreased the anchorage-independent growth in both T24T and UMUC3 cells (Figures 1C–F).

Moreover, the inhibition of miR-146b significantly reduced the monolayer growth of UMUC3 and T24T, accompanied by inducing G0/G1 cell cycle arrest in UMUC3 cells (Figures 1G, H). To further determine the potent oncogenic activity of miR-146b *in vivo*, UMUC3 (miR-146b inhibitor) and UMUC3 (nonsense) cells were subcutaneously injected into nude mice. Unexpectedly, the inhibition of miR-146b dramatically decreased UMUC3 xenograft tumor growth and reduced tumor burden (weight) as compared to the UMUC3 (nonsense) group ($p < 0.01$, n = 5) (Figures 1I–K). In general, a novel positive regulatory effect of miR-146b on human BCa cell growth has been discovered.

3.2 Cyclin D1 protein mediated miR-146b-induced human BCa cell proliferation

In order to elucidate the mechanism of miR-146b involved in the regulation of G0/G1 cell cycle transition, we first performed Western blotting to detect the potential G0/G1 transition regulators. As the result showed, the knockdown of miR-146b exerted no remarkable effect on CDK4, CDK6, and p27 protein

10.3389/fonc.2025.1565638

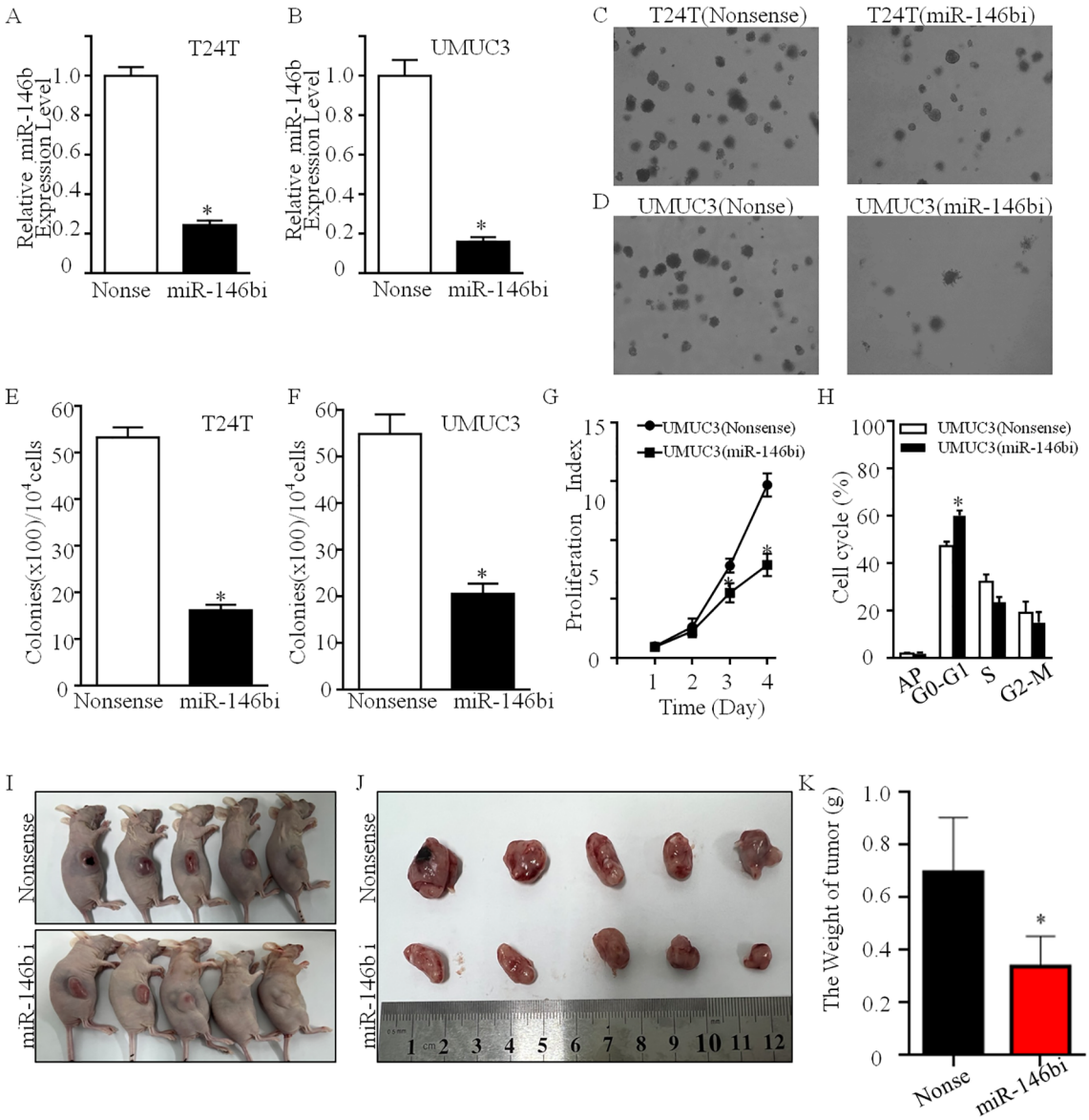

FIGURE 1
MiR-146b overexpression was crucial for anchorage-independent growth of human BCa cells. **(A, B)** MiR-146b inhibitor and its nonsense control plasmids were stably transfected into T24T **(A)** and UMUC3 **(B)** cells, and stable transfectants were identified by real-time PCR. Bars represent the mean ± SD, Student's *t*-test was used to determine the p-value, and the asterisk (*) indicates a significant decrease relative to nonsense control cells (*p < 0.05). **(C, D)** A soft agar assay was used to determine the effect of miR-3687 down-expression on UMUC3 and T24T anchorage-independent growth, and the images were captured under microscopy. **(E, F)** The number of colonies was counted with more than 32 cells of each colony, and the results were presented as colonies per 10,000 cells, and the bars show mean ± SD from three independent experiments. The asterisk (*) indicates a significant decrease in comparison to that of nonsense control transfectants (*p < 0.05). **(G)** UMUC3 transfectants were plated in 96-well plates at a density of 5,000 cells per well. The cell culture medium was then replaced with 0.1% FBS DMEM and cultured for 12 h The cells were replaced with normal medium and cultured for another 1, 2, 3, or 4 days. Subsequently, an ATP activity assay was performed using protocol described in the section "Materials and Methods". The double asterisk (*) indicates significant decrease from nonsense control (p < 0.05). **(H)** The indicated cells (2×10^5) were seeded into a 6-well plate and cultured overnight. Following synchronization in 0.1% FBS for 12 h, the medium was replaced with 10% FBS DMEM for another 12 h, and the cells were then stained with propidium iodide for cell cycle analysis as described in the section of "Materials and Methods". The results represented one of three independent experiments. BALB/c athymic nude mice were subcutaneously injected with UMUC3 (miR-146bi) cells or their nonsense control transfectants. The mice were euthanized after 4–5 weeks, and xenograft tumors in the mice injected with the indicated UMUC3 transfectants were removed, imaged, and weighed **(I, J)**. The results of the tumor weight in the mice injected with the UMUC3 transfectants **(K)** were presented as means ± SD. *Significant decrease relative to nonsense control cells (p < 0.05). BCa, bladder cancer; FBS, fetal bovine serum; DMEM, Dulbecco's modified Eagle's medium.

expression, while specifically decreasing Cyclin D1 protein abundance in both UMUC3 and T24T cells (Figures 2A, B). Therefore, we supposed that Cyclin D1 may be the miR-146b downstream effector involved in inducing G0/G1 phase arrest and promoting human BCa cell proliferation. To test this notion, we stably transfected HA-Cyclin D1 into UMUC3 (miR-146bi) cells (Figure 2B). The ectopic expression of HA-Cyclin D1 reversed the reduction of miR-146bi on anchorage-independent growth and

10.3389/fonc.2025.1565638

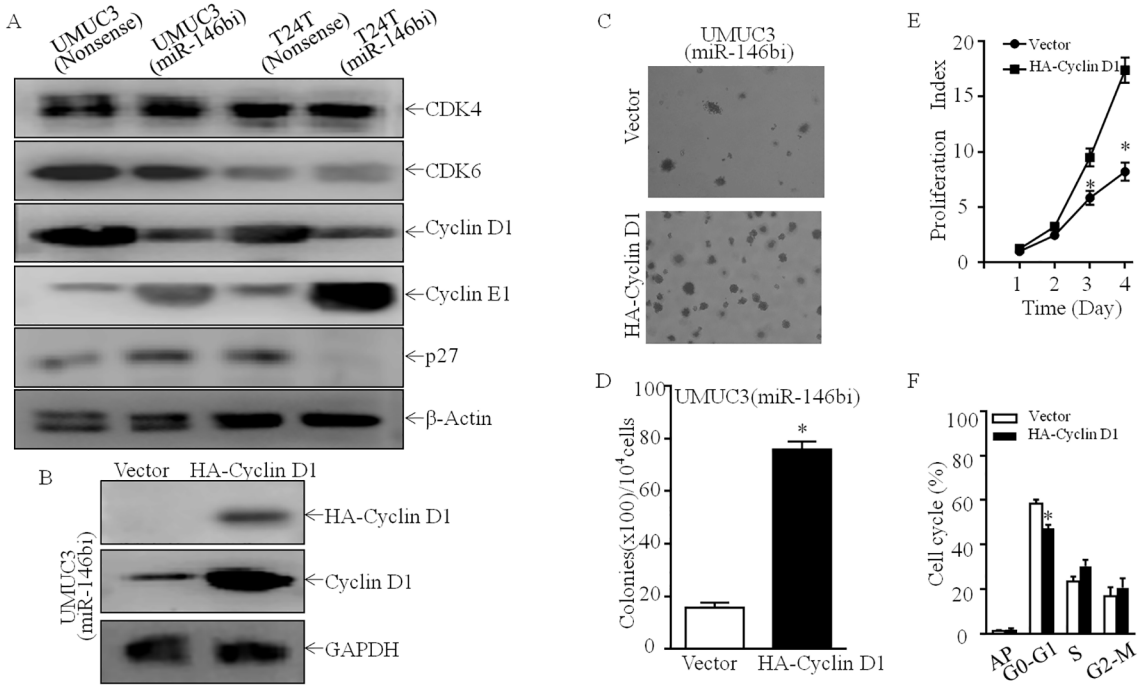

FIGURE 2
Cyclin D1 upregulation mediates miR-146b promotion of human BCa anchorage-independent growth. **(A)** The indicated cell extracts were subjected to Western blotting to determine the expression of CDK4, CDK6, Cyclin D1, Cyclin E1, and p27. β-Actin was used as a protein loading control. **(B)** HA-tagged Cyclin D1 constructs were stably transfected into UMUC3 (miR-146bi) cells. The overexpressed efficiency of Cyclin D1 protein was assessed by Western blotting. **(C, D)** A soft agar assay was used to determine the effect of Cyclin D1 overexpression on anchorage-independent growth of UMUC3 (miR-146bi); the number of colonies was counted under microscopy **(C)**, and the results were presented as colonies per 10,000 cells **(D)**. **(E)** The effect of Cyclin D1 on monolayer proliferation rates of UMUC3 (miR-146bi) cells was evaluated by ATP assay. Results are means ± SD; *significant change relative to vector control cells ($p < 0.05$). **(F)** The indicated cells were seeded in 6-well plates and cultured to 70%–80% confluence. After synchronization, the cells were cultured in complete medium for another 24 h and then subjected to cell cycle analysis (n = 3). BCa, bladder cancer.

monolayer growth, as compared with those observed in their scramble nonsense transfectants (Figures 2C–E).

Furthermore, the ectopic expression of HA-Cyclin D1 in UMUC3 (miR-146bi) cells also inhibited G0/G1 cell cycle arrest, and the results of flow cytometry also indicated that UMUC3 (miR-146bi/HA-Cyclin D1) exhibited a reverse effect of miR-146bi on inducing G0/G1 cell cycle arrest (Figure 2F). In conclusion, the results indicated that Cyclin D1 is a critical downstream effector for miR-146b mediating bladder cancer cell growth.

3.3 MiR-146b increased Cyclin D1 transcription by promoting C-MYC protein expression

To ascertain the mechanism of miR-146b upregulating Cyclin D1 expression, the mRNA expression of *cyclin* D1 was first assessed. As shown in Figure 3A, *cyclin d1* mRNA expression was profoundly downregulated in UMUC3 (miR-146bi) transfectant cells in comparison to UMUC3 (nonsense) cells. Subsequently, it was found that the Cyclin D1 promoter-driven luciferase reporter transcription activity in UMUC3 (miR-146bi) cells was much lower than in UMUC3 (nonsense) cells (Figure 3B), indicating the possibility of miR-146b increasing the transcription of *cyclin d1* mRNA. To verify this, we tried to conduct a bioinformatics analysis of the −1,407 to −167 region of the Cyclin D1 promoter sequence using the TFANSFAC Transcription Factor Binding Sites Software (Biological Database, Wolfenbüttel, Germany). The results showed that putative DNA-binding sites of Elk1, AP1, C-MYC, and Sp1 were involved in the Cyclin D1 promoter region (Figure 3C). Consequently, we tried to determine the effect of miR-146b inhibitor on the protein expression of the indicated transcription factors.

As shown in Figure 3D, downregulation of C-MYC protein expression was discovered in UMUC3 (miR-146bi) cells, as compared to UMUC3 (nonsense) cells with no marked influence on Elk1, c-Jun, or Sp1 protein expression. Our previous study has shown that C-MYC is a promotive transcription factor of Cyclin D1 by directly binding to its promoter region, which plays a critical role in human bladder cancer cell tumorigenicity (19). Thus, we suggested that C-MYC may play a role in miR-146bi inhibition of Cyclin D1 transcription. To verify that C-MYC was critical for miR-146b promotion of human BCa cell proliferation, we transfected UMUC3 (miR-146bi) cells with the C-MYC-P3EF1a plasmid (Figure 4A). Consistently, the ectopic expression of C-MYC increased the mRNA expression and promoter activity of Cyclin D1, which remarkably increased the anchorage-independent growth ability of UMUC3 (miR-146bi/C-MYC) transfectants (Figures 4B–E). In conclusion, the above results strongly

10.3389/fonc.2025.1565638

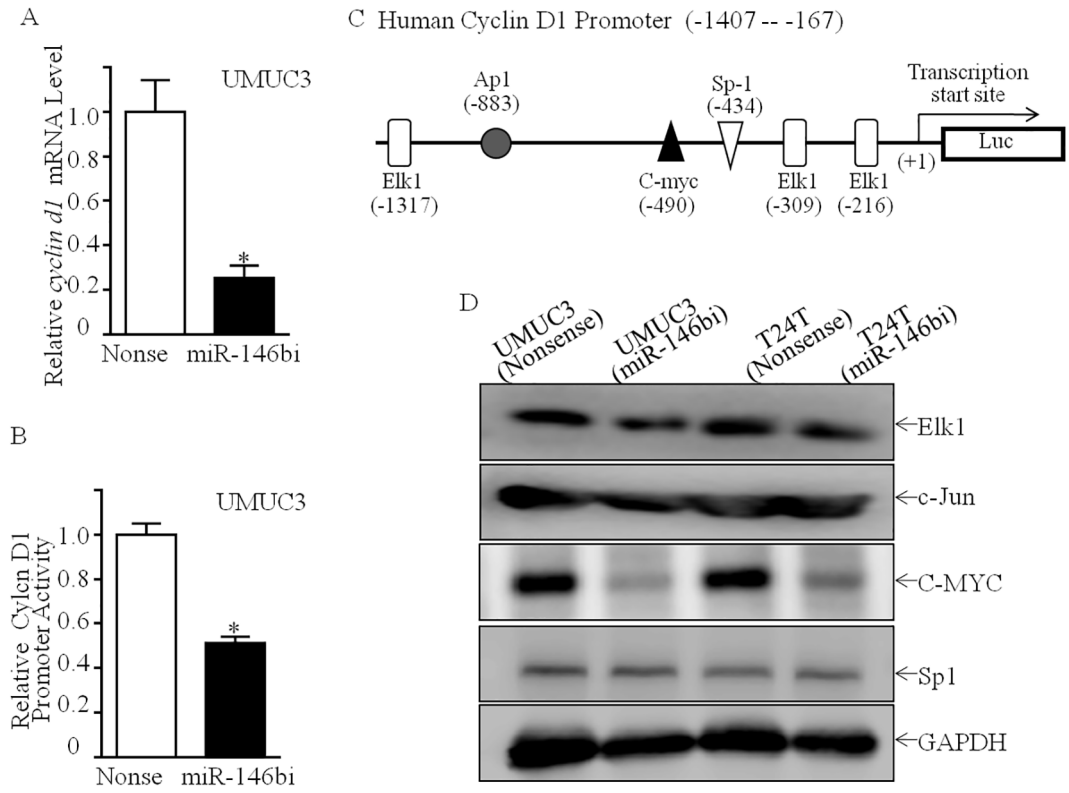

FIGURE 3
Inhibition of miR-146b attenuated Cyclin D1 transcription with downregulation of C-MYC protein. **(A)** Relative *cyclin d1* mRNA expression detected in UMUC3 (miR-146bi) and UMUC3 (nonsense) cells. **(B)** UMUC3 (nonsense) versus UMUC3 (miR-146bi) cells were transiently transfected with a *cyclin d1* promoter-driven luciferase reporter together with pRL-TK. Transfectants were seeded into 96-well plates to determine *cyclin d1* promoter transcriptional activity. pRL-TK was used as the internal control to normalize transfection efficiency. Bars indicate means ± SD from three replicate assays. **(C)** Potential transcriptional factor binding sites in human cyclin d1 promoter region were analyzed via the TRANSFAC 8.3 engine online. **(D)** Cell lysates from indicated cells were evaluated for Elk1, c-Jun, C-MYC, and Sp1 protein expression. GAPDH served as the loading control. The asterisk (*) indicates a statistically significant difference compared to the control (*p < 0.05).

indicated that C-MYC is the key factor mediating miR-146b, increasing BCa growth by promoting Cyclin D1 transcription.

3.4 SMAD4 was required for miR-146b promotion of C-MYC at the transcriptional level

In order to study the molecular mechanism of miR-146b upregulating C-MYC protein expression, we first tested the effect of miR-146b on *c-myc* mRNA level. We found that *c-myc* mRNA was significantly decreased in UMUC3 (miR-146bi) cells (Figure 5A). Furthermore, *c-myc* promoter-driven luciferase reporter activity was also inhibited in UMUC3 (miR-146bi) cells as compared with its scramble nonsense transfectants (Figure 5B), suggesting that the indicated transcription factor(s) involved in the −1,225 to −14 region of the promoter participated in miR-146b promoting *c-myc* promoter transcription. Therefore, we performed bioinformatics analysis to figure out the potential transcriptional factors (Figure 5C) and then detected their protein expression (Ap1, Elk1, Ets1, Smad4, and Sp1). The results indicated that only SMAD4 showed high expression, while others exhibited no remarkable differences (Figures 3D, 5D, E), revealing that SMAD4 may be critical for regulating C-MYC expression. Thus, we knocked down SMAD4 in UMUC3 (miR-146bi) cells using shRNAs specifically targeting human SMAD4, and UMUC3 (miR-146bi/shSMAD4#1), UMUC3 (miR-146bi/shSMAD4#2), and their scramble transfectant UMUC3 (miR-146bi/nonsense) were established (Figure 6A). As expected, the knockdown of SMAD4 increased the protein expression of C-MYC and Cyclin D1 (Figure 6A), *c-myc* mRNA expression (Figure 6B), and *c-myc* promoter activity (Figure 6C), as well as BCa cell growth (Figures 6D, E), demonstrating that SMAD4 was indeed an intermediate regulator linking miR-146b to C-MYC and responsible for BCa tumorigenic growth. In general, miR-146 inhibits SMAD4 expression, consequently increasing *c-myc* transcription, further promoting *cyclin d1* mRNA transcription and protein expression, and finally elevating BCa cell anchorage-independent growth.

3.5 MiR-146b decreased *smad4* mRNA stability by directly targeting its 3′-UTR

To clarify the molecular mechanism of miR-146b inhibiting SMAD4 expression, we first detected *smad4* mRNA abundance in

10.3389/fonc.2025.1565638

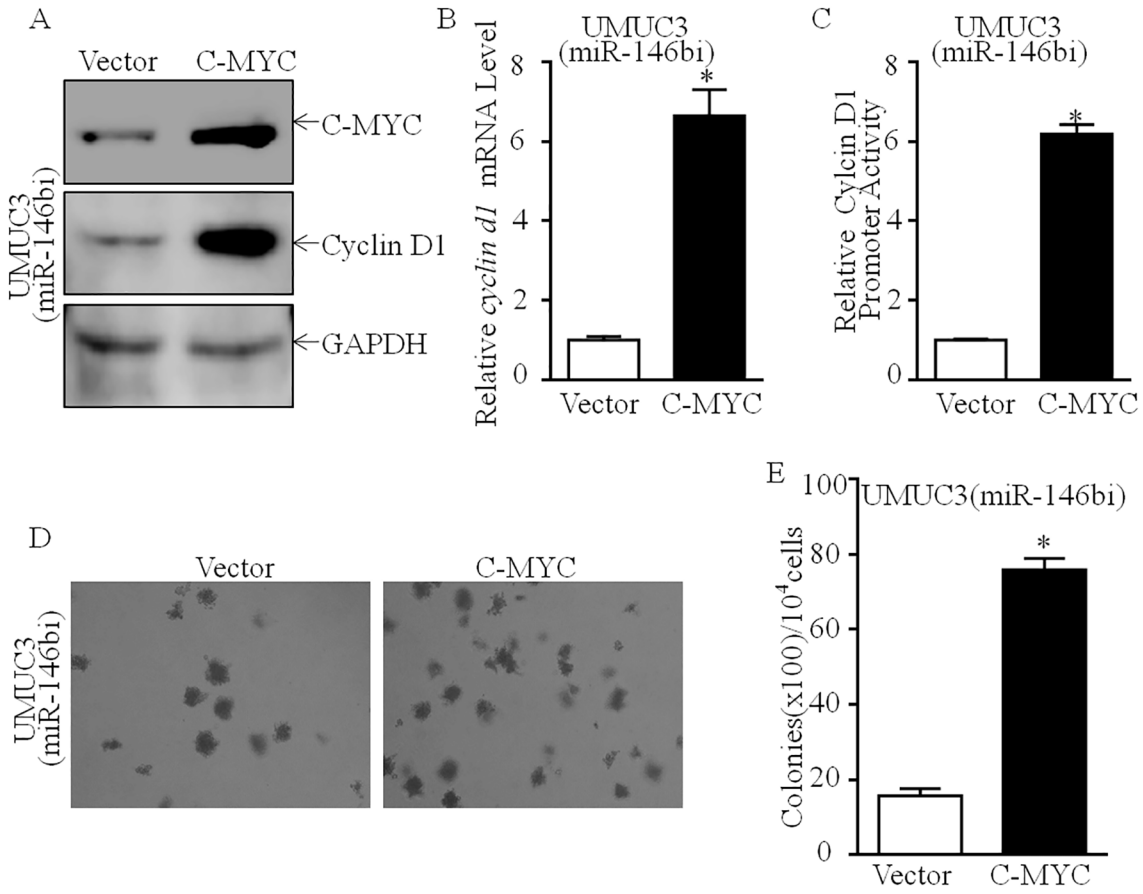

FIGURE 4
Effects of C-MYC on promotion of cyclin d1 transcription and human BCa anchorage-independent growth. **(A)** C-MYC overexpressed constructs were stably transfected into UMUC3 (miR-146bi) cells. The C-MYC overexpressed efficiency and its downstream Cyclin D1 expression were assessed by Western blotting. GAPDH was used as a protein loading control. **(B)** Relative *cyclin d1* mRNA expression detected in UMUC3 (miR-146bi/Vector) and UMUC3 (miR-146bi/C-MYC) cells. **(C)** UMUC3 (miR-146bi/Vector) and UMUC3 (miR-146bi/C-MYC) cells were transiently transfected with a *cyclin d1* promoter-driven luciferase reporter together with pRL-TK. Transfectants were seeded into 96-well plates to determine *cyclin d1* promoter transcriptional activity. pRL-TK was used as the internal control to normalize transfection efficiency. Bars indicate means ± SD from three replicate assays. **(D)** The stable transfectants as indicated were subjected to anchorage-independent soft agar growth assay. Representative images of colonies were photographed under an Olympus DP71. **(E)** The number of colonies was counted with more than 32 cells of each colony, and the results were presented as colonies per 10,000 cells. The bars show mean ± SD from three independent experiments, and the asterisk (*) indicates a significant increase in comparison to vector transfectants as indicated (*$p < 0.05$). BCa, bladder cancer.

UMUC3 cells. As shown in Figure 7A, miR-146b inhibition elevated *smad4* mRNA expression. Therefore, we supposed that miR-146b destabilized *smad4* mRNA. The result exhibited that miR-146b inhibition delayed the *smad4* mRNA degradation rates (Figure 7B). MiRNAs function post-transcriptionally usually by base-pairing to target mRNA 3′-UTR to inhibit protein synthesis (20). Thus, we next detected the 3′-UTR activity of *smad4* mRNA between UMUC3 (miR-146bi) and UMUC3 (nonsense) cells. As shown in Figure 7C, miR-146b inhibition improved the *smad4* mRNA 3′-UTR activity as compared to the control cells, suggesting that miR-146b may be involved in this regulation. Thereby, we performed bioinformatics research on the potential targeted miRNA of smad4 mRNA 3′-UTR using TargetScan (v7.0; targetscan.org) (21). The results exhibited that there were multiple putative miRNA binding sites in *smad4* mRNA 3′-UTR, surprisingly including the binding sites for miR-146b (Figure 7D).

To ascertain whether miR-146b could directly bind to *smad4* mRNA 3′-UTR to stabilize its mRNA, as shown in Figure 7D, we constructed the plasmid that miR-146b binding site in *smad4* mRNA 3′-UTR-luciferase reporter was mutated. Then, we co-transfected the wild-type or the mutation plasmids with pRL-TK into either UMUC3 (nonsense) or UMUC3(miR-146bi) cells transiently. We found that the luciferase activity of wild-type *smad4* mRNA 3′-UTR in UMUC3 (miR-146bi) cells was much higher than in UMUC3 (nonsense), whereas the mutation decreased the effect of miR-146b inhibition (Figure 7E), revealing that the direct binding of miR-146b to *smad4* mRNA 3′-UTR is critical for miR-146b stabilization of *smad4* mRNA. In summary, our results revealed that overexpressed miR-146b attenuated *smad4* mRNA expression by directly binding to its 3′-UTR, therefore promoting *c-myc* mRNA transcription, in turn increasing *cyclin D1* mRNA transcription and protein expression and finally

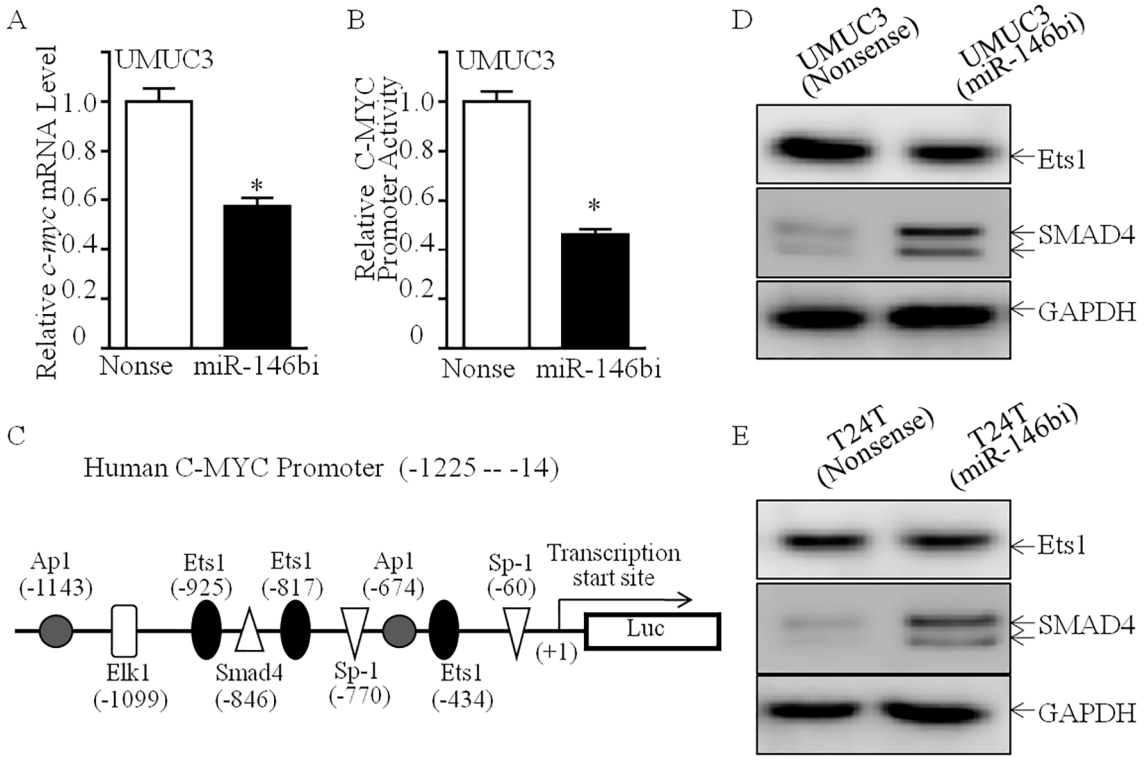

FIGURE 5
MiR-146b overexpression inhibited *c-myc* mRNA transcription in human BCa cells. **(A)** Relative *c-myc* mRNA expression detected in UMUC3 (miR-146bi) and UMUC3 (nonsense) cells. **(B)** UMUC3 (nonsense) versus UMUC3 (miR-146bi) cells were transiently transfected with a *c-myc* promoter-driven luciferase reporter together with pRL-TK. Transfectants were seeded into 96-well plates to determine *c-myc* promoter transcriptional activity. pRL-TK was used as the internal control to normalize transfection efficiency. Bars indicate means ± SD from three replicate assays. **(C)** Potential transcriptional factor binding sites in human *c-myc* promoter region were analyzed via the TRANSFAC 8.3 engine online. **(D, E)** Cell lysates from indicated cells were evaluated for Ets1 and SMAD4 protein expression. GAPDH served as the loading control. BCa, bladder cancer. The asterisk (*) indicates a statistically significant difference compared to the control (*$p < 0.05$).

promoting BCa cell anchorage-independent growth as shown in Figure 7F.

4 Discussion

In recent years, accumulating evidence demonstrated microRNAs as negative regulators of gene expression by directly binding with mRNA sequences to repress transcript destabilization or translation (22, 23). A growing number of studies have shown that the dysregulation of miRNAs leads to the progression of multiple cancers, including bladder cancer (24). Nevertheless, the aberrant expression of specific miRNAs exerting the actual functions on proliferation, metastasis, and progression of BCa is still unclear. MiR-146b is a member of the miR-146 family, which is encoded by independent genes located on human chromosomes 10 (25). Several studies have reported that miR-146b is widely upregulated and plays an important oncogenic role in multiple cancers, such as cervical cancer (7), colon cancer (8), and thyroid cancer (26). Our previous data illustrate that the drastic upregulation of miR-146b in BCa tissues and cell lines was discovered as expected, as compared to its adjacent normal urothelial tissues and the normal urothelial cell line, respectively. Moreover, miR-146b overexpression promotes the invasion ability of human bladder cancer by increasing MMP2 protein expression (10). However, its role in the malignant growth and proliferation of BCa has not been fully studied. In this research, the loss-of-function study demonstrated that the inhibition of miR-146b could repress the proliferation and anchorage-independent growth of BCa cells, which suggested miR-146b as an oncogene in BCa. While our data suggest that miR-146b directly regulates the SMAD4/C-MYC/Cyclin D1 axis, it is important to note that miR-146b may not be the only regulator of this pathway. Other miRNAs and transcription factors could also influence the expression of SMAD4, C-MYC, and Cyclin D1, further modulating bladder cancer cell growth and proliferation. For instance, miRNAs such as the miR-17-92 cluster and miR-26a have been implicated in regulating components of the SMAD4/C-MYC/Cyclin D1 axis in other cancer types. Future studies focusing on the combined effects of miR-146b and other regulatory elements may offer a more comprehensive understanding of the intricate regulatory networks governing bladder cancer progression.

Our further study indicated that the G0/G1 phase arrest could be responsible for miR-146b inhibition inducing cell proliferation

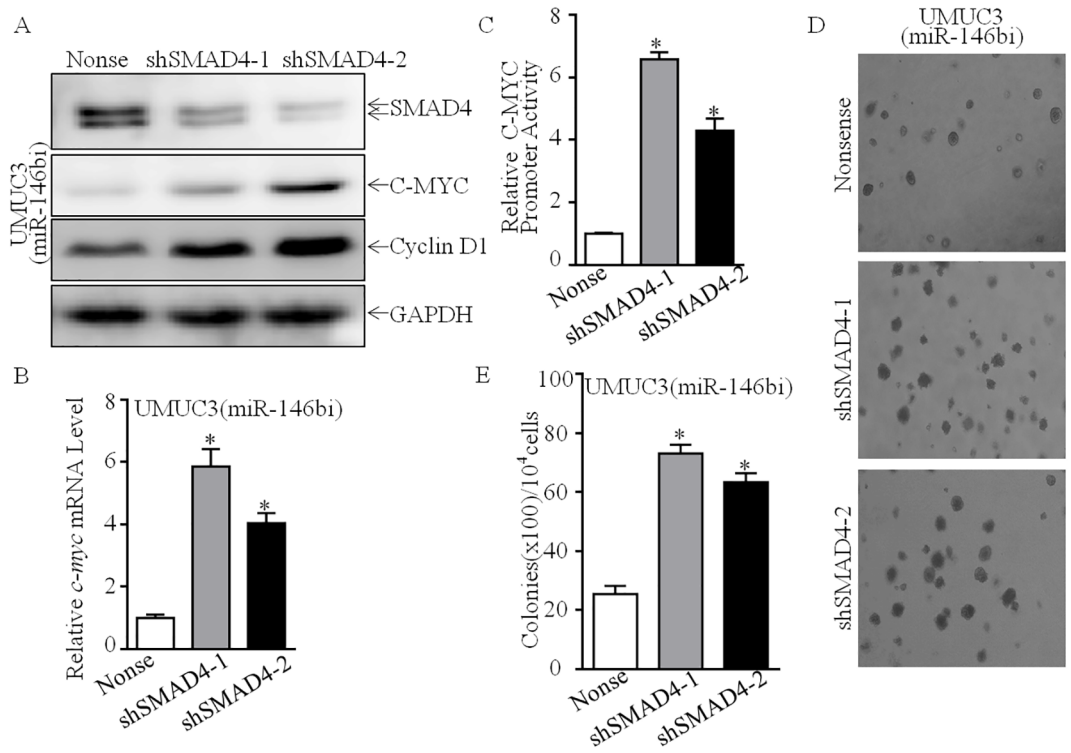

FIGURE 6
SMAD4 was a miR-146b-regulated transcription factor mediating Cyclin D1 upregulation in human BCa cells. **(A)** SMAD4 knockdown constructs were stably transfected into UMUC3 (miR-146bi) cells. The SMAD4 knockdown efficiency and its downstream C-MYC, Cyclin D1 expression were assessed by Western blotting. GAPDH was used as a protein loading control. **(B)** Relative *c-myc* mRNA expression detected in UMUC3 (miR-146bi/nonsense), UMUC3 (miR-146bi/shSMAD4-1) and UMUC3 (miR-146bi/shSMAD4-2) cells. **(C)** UMUC3 (miR-146bi/nonsense), UMUC3 (miR-146bi/shSMAD4-1), and UMUC3 (miR-146bi/shSMAD4-2) cells were transiently transfected with a *c-myc* promoter-driven luciferase reporter together with pRL-TK. Transfectants were seeded into 96-well plates to determine *c-myc* promoter transcriptional activity. pRL-TK was used as the internal control to normalize transfection efficiency. Bars indicate means ± SD from three replicate assays. **(D)** The stable transfectants as indicated were subjected to anchorage-independent soft agar growth assay. Representative images of colonies were photographed under an Olympus DP71. **(E)** The number of colonies was counted with more than 32 cells of each colony, and the results were presented as colonies per 10,000 cells. The bars show mean ± SD from three independent experiments, and the asterisk (*) indicates a significant increase in comparison to nonsense transfectants as indicated (*$p < 0.05$). BCa, bladder cancer.

impairment. Cyclin D1, a critical regulator, controls the cell cycle progression from the G0–G1 phase to the S phase by forming a complex with CDK4/6 (27, 28). Deregulation of Cyclin D1 expression and/or activity is common in human cancers including bladder cancer (29), colon cancer (30), and breast cancer (31). Cyclin D1 has been reported to be responsible for miR-576-3p overexpression inhibiting human bladder cancer proliferation by directly binding with its 3′-UTR (32). Isorhapontigenin exerts cancer-inhibitory effects on the growth of patient-derived glioblastoma spheres by inhibiting Cyclin D1 expression by regulating the miR-145/SOX2 axis (33). Long non-coding RNA (lncRNA) DILA1 could interact with the Thr286 of Cyclin D1 for repressing its phosphorylation and subsequent degradation, thereby promoting the Cyclin D1 protein expression and finally contributing to tamoxifen resistance in breast cancer (34). In the current study, miR-146b inhibition decreased Cyclin D1 protein expression. Ectopically expressed HA-Cyclin D1 in UMUC3 (miR-146bi) cells expectably reversed the reduction of miR-146bi on monolayer and anchorage-independent growth, indicating that Cyclin D1 is responsible for miR-146bi-mediated G0/G1 cell cycle arrest and the inhibition of anchorage-independent growth in BCa cells.

Oncoprotein C-MYC is critical for the formation and progression of various cancers by triggering the transcription of downstream oncogene or tumor suppressor genes (35). C-MYC could collaborate with TGF-α, epidermal growth factor receptor, Ras, PI3K/Akt, or NF-κB to the regulation of Cyclin D1 (36, 37). Coordination of C-MYC with Cyclin D1 not only accelerates tumor formation but also may drive tumor progression to a more aggressive phenotype (38). Our previous study has shown that *c-myc* mRNA impairment is crucial for p63α inhibition of Cyclin D1 gene transcription and bladder cancer cell tumorigenicity (19). In the present study, we explored the mechanism underlying miR-146b promoting Cyclin D1 promoter activity and focused on the contribution of C-MYC on Cyclin D1 promoter activity. We found that miR-146b inhibition could reduce Cyclin D1 mRNA expression through the inhibition of its promoter activity, which is mediated by decreasing C-MYC protein expression. Moreover, the ectopic expression of C-MYC reversed not only the inhibition effect on Cyclin D1 expression but also the anchorage-independent

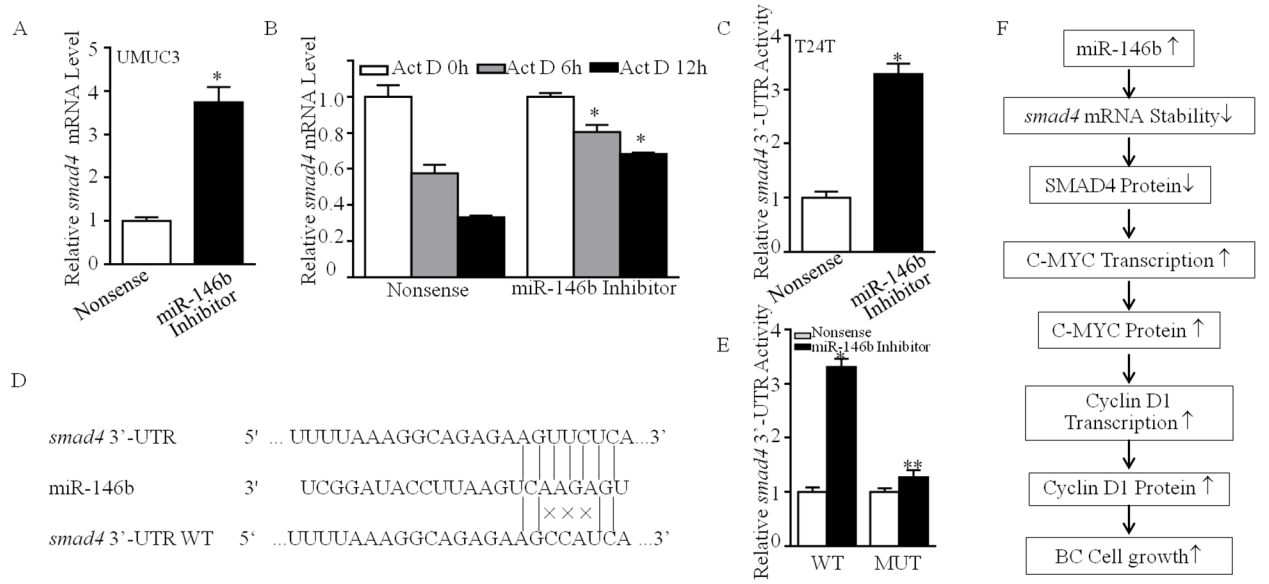

FIGURE 7
MiR-146b was responsible for destabilization of *smad4* mRNA by direct binding to its 3′-UTR. **(A)** UMUC3 (miR-146bi) and UMUC3 (nonsense) cells were cultured in 6-well plates till cell density reached 70%–80%. Following synchronization for 12 h, the medium was then replaced with 10% FBS DMEM for another 12 h The cells were extracted for total RNA with TRIzol reagent. Real-time PCR was used to determine *smad4* mRNA expression, and gapdh was used as an internal control. Data represent mean ± SD (*p < 0.05). **(B)** UMUC3 (miR-146bi) and UMUC3 (nonsense) cells were seeded into 6-well plates. After synchronization, the indicated cells were treated with Actinomycin D (Act D) for the indicated time points. Total RNA was then isolated and subjected to real-time PCR analysis for mRNA levels of *smad4*, and *gapdh* was used as an internal control. Bars represent mean ± SD from three independent experiments. Student's *t*-test was utilized to determine the p-value. The asterisk (*) indicates a significant increase in comparison to UMUC3 (nonsense) cells (*p < 0.05). **(C)** The pMIR-*SMAD4 3′-UTR* reporter was transiently transfected into the indicated cells, and luciferase activity of each transfectant was evaluated. The luciferase activity was presented as a relative to nonsense transfectant normalized using pRL-TK as an internal control. The bars show mean ± SD from three independent experiments. The symbol (*) indicates a significant increase in UMUC3 (miR-146bi) in comparison to nonsense transfectant (p < 0.05). **(D)** The predicted miR-146b binding site existed in the 3′-UTR of *smad4* mRNA, and its mutants (MUTs) were generated in the binding site. **(E)** The pMIR-*smad4* 3′-UTR reporters (WT and MUT) were co-transfected with pRL-TK into the indicated cells. Twenty-four hours post-transfection, the transfectants were extracted for determination of the luciferase activity, and TK was used as the internal control. Luciferase activity of each transfectant was evaluated, and the results were presented as relative *SMAD4 3′-UTR* activity. The bars show mean ± SD from three independent experiments. The double asterisk (**) indicates a significant inhibition of *3′-UTR* activity in mutant transfectant in comparison to mutant of WT *smad4 3′-UTR* luciferase reporter transfectant (p < 0.05). **(F)** The proposed mechanisms underlying miR-146b overexpression in the promotion of human BCa cells growth: miR-146b overexpression destabilizes *smad4* mRNA, which further elevates *c-myc* mRNA transcription, in turn promoting the transcription of *cyclin d1* and protein expression, and finally increases the transition of cell cycle G0/G1 phase and the anchorage-independent growth of human BCa cells. FBS, fetal bovine serum; DMEM, Dulbecco's modified Eagle's medium; BCa, bladder cancer.

growth by knockdown miR-146b in BCa cells. Taken together, our study provides evidence that targeting C-MYC and Cyclin D1 may be a good strategy for bladder cancer prevention.

Heterozygous or homozygous deletion of SMAD4 was first discovered in pancreatic ductal adenocarcinoma (39) and later detected in various types of cancers, such as colorectal cancer (40), cholangiocarcinoma (41), gastric cancer (42), and prostate cancer (43), although with lower frequencies to some extent. In bladder cancer, SMAD4 overexpression decreased bladder cancer cell proliferation, migration, and invasion abilities (44). Herein, the knockdown of miR-146b stabilized *smad4* mRNA and promoted its protein expression by directly binding with its 3′-UTR. Knockdown of SMAD4 in UMUC3 (miR-146bi) cells reversed the inhibition of anchorage-independent growth of BCa, indicating the consistent suggestion that SMAD4 may be a tumor suppressor for BCa tumorigenic growth. As the core mediator of the canonical TGF-β signaling pathway, SMAD4 plays a pivotal role in the switch of TGF-β function on tumorigenesis (45). The canonical TGF-β/SMAD4 signaling pathway plays a tumor suppressive role at early stages, mainly by inducing G0/G1 cell cycle arrest and apoptosis (46). Moreover, SMAD4 mediates the inhibitory effect of TGF-β on C-MYC expression by forming a complex with SMAD3, E2F4/5, and p107 at the TGF-β inhibitory element (TIE) element on the *c-myc* promoter (47). Consistently, in this study, we found that the knockdown of SMAD4 in UMUC3 (miR-146bi) cells promoted C-MYC transcription and protein expression. The results of the ChIP assay showed that SMAD4 could directly bind with the *c-myc* promoter.

Our findings provide novel insights into the role of miR-146b in regulating the SMAD4/C-MYC/Cyclin D1 axis in bladder cancer, aligning with previous studies demonstrating miR-146b's oncogenic potential in various malignancies. In colorectal cancer, miR-146b has been shown to regulate cancer cell proliferation and invasion, similarly enhancing the transcription of Cyclin D1 and other cell cycle regulators through its modulation of key signaling pathway state cancer; miR-146b also promotes cell growth by targeting PTEN and activating the PI3K/AKT pathway, which can intersect with the mechanisms we can observe in bladder cancer. In cervical cancer, miR-146b enhances proliferation and metastasis by

regulating inflammatory pathways, a mechanism that could potentially overlap with its effects on the TGF-β/SMAD signaling axis in bladder cancer. These studies and our findings underscore the central role of miR-146b in promoting cancer progression through the regulation of cell cycle-related proteins such as Cyclin D1, C-MYC, and other pivotal regulators. However, it is important to recognize that miR-146b may not be the only regulator of this axis. Other miRNAs, such as the miR-17-92 cluster, have been implicated in modulating the same pathway in different cancers. Future research should explore the cooperative regulation of this axis by multiple miRNAs and transcription factors, providing a more comprehensive understanding of the regulatory networks involved in bladder cancer progression. Although our study provides valuable insights into the role of miR-146b in bladder cancer, there are several limitations that should be acknowledged. First, our study mainly relied on the use of the UMUC3 and T24T cell lines and athymic nude mice, which may not fully recapitulate the complexity of human bladder cancer, especially with regard to tumor heterogeneity and the tumor microenvironment. Furthermore, while our findings suggest a significant role for miR-146b in regulating the SMAD4/C-MYC/Cyclin D1 axis, other potential pathways or factors may also contribute to the observed effects. Future research should explore additional bladder cancer models, including PDXs or GEMMs, to better reflect tumor biology and therapeutic responses. Additionally, the potential off-target effects of miR-146b inhibition were not fully addressed in this study, and future work should include controls to evaluate these effects more comprehensively. Lastly, while we focused on the miR-146b-induced regulation of Cyclin D1 and C-MYC, additional miRNAs or transcription factors may cooperate in modulating this axis, warranting further investigation into the broader regulatory network involved in bladder cancer progression.

While our study highlights miR-146b as a promising therapeutic target in bladder cancer, it is important to consider the challenges associated with miRNA-based therapies. MiRNA therapies face several obstacles, including the efficient delivery of miRNA mimics or inhibitors to target tissues, off-target effects, and potential immune responses. Additionally, the systemic delivery of miRNAs is often hindered by their instability in the bloodstream and rapid degradation by nucleases. Recent advancements in nanotechnology, such as liposomes and nanoparticles, hold promise for improving the targeted delivery and stability of miRNA-based therapies. Furthermore, the specificity of miRNA inhibition or overexpression can be fine-tuned by employing modified RNA molecules with reduced off-target effects. Therefore, while miR-146b-based therapies show potential, future research should focus on optimizing delivery methods, minimizing off-target effects, and assessing the safety and efficacy of miRNA-based approaches in preclinical and clinical trials.

In conclusion, miR-146b overexpression promotes proliferation and anchorage-independent growth of human BCa cells by enhancing SMAD4/C-MYC/Cyclin D1 pathway activation. MiR-146b overexpression destabilizes *smad4* mRNA by directly binding to its 3′-UTR, further elevating *c-myc* mRNA transcription, followed by promoting *cyclin D1* mRNA transcription and protein expression, and finally promoting the transition of cell cycle G0/G1 phase and the anchorage-independent growth of human BCa cells. The observed regulation of the SMAD4/C-MYC/Cyclin D1 axis by miR-146b underscores its potential as a key modulator in bladder cancer progression. However, it is essential to recognize that this pathway may be influenced by other factors beyond miR-146b. Other miRNAs, such as the miR-17-92 cluster, have been shown to target SMAD4 and C-MYC in different cancers, suggesting that multiple miRNAs may cooperatively regulate the same pathway. Additionally, transcription factors and signaling molecules such as TGF-β and SMAD2/3 may also play roles in modulating this axis. Further investigation into these alternative regulatory mechanisms will help provide a more complete picture of the molecular drivers of bladder cancer and may reveal additional therapeutic targets. Our new findings together with previous data of miR-146b promoting bladder cancer invasion suggest that the miR-146b could serve as a promising prognostic and therapeutic target for bladder cancer management.

5 Conclusions

In conclusion, our study demonstrates that miR-146b plays a crucial role in promoting the proliferation and tumorigenic growth of BCa cells through the modulation of the SMAD4/C-MYC/Cyclin D1 axis. Specifically, miR-146b overexpression leads to the destabilization of SMAD4 mRNA by directly binding to its 3'-UTR, thereby decreasing SMAD4 expression. This reduction in SMAD4 facilitates the transcription of C-MYC, which, in turn, upregulates Cyclin D1 expression, driving the G0/G1 cell cycle transition and enhancing BCa cell proliferation. Furthermore, our findings highlight that miR-146b not only is involved in the regulation of key cell cycle regulators but also plays a significant role in promoting anchorage-independent growth, a critical hallmark of tumorigenic potential. The therapeutic implications of these findings are noteworthy, as targeting miR-146b could provide a novel strategy for controlling BCa cell growth by disrupting this oncogenic pathway.

This study presents a new mechanistic insight into the role of miR-146b in bladder cancer and its potential as a therapeutic target. Given that miR-146b has already been implicated in various cancer types, its involvement in BCa suggests that it may serve as both a biomarker for prognosis and a target for therapeutic intervention. Future studies should focus on validating these findings in clinical settings and exploring potential miR-146b-based therapies for BCa treatment.

Data availability statement

The original contributions presented in the study are included in the article/supplementary material. Further inquiries can be directed to the corresponding authors.

Ethics statement

The studies involving humans were approved by Affiliated Jinhua Hospital, Zhejiang University School of Medicine. The studies were conducted in accordance with the local legislation and institutional requirements. Written informed consent for participation was not required from the participants or the participants' legal guardians/next of kin in accordance with the national legislation and institutional requirements. The animal study was approved by Affiliated Jinhua Hospital, Zhejiang University School of Medicine. The study was conducted in accordance with the local legislation and institutional requirements.

Author contributions

JLZ: Conceptualization, Data curation, Methodology, Writing – original draft, Writing – review & editing. ZZ: Data curation, Writing – original draft. ZY: Data curation, Writing – review & editing. LD: Data curation, Writing – review & editing. CL: Data curation, Writing – review & editing. XW: Data curation, Writing – review & editing. PS: Data curation, Writing – review & editing. JZ: Data curation, Writing – review & editing. WL: Conceptualization, Writing – review & editing. JL: Conceptualization, Writing – review & editing.

Funding

The author(s) declare that financial support was received for the research and/or publication of this article. This research was partially supported by grants from the Natural Science Foundation of China (NSFC 82103872), Ningbo Natural Science Foundation (2023J026), Technology Project of Zhejiang Provincial Health Commission (2022KY346), and Ningbo Medical Technology Programme (2020Y42).

Conflict of interest

The authors declare that the research was conducted in the absence of any commercial or financial relationships that could be construed as a potential conflict of interest.

Generative AI statement

The author(s) declare that no Generative AI was used in the creation of this manuscript.

Publisher's note

References

1. Sanli O, Dobruch J, Knowles MA, Burger M, Alemozaffar M, Nielsen ME, et al. Bladder cancer. *Nat Rev Dis Primers*. (2017) 3:17022. doi: 10.1038/nrdp.2017.22

2. Torre LA, Bray F, Siegel RL, Ferlay J, Lortet-Tieulent J, Jemal A. Global cancer statistics, 2012. *CA Cancer J Clin*. (2015) 65:87–108. doi: 10.3322/caac.21262

3. Ploussard G, Shariat SF, Dragomir A, Kluth LA, Xylinas E, Masson-Lecomte A, et al. Conditional survival after radical cystectomy for bladder cancer: evidence for a patient changing risk profile over time. *Eur Urol*. (2014) 66:361–70. doi: 10.1016/j.eururo.2013.09.050

4. Di Leva G, Garofalo M, Croce CM. MicroRNAs in cancer. *Annu Rev Pathol*. (2014) 9:287–314. doi: 10.1146/annurev-pathol-012513-104715

5. Rupaimoole R, Slack FJ. MicroRNA therapeutics: towards a new era for the management of cancer and other diseases. *Nat Rev Drug Discovery*. (2017) 16:203–22. doi: 10.1038/nrd.2016.246

6. Lujambio A, Lowe SW. The microcosmos of cancer. *Nature*. (2012) 482:347–55. doi: 10.1038/nature10888

7. Yao S, Xu J, Zhao K, Song P, Yan Q, Fan W, et al. Down-regulation of HPGD by miR-146b-3p promotes cervical cancer cell proliferation, migration, and anchorage-independent growth through activation of STAT3 and AKT pathways. *Cell Death Dis*. (2018) 9:1055. doi: 10.1038/s41419-018-1059-y

8. Zhu Y, Wu G, Yan W, Zhan H, Sun P. miR-146b-5p regulates cell growth, invasion, and metabolism by targeting PDHB in colorectal cancer. *Am J Cancer Res*. (2017) 7:1136–50.

9. Gao S, Zhao Z, Wu R, Wu L, Tian X, Zhang Z. MiR-146b inhibits autophagy in prostate cancer by targeting the PTEN/Akt/mTOR signaling pathway. *Aging*. (2018) 10:2113–21. doi: 10.18632/aging.101780

10. Zhu J, Xu C, Ruan L, Wu J, Li Y, Zhang X. MicroRNA-146b overexpression promotes human bladder cancer invasion via enhancing ETS2-mediated MMP2 mRNA transcription. *Mol Ther Nucleic Acids*. (2019) 16:531–42. doi: 10.1016/j.omtn.2019.04.007

11. Al-Nakhle HH. Unraveling the multifaceted role of the miR-17-92 cluster in colorectal cancer: from mechanisms to biomarker potential. *Curr Issues Mol Biol*. (2024) 46:1832–50. doi: 10.3390/cimb46030120

12. Chen L, Zheng J, Zhang Y, Yang L, Wang J, Ni J, et al. Tumor-specific expression of microRNA-26a suppresses human hepatocellular carcinoma growth via cyclin-dependent and -independent pathways. *Mol Ther*. (2011) 19:1521–8. doi: 10.1038/mt.2011.64

13. Shan J, Zhao W, Gu W. Suppression of cancer cell growth by promoting cyclin D1 degradation. *Mol Cell*. (2009) 36:469–76. doi: 10.1016/j.molcel.2009.10.018

14. Fang Y, Cao Z, Hou Q, Ma C, Yao C, Li J, et al. Cyclin D1 downregulation contributes to anticancer effect of isorhapontigenin on human bladder cancer cells. *Mol Cancer Ther*. (2013) 12:1492–503. doi: 10.1158/1535-7163.MCT-12-0922

15. Liao DJ, Thakur A, Wu J, Biliran H, Sarkar FH. Perspectives on c-Myc, Cyclin D1, and their interaction in cancer formation, progression, and response to chemotherapy. *Crit Rev Oncog*. (2007) 13:93–158. doi: 10.1615/CritRevOncog.v13.i2.10

16. Zhu J, Li Y, Chen C, Ma J, Sun W, Tian Z, et al. NF-κB p65 overexpression promotes bladder cancer cell migration via FBW7-mediated degradation of RhoGDIα protein. *Neoplasia*. (2017) 19:672–83. doi: 10.1016/j.neo.2017.06.002

17. Zhu J, Li Y, Tian Z, Hua X, Gu J, Li J, et al. ATG7 overexpression is crucial for tumorigenic growth of bladder cancer *in vitro* and *in vivo* by targeting the ETS2/miRNA196b/FOXO1/p27 axis. *Mol Ther Nucleic Acids*. (2017) 7:299–313. doi: 10.1016/j.omtn.2017.04.012

18. Huang H, Zhu J, Li Y, Zhang L, Gu J, Xie Q, et al. Upregulation of SQSTM1/p62 contributes to nickel-induced Malignant transformation of human bronchial epithelial cells. *Autophagy*. (2016) 12:1687–703. doi: 10.1080/15548627.2016.1196313

19. Li X, Tian Z, Jin H, Xu J, Hua X, Yan H, et al. Decreased c-Myc mRNA stability via the microRNA 141-3p/AUF1 axis is crucial for p63α inhibition of cyclin D1 gene

transcription and bladder cancer cell tumorigenicity. *Mol Cell Biol*. (2018) 38:e00273–18. doi: 10.1128/MCB.00273-18

20. Fabian MR, Sonenberg N, Filipowicz W. Regulation of mRNA translation and stability by microRNAs. *Annu Rev Biochem*. (2010) 79:351–79. doi: 10.1146/annurev-biochem-060308-103103

21. Lewis BP, Shih IH, Jones-Rhoades MW, Bartel DP, Burge CB. Prediction of mammalian microRNA targets. *Cell*. (2003) 115:787–98. doi: 10.1016/s0092-8674(03)01018-3

22. Jonas S, Izaurralde E. Towards a molecular understanding of microRNA-mediated gene silencing. *Nat Rev Genet*. (2015) 16:421–33. doi: 10.1038/nrg3965

23. Sohel MMH. Circulating microRNAs as biomarkers in cancer diagnosis. *Life Sci*. (2020) 248:117473. doi: 10.1016/j.lfs.2020.117473

24. Catto JW, Alcaraz A, Bjartell AS, De Vere White R, Evans CP, Fussel S, et al. MicroRNA in prostate, bladder, and kidney cancer: a systematic review. *Eur Urol*. (2011) 59:671–81. doi: 10.1016/j.eururo.2011.01.044

25. Hermann H, Runnel T, Aab A, Baurecht H, Rodriguez E, Magilnick N, et al. miR-146b probably assists miRNA-146a in the suppression of keratinocyte proliferation and inflammatory responses in psoriasis. *J Invest Dermatol*. (2017) 137:1945–54. doi: 10.1016/j.jid.2017.05.012

26. Ramírez-Moya J, Wert-Lamas L, Santisteban P. MicroRNA-146b promotes PI3K/AKT pathway hyperactivation and thyroid cancer progression by targeting PTEN. *Oncogene*. (2018) 37:3369–83. doi: 10.1038/s41388-017-0088-9

27. Keenan SM, Lents NH, Baldassare JJ. Expression of cyclin E renders cyclin D-CDK4 dispensable for inactivation of the retinoblastoma tumor suppressor protein, activation of E2F, and G1-S phase progression. *J Biol Chem*. (2004) 279:5387–96. doi: 10.1074/jbc.M310383200

28. Singh RP, Agarwal C, Agarwal R. Inositol hexaphosphate inhibits growth, and induces G1 arrest and apoptotic death of prostate carcinoma DU145 cells: modulation of CDKI-CDK-cyclin and pRb-related protein-E2F complexes. *Carcinogenesis*. (2003) 24:555–63. doi: 10.1093/carcin/24.3.555

29. Lopez-Beltran A, Luque RJ, Alvarez-Kindelan J, Quintero A, Merlo F, Carrasco JC, et al. Prognostic factors in stage T1 grade 3 bladder cancer survival: the role of G1-S modulators (p53, p21Waf1, p27kip1, Cyclin D1, and Cyclin D3) and proliferation index (ki67-MIB1). *Eur Urol*. (2004) 45:606–12. doi: 10.1016/j.eururo.2003.11.011

30. Ogino S, Nosho K, Irahara N, Kure S, Shima K, Baba Y, et al. A cohort study of cyclin D1 expression and prognosis in 602 colon cancer cases. *Clin Cancer Res*. (2009) 15:4431–8. doi: 10.1158/1078-0432.CCR-08-3330

31. Zhong Z, Yeow WS, Zou C, Wassell R, Wang C, Pestell RG, et al. Cyclin D1/cyclin-dependent kinase 4 interacts with filamin A and affects the migration and invasion potential of breast cancer cells. *Cancer Res*. (2010) 70:2105–14. doi: 10.1158/0008-5472.CAN-08-1108

32. Liang Z, Li S, Xu X, Xu X, Wang X, Wu J, et al. MicroRNA-576-3p inhibits proliferation in bladder cancer cells by targeting cyclin D1. *Molecules Cells*. (2015) 38:130–7. doi: 10.14348/molcells.2015.2146

33. Xu Z, Zeng X, Xu J, Xu D, Li J, Jin H, et al. Isorhapontigenin suppresses growth of patient-derived glioblastoma spheres through regulating miR-145/SOX2/cyclin D1 axis. *Neuro Oncol*. (2016) 18:830–9. doi: 10.1093/neuonc/nov298

34. Shi Q, Li Y, Li S, Jin L, Lai H, Wu Y, et al. LncRNA DILA1 inhibits cyclin D1 degradation and contributes to tamoxifen resistance in breast cancer. *Nat Commun*. (2020) 11(1):5513. doi: 10.1038/s41467-020-19349-w

35. Tang J, Yan T, Bao Y, Shen C, Yu C, Zhu X, et al. LncRNA GLCC1 promotes colorectal carcinogenesis and glucose metabolism by stabilizing c-Myc. *Nat Commun*. (2019) 10:3499. doi: 10.1038/s41467-019-11447-8

36. Biliran H Jr, Banerjee S, Thakur A, Sarkar FH, Bollig A, Ahmed F, et al. c-Myc-induced chemosensitization is mediated by suppression of cyclin D1 expression and nuclear factor-kappa B activity in pancreatic cancer cells. *Clin Cancer Res*. (2007) 13:2811–21. doi: 10.1158/1078-0432.CCR-06-1844

37. Ahn H, Im E, Lee DY, Lee HJ, Jung JH, Kim SH. Antitumor effect of pyrogallol via miR-134 mediated S phase arrest and inhibition of PI3K/AKT/Skp2/cMyc signaling in hepatocellular carcinoma. *Int J Mol Sci*. (2019) 20:3985. doi: 10.3390/ijms20163985

38. Chen J, Li X, Cheng Q, Ning D, Ma J, Zhang ZP, et al. Effects of cyclin D1 gene silencing on cell proliferation, cell cycle, and apoptosis of hepatocellular carcinoma cells. *J Cell Biochem*. (2018) 119:2368–80. doi: 10.1002/jcb.v119.2

39. Pan S, Brentnall TA, Chen R. Proteome alterations in pancreatic ductal adenocarcinoma. *Cancer Lett*. (2020) 469:429–36. doi: 10.1016/j.canlet.2019.11.020

40. Fleming NI, Jorissen RN, Mouradov D, Christie M, Sakthianandeswaren A, Palmieri M, et al. SMAD2, SMAD3, and SMAD4 mutations in colorectal cancer. *Cancer Res*. (2013) 73:725–35. doi: 10.1158/0008-5472.CAN-12-2706

41. Qiao P, Li G, Bi W, Yang L, Yao L, Wu D. MicroRNA-34a inhibits epithelial mesenchymal transition in human cholangiocarcinoma by targeting Smad4 through transforming growth factor-beta/Smad pathway. *BMC Cancer*. (2015) 15:469. doi: 10.1186/s12885-015-1359-x

42. Ma C, Wang X, Yang F, Zang Y, Liu J, Wang X, et al. Circular RNA hsa_circ_0004872 inhibits gastric cancer progression via the miR-224/Smad4/ADAR1 successive regulatory circuit. *Mol Cancer*. (2020) 19:157. doi: 10.1186/s12943-020-01268-5

43. Ding Z, Wu CJ, Chu GC, Xiao Y, Ho D, Zhang J, et al. SMAD4-dependent barrier constrains prostate cancer growth and metastatic progression. *Nature*. (2011) 470:269–73. doi: 10.1038/nature09677

44. Hirata H, Ueno K, Shahryari V, Tanaka Y, Tabatabai ZL, Hinoda Y, et al. Oncogenic miRNA-182-5p targets Smad4 and RECK in human bladder cancer. *PloS One*. (2012) 7:e51056. doi: 10.1371/journal.pone.0051056

45. Zhao M, Mishra L, Deng CX. The role of TGF-beta/SMAD4 signaling in cancer. *Int J Biol Sci*. (2018) 14:111–23. doi: 10.7150/ijbs.23230

46. Zhou J, Zhang C, Zhou B, Jiang D. miR-183 modulated cell proliferation and apoptosis in ovarian cancer through the TGF-beta/Smad4 signaling pathway. *Int J Mol Med*. (2019) 43:1734–46. doi: 10.3892/ijmm.2019.4082

47. Chen CR, Kang Y, Siegel PM, Massague J. E2F4/5 and p107 as Smad cofactors linking the TGFbeta receptor to c-myc repression. *Cell*. (2002) 110:19–32. doi: 10.1016/s0092-8674(02)00801-2

frontiers | Frontiers in Pharmacology

TYPE Original Research
PUBLISHED 01 April 2025
DOI 10.3389/fphar.2025.1573611

OPEN ACCESS

EDITED BY
Lei Yin,
Shanghai Jiaotong University School of Medicine, China

REVIEWED BY
Yousheng Yao,
Sun Yat-sen Memorial Hospital, China
Yonghao Chen,
West China Hospital, Sichuan University, China

*CORRESPONDENCE
Song Fan,
fansong@ahmu.edu.cn
Peng Guo,
jysrmyyqingtian@163.com

†These authors have contributed equally to this work to this article

RECEIVED 09 February 2025
ACCEPTED 10 March 2025
PUBLISHED 01 April 2025

CITATION
Wu J, Wu W, Qin J, Chen Z, Zhong R, Guo P and Fan S (2025) Exploring the impact of cuproptosis on prostate cancer prognosis *via* RNA methylation regulation based on single cell and bulk RNA sequencing data.
Front. Pharmacol. 16:1573611.
doi: 10.3389/fphar.2025.1573611

Exploring the impact of cuproptosis on prostate cancer prognosis *via* RNA methylation regulation based on single cell and bulk RNA sequencing data

Junchao Wu[1,2,3†], Wentian Wu[4†], Jiaxuan Qin[1,2,3†], Ziqi Chen[1,2,3], Rongfang Zhong[5], Peng Guo[6*] and Song Fan[1,2,3*]

[1]Department of Urology, The First Affiliated Hospital of Anhui Medical University, Hefei, China, [2]Institute of Urology, Anhui Medical University, Hefei, China, [3]Anhui Province Key Laboratory of Urological and Andrological Diseases Research and Medical Transformation, Hefei, China, [4]Department of Oncology, The First Affiliated Hospital of Anhui Medical University, Hefei, China, [5]Department of Urology, The University of Hong Kong-Shenzhen Hospital, Shenzhen, China, [6]Department of Urology, The Affiliated Jiangyin Hospital of Nantong University, Wuxi, China

Background: Cuproptosis, along with RNA methylation regulators, has recently come to the fore as innovative mechanisms governing cell death, exerting profound impact on the onset and progression of multiple cancers. Nonetheless, the prognostic implications and underlying regulatory mechanisms of them associated with prostate cancer (PCa) remain to be thoroughly investigated.

Methods: Genomic and clinical data for PCa from The Cancer Genome Atlas datasets were analyzed to identify a prognostic model through univariate and Least Absolute Shrinkage and Selection Operator Cox regression analyses that were validated utilizing external datasets. We used receiver operating characteristic curves and C-index to evaluate the accuracy of our prognostic model. In conjunction with this, we conducted single-cell RNA sequencing (scRNA-seq) analyses to investigate underlying mechanisms and evaluate the degree of immune infiltration, as well as to assess patients' responses to diverse chemotherapy agents. Especially, qPCR assay was utilized to unveil the expression of signature genes in PCa.

Results: We meticulously selected six Cuproptosis-Associated RNA Methylation Regulators (CARMRs) to establish a risk prognosis model, which was further verified to obtain enhanced predictive capacity in external validation cohorts. Insights from immune infiltration and scRNA-seq analyses have elucidated the immune characteristics of PCa, and highlighted the immunosuppressive role of regulatory T cells on immune response. Additionally, drug susceptibility analysis demonstrated that patients with PCa in the low-risk category derived better benefit from bicalutamide treatment, whereas those in the high-risk group exhibited a favor response to adriamycin and docetaxel treatments. The qPCR and immunohistochemistry (IHC) staining assays also reveal the a dramatically altered expression pattern of TRDMT1 and ALYREF in PCa tissues.

Conclusion: In general, we established a model involving CARMRs that can better predict the risk of recurrence of PCa and have identified the possible mechanisms affecting PCa progression, thereby promoting further research in this field.

KEYWORDS

prostate cancer, cuproptosis, RNA methylation regulators, immunotherapy, chemotherapy agent

1 Introduction

Prostate cancer (PCa) is a global health issue. According to the statistics from GLOBOCAN 2020, PCa serves as the second most common cancer in men worldwide following lung cancer, and it is particularly endemic in 112 countries (Sung et al., 2021). Localized PCa is primarily treated through radical prostatectomy combined with radiotherapy, whereas high-risk PCa is managed *via* androgen deprivation therapy (ADT) (Sekhoacha et al., 2022). Nevertheless, long-term ADT treatment may contribute to the occurrence of castration-resistant PCa (CRPC), resulting in a higher risk of metastasis and poorer recurrence-free survival (RFS) (Bach et al., 2014; Teo et al., 2019). Nowadays, clinical diagnostic biomarkers used to screen the public for PCa, such as prostate specific antigen, lack specificity and the Gleason score can be easily affected by sampling error and subjectivity. In contrast, genotyping-based classification can be crucial in identifying specific subtypes of PCa and promoting individualized treatment (Kench et al., 2022; Ye et al., 2020). Therefore, exploring novel biomarkers for predicting the prognosis of PCa and improving treatment accuracy is of great significance.

Cuproptosis, a novel non-apoptotic mode of cell death, is mediated by copper-dependent mitochondria and occurs through direct binding of copper to the acylation components in the tricarboxylic acid cycle. Increased intracellular levels of copper ions can induce cuproptosis (Chen et al., 2022). Recent research has shown that copper levels in tumor tissues are 2–3 times higher than those in normal tissues (Gupte and Mumper, 2009). As a common form of cell death, cuproptosis has the capacity to regulate the DLAT/mTOR pathway to enhance the autophagy of PCa cells and reverse their resistance to chemotherapy drugs (Wen et al., 2023). Given that cuproptosis induces cell death *via* changing mitochondrial metabolism, the drugs that enhance this dependency, such as enzalutamide could build on synergies (Gao et al., 2024). The discovery of cuproptosis, which needs further research, may provide ideas for the exploration of novel therapeutic targets for cancer treatment. Moreover, gaining an insight into the mechanism and associated signaling pathways of cuproptosis would provide new options for reversing drug resistance in PCa.

On the other hand, RNA methylation modifications participate broadly in biological processes and correlate with proliferation, metastasis, cellular stress, and the immune response to cancer (Yang et al., 2021; Chen et al., 2019). The RNA methylation categories of significance included N6-methyladenosine (m6A), 5-methylcytosine (m5C), N7-methylguanosine (m7G), and N1-methyladenosine (m1A) (Long et al., 2023). Among these, the m6A modification is the most widely distributed in living organisms and is known to be involved in multiple processes of RNA synthesis (An and Duan, 2022). For example, YTHDF2 has been shown to induce the proliferation of PCa cells through an m6A--dependent mechanism (Li et al., 2020). Elevated methylation levels of EI3C mRNA may contribute to metastasis by activating the MAPK pathway (Ding et al., 2022). Additionally, METTL3 (Haigh et al., 2022), VIRMA (Barros-Silva et al., 2020), FTO (Zhang J. et al., 2023), and RBM15 (Wang et al., 2023) are known to play key roles in controlling the extent of methylation to impact the survival, progression and drug-resistance of patients with PCa by serving as "writers". RNA methylation has also shown a strong correlation with genetic variation, alternative splicing, and immune phenotypes. We speculate that the tumor microenvironment (TME) would be remodeled when the methylation level increased (Zhao et al., 2021). RNA methylation modifications have been implicated in various cancers making them potential biomarkers for cancer diagnosis and treatment.

To conclude, rational prognostic models were formerly established involving Cuproptosis-Associated RNA Methylation Regulators (CARMRs) to provide fresh insights into the development of new targets and patient immunotherapy in colorectal cancer and hepatocellular carcinoma (Li et al., 2023; Zhao et al., 2024a). CARMRs may help characterize the immune status, be essential for proliferation and invasiveness, and predict patient prognosis. Hence, we constructed a CARMR-based prognostic model to explore the potential mechanism of transfer and drug resistance in PCa.

In this study, we constructed a prognostic model utilizing CARMRs in patients with PCa to divide them into high- and low-risk groups, predict RFS, the landscape of TME, and drug sensitivity. We believe that clinicians can better identify the PCa stage and guide individualized treatment through our approach described here. The workflow of this study is shown in Figure 1.

2 Materials and methods

2.1 Datasets acquisition and preprocessing

Two PCa cohorts were included in this study. The Cancer Genome Atlas Prostate Adenocarcinoma (TCGA-PRAD) cohort was downloaded from the Genomic Data Commons. We deleted patients with missing data, and eventually enrolled 488 patients with complete expression profile data and clinical information. We transformed Transcripts Per Million (TPM) data to a $\log_2$ (TPM) format to achieve better comparability. Subsequently, the Gene Expression Omnibus (GEO) cohorts from three eligible GEO datasets, GSE21032 (n = 138) (Taylor et al., 2010), GSE116918 (n = 223) (Jain et al., 2018), and GSE46602 (n = 36) (Mortensen et al., 2015) were utilized as validation cohorts.

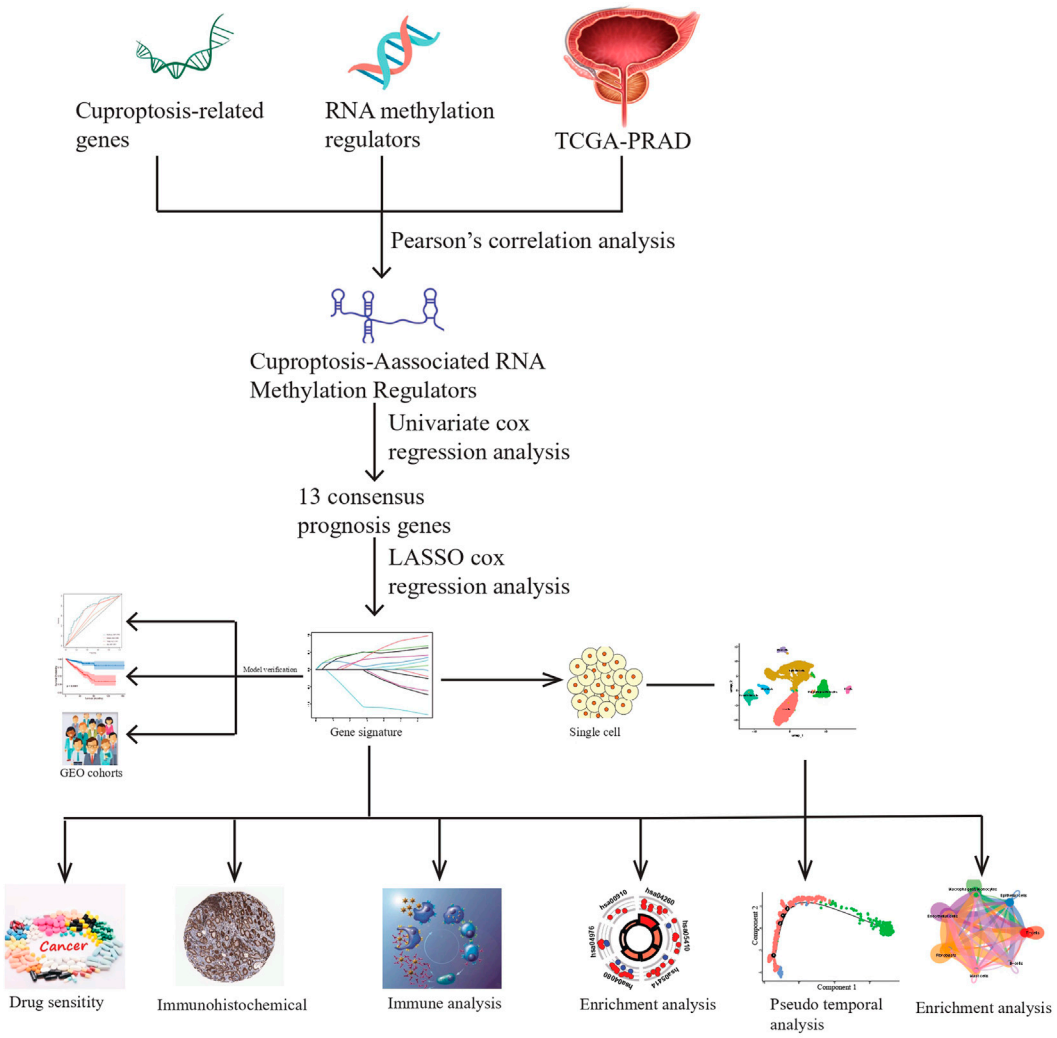

FIGURE 1
A schematic showing the workflow of the study.

The baseline information of all cohorts above has been summarized in Table 1. We removed potential cross-dataset batch effects using the "sva" library of R software package implemented *via* an empirical Bayes framework (Leek et al., 2012). A single-cell dataset (GSE193337) (Heidegger et al., 2022) was extracted from the GEO database. The baseline information of samples from the single-cell dataset was summarized in Table 2 and the single-cell RNA sequencing (scRNA-seq) data of four PCa samples were utilized for our study.

2.2 Identification of prognostic CARMRs

We identified 13 cuproptosis-related genes and 59 RNA methylation regulators, which were treated as the focus of our study based on previous literature (Chen YS. et al., 2021; He et al., 2022; Li M. et al., 2022; Tsvetkov et al., 2022). A Pearson correlation analysis was employed to identify CARMRs, and filter conditions were set to $|R| \geq 0.4$, $P < 0.001$. Further, we conducted a univariate Cox regression analysis utilizing "survival" package (Liu et al., 2021) and $P < 0.05$ was designated as a threshold to identify CARMRs that were correlated with RFS.

2.3 Construction and validation of a prognostic model and nomogram

Based on the results of our univariable Cox regression analysis, we used least absolute shrinkage and selection operator regression analysis (LASSO) regression analysis (Li Y. et al., 2022) to select combinations of genes that were rationally narrowed by the glmnet software package, in order to minimize the risk of overfitting. Through cross-verification, we selected the penalty parameter (λ) value with the least average error to construct the model. Finally, we selected six prognostic CARMRs to construct a risk model, and calculated the risk scores for each patient with PCa according to the following equation:

TABLE 1 Summary of the clinicopathological parameters of the four enrolled datasets.

Items	TCGA-PRAD (n = 488)	MSKCC(n = 138)	GEO116918 (n = 223)	GEO46602 (n = 36)
Age				
≤60	219	87	31	15
>60	269	51	192	21
Pathological T stage				
T1 + T2	187	86	127	19
T3 + T4	301	52	96	17
Gleason score				
≤7	287	117	127	32
>7	201	21	96	4
Status				
Recurrence free	396	103	172	14
Recurred	92	35	51	22

TABLE 2 After filtering, basic quality control statistics for the respective combined datasets, and patient samples are characterized in the table below.

Dataset	Sample	Number of cells	Number of genes
GSE193337	GSM5793828	2,420	19,815
	GSM5793829	5,724	21,344
	GSM5793831	5,087	21,890
	GSM5793832	5,964	21,530

$$\text{Risk score} = \sum_{i=1}^{n} (\text{coef}_i * \exp_i)$$

where $coef_i$ and exp_i terms represent the coefficients and expression values of the prognostic genes, respectively. Defining the median risk score of the TCGA cohort as the cutoff value, the patients of the TCGA and GEO cohort could be separated into high- and low-risk groups. Time-dependent receiver operating characteristic (ROC) curves and Kaplan-Meier (KM) curves were used to evaluate the predictive performance of our prognostic model in the TCGA-PRAD and GEO cohorts. Combining clinicopathological factors with prognostic significance, we constructed a nomogram for the TCGA-PRAD cohort *via* the "regplot" package to predict 1-, 3- and 5-year risk of recurrence for patients with PCa. We then computed the C-index value to show the predictive performance of our nomogram and other clinicopathological parameters. The calibration curve also evaluated the efficacy of the nomogram. Finally, we analyzed the relationship between different independent factors and risk scores and plotted the KM curves in the clinicopathological subgroup to further verify the capability of this approach.

2.4 Function enrichment analysis

The differentially expressed genes (DEGs) of the high-risk and low-risk group patients with PCa were determined using the "DESeq2" package with the threshold of $|\log_2 \text{foldChange}| \geq 0.5$ and adjusted $P < 0.05$. We then investigated biological structure and function, using gene ontology (GO) enrichment and Kyoto Encyclopedia of Genes and Genome (KEGG) enrichment analyses to identify pathways enriched in PCa. The changes in signaling pathways and interactions of DEGs were depicted by Gene Set Enrichment Analysis (GSEA). Various software packages, namely "clusterProfiler" (Wu et al., 2021), "org.Hs.e.g.db" (Qing et al., 2022) and the R software package, were employed.

2.5 Drug sensitivity and immune infiltration analysis

Understanding the responsiveness of patients carrying various levels of risk of PCa recurrence due to the administration of common chemotherapeutic agents contributes to developing individualized treatment plans for patients with PCa. Therefore, we used the "pRRophetic" software package to calculate the half maximum inhibitory concentration (IC_{50}) value of adriamycin, bicalutamide and docetaxel in different risk of PCa recurrence subgroups. In order to explore the relationship between risk score and TME, the CIBERSORT (Craven et al., 2021) algorithm was utilized to investigate the differential proportions of 22 kinds of immune cells between high- and low-risk groups in patients with PCa. The ESTIMATE algorithm (Xu et al., 2021) was utilized to calculate estimate score, immune score, stromal score and tumor purity. We utilized the ssGSEA algorithm (Ye et al., 2019) to validate the accuracy of immune infiltration analysis. Finally, we analyzed the expression of TRDMT1 and ALYREF in tumor and normal histopathology tissue sections acquired from the Human Protein Atlas database (www.proteinatlas.org).

2.6 Quality control and annotation of single-cell RNA sequencing data

The "Seurat_v5" software package was used to further process single-cell RNA sequencing data derived from PCa samples (Yu et al., 2022). First, we constructed single cell objects by the CreateSeuratObject method. With the threshold of RNA features ranging from 300 to 7,000 and the proportion of a mitochondrial gene set to less than 5%, eligible cells were selected and retained for further analysis. We employed the "NormalizeData" algorithm to standardize the data and selected the top 20 components and first

2,000 variably expressed genes for follow-up analysis, while "ScaleData" was used to center and scale the highly variable genes. We conducted principal component analysis (PCA) to reduce the dimensionality of the data, and the PCA number was adjusted to 15. The "Harmony" algorithm was applied to integrated single-cell data from different datasets to eliminate potential batch effects. Subsequently, we defined a category of genes with the same expression patten as a cluster and utilized the software function of uniform manifold approximation and projection (UMAP) to depict the distribution of each cluster. Cell annotation was performed by artificiality, and the cell markers were referred from CellMarker2.0.

2.7 Cell-cell communication and pseudotime analysis

We applied "Cellchat" from R software package to reveal and visualize the cell-cell interactions and possible signaling pathways involved (Yu et al., 2022). After identifying the prognostic genes primarily distributed in T cells, we subdivided and annotated the T cell cluster on the basis of cell markers obtained from previous studies (resolution = 0.5). We investigated the transition of different subtypes utilizing the "Monocle" application from R software package. The resulting cell state plots and cell type maps revealed the developmental trajectory of PCa.

2.8 Quantitative real-time PCR (qRT-PCR)

The RNA extraction was performed using the Trizol reagent (Beijing ComWin Biotech Co., Ltd.) from prostate normal and cancer cell lines RWPE-1, LNCaP, C42, PC3 (Wuhan Pricella Biotech Co., Ltd.). For cDNA synthesis, reverse transcription was conducted using the TaKaRa (Dalian TaKaRa Biotech Co., Ltd.) kit according to the manufacturer's instructions. GAP was employed as an internal reference gene to normalize relative expressions of lncRNA with the $2^{-\Delta\Delta CT}$ method. The specific primers in our study were as follows: TRDMT1 (forward: 5′-CGGGTGCTGGAGCTATACAG-3′, reverse:5′-CGACAGTGTTGACATCAATGGC-3′); ALYREF (5′-GCAGGC CAAAACAACTTCCC -3′, 5′-AGTTCCTGAATATCGGCGTCT -3′).

2.9 Statistical analysis

All statistical analyses were carried out using R software package (version 4.2.0). The continuous data were analyzed by independent t-test, Wilcoxon test or Fisher's exact test, which was considered to analyze classified data. $P < 0.05$ was considered to be statistically significant.

3 Results

3.1 Identification of cuproptosis-associated RNA methylation regulators (CARMRs) and construction of a prognostic model involving CARMRs

We conducted Pearson's correlation analysis between cuproptosis-related genes and RNA methylation regulators: by setting filter criteria, a total of 48 CARMRs were selected for further study (Figure 2A). To screen out CARMRs correlated with RFS, we performed univariate Cox regression analysis and identified 13 CARMRs significantly associated with prognosis ($P < 0.05$) (Figure 2B). The results revealed that only TRDMT1 exhibited a protective effect, whereas the remaining 12 genes (NEK2, SMCA, ALYREF, BLM, DNMT1, DNMT3B, TOP2A, TRMT61A, HMMR, EXO1, HNRNPA2B1, INCENP) were identified as risk factors for the recurrence of PCa. Further, we conducted LASSO Cox regression analysis to minimize model overfitting and determine the optimal λ value (Figure 2C). Ultimately, a six-CARMR signature, comprising a set of genes, was selected for the construction of a prognostic model assessing the risk of recurrence within PCa and the association between cuproptosis-related genes and the six select RNA methylation regulators was vividly visualized using a Sankey diagram (Figure 2D). Risk scores were calculated as follows: Risk Score = (0.458731758 × ALYREF) + (0.208975015 × DNMT1) + (0.462010845 × DNMT3B) + (0.136363177 × EXO1) + (0.219757226 × HNRNPA2B1) + (−0.864908568 × TRDMT1), and the gene coefficient was derived from the results of the LASSO regression analysis. Setting the median risk score of the TCGA cohort as the cutoff value based on equations, all patients could be separated into high- and low-risk PCa recurrence groups. The risk factor association plot depicted the distribution of risk scores, PCa recurrence status, and expression levels of the model genes among patients in the high- and low-risk groups, respectively (Figure 2E). The KM curves revealed that the high-risk group had a significantly worse prognosis than that of the low-risk group ($P < 0.001$) (Figure 2G). In order to measure the efficacy of our prognostic model, ROC curves were employed to evaluate the sensitivity and specificity of the model. The results demonstrated that the area under the curve (AUC) for predicting 1-, 3-, and 5-year RFS were 0.724, 0.739, and 0.711, respectively and the predictive performance of the risk scores was better than other clinicopathological parameters (Figures 2H,I), indicating that the constructed model possessed a favorable predictive capability. To further validate our prognostic model, we applied the approaches mentioned above to the GEO cohort data. After separating patients into diverse risk groups, we discovered that the expression levels of the prognostic genes varied among patients and recurred patients were concentrated in the high-risk group (Figure 2F). The KM curve revealed a satisfactory separation of patients ($P < 0.001$) (Figure 2J). Complementary to this, AUC values of ROC curves were all over 0.700, indicating the superior predictive performance of our prognostic model, and the clinical ROC curve confirmed the reliable predictive capability of the computed risk scores (Figures 2K,L).

3.2 Nomogram based on independent prognostic factors in patients with PCa and correlation between the CARMR signature genes and clinicopathological traits

The nomogram integrated independent prognostic factors which were filtered utilizing a univariate Cox regression analysis, and multiple line segments were displayed in a specific proportion to

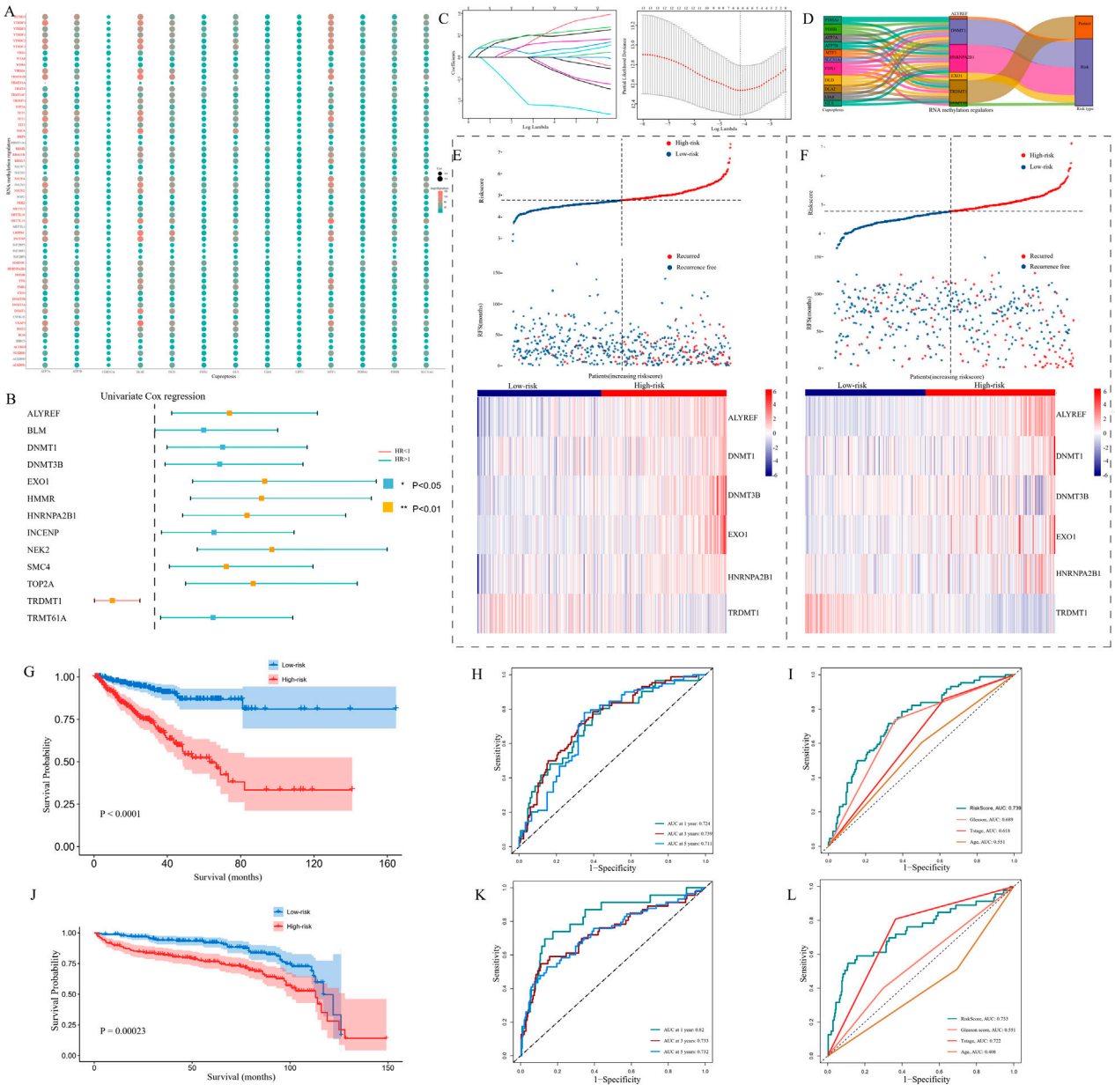

FIGURE 2
The construction and validation of a prognostic model. **(A)** An association between 13 copper death-related genes and 56 RNA methylation regulatory genes is presented by a dot plot. **(B)** Univariate Cox regression analysis results showing that Cuproptosis-Associated RNA Methylation Regulators (CARMRs) were associated with the prognosis of patients with PCa. **(C)** Selection of prognostic CARMRs on the basis of the optimal λ calculated by LASSO regression analysis. **(D)** Sankey diagram revealing the correlation between cuproptosis-related genes and RNA methylation regulatory genes. **(E,F)** Risk maps depicting the distribution of patient status and the expression profiles of prognostic genes in TCGA and GEO cohorts. **(G–I)** KM curve, Time-independent ROC curve, and clinical ROC curve in a TCGA cohort. **(J–L)** Validation of our prognostic model by conducting KM curve, time ROC curve, and clinical ROC curve analyses in a GEO cohort. $^{*}P < 0.05$,$^{**}P < 0.01$,$^{***}P < 0.001$.

quantify the 1-, 3-and 5-year probability of PCa recurrence in patients with PCa (Figure 3A). To evaluate the discriminatory ability of the model, we calculated the C-index for the Gleason score, nomogram, pathological T stage and risk score, which were 0.672, 0.740, 0.613 and 0.719, respectively. These results were displayed as a bar plot and indicated that the nomogram had the highest accuracy in predicting PCa recurrence compared with a single norm (Figure 3B). Additionally, calibration curves demonstrated good consistency between the actual and the predicted RFS. To further analyze the relationship between the recurrence risk score and clinicopathological parameters, we grouped the patients in the TCGA-PRAD cohort according to age, Gleason score, and pathological T stage score (Figures 3C,F,I). The results demonstrated that age, Gleason score and T stage score were positively correlated with the risk of PCa recurrence score ($P < 0.05$). KM curves indicated that the CARMR signature set of genes had predictive value for RFS in different stratified cohorts ($P < 0.05$) (Figures 3D,E,G,H,J,K).

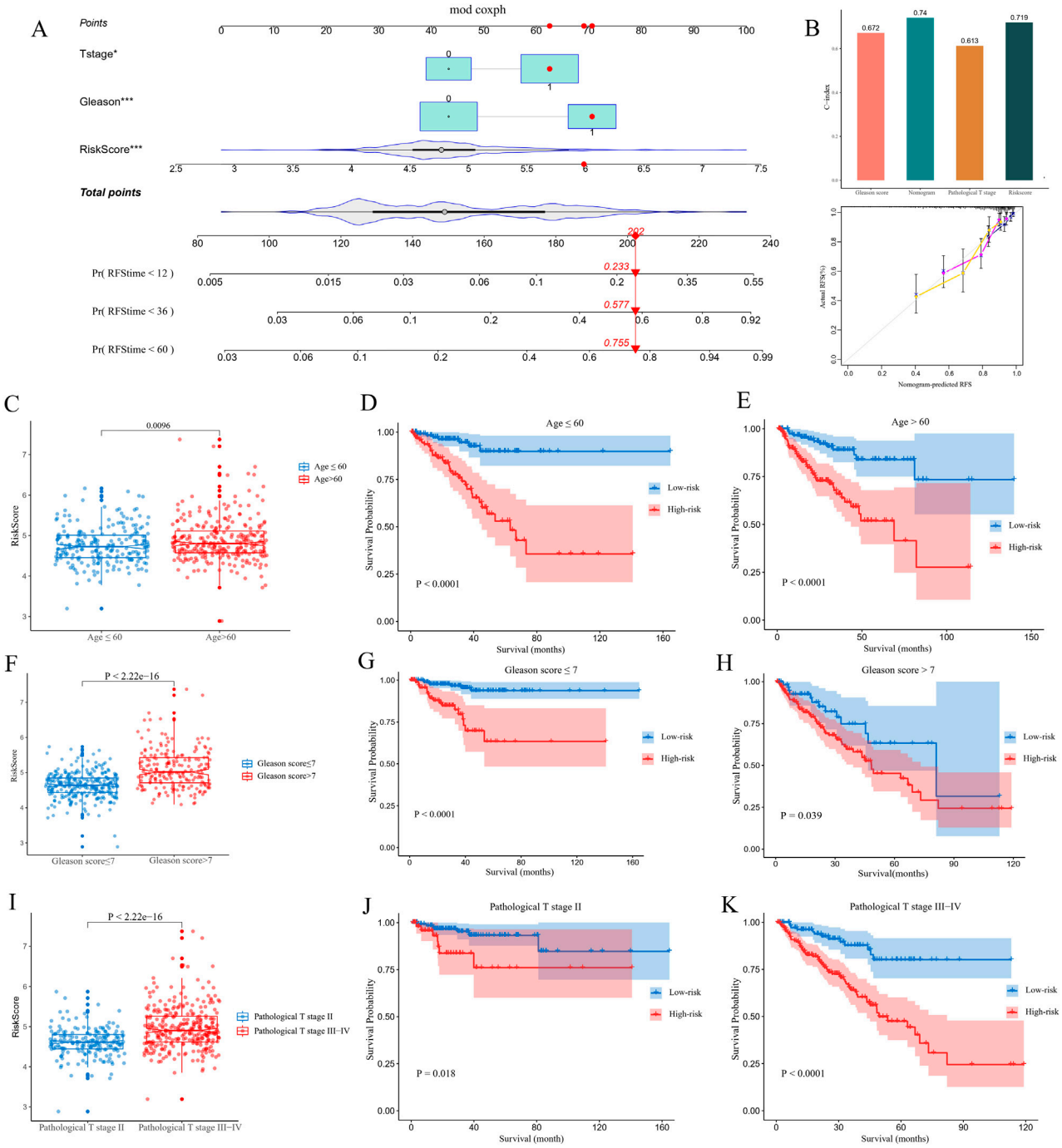

FIGURE 3
Construction of a nomogram and conducting clinicopathological subgroup analysis. **(A)** A nomogram was utilized to predict 1-, 3- and 5-year recurrence-free survival (RFS) values for patients with PCa in a TCGA cohort. **(B)** C-index, calibration curve of nomogram, and other clinicopathological factors were utilized to evaluate the accuracy of the nomogram. **(C,F and I)** Comparisons of risk score differences between various clinicopathological factor subgroups. **(D,E,G,H,J and K)** KM analysis was conducted to identify survival differences between high- and low-risk groups of patients with PCa in different subgroups.

3.3 Functional enrichment analysis and drug sensitivity analysis

An enrichment analysis was conducted on the DEGs between the high- and low-risk groups. The GO analysis results revealed that the enriched biological processes included muscle system processes, muscle organ development, muscle contraction, striated muscle contraction, assembly of muscle fibers, and striated muscle cell development. The enriched cellular components included sarcomeres, muscle fibers, contractile

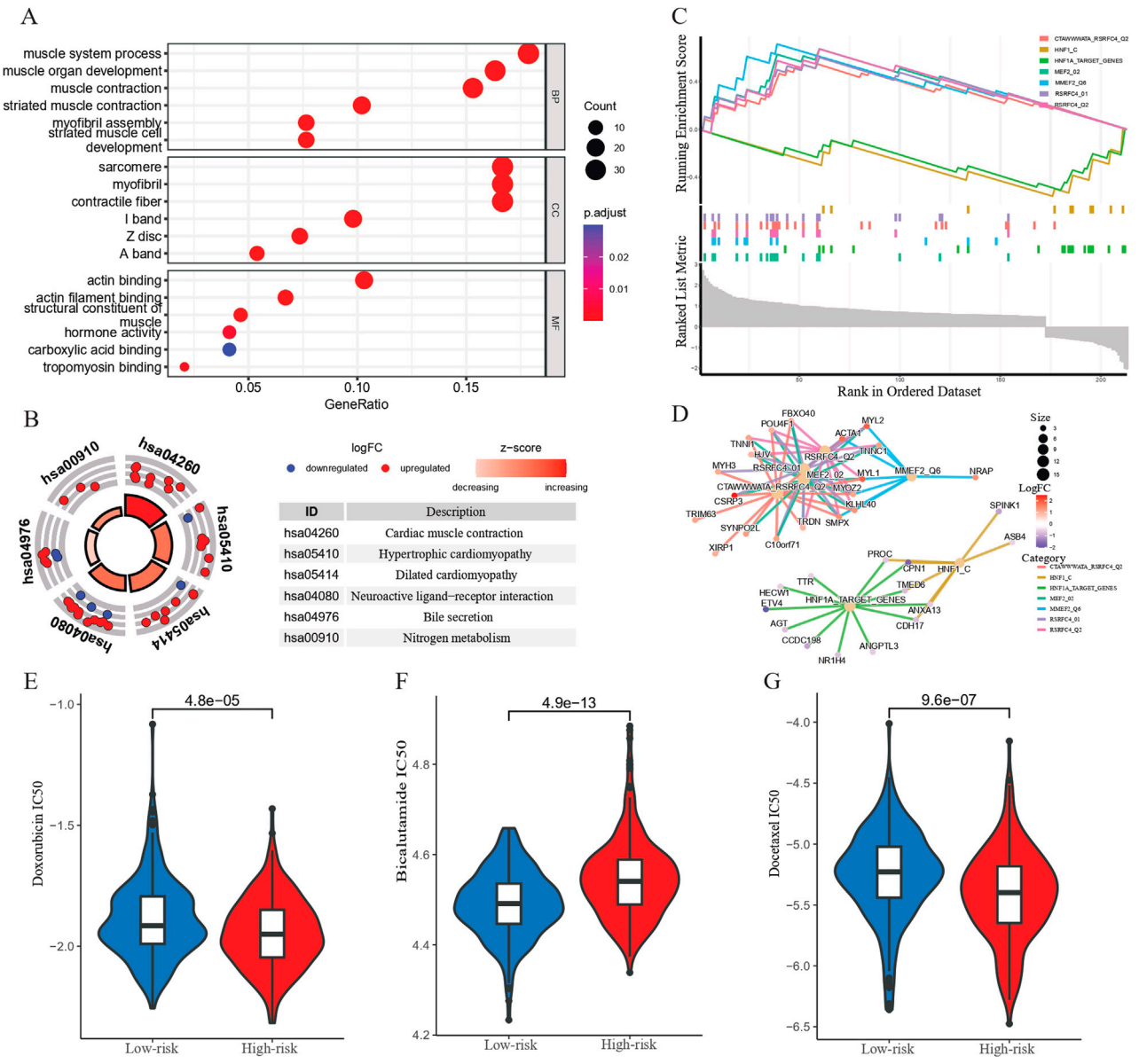

FIGURE 4
Functional enrichment analysis and chemotherapeutic response prediction of prognostic genes. **(A)** GO enrichment analysis of CARMRs. **(B)** KEGG enrichment analysis of CARMRs. **(C)** GSEA of CARMRs. **(D)** The interaction of genes in different enriched pathways. **(E–G)** Predicting the IC_{50} value in high- and low-risk groups of patients with PCa to doxorubicin, bicalutamide and docetaxel therapy.

fibers, M-lines, Z-discs, and A-bands. The molecular functions enriched included actin binding, actin filament binding, muscle structural constituent, hormone activity, carboxylic acid binding, and myosin binding (Figure 4A). KEGG analysis demonstrated that the CARMR signature set of genes was involved in pathways related to cardiac muscle contraction, hypertrophic cardiomyopathy, dilated cardiomyopathy, neuroactive ligand-receptor interaction, bile secretion, nitrogen metabolism, and adrenergic signaling in cardiac myocytes (Figure 4B). The GSEA profile showed that the HNF1_C and HNF1A_TARGET_GENES pathways were downgraded, while other pathways were upgraded (Figure 4C). In addition, the gene interaction network diagram revealed promising interactions among the DEGs enriched in various pathways (Figure 4D).

In order to gain a deeper understanding of the drug response, we performed a drug sensitivity analysis of the high- and low-risk groups of patients with PCa. By comparing the IC_{50} values of chemotherapy drugs for treating PCa, we found that the high-risk group had a higher IC_{50} value for bicalutamide than the low-risk group ($P < 0.001$), whereas the IC_{50} values for doxorubicin and docetaxel were lower for the high-risk group as shown in the boxplot, which implies that the high-risk group showed a higher sensitivity to doxorubicin ($P < 0.001$) and docetaxel ($P < 0.001$) compared to the low-risk group (Figures 4E–G). These results may be used to guide personalized therapy.

3.4 Immune cell infiltration and correlation analysis

A violin plot was generated utilizing the Cibersort algorithm to illustrate the proportions of immune cell infiltration in patients with PCa, and the Wilcoxon test was employed to assess the differences in immune cell populations between the high- and low-risk groups. The types of immune cells exhibiting significant differences between the two groups included plasma cells, T regulatory cells (Tregs), M0 macrophages, M2 macrophages, and resting Mast cells (Figure 5A). Further, the results demonstrated that estimate score (Figure 5B), immune score (Figure 5C) and stromal score (Figure 5D) values were elevated in the high-risk group compared with those in the low-risk group ($P < 0.05$). However, there was no difference between the two risk groups in terms of tumor purity. In addition, utilizing the ssGSEA method, we found that the high-risk group exhibited higher levels of activated $CD4^+$ T cells, activated $CD8^+$ T cells, CD56dim natural killer cells, myeloid-derived suppressor cells (MDSC), memory B cells, nature killer cells and regulatory T cells, whereas it showed a reduction in the levels of activated B cells, immature dendritic cells, mast cells, neutrophils and Type 17 T helper cells (Figure 5E). To delineate the expression profiles of signature genes, we initially investigated the IHC results obtained from the Human Protein Atlas (HPA) dataset, and ascertained the downregulated expression of TRDMT1 and the upregulated expression ALYREF in PCa tissues compared to normal tissues (Figures 5F,H). Furthermore, qPCR assay was employed across a range of diverse cell lines and also demonstrated the decreasing expression trend for TRDMT1 from normal to malignant cells (Figure 5G). Conversely, the expression level of ALYREF exhibited an opposite trend (Figure 5I).

3.5 Distribution of prognostic genes in single-cell landscape

To further explore the expression profiles of prognostic genes in depth, we probed gene expression in PCa tissue at the single-cell level from a GEO dataset (GSE193337). We extracted the scRNA-seq data of four samples from patients with PCa. The baseline characteristics of patients have been described previously (Heidegger et al., 2022). Utilizing stringent data quality control, we extracted 23,697 cells and 17,618 genes to construct a PCa single-cell atlas. To eliminate the batch effect between distinct samples, we applied harmony function and further establish an initial diagram of PCa tissues. The plots before and after batch effect removal were depicted in Supplementary Figures S1A and B. The Seurat software package was employed to reduce the dimensionality of data. We successfully classified the cells into 14 clusters. We utilized recognized cell markers (Heidegger et al., 2022; Kfoury et al., 2021; Ma et al., 2020; Zaidi et al., 2024), and all clusters were annotated as B cells, epithelial cells, endothelial cells, fibroblasts, mast cells, macrophages, monocytes, and T cells (Figures 6A,B). Notably, we discovered that epithelial cells and T cells were the top two abundant cells in the four samples (as shown in the histogram), implying that these cell types figured prominently in the development of PCa (Figure 6C). We investigated the distribution of prognostic genes in all cell types, and discovered that DNMT1, EXO1 and HNRNPA2B1 were primarily distributed in T cells, whereas DNMT3B was detected in endothelial cells (Figures 6D–G). TRDMT1 and ALYREF were both expressed by T cells and epithelial cells (Figures 6H,I). To identify the cell clusters enriched in prognostic genes, we scored individual cells for their prognostic gene signature and found that the prognostic genes were strongly enriched in a subtype of cells within the T-cell cluster compared with other cell types utilizing ANOVA analysis ($P < 0.001$) (Figures 6J,K).

3.6 Intracellular interactions, pseudotime, and function enrichment analysis revealing the role of T cells

Our cell-cell interaction analysis indicated that in terms of interaction numbers and weights, T cells had the strongest correlation with other cell types (Figures 7A,B). We identified several intercellular signaling pathways in seven key epithelial cell clusters (Figure 7C). Based on the analyses of four significant pathways consisting of COLLAGEN, MHC-I, APP and MIF signaling pathways (Supplementary Figures S1C–F), we delineated that T cells exerted predominant impact on the alteration of TME and needed in-depth investigation. In order to further define the potential role of T cells in the tumorigenesis of PCa, we extracted a subset of T cells and further subdivided them into four subtypes including $CD4^+$ conventional T cells (CCR7), $CD4^+$ regulatory T cells (FOXP3), $CD8^+$ naïve T cells (LAG3), and $CD8^+$ effector T cells (GZMA) based on conventional cell markers (Figure 7D) (Guo et al., 2018; Bian et al., 2024; Tuong et al., 2021). We modeled the developmental trajectory of cells by conducting pseudotime analysis. Cell trajectory profiles showed that T cells underwent evolutionary development (Figure 7E). We observed that $CD4^+$ conventional T cells and $CD8^+$ naïve T cells were gradually transformed into $CD4^+$ regulatory T cells and $CD8^+$ effector T cells (Figure 7F).

To explore the biological function of T cells in patients with PCa, we conducted GO, KEGG and GSEA-based gene enrichment analyses. First, GO analysis revealed the role of the enriched genes in biological processes, cellular components and molecular functions, respectively. We discovered that T cells primarily played a role in the regulation of cell-cell adhesion, mononuclear cell differentiation, lymphocyte differentiation, positive regulation of cytokine production, leukocyte cell–cell adhesion, external side of plasma membrane, actin binding, GTPase regulator activity, and nucleoside-triphosphatase regulator activity (Figure 7G). Additionally, KEGG analysis indicated that biological processes, such as human T-cell leukemia virus 1 infection, Epstein-Barr virus infection, T cell receptor signaling pathway, natural killer cell-mediated cytotoxicity, human immunodeficiency virus 1 infection, and human cytomegalovirus infection were correlated with T cells (Figure 7H). Finally, we discovered that CIITA_TARGET_GENES, HSF2_TARGET_GENES, KLF3_TARGET_GENES and MORC2_TARGET_GENES pathways were downgraded in PCa, based on the GSEA results (Figure 7I).

4 Discussion

Due to the failures of post-prostatectomy and radiotherapy in curing recurrent and locally advanced PCa, it is reasonable to attach great importance to novel immunotherapy (Sokoloff et al., 2004). Having previously shown that checkpoint inhibitors could bring

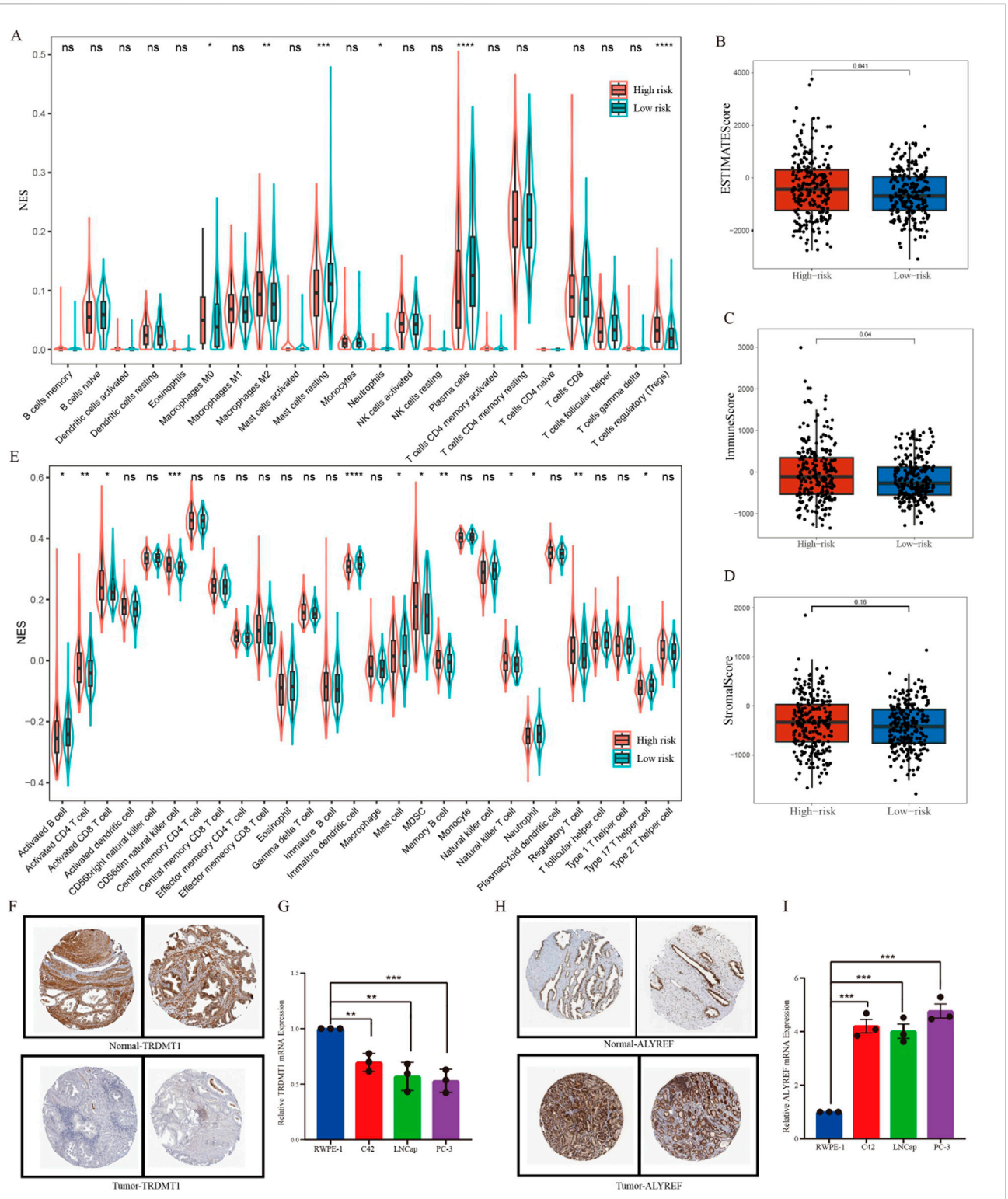

FIGURE 5
Immune cell infiltration analysis. **(A)** The differences in the enrichment scores of 22 types of immune cells between two risk subgroups. **(B–D)** Comparisons of the differences between two risk subgroups in terms of estimate score, immune score, and stromal score. **(E)** A violin chart showing the differences in the proportions of 28 immune cells between high-risk and low-risk groups of patients with prostate cancer. **(F)** Representative pictures showing the different protein levels of TRDMT1 from HPA. **(G)** Expression of TRDMT1 in normal prostate cell and prostate cancer cells. **(H)** Representative pictures showing the different protein levels of ALYREF from HPA. **(I)** Expression of ALYREF in normal prostate cell and prostate cancer cells. $^{*}P < 0.05$,$^{**}P < 0.01$,$^{***}P < 0.001$.

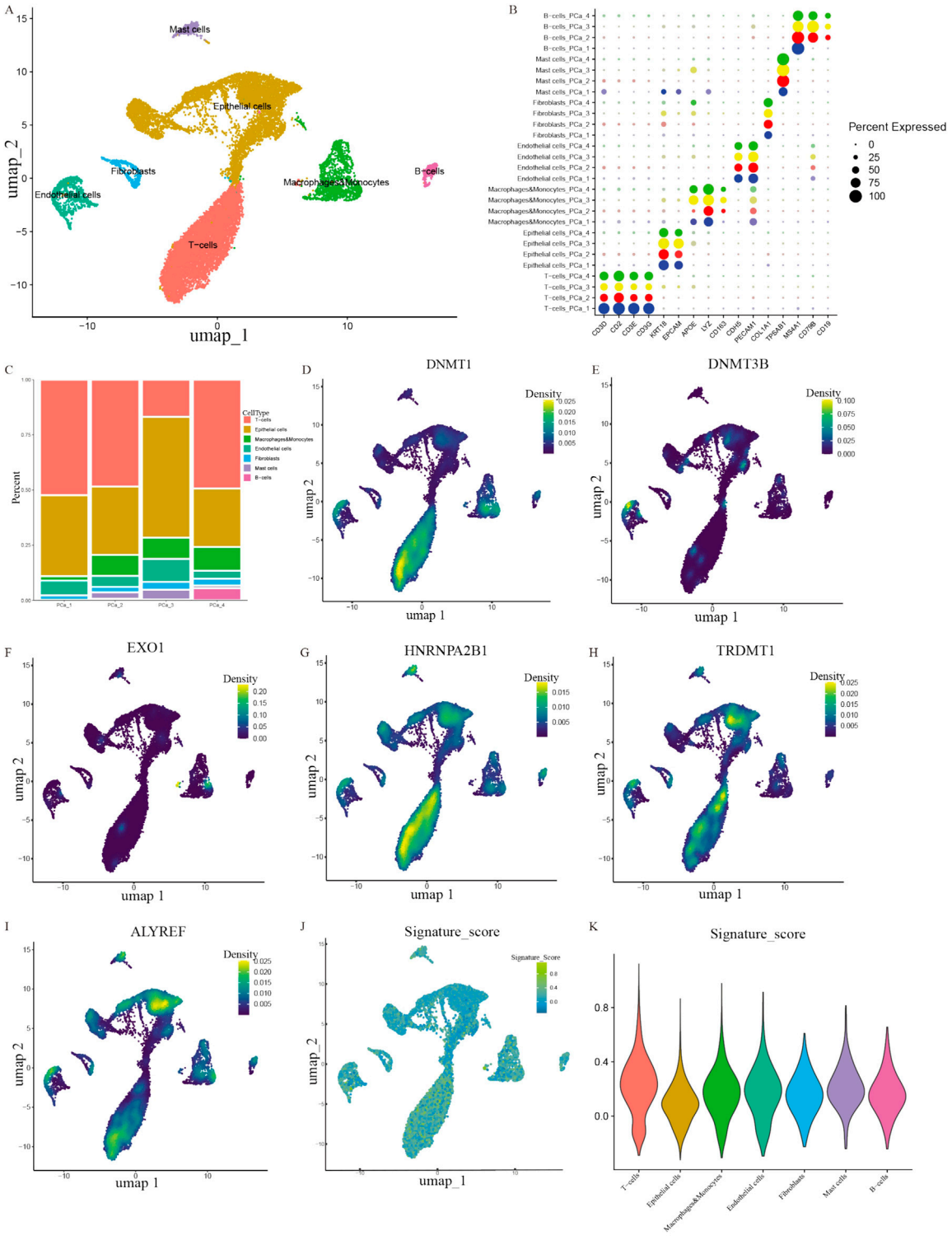

FIGURE 6
Exploring the distribution of prognostic genes. **(A)** A plot of the different types of cells. **(B)** A bubble plot of the expression of diagnostic marker genes in each cell cluster. **(C)** Cell proportions in four PCa samples. **(D–I)** The distribution of prognostic genes in different clusters. **(J–K)** UMAP map and violin plot indicating the enrichment of gene signatures in PCa tissues.

favorable healing efficacy for patients with PCa, we have now explored a signature set of CARMR genes for anticipating the prognosis and drug response of patients with PCa in this report (Vietri et al., 2021; Pritchard et al., 2016). Additionally, cell death may maintain the balance through removing tumor cells, and this cell function was defective in metastatic and castration-resistant advanced PCa (Campbell and Leung, 2021; Zhu M. et al., 2023). Cuproptosis, as a newly discovered form of cell death, differs from

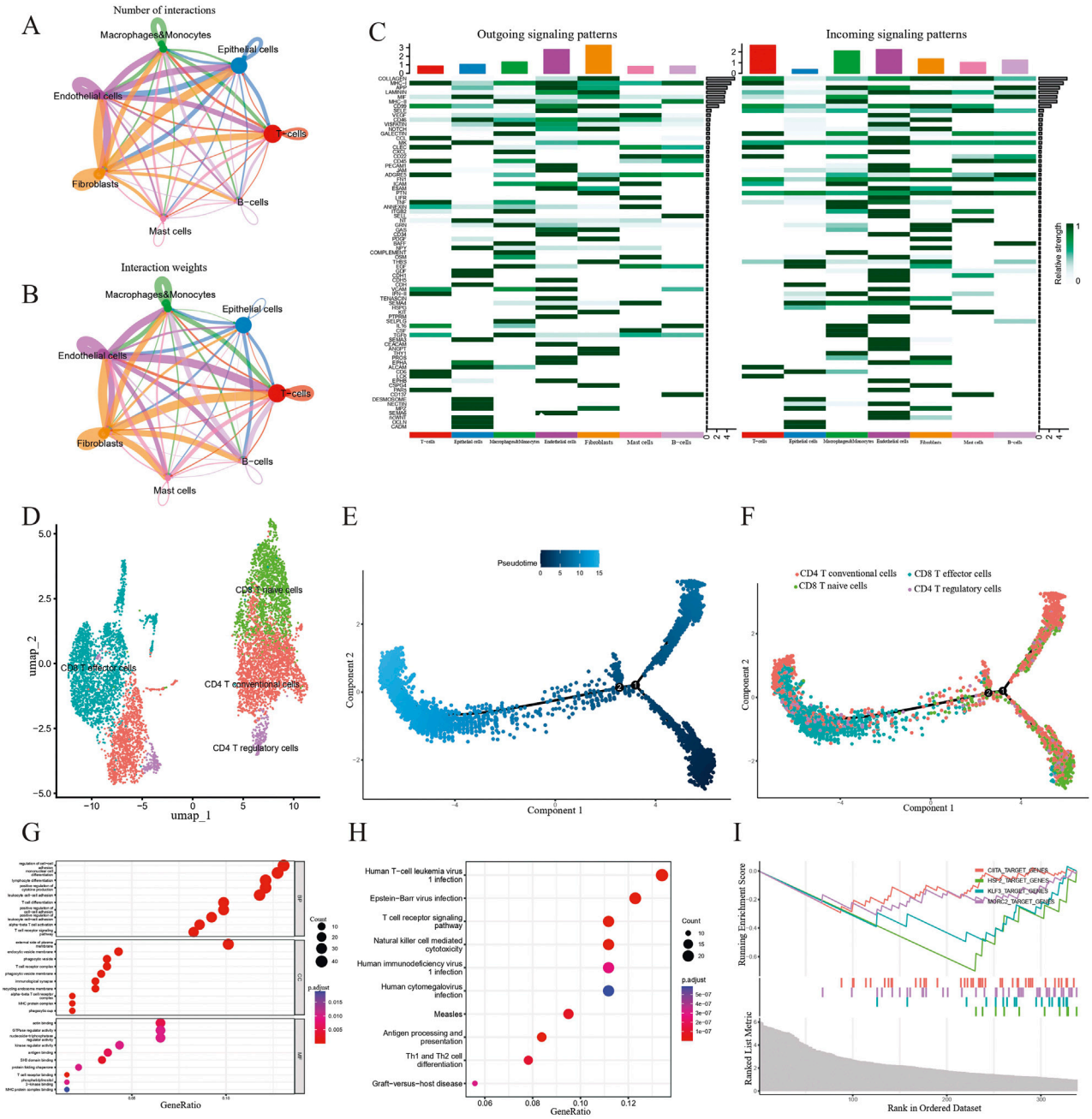

FIGURE 7
Investigating the role of T cells in the development of PCa. **(A and B)** Cell-cell communication analysis in terms of weighted interactions. **(C)** A heatmap showing signaling pathways in seven clusters. **(D)** Subgroups of T cell clusters depicted *via* a UMAP map. **(E)** Displaying the beginnings and endings of pseudo-time trajectories. The colors from dark to light represent the order of pseudo-time. **(F)** Pseudo-time analysis revealing the transition from CD4$^+$ T conventional cells and CD8$^+$ T naive cells to CD8$^+$ T effector cells and CD4$^+$ T regulatory cells. **(G–I)** GO, KEGG enrichment analysis and GSEA indicating the potential function of T cell-related genes.

other cell death modalities in its reliance on mitochondrial respiration (Tsvetkov et al., 2022). Meanwhile, growing evidence suggests that RNA-based epigenetic pathways are dysregulated in human diseases and may be ideal targets for cancer treatment (Barbieri and Kouzarides, 2020). In this research scenario, we investigated the potential connection between CARMRs and PCa.

First, we conducted univariate Cox regression and Lasso regression analyses to screen for RFS-related CARMRs and established a model to better predict prognosis and guide the stratified treatment of patients with PCa. An ROC curve was generated to validate the robust prognostic accuracy of the model. Ultimately, six CARMRs (ALYREF, DNMT1, DNMT3B, EXO1, HNRNPA2B1, TRDMT1) were included in our analysis to establish a prognostic model for estimating the risk of PCa recurrence. By reviewing previous studies, we discovered that prognostic genes played a key role in the tumorigenesis and

TABLE 3 The biological functions and potential roles of CARMRs.

Gene name	Main function	Signaling pathways	Role in prostate cancer progression
ALYREF	Involved in mRNA export from the nucleus	CDK13/NSUN5/ACC1 pathway	inducing
DNMT1	Maintains DNA methylation patterns during DNA replication	PI3K-Akt signaling pathway	inducing
DNMT3B	Responsible for *de novo* DNA methylation	PI3K-Akt signaling pathway	inducing
EXO1	Involved in DNA repair, particularly in the 5′ to 3′ exonuclease activity	P53 signaling pathway	inducing
HNRNPA2B1	Involving in mRNA processing and transport	TGF-β and FOXO pathways	inducing
TRDMT1	Catalyzes the methylation of tRNAs	—	inducing

advancement of PCa. Initially, ALYREF is determined to function as a reader of the 5-methylcytosine modification, playing a crucial role in stabilizing the associated mRNA and modulating its expression at the post-transcription level, thereby involving in cellular metabolism and movement (Zhang et al., 2021; Zhao et al., 2024b; Nulali et al., 2024). Building on a prior study, we propose a hypothesis that ALYREF may interact with the 5-methylcytosine modification on ACC1 mRNA and trigger the proliferation and lipid synthesis of PCa cells through activating the CDK13/NSUN5/ACC1 pathway (Zhang Y. et al., 2023). The DNMT3 gene family includes DNMT3A and DNMT3B, which are capable of methylating CpG sites and stably maintaining methylation patterns (Chen et al., 2003). By interacting with PI3K-Akt signaling pathway, DNMT3B and DNMT1 effectively silence the expression of tumor suppressor gene by increasing methylation levels and facilitate the malignant transformation of PCa cells (Agarwal et al., 2013; Zhu et al., 2021). EOX1 regulates the reprogramming of lipid metabolism by suppressing the P53 signaling pathway and promotes the progression of PCa (Wang et al., 2024). Moreover, distinct from other CARMRs, HNRNPA2B1 assumes a pivotal role in N6-methyladenosine methylation to regulate the TGF-β and FOXO pathways, influencing the phenotype of PCa and its response to conventional treatment (Qi et al., 2023; Liyanage et al., 2024). Consequently, CARMRs appear to modulate metabolism by amplifying the function of specific mRNAs, thereby modifying the phenotype of PCa. The summary of biological functions of the CARMRs were listed in Table 3.

We carried out univariate Cox regression analysis to explore the role of clinicopathological parameters in the prognosis of PCa and our results showed the prognostic value of age, Gleason score, and pathological T stage and a correlation with risk score. We integrated all the factors to ascertain the status and advancement of this disease. We employed gene functional enrichment analysis to identify the potential functions of CARMRs in PCa: our data showed that CARMRs were correlated with muscle organ development and muscle fiber movement. Previous studies have shown that ADT treatment for PCa may lead to muscle atrophy and weakness through reducing Ca^{2+}-sensitivity in Type I and II muscle fibers (Lamboley et al., 2018). Conversely, the organism of PCa patients tended to add the abundance and contraction ability of skeletal muscle to positively regulate the TME (Rocha-Rodrigues et al., 2021). Except for the adaptive regulatory, muscle cells produced more interleukins 4 and 13 for the growth of cancer stem cells and their interaction was essential for the cancer cell fusion and the generation of drug-sensitive phenotype (Uygur et al., 2019). Moreover, other studies have shown that cardiac and skeletal muscle mass is reduced in the absence of anti-cancer treatment (Baumfalk et al., 2019; Rollins et al., 2017). In this case, it is possible that tumor cells fuse together, inducing higher cytokine production from adjacent skeletal muscle cells and generate a metastatic phenotype by increasing myosin content. Besides, cardiac and skeletal muscle cells in other regions were consumed accordingly. Our point of view may be validated if there is evidence that the myosin expression profile in PCa influences the formation of a metastatic phenotype (Makowska et al., 2015). The evaluation of chemotherapy drugs indicated that doxorubicin and docetaxel were more effective when applied to patients with a high-risk of PCa recurrence. Studies have also demonstrated that doxorubicin and docetaxel exhibit anti-tumor activity in metastatic PCa (Petrioli et al., 2008; Fizazi et al., 2022).

It is well-established that immune responses play a dominant role in tumor development and anti-tumor therapy. To guide immunotherapy of patients with PCa, we investigated the immune infiltration in PCa tissue (Hawley et al., 2023). As key components of TME, immune cells and stromal cells are significantly correlated with immune therapy and prognosis of PCa. From the results of our study, the high-risk group exhibited increased abundance of M0 macrophages, M2 macrophages, and Tregs, and a significant reduction in plasma cells and mast cells. M0 macrophages are a plastic cell population that can change their phenotype under the influence of environmental signals such as radiation injury, potentially transitioning to tumor-associated macrophages (TAMs) (Qiu et al., 2018). TAMs are known to impact tumor progression through cell proliferation, angiogenesis, adaptive immune control, and metastasis, making them an attractive therapeutic target in PCa immune therapy (Jairath et al., 2020). To be specific, circSMARCC1 could activate the miR-1322/CCL20/CCR6 signaling pathway and induce the proliferation of TAMs to impact tumorigenesis (Xie et al., 2022). M2 macrophages may be polarized to influence metastasis and excessive proliferation of PCa cells *via* the IL17/CTSK/EMT axis (Wu et al., 2022). Referring to previous studies, Tregs have been shown to inhibit TME in various cancers, and to induce bone metastasis in PCa, which portends a poor prognosis (Liu et al., 2023; Meng et al., 2021; Alvisi et al., 2022; Boucher et al., 2023). Tregs are known to utilize the GIT/PAK/PIX complex to downgrade the anti-tumor response (Pedros et al., 2017). Clinical analysis has also corroborated the positive correlation between patient mortality

rate and the degree of M2 macrophage and Tregs infiltration (Erlandsson et al., 2019). In conclusion, we reasoned that the study of TME may provide new ideas for regulating the immune status of tumor tissues, inhibiting tumor growth, and achieving a better prognosis.

To some extent, IC_{50} values had the capacity to characterize the natural response of PCa cells to chemotherapy agents (Xu et al., 2022). Our drug sensitivity analysis showed that doxorubicin and docetaxel may achieve better healing efficacy when applied to high-risk PCa subgroups. In an animal experiment, docetaxel was confirmed to remodel TME and enhance lymphocyte infiltration through activating the cGAS/STING pathway in PCa (Ma et al., 2022). Additionally, by conducting clinical trials, we found that doxorubicin and docetaxel combined with epirubicin demonstrated favorable efficacy in patients with advanced hormone-refractory PCa (Petrioli et al., 2008; Tannock et al., 2004; Petrylak et al., 2004). ALYRFE, functioning as a binding protein, can participate in diverse regulatory mechanisms, consisting of pre-mRNA processing, mRNA stability and mRNA methylation and facilitate the emergence of malignant phenotypes and the development of drug resistance (Zhao Y. et al., 2024; Zhong et al., 2024). Furthermore, across various tumor types, it has been observed that the increased transformation of ALYRFE into the nucleus leads to the elevated levels of 5-methylcytosine methylation, thereby promoting the drug resistance through the activation of a distinct molecular pathways (Shi et al., 2025; Huang et al., 2025; Xu et al., 2020). Similarly, TRDMT1 is capable of methylate both tRNA and mRNA, thereby promoting the stability of RNA and enhancing protein synthesis (Lewinska et al., 2023). An increase in expression of TRDMT1 and corresponding methylation levels results in the heightened resistance observed in multiple cancer cells (Lewińska et al., 2022; Lai et al., 2025). Conclusively, the CARMRs contribute to the therapeutic failure through enhancing the methylation levels. Furthermore, these findings may offer novel perspectives for addressing resistance issues in advanced PCa, potentially leading to the development of more effective treatment strategies.

We explored the relationship between prognostic genes and TME at the single-cell level. Our findings showed that most of the enriched genes were expressed in epithelial cells and T cells, which constitute the majority of tumor tissue and play an important role in the progression of PCa. The analysis of cell-cell interactions illustrated the strong interactions between T cells and others, which indicated that the heterogeneity of T cells could guide immunotherapy and determine patient prognosis. We subdivided T cells and modeled the developmental trajectory of T cells. $CD8^+$ T effector cells and $CD4^+$ T regulatory cells evolved from $CD4^+$ T conventional cells and $CD8^+$ T naïve cells. Therefore, we hypothesized that the expression of prognostic genes may promote the transition to $CD4^+$ T regulatory cells and contribute to the poor prognosis. According to the results of our functional enrichment analysis, prognostic genes may be crucial in the differentiation of immune cells. Referring to other studies, we acknowledge that immune cell differentiation may cause immunosuppressive phenotypes. When monocytes transform to dendritic cells *via* tumor stroma-derived factors, the expression of CD14 and PD-L1 may elevate and hinder the destruction of immune cells in PCa (Spary et al., 2014). Alternatively, inhibiting the differentiation of MDSC and enhancing the proliferation of T cells may reverse its immune phenotype (Peng et al., 2022). Further, we noticed that target genes comprising CIITA, HSF2, KLF3 and MORC2 are strongly linked with RNA methylation (Mishra et al., 2010; Zhu J. et al., 2023; Tan et al., 2023; Chen F. et al., 2021). Of note, HSF2 impacts cell-cell adhesion and is positively correlated with a favorable prognosis (Björk et al., 2016). These observations are consistent with our GSEA results. Our current findings show that CARMRs may reshape TME by affecting the differentiation of immune cells. Eventually, this leads to enhancement of an invasive phenotype in PCa.

However, our study has some limitations. First, our analysis was based on a secondary analysis of public database data. These retrospective data were subject to selection biases, and this may have affected the accuracy of our analytical results. Additionally, there was a lack of a sufficient number of PCa samples to validate the applicability of the model, and the specific mechanisms by which the model genes may regulate PCa development remain elusive. Selection and sample biases may have been generated in our study since the clinical samples were selected from variously sourced datasets. Therefore, further *in vitro* and *in vivo* experimentation is needed to validate our results. Utilizing cell line experimentation, we would be able to compare the expression of prognostic genes of different invasive capacities in PCa cells to support our results.

5 Conclusion

To summarize, we have identified a correlation between RNA methylation and cuproptosis and were able to select six CARMRs to construct a risk stratification model for patients with PCa. Additionally, the relationship between TME and risk subgroups was analyzed by integrating single cell and bulk sequencing data to enable individualized immunotherapy. Through an in-depth investigation, we believe that our study has revealed a potential mechanism of PCa tumorigenesis that will support a higher efficacy therapeutic program.

Data availability statement

The original contributions presented in the study are included in the article/Supplementary Material, further inquiries can be directed to the corresponding authors.

Author contributions

JW: Conceptualization, Data curation, Resources, Software, Writing–original draft. WW: Formal Analysis, Investigation, Methodology, Writing–original draft. JQ: Resources, Software, Supervision, Validation, Writing–review and editing. ZC: Formal Analysis, Investigation, Methodology, Writing–original draft. RZ: Writing–review and editing, Resources, Validation. PG: Funding acquisition, Resources, Writing–review and editing, Methodology, Software, Validation. SF: Funding acquisition, Resources, Writing–review and editing, Conceptualization, Formal Analysis, Investigation, Project administration.

Funding

The author(s) declare that financial support was received for the research and/or publication of this article. This work was supported by the Natural Science Foundation of Anhui Province (2208085MH208), the Key Research and Development Program of Anhui Province (2022e07020037) and the Scientific Research and Practical Innovation Project of Postgraduates of Anhui Medical University (YJS20230188).

Conflict of interest

The authors declare that the research was conducted in the absence of any commercial or financial relationships that could be construed as a potential conflict of interest.

Generative AI statement

The author(s) declare that no Generative AI was used in the creation of this manuscript.

Publisher's note

Supplementary material

The Supplementary Material for this article can be found online at: https://www.frontiersin.org/articles/10.3389/fphar.2025.1573611/full#supplementary-material

SUPPLEMENTARY FIGURE S1
Integrating single-cell data of PCa cells, intercellular communication analysis and the alteration of genes in pseudotime analysis. **(A-B)** The single-cell atlas of PCa before and after harmony processes. **(C-F)** Heatmaps depicting the network centrality scores and potential roles of the top four signaling. **(G)** Heatmaps manifesting the expression of differentially expressed genes (DEGs) with the timing changes.

References

Agarwal, S., Amin, K. S., Jagadeesh, S., Baishay, G., Rao, P. G., Barua, N. C., et al. (2013). Mahanine restores RASSF1A expression by down-regulating DNMT1 and DNMT3B in prostate cancer cells. *Mol. cancer* 12 (1), 99. doi:10.1186/1476-4598-12-99

Alvisi, G., Termanini, A., Soldani, C., Portale, F., Carriero, R., Pilipow, K., et al. (2022). Multimodal single-cell profiling of intrahepatic cholangiocarcinoma defines hyperactivated Tregs as a potential therapeutic target. *J. Hepatol.* 77 (5), 1359–1372. doi:10.1016/j.jhep.2022.05.043

An, Y., and Duan, H. (2022). The role of m6A RNA methylation in cancer metabolism. *Mol. cancer* 21 (1), 14. doi:10.1186/s12943-022-01500-4

Bach, C., Pisipati, S., Daneshwar, D., Wright, M., Rowe, E., Gillatt, D., et al. (2014). The status of surgery in the management of high-risk prostate cancer. *Nat. Rev. Urol.* 11 (6), 342–351. doi:10.1038/nrurol.2014.100

Barbieri, I., and Kouzarides, T. (2020). Role of RNA modifications in cancer. *Nat. Rev. Cancer* 20 (6), 303–322. doi:10.1038/s41568-020-0253-2

Barros-Silva, D., Lobo, J., Guimarães-Teixeira, C., Carneiro, I., Oliveira, J., Martens-Uzunova, E. S., et al. (2020). VIRMA-dependent N6-methyladenosine modifications regulate the expression of long non-coding RNAs CCAT1 and CCAT2 in prostate cancer. *Cancers (Basel)* 12 (4), 771. doi:10.3390/cancers12040771

Baumfalk, D. R., Opoku-Acheampong, A. B., Caldwell, J. T., Ade, C. J., Copp, S. W., Musch, T. I., et al. (2019). Effects of prostate cancer and exercise training on left ventricular function and cardiac and skeletal muscle mass. *J. Appl. Physiol.* 126 (3), 668–680. doi:10.1152/japplphysiol.00829.2018

Bian, X., Wang, W., Abudurexiti, M., Zhang, X., Ma, W., Shi, G., et al. (2024). Integration analysis of single-cell multi-omics reveals prostate cancer heterogeneity. *Adv. Sci.* 11 (18), e2305724. doi:10.1002/advs.202305724

Björk, J. K., Åkerfelt, M., Joutsen, J., Puustinen, M. C., Cheng, F., Sistonen, L., et al. (2016). Heat-shock factor 2 is a suppressor of prostate cancer invasion. *Oncogene* 35 (14), 1770–1784. doi:10.1038/onc.2015.241

Boucher, Y., Posada, J. M., Subudhi, S., Kumar, A. S., Rosario, S. R., Gu, L., et al. (2023). Addition of losartan to FOLFIRINOX and chemoradiation reduces immunosuppression-associated genes, Tregs, and FOXP3^{+} cancer cells in locally advanced pancreatic cancer. *Clin. Cancer Res.* 29 (8), 1605–1619. doi:10.1158/1078-0432.CCR-22-1630

Campbell, K. J., and Leung, H. Y. (2021). Evasion of cell death: a contributory factor in prostate cancer development and treatment resistance. *Cancer Lett.* 520, 213–221. doi:10.1016/j.canlet.2021.07.045

Chen, F., Fan, Y., Liu, X., Zhang, J., Shang, Y., Zhang, B., et al. (2021b). Pan-cancer integrated analysis of HSF2 expression, prognostic value and potential implications for cancer immunity. *Front. Mol. Biosci.* 8, 789703. doi:10.3389/fmolb.2021.789703

Chen, L., Min, J., and Wang, F. (2022). Copper homeostasis and cuproptosis in health and disease. *Signal Transduct. Target. Ther.* 7 (1), 378. doi:10.1038/s41392-022-01229-y

Chen, T., Ueda, Y., Dodge, J. E., Wang, Z., and Li, E. (2003). Establishment and maintenance of genomic methylation patterns in mouse embryonic stem cells by Dnmt3a and Dnmt3b. *Mol. Cell. Biol.* 23 (16), 5594–5605. doi:10.1128/mcb.23.16.5594-5605.2003

Chen, X. Y., Zhang, J., and Zhu, J. S. (2019). The role of m(6)A RNA methylation in human cancer. *Mol. cancer* 18 (1), 103. doi:10.1186/s12943-019-1033-z

Chen, Y. S., Yang, W. L., Zhao, Y. L., and Yang, Y. G. (2021a). Dynamic transcriptomic ^{m5C} and its regulatory role in RNA processing. *Wiley Interdiscip. Rev. RNA.* 12 (4), e1639. doi:10.1002/wrna.1639

Craven, K. E., Gökmen-Polar, Y., and Badve, S. S. (2021). CIBERSORT analysis of TCGA and METABRIC identifies subgroups with better outcomes in triple negative breast cancer. *Sci. Rep.* 11 (1), 4691. doi:10.1038/s41598-021-83913-7

Ding, L., Wang, R., Zheng, Q., Shen, D., Wang, H., Lu, Z., et al. (2022). circPDE5A regulates prostate cancer metastasis via controlling WTAP-dependent N6-methyladenisine methylation of EIF3C mRNA. *J. Exp. Clin. Cancer Res.* 41 (1), 187. doi:10.1186/s13046-022-02391-5

Erlandsson, A., Carlsson, J., Lundholm, M., Fält, A., Andersson, S. O., Andrén, O., et al. (2019). M2 macrophages and regulatory T cells in lethal prostate cancer. *Prostate* 79 (4), 363–369. doi:10.1002/pros.23742

Fizazi, K., Foulon, S., Carles, J., Roubaud, G., McDermott, R., Fléchon, A., et al. (2022). Abiraterone plus prednisone added to androgen deprivation therapy and docetaxel in *de novo* metastatic castration-sensitive prostate cancer (PEACE-1): a multicentre, open-label, randomised, phase 3 study with a 2 × 2 factorial design. *Lancet* 399 (10336), 1695–1707. doi:10.1016/S0140-6736(22)00367-1

Gao, X., Zhao, H., Liu, J., Wang, M., Dai, Z., Hao, W., et al. (2024). Enzalutamide sensitizes castration-resistant prostate cancer to copper-mediated cell death. *Adv. Sci.* 11 (30), e2401396. doi:10.1002/advs.202401396

Guo, X., Zhang, Y., Zheng, L., Zheng, C., Song, J., Zhang, Q., et al. (2018). Global characterization of T cells in non-small-cell lung cancer by single-cell sequencing. *Nat. Med.* 24 (7), 978–985. doi:10.1038/s41591-018-0045-3

Gupte, A., and Mumper, R. J. (2009). Elevated copper and oxidative stress in cancer cells as a target for cancer treatment. *Cancer Treat. Rev.* 35 (1), 32–46. doi:10.1016/j.ctrv.2008.07.004

Haigh, D. B., Woodcock, C. L., Lothion-Roy, J., Harris, A. E., Metzler, V. M., Persson, J. L., et al. (2022). The METTL3 RNA methyltransferase regulates transcriptional networks in prostate cancer. *Cancers (Basel)* 14 (20), 5148. doi:10.3390/cancers14205148

Hawley, J. E., Obradovic, A. Z., Dallos, M. C., Lim, E. A., Runcie, K., Ager, C. R., et al. (2023). Anti-PD-1 immunotherapy with androgen deprivation therapy induces robust immune infiltration in metastatic castration-sensitive prostate cancer. *Cancer Cell* 41 (11), 1972–1988.e5. doi:10.1016/j.ccell.2023.10.006

He, R., Man, C., Huang, J., He, L., Wang, X., Lang, Y., et al. (2022). Identification of RNA methylation-related lncRNAs signature for predicting hot and cold tumors and prognosis in colon cancer. *Front. Genet.* 13, 870945. doi:10.3389/fgene.2022.870945

Heidegger, I., Fotakis, G., Offermann, A., Goveia, J., Daum, S., Salcher, S., et al. (2022). Comprehensive characterization of the prostate tumor microenvironment identifies CXCR4/CXCL12 crosstalk as a novel antiangiogenic therapeutic target in prostate cancer. *Mol. Cancer* 21 (1), 132. doi:10.1186/s12943-022-01597-7

Huang, S., Shi, D., Dai, S., Jiang, X., Wang, R., Yang, M., et al. (2025). RNF31 induces paclitaxel resistance by sustaining ALYREF cytoplasmic-nuclear shuttling in human triple-negative breast cancer. *Clin. Transl. Med.* 15 (2), e70203. doi:10.1002/ctm2.70203

Jain, S., Lyons, C. A., Walker, S. M., McQuaid, S., Hynes, S. O., Mitchell, D. M., et al. (2018). Validation of a Metastatic Assay using biopsies to improve risk stratification in patients with prostate cancer treated with radical radiation therapy. *Ann. Oncol.* 29 (1), 215–222. doi:10.1093/annonc/mdx637

Jairath, N. K., Farha, M. W., Srinivasan, S., Jairath, R., Green, M. D., Dess, R. T., et al. (2020). Tumor immune microenvironment clusters in localized prostate adenocarcinoma: prognostic impact of macrophage enriched/plasma cell non-enriched subtypes. *J. Clin. Med.* 9 (6), 1973. doi:10.3390/jcm9061973

Kench, J. G., Amin, M. B., Berney, D. M., Compérat, E. M., Cree, I. A., Gill, A. J., et al. (2022). WHOClassification of Tumours fifth edition: evolving issues in the classification, diagnosis, and prognostication of prostate cancer. *Histopathology* 81 (4), 447–458. doi:10.1111/his.14711

Kfoury, Y., Baryawno, N., Severe, N., Mei, S., Gustafsson, K., Hirz, T., et al. (2021). Human prostate cancer bone metastases have an actionable immunosuppressive microenvironment. *Cancer Cell* 39 (11), 1464–1478.e8. doi:10.1016/j.ccell.2021.09.005

Lai, J., Chen, L., Li, Q., Zhao, G., Li, X., Guo, D., et al. (2025). tRNA methyltransferase DNMT2 promotes hepatocellular carcinoma progression and enhances Bortezomib resistance through inhibiting TNFSF10. *Cell. Signal.* 127, 111533. doi:10.1016/j.cellsig.2024.111533

Lamboley, C. R., Xu, H., Dutka, T. L., Hanson, E. D., Hayes, A., Violet, J. A., et al. (2018). Effect of androgen deprivation therapy on the contractile properties of type I and type II skeletal muscle fibres in men with non-metastatic prostate cancer. *Clin. Exp. Pharmacol. Physiol.* 45 (2), 146–154. doi:10.1111/1440-1681.12873

Leek, J. T., Johnson, W. E., Parker, H. S., Jaffe, A. E., and Storey, J. D. (2012). The sva package for removing batch effects and other unwanted variation in high-throughput experiments. *Bioinformatics* 28 (6), 882–883. doi:10.1093/bioinformatics/bts034

Lewinska, A., Adamczyk-Grochala, J., and Wnuk, M. (2023). TRDMT1-mediated RNA C-5 methylation as a novel target in anticancer therapy. *Biochimica Biophys. Acta Rev. Cancer* 1878 (6), 188964. doi:10.1016/j.bbcan.2023.188964

Lewińska, A., Wróbel, K., Błoniarz, D., Adamczyk-Grochala, J., Wołowiec, S., and Wnuk, M. (2022). Lapatinib- and fulvestrant-PAMAM dendrimer conjugates promote apoptosis in chemotherapy-induced senescent breast cancer cells with different receptor status. *Biomater. Adv.* 140, 213047. doi:10.1016/j.bioadv.2022.213047

Li, D., Shi, Z., Liu, X., Jin, S., Chen, P., Zhang, Y., et al. (2023). Identification and development of a novel risk model based on cuproptosis-associated RNA methylation regulators for predicting prognosis and characterizing immune status in hepatocellular carcinoma. *Hepatol. Int.* 17 (1), 112–130. doi:10.1007/s12072-022-10460-2

Li, J., Xie, H., Ying, Y., Chen, H., Yan, H., He, L., et al. (2020). YTHDF2 mediates the mRNA degradation of the tumor suppressors to induce AKT phosphorylation in N6-methyladenosine-dependent way in prostate cancer. *Mol. Cancer* 19 (1), 152. doi:10.1186/s12943-020-01267-6

Li, M., Tao, Z., Zhao, Y., Li, L., Zheng, J., Li, Z., et al. (2022a). 5-methylcytosine RNA methyltransferases and their potential roles in cancer. *J. Transl. Med.* 20 (1), 214. doi:10.1186/s12967-022-03427-2

Li, Y., Lu, F., and Yin, Y. (2022b). Applying logistic LASSO regression for the diagnosis of atypical Crohn's disease. *Sci. Rep.* 12 (1), 11340. doi:10.1038/s41598-022-15609-5

Liu, S., Tao, Z., Lou, J., Li, R., Fu, X., Xu, J., et al. (2023). CD4(+)CCR8(+) Tregs in ovarian cancer: a potential effector Tregs for immune regulation. *J. Transl. Med.* 21 (1), 803. doi:10.1186/s12967-023-04686-3

Liu, T. T., Li, R., Huo, C., Li, J. P., Yao, J., Ji, X. L., et al. (2021). Identification of CDK2-related immune forecast model and ceRNA in lung adenocarcinoma, a pan-cancer analysis. *Front. Cell Dev. Biol.* 9, 682002. doi:10.3389/fcell.2021.682002

Liyanage, C., Fernando, A., Chamberlain, A., Moradi, A., and Batra, J. (2024). RNA m6a methylation regulator expression in castration-resistant prostate cancer progression and its genetic associations. *Cancers (Basel)* 16 (7), 1303. doi:10.3390/cancers16071303

Long, S., Yan, Y., Xu, H., Wang, L., Jiang, J., Xu, Z., et al. (2023). Insights into the regulatory role of RNA methylation modifications in glioma. *J. Transl. Med.* 21 (1), 810. doi:10.1186/s12967-023-04653-y

Ma, X., Guo, J., Liu, K., Chen, L., Liu, D., Dong, S., et al. (2020). Identification of a distinct luminal subgroup diagnosing and stratifying early stage prostate cancer by tissue-based single-cell RNA sequencing. *Mol. Cancer* 19 (1), 147. doi:10.1186/s12943-020-01264-9

Ma, Z., Zhang, W., Dong, B., Xin, Z., Ji, Y., Su, R., et al. (2022). Docetaxel remodels prostate cancer immune microenvironment and enhances checkpoint inhibitor-based immunotherapy. *Theranostics* 12 (11), 4965–4979. doi:10.7150/thno.73152

Makowska, K. A., Hughes, R. E., White, K. J., Wells, C. M., and Peckham, M. (2015). Specific myosins control actin organization, cell morphology, and migration in prostate cancer cells. *Cell Rep.* 13 (10), 2118–2125. doi:10.1016/j.celrep.2015.11.012

Meng, F., Han, X., Min, Z., He, X., and Zhu, S. (2021). Prognostic signatures associated with high infiltration of Tregs in bone metastatic prostate cancer. *Aging* 13 (13), 17442–17461. doi:10.18632/aging.203234

Mishra, D. K., Chen, Z., Wu, Y., Sarkissyan, M., Koeffler, H. P., and Vadgama, J. V. (2010). Global methylation pattern of genes in androgen-sensitive and androgen-independent prostate cancer cells. *Mol. Cancer Ther.* 9 (1), 33–45. doi:10.1158/1535-7163.MCT-09-0486

Mortensen, M. M., Høyer, S., Lynnerup, A. S., Ørntoft, T. F., Sørensen, K. D., Borre, M., et al. (2015). Expression profiling of prostate cancer tissue delineates genes associated with recurrence after prostatectomy. *Sci. Rep.* 5, 16018. doi:10.1038/srep16018

Nulali, J., Zhang, K., Long, M., Wan, Y., Liu, Y., Zhang, Q., et al. (2024). ALYREF-Mediated RNA 5-methylcytosine modification promotes hepatocellular carcinoma progression via stabilizing EGFR mRNA and pSTAT3 activation. *Int. J. Biol. Sci.* 20 (1), 331–346. doi:10.7150/ijbs.82316

Pedros, C., Canonigo-Balancio, A. J., Kong, K. F., and Altman, A. (2017). Requirement of Treg-intrinsic CTLA4/PKCη signaling pathway for suppressing tumor immunity. *JCI insight.* 2 (23), e95692. doi:10.1172/jci.insight.95692

Peng, S., Hu, P., Xiao, Y. T., Lu, W., Guo, D., Hu, S., et al. (2022). Single-cell analysis reveals EP4 as a target for restoring T-cell infiltration and sensitizing prostate cancer to immunotherapy. *Clin. Cancer Res.* 28 (3), 552–567. doi:10.1158/1078-0432.CCR-21-0299

Petrioli, R., Fiaschi, A. I., Francini, E., Pascucci, A., and Francini, G. (2008). The role of doxorubicin and epirubicin in the treatment of patients with metastatic hormone-refractory prostate cancer. *Cancer Treat. Rev.* 34 (8), 710–718. doi:10.1016/j.ctrv.2008.05.004

Petrylak, D. P., Tangen, C. M., Hussain, M. H., Lara, P. N., Jr., Jones, J. A., Taplin, M. E., et al. (2004). Docetaxel and estramustine compared with mitoxantrone and prednisone for advanced refractory prostate cancer. *N. Engl. J. Med.* 351 (15), 1513–1520. doi:10.1056/nejmoa041318

Pritchard, C. C., Mateo, J., Walsh, M. F., De Sarkar, N., Abida, W., Beltran, H., et al. (2016). Inherited DNA-repair gene mutations in men with metastatic prostate cancer. *N. Engl. J. Med.* 375 (5), 443–453. doi:10.1056/NEJMoa1603144

Qi, F., Shen, W., Wei, X., Cheng, Y., Xu, F., Zheng, Y., et al. (2023). CSNK1D-mediated phosphorylation of HNRNPA2B1 induces miR-25-3p/miR-93-5p maturation to promote prostate cancer cell proliferation and migration through m(6)A-dependent manner. *Cell. Mol. life Sci.* 80 (6), 156. doi:10.1007/s00018-023-04798-5

Qing, J., Li, C., Hu, X., Song, W., Tirichen, H., Yaigoub, H., et al. (2022). Differentiation of T Helper 17 cells may mediate the abnormal humoral immunity in IgA nephropathy and inflammatory bowel disease based on shared genetic effects. *Front. Immunol.* 13, 916934. doi:10.3389/fimmu.2022.916934

Qiu, S. Q., Waaijer, S. J. H., Zwager, M. C., de Vries, E. G. E., van der Vegt, B., and Schröder, C. P. (2018). Tumor-associated macrophages in breast cancer: innocent bystander or important player? *Cancer Treat. Rev.* 70, 178–189. doi:10.1016/j.ctrv.2018.08.010

Rocha-Rodrigues, S., Matos, A., Afonso, J., Mendes-Ferreira, M., Abade, E., Teixeira, E., et al. (2021). Skeletal muscle-adipose tissue-tumor Axis: molecular mechanisms linking exercise training in prostate cancer. *Int. J. Mol. Sci.* 22 (9), 4469. doi:10.3390/ijms22094469

Rollins, K. S., Esau, P. J., Gittemeier, E. M., Opoku-Acheampong, A. B., Behnke, B. J., Copp, S. W., et al. (2017). Prostate Cancer Reduces Endurance Exercise Capacity in the Rat: Possible Roles of Reduced Cardiac Mass and Function. *The FASEB Journal*, 31. doi:10.1096/fasebj.31.1_supplement.1020.14

Sekhoacha, M., Riet, K., Motloung, P., Gumenku, L., Adegoke, A., and Mashele, S. (2022). Prostate cancer review: genetics, diagnosis, treatment options, and alternative approaches. *Molecules* 27 (17), 5730. doi:10.3390/molecules27175730

Shi, C. J., Pang, F. X., Lei, Y. H., Deng, L. Q., Pan, F. Z., Liang, Z. Q., et al. (2025). 5-methylcytosine methylation of MALAT1 promotes resistance to sorafenib in hepatocellular carcinoma through ELAVL1/SLC7A11-mediated ferroptosis. *Drug Resist. Updat* 78, 101181. doi:10.1016/j.drup.2024.101181

Sokoloff, M. H., Rinker-Schaeffer, C. W., Chung, L. W., and Brendler, C. B. (2004). Adjunctive therapy for men with high risk localized and locally advanced prostate cancer: targeting disseminated tumor cells. *J. Urol.* 172 (6 Pt 2), 2539–2544. doi:10.1097/01.ju.0000145044.97177.09

Spary, L. K., Salimu, J., Webber, J. P., Clayton, A., Mason, M. D., and Tabi, Z. (2014). Tumor stroma-derived factors skew monocyte to dendritic cell differentiation toward a suppressive CD14(+) PD-L1(+) phenotype in prostate cancer. *Oncoimmunology* 3 (9), e955331. doi:10.4161/21624011.2014.955331

Sung, H., Ferlay, J., Siegel, R. L., Laversanne, M., Soerjomataram, I., Jemal, A., et al. (2021). Global cancer statistics 2020: GLOBOCAN estimates of incidence and mortality worldwide for 36 cancers in 185 countries. *CA Cancer J. Clin.* 71 (3), 209–249. doi:10.3322/caac.21660

Tan, Y., Zheng, T., Su, Z., Chen, M., Chen, S., Zhang, R., et al. (2023). Alternative polyadenylation reprogramming of MORC2 induced by NUDT21 loss promotes KIRC carcinogenesis. *JCI insight* 8 (18), e162893. doi:10.1172/jci.insight.162893

Tannock, I. F., de Wit, R., Berry, W. R., Horti, J., Pluzanska, A., Chi, K. N., et al. (2004). Docetaxel plus prednisone or mitoxantrone plus prednisone for advanced prostate cancer. *N. Engl. J. Med.* 351 (15), 1502–1512. doi:10.1056/nejmoa040720

Taylor, B. S., Schultz, N., Hieronymus, H., Gopalan, A., Xiao, Y., Carver, B. S., et al. (2010). Integrative genomic profiling of human prostate cancer. *Cancer Cell* 18 (1), 11–22. doi:10.1016/j.ccr.2010.05.026

Teo, M. Y., Rathkopf, D. E., and Kantoff, P. (2019). Treatment of advanced prostate cancer. *Annu. Rev. Med.* 70, 479–499. doi:10.1146/annurev-med-051517-011947

Tsvetkov, P., Coy, S., Petrova, B., Dreishpoon, M., Verma, A., Abdusamad, M., et al. (2022). Copper induces cell death by targeting lipoylated TCA cycle proteins. *Science* 375 (6586), 1254–1261. doi:10.1126/science.abf0529

Tuong, Z. K., Loudon, K. W., Berry, B., Richoz, N., Jones, J., Tan, X., et al. (2021). Resolving the immune landscape of human prostate at a single-cell level in health and cancer. *Cell Rep.* 37 (12), 110132. doi:10.1016/j.celrep.2021.110132

Uygur, B., Leikina, E., Melikov, K., Villasmil, R., Verma, S. K., Vary, C. P. H., et al. (2019). Interactions with muscle cells boost fusion, stemness, and drug resistance of prostate cancer cells. *Mol. Cancer Res.* 17 (3), 806–820. doi:10.1158/1541-7786.MCR-18-0500

Vietri, M. T., D'Elia, G., Caliendo, G., Resse, M., Casamassimi, A., Passariello, L., et al. (2021). Hereditary prostate cancer: genes related, target therapy and prevention. *Int. J. Mol. Sci.* 22 (7), 3753. doi:10.3390/ijms22073753

Wang, H., Liu, J., Zhu, X., Yang, B., He, Z., and Yao, X. (2023). AZGP1P2/UBA1/RBM15 cascade mediates the fate determinations of prostate cancer stem cells and promotes therapeutic effect of docetaxel in castration-resistant prostate cancer via TPM1 m6A modification. *Research.* 6, 0252. doi:10.34133/research.0252

Wang, Z., Chao, Z., Wang, Q., Zou, F., Song, T., Xu, L., et al. (2024). EXO1/P53/SREBP1 axis-regulated lipid metabolism promotes prostate cancer progression. *J. Transl. Med.* 22 (1), 104. doi:10.1186/s12967-023-04822-z

Wen, H., Qu, C., Wang, Z., Gao, H., Liu, W., Wang, H., et al. (2023). Cuproptosis enhances docetaxel chemosensitivity by inhibiting autophagy via the DLAT/mTOR pathway in prostate cancer. *FASEB J.* 37 (9), e23145. doi:10.1096/fj.202300980r

Wu, N., Wang, Y., Wang, K., Zhong, B., Liao, Y., Liang, J., et al. (2022). Cathepsin K regulates the tumor growth and metastasis by IL-17/CTSK/EMT axis and mediates M2 macrophage polarization in castration-resistant prostate cancer. *Cell death and Dis.* 13 (9), 813. doi:10.1038/s41419-022-05215-8

Wu, T., Hu, E., Xu, S., Chen, M., Guo, P., Dai, Z., et al. (2021). clusterProfiler 4.0: a universal enrichment tool for interpreting omics data. *Innov. Camb.* 2 (3), 100141. doi:10.1016/j.xinn.2021.100141

Xie, T., Fu, D. J., Li, Z. M., Lv, D. J., Song, X. L., Yu, Y. Z., et al. (2022). CircSMARCC1 facilitates tumor progression by disrupting the crosstalk between prostate cancer cells and tumor-associated macrophages via miR-1322/CCL20/CCR6 signaling. *Mol. Cancer* 21 (1), 173. doi:10.1186/s12943-022-01630-9

Xu, Q., Chen, S., Hu, Y., and Huang, W. (2021). Landscape of immune microenvironment under immune cell infiltration pattern in breast cancer. *Front. Immunol.* 12, 711433. doi:10.3389/fimmu.2021.711433

Xu, Y., Pachnikova, G., Wang, H., Wu, Y., Przybilla, D., Schäfer, R., et al. (2022). IC_{50}: an unsuitable measure for large-sized prostate cancer spheroids in drug sensitivity evaluation. *Bosnian J. Basic Med. Sci.* 22 (4), 580–592. doi:10.17305/bjbms.2022.7279

Xu, Z., Li, X., Li, H., Nie, C., Liu, W., Li, S., et al. (2020). Suppression of DDX39B sensitizes ovarian cancer cells to DNA-damaging chemotherapeutic agents via destabilizing BRCA1 mRNA. *Oncogene* 39 (47), 7051–7062. doi:10.1038/s41388-020-01482-x

Yang, B., Wang, J. Q., Tan, Y., Yuan, R., Chen, Z. S., and Zou, C. (2021). RNA methylation and cancer treatment. *Pharmacol. Res.* 174, 105937. doi:10.1016/j.phrs.2021.105937

Ye, L., Zhang, T., Kang, Z., Guo, G., Sun, Y., Lin, K., et al. (2019). Tumor-infiltrating immune cells act as a marker for prognosis in colorectal cancer. *Front. Immunol.* 10, 2368. doi:10.3389/fimmu.2019.02368

Ye, S., Wang, H., He, K., Shen, H., Peng, M., Nian, Y., et al. (2020). Gene set based systematic analysis of prostate cancer and its subtypes. *Future Oncol.* 16 (2), 4381–4393. doi:10.2217/fon-2019-0459

Yu, L., Shen, N., Shi, Y., Shi, X., Fu, X., Li, S., et al. (2022). Characterization of cancer-related fibroblasts (CAF) in hepatocellular carcinoma and construction of CAF-based risk signature based on single-cell RNA-seq and bulk RNA-seq data. *Front. Immunol.* 13, 1009789. doi:10.3389/fimmu.2022.1009789

Zaidi, S., Park, J., Chan, J. M., Roudier, M. P., Zhao, J. L., Gopalan, A., et al. (2024). Single-cell analysis of treatment-resistant prostate cancer: implications of cell state changes for cell surface antigen-targeted therapies. *Proc. Natl. Acad. Sci. U. S. A.* 121 (28), e2322203121. doi:10.1073/pnas.2322203121

Zhang, J., Wei, J., Sun, R., Sheng, H., Yin, K., Pan, Y., et al. (2023a). A lncRNA from the FTO locus acts as a suppressor of the m(6)A writer complex and p53 tumor suppression signaling. *Mol. Cell* 83 (15), 2692–2708.e7. doi:10.1016/j.molcel.2023.06.024

Zhang, Q., Liu, F., Chen, W., Miao, H., Liang, H., Liao, Z., et al. (2021). The role of RNA m(5)C modification in cancer metastasis. *Int. J. Biol. Sci.* 17 (13), 3369–3380. doi:10.7150/ijbs.61439

Zhang, Y., Chen, X. N., Zhang, H., Wen, J. K., Gao, H. T., Shi, B., et al. (2023b). CDK13 promotes lipid deposition and prostate cancer progression by stimulating NSUN5-mediated m5C modification of ACC1 mRNA. *Cell death Differ.* 30 (12), 2462–2476. doi:10.1038/s41418-023-01223-z

Zhao, Y., Sun, H., Zheng, J., and Shao, C. (2021). Analysis of RNA m(6)A methylation regulators and tumour immune cell infiltration characterization in prostate cancer. *Artif. Cells, Nanomedicine, Biotechnol.* 49 (1), 407–435. doi:10.1080/21691401.2021.1912759

Zhao, Y., Xing, C., and Peng, H. (2024c). ALYREF (Aly/REF export factor): a potential biomarker for predicting cancer occurrence and therapeutic efficacy. *Life Sci.* 338, 122372. doi:10.1016/j.lfs.2023.122372

Zhao, Z., Miao, Z., Hou, Y., Zhong, Y., Zhang, X., and Fang, X. (2024a). A novel signature constructed by cuproptosis-related RNA methylation regulators suggesting downregulation of YTHDC2 may induce cuproptosis resistance in colorectal cancer. *Int. Immunopharmacol.* 139, 112691. doi:10.1016/j.intimp.2024.112691

Zhao, Z., Zhou, Y., Lv, P., Zhou, T., Liu, H., Xie, Y., et al. (2024b). NSUN4 mediated RNA 5-methylcytosine promotes the malignant progression of glioma through improving the CDC42 mRNA stabilization. *Cancer Lett.* 597, 217059. doi:10.1016/j.canlet.2024.217059

Zhong, L., Wu, J., Zhou, B., Kang, J., Wang, X., Ye, F., et al. (2024). ALYREF recruits ELAVL1 to promote colorectal tumorigenesis via facilitating RNA m5C recognition and nuclear export. *NPJ Precis. Oncol.* 8 (1), 243. doi:10.1038/s41698-024-00737-0

Zhu, A., Hopkins, K. M., Friedman, R. A., Bernstock, J. D., Broustas, C. G., and Lieberman, H. B. (2021). DNMT1 and DNMT3B regulate tumorigenicity of human prostate cancer cells by controlling RAD9 expression through targeted methylation. *Carcinogenesis* 42 (2), 220–231. doi:10.1093/carcin/bgaa088

Zhu, J., Teng, H., Zhu, X., Yuan, J., Zhang, Q., and Zou, Y. (2023b). Pan-cancer analysis of Krüppel-like factor 3 and its carcinogenesis in pancreatic cancer. *Front. Immunol.* 14, 1167018. doi:10.3389/fimmu.2023.1167018

Zhu, M., Liu, D., Liu, G., Zhang, M., and Pan, F. (2023a). Caspase-linked programmed cell death in prostate cancer: from apoptosis, necroptosis, and pyroptosis to PANoptosis. *Biomolecules* 13 (12), 1715. doi:10.3390/biom13121715

frontiers | Frontiers in Pharmacology

TYPE Original Research
PUBLISHED 15 April 2025
DOI 10.3389/fphar.2025.1584502

OPEN ACCESS

EDITED BY
Lei Yin,
Shanghai Jiaotong University School of Medicine, China

REVIEWED BY
Cangcang Xu,
Hunan Normal University, China
Sentai Ding,
Shandong Provincial Hospital, China

*CORRESPONDENCE
Haitao Niu,
niuht0532@126.com
Ye Liang,
liangye82812@163.com

RECEIVED 27 February 2025
ACCEPTED 04 April 2025
PUBLISHED 15 April 2025

CITATION
Yuan Y, Chu G, Ma Q, Liang Z, Liang Y and Niu H (2025) Multiscale screening and identifying specific targets for artesunate in suppressing bladder cancer.
Front. Pharmacol. 16:1584502.
doi: 10.3389/fphar.2025.1584502

Multiscale screening and identifying specific targets for artesunate in suppressing bladder cancer

Yi Yuan[1], Guangdi Chu[1], Qingyue Ma[2], Zhijuan Liang[3], Ye Liang[3]* and Haitao Niu[1,3]*

[1]Department of Urology, The Affiliated Hospital of Qingdao University, Qingdao, China, [2]Department of Ophthalmology, The Affiliated Hospital of Qingdao University, Qingdao, China, [3]Key Laboratory, Department of Urology and Andrology, The Affiliated Hospital of Qingdao University, Qingdao, China

Background: Bladder cancer (BLCA) is a highly aggressive urinary malignancy with high mortality in advanced stages, posing a significant health risk. Artesunate (ART), a derivative of artemisinin, has been demonstrated with potent anti-tumor activity in some studies, yet its specific targets for BLCA and the molecular mechanisms have not been fully elucidated.

Purpose: This study screened potential targets of ART against BLCA through network pharmacology, followed by molecular docking simulations and experimental validation *in vitro* and *in vivo* to elucidate the underlying mechanisms.

Methods: This study identified the critical targets of BLCA and ART by employing multiscale screening from public databases, and a protein-protein interaction (PPI) network was constructed. Molecular docking simulations confirmed the stable binding of ART to the identified tumor-related targets promoting BLCA progression. These computational findings were further validated through experiments *in vivo* and *in vitro*, ensuring robust and reliable results.

Results: Based on network pharmacology analysis, the effects of ART on BLCA were multifaceted. Molecular docking simulations confirmed the binding stability of ART with core targets. The experiments *in vitro* proved that ART could inhibit BLCA cell proliferation and migration by downregulating the expression of BCL-2, inducing Caspase 3-mediated apoptosis, resulting in cell cycle arrest and suppressing the PI3K/Akt/mTOR classical pathway involved in BLCA growth and metabolism. Studies *in vivo* also confirmed that ART had significant anti-tumor effects with minimal side effects.

Conclusion: This study identified the mechanism by which ART inhibited BLCA through multiple specific targets, revealing its potential anti-cancer pathways and laying the foundation for the clinical application of traditional Chinese medicine in BLCA therapy.

KEYWORDS

artesunate, anti-tumor mechanism, bladder cancer, network pharmacology, molecular docking

1 Introduction

Bladder cancer (BLCA) is the most common malignancy of the urinary system. According to statistics, in 2024, the United States has 83,190 new cases of BLCA, with 16,840 deaths attributed to the disease (Siegel et al., 2024). At initial diagnosis, approximately 70%–75% of patients present with non-muscle-invasive bladder cancer (NMIBC), 20%–25% with muscle-invasive bladder cancer (MIBC) and about 5% have distant metastases. Despite the improvements in patient survival brought about by current treatment methods, including surgical resection, intravesical instillation therapy and recently developed immunotherapy, several challenges remain, such as significant side effects, poor patient tolerance and limited efficacy. Therefore, it is crucial to develop novel treatment strategies, particularly those that are highly effective and have fewer side effects, to improve the survival rate and quality of life of BLCA patients (Witjes et al., 2021; Hermans et al., 2018).

Network pharmacology, as an emerging research tool, integrates systems biology, multidimensional data analysis and bioinformatics to support drug development and precision medicine. Unlike the traditional "single drug-single target" research model, network pharmacology systematically identifies potential drug targets, deeply analyzes their complex biological mechanisms and facilitates the development of personalized treatment strategies. Its core principle is to use computer simulations and huge data analysis to construct a "drug-target-disease" network, comprehensively elucidating the multi-target action mechanisms of drugs, predicting potential therapeutic targets and exploring possible drug combination strategies (Zhao et al., 2023). In the study of natural compounds, network pharmacology exhibits unique advantages. Natural compounds often possess complex chemical structures and multiple biological activities, allowing them to act on several signaling pathways and molecular targets simultaneously, thereby achieving synergistic anti-cancer effects. Therefore, network pharmacology is particularly important in elucidating the multi-target anti-cancer mechanisms of natural compounds. Compared to the traditional single-target drug development model, network pharmacology systematically constructs and analyzes the multidimensional biological interaction networks of natural compounds, providing crucial theoretical support for uncovering their anti-cancer mechanisms, identifying key targets and optimizing precision treatment strategies. This approach not only facilitates a comprehensive understanding of the pharmacological actions of natural compounds but also promotes the development and clinical translation of novel anti-cancer drugs.

Artesunate (ART) is a semi-synthetic derivative of artemisinin, which is derived from *Artemisia annua*. The discovery of artemisinin was awarded the Nobel Prize in Physiology or Medicine in 2015 for its outstanding anti-malarial activity. Recent studies have demonstrated that ART exhibited significant anti-cancer activity in various malignancies by blocking tumor-associated signaling pathways through multiple mechanisms (Efferth, 2017). For example, ART enhanced the radiosensitivity of esophageal cancer cells by inhibiting DNA damage repair (Fei et al., 2018); induced ROS-dependent apoptosis and ferroptosis in non-small cell lung cancer (Zhang et al., 2021); and targeted oral squamous cell carcinoma by inhibiting the AKT/AMPK/mTOR pathway (Xiao et al., 2020). Additionally, relevant studies *in vitro* have shown that ART, when combined with gemcitabine, can reverse gemcitabine resistance in pancreatic cancer cells (Yao et al., 2022). In terms of clinical applications, ART has made significant progress, demonstrating satisfactory efficacy and safety. For instance, in an open-label phase I clinical trial (ARTIC M33/2), 13 patients with metastatic breast cancer continued receiving ART as adjunct therapy after the trial ended. The results showed enhanced therapeutic efficacy, well tolerance and fewer side effects (von Hagens et al., 2019). Furthermore, 28 patients who received intravaginal ART implants for the treatment of CIN2/3 (cervical intraepithelial neoplasia grade 2/3) also exhibited favorable safety and tolerance (Trimble et al., 2020).

Currently, research on ART in BLCA primarily focuses on its mechanisms of drug resistance. Studies have found that in BLCA, ART can induce cell cycle arrest, trigger mitochondrial dysfunction, activate autophagy and mediate apoptosis in cisplatin-resistant BLCA cells (Li et al., 2024). Additionally, ART can generate reactive oxygen species (ROS), causing intracellular redox imbalance and making it a potential candidate for combination therapy with cisplatin in BLCA treatment (Chen et al., 2023). Furthermore, ART can promote tumor cell apoptosis by activating autophagy in BLCA cells (Zhou et al., 2020). However, the precise mechanism of ART in the treatment of BLCA remains to be fully elucidated. This study will integrate network pharmacology, molecular docking and experiments *in vitro* and *in vivo* to systematically explore the multi-target mechanisms of ART in BLCA, providing new insights and potential therapeutic strategies for precision treatment.

2 Methods

2.1 Cell culture and regents

Human BLCA cell lines T24 and UMUC3 were sourced from the Chinese Academy of Sciences Cell Bank. They were maintained in RPMI-1640 or DMEM with 10% FBS, incubated at 5% CO_2 at 37°C. ART was purchased from MCE (HY-N0193; China). The drug powder was dissolved in DMSO (HY-Y0320; MCE; China) and then diluted in cell culture medium to the required concentration prior to use.

2.2 Network pharmacology analysis

A search for "artesunate" identified 201 targets, while "bladder cancer" yielded 4,555 targets. The intersection of these targets, along with transcriptome and clinical data from TCGA and GEO, was analyzed using Venny 2.1. Interactions between these targets were investigated using a PPI network built with STRING and represented visually through Cytoscape 3.10.1, with network centrality assessed using CytoNCA. GO and KEGG analyses were

Abbreviations: ART, artesunate; BLCA, bladder cancer; NMIBC, non-muscle-invasive bladder cancer; MIBC, muscle-invasive bladder cancer; PPI, protein-protein interaction.

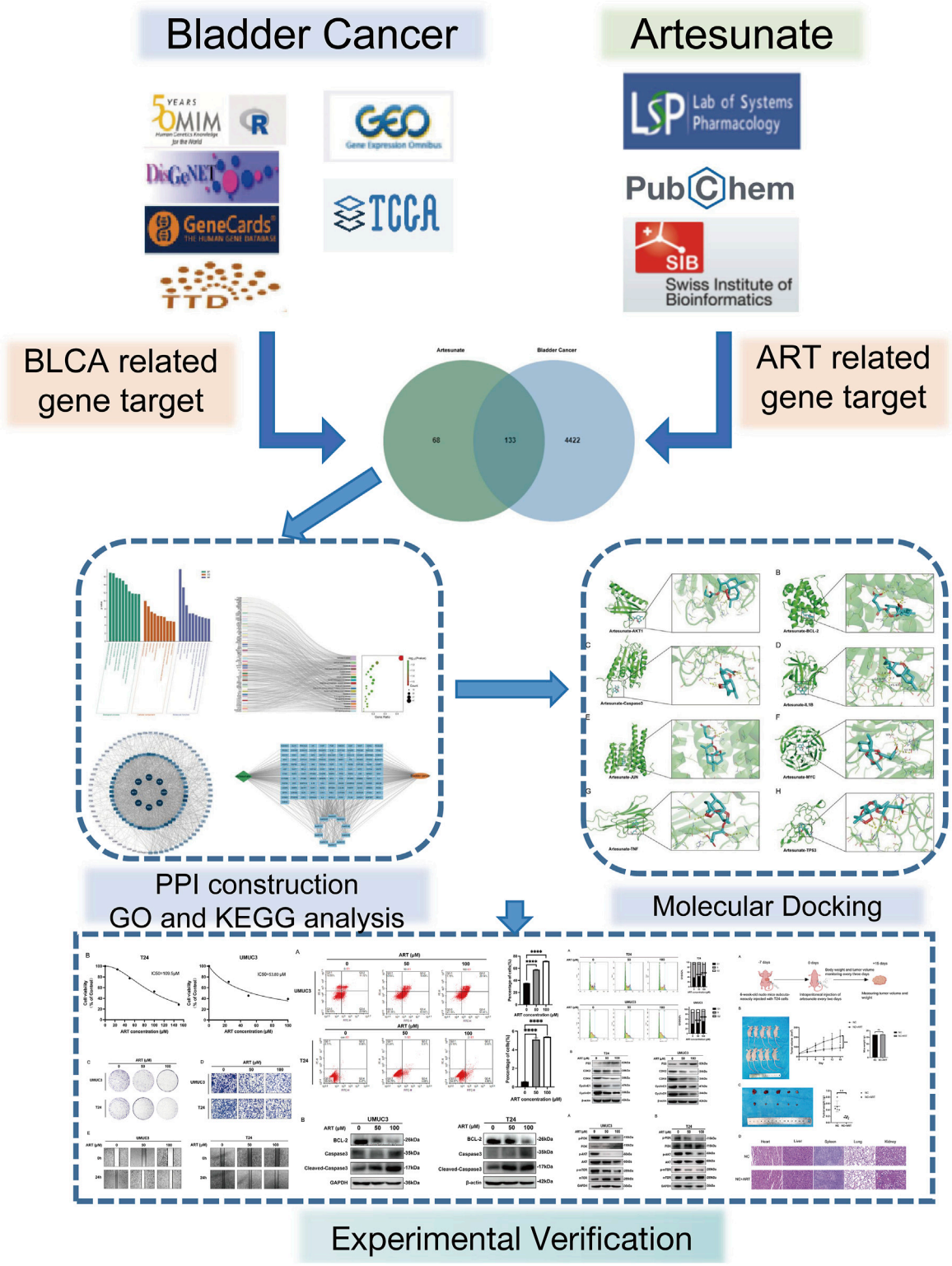

GRAPHICAL ABSTRACT
Flow of the research.

conducted using DAVID v6.8 and KEGG databases respectively, with results visualized using charts from the Bioinformatics platform.

2.3 Molecular docking

Gene IDs for core targets were obtained from UniProt and 3D protein structures were sourced from the PDB (https://www.rcsb.org/). The structure of ART was converted and optimized using Chem3D. Docking simulations were conducted with AutoDock Vina and the results were visualized using PyMOL. Binding energies were interpreted as follows: values below 0 kcal/mol indicated the ability of binding, below -5 kcal/mol indicated strong affinity and below -7 kcal/mol indicated extremely strong affinity (Ge et al., 2023).

2.4 MTT assay

Cells were seeded at a density of 2000 cells per well in a 96-well plate and allowed to adhere overnight. The following day, cells were treated with varying concentrations of ART and incubated for 24 h. Subsequently, 20 μL of MTT solution (5 mg/mL in PBS) was added to each well, and the plate was incubated for an additional 4 h at 37°C. After incubation, the medium containing MTT was carefully removed, and 150 μL of DMSO was added to dissolve the formazan crystals. The optical density (OD) was measured at 490 nm using enzyme-labeled instrument to quantify cell viability.

2.5 Colony formation

The BLCA cells T24 and UMUC3 were pretreated with varying concentrations of ART for 24 h. After pretreatment, 500 cells per well were seeded into six-well plates and cultured for 14 days to allow colony formation. At the end of the incubation period, colonies were fixed with 4% paraformaldehyde for 20 min and stained with 0.2% crystal violet solution for 30 min. Excess stain was rinsed off with distilled water, and the plates were air-dried before imaging and counting the colonies.

2.6 Cell migration

After pretreatment with varying concentrations of ART for 24 h, cells were resuspended in serum-free medium and seeded into the upper chambers of Transwell inserts with an 8 μm pore size. The lower chambers were filled with complete medium containing 10% serum as a chemoattractant. The plates were incubated in a 37°C cell incubator for 24 h. After incubation, migrated cells on the bottom surface of the membrane were fixed with 4% paraformaldehyde for 20 min and stained with 0.1% crystal violet for 30 min. The stained membranes were washed with distilled water, air-dried and non-migrated cells on the upper surface of the membrane were gently removed using a cotton swab. The membranes were then visualized under a microscope for analysis.

2.7 Flow cytometry

Cell cycle and apoptosis analyses were performed using flow cytometry with DNA-binding dyes and apoptosis markers. After pretreating the cells with ART at concentrations of 0, 50 and 100 μM for 24 h, the cells were harvested and stained with propidium iodide (PI) solution to assess cell cycle distribution. Additionally, apoptosis was evaluated by labeling the cells with Annexin V-FITC to detect early apoptosis and PI to label late apoptotic or dead cells. The samples were then analyzed using flow cytometry to determine the distribution of cells in the G0/G1, S and G2/M phases, and to quantify the populations of early and late apoptotic cells. Data analysis was conducted using Novepress software to assess the fluorescence intensity and determine the percentage of cells in each phase and apoptosis stage.

2.8 Western blot (WB)

Cells exposed to 0, 50 and 100 μM concentrations of ART for 48 h were lysed using RIPA buffer to ensure optimal protein extraction. The lysates were resolved by SDS-PAGE and transferred to PVDF membranes. Following overnight incubation at 4°C with primary antibodies, the membranes were treated with HRP-conjugated secondary antibodies for 1 h and protein signals were detected using chemiluminescence (ECL) (WBK1S0100; millipore; United States) Detailed information regarding the antibodies used can be found in (Supplementary Table 1).

2.9 Subcutaneous xenograft tumor model

Four-week-old female nude mice were purchased from Beijing Vital River Laboratory Animal Technology Co., Ltd. (Beijing; China). Following a 2-week acclimation period, tumor cells (1×10^7 per mouse) were injected into the right axillae of the mice. Subsequently, the mice were randomly allocated into two groups. The ART group received 90 mg/kg of ART via intraperitoneal injection, while the control group was administered an equivalent volume of physiological saline. After 15 days of treatment, the mice were euthanized, and subcutaneous tumors were harvested and quantitatively measured. Moreover, tissues from the heart, liver, spleens, lungs and kidneys were collected for histopathological analysis using hematoxylin and eosin (HE) staining.

2.10 Statistical analysis

Data were processed and analyzed using Prism 8.0.1, employing one-way ANOVA and unpaired t-tests for statistical evaluation, and were presented as the mean of three independent samples. Statistical significance is indicated as $^{*}p < 0.05$, $^{**}p < 0.01$, $^{***}p < 0.001$, $^{****}p < 0.0001$.

3 Results

3.1 Potential targets of ART for BLCA treatment

Conducted differential gene expression analysis between BLCA and adjacent tissues in the GEO and TCGA databases and visualized the results (Figures 1A,B). Performed an intersection analysis with BLCA-related gene targets retrieved from the OMIM, Gene-Cards, DisGeNET and TTD databases, resulting in 4,555 disease targets. By searching PubChem, TCMSP databases and predicting with Swiss Target Prediction, 201 potential targets of ART were identified. An intersection analysis of the 201 ART-related target genes and 4555 BLCA-related target genes resulted in 133 intersecting genes, which can be considered potential therapeutic candidate targets of ART for BLCA. The intersection results were displayed in Figure 1C. Following this, a drug-disease-target network of 133 genes was constructed using Cytoscape 3.10.1 software, demonstrating the interaction between ART and BLCA (Figure 1D). GO enrichment analysis identified 812 significant GO terms ($p < 0.05$), including 622 biological processes (BP), 66 cellular components (CC) and 124 molecular functions (MF) (Supplementary Table 2). The 10 most significantly enriched terms for each category were presented visually (Figure 1E), suggesting ART may counteract BLCA by regulating proteins and enzymes in these pathways. KEGG enrichment analysis revealed 175 significant pathways ($p < 0.05$) (Supplementary Table 3), with key tumor-related pathways like "cancer pathways," "apoptosis" and "p53 signaling pathway" being prominent (Figure 1F). To investigate ART's interaction with BLCA intersecting targets, 133 targets were analyzed using the STRING database and visualized with Cytoscape 3.10.1, creating a disease-drug-pathway-target network (Figure 1G). In the PPI network, darker and more central nodes indicated stronger interactions with central nodes representing core targets (AKT1, BCL-2, Caspase 3, IL1B, JUN, MYC, TNF, TP53) (Figure 1H). The analysis showed that these targets were involved in several tumor-related pathways (Supplementary Table 2), suggesting ART may affect BLCA by modulating these tumor-related processes.

According to these results, ART was expected to inhibit cancer by affecting specific physiological processes and key molecules in cancer. To confirm this hypothesis, additional molecular docking and experimental validation were next be performed.

3.2 The patterns of molecular docking simulation

To gain deeper insight into the role of ART in BLCA, this research further employed molecular docking simulations to comprehensively simulate the interactions between ART and the identified core targets. Specifically, ART formed multiple hydrogen bonds within the binding pockets of certain target proteins and interacted with key amino acid residues. These interactions may influence the conformational stability of target proteins and their functional roles in signaling pathways. Detailed information on binding affinity, hydrogen bond sites and bond lengths were provided in Table 1, while the visualized binding conformations of ART with core targets were presented in Figure 2. The docking results revealed that the binding affinities of ART with core targets ranged from −6.7 to −8.2 kcal/mol, indicating strong binding interactions between ART and these proteins.

The above findings suggested that ART exhibited high-affinity binding to multiple key genes involved in tumor progression, playing a crucial role in tumor cell proliferation, migration and apoptosis. For instance, ART demonstrated a strong binding affinity with BCL-2, a critical anti-apoptotic protein that inhibited mitochondrial outer membrane permeability, thereby preventing cytochrome C release and suppressing apoptosis pathway activation (Iqbal et al., 2019). This suggested that ART may regulate BLCA cell apoptosis by targeting BCL-2. Moreover, ART exhibited strong binding interactions with Caspase 3 (CASP3), an essential executioner of apoptosis, implying that ART may mediate the activation of intrinsic or extrinsic apoptotic pathways, promoting programmed tumor cell death and exerting its anti-BLCA effects (Yang et al., 2017).

Additionally, ART displayed a strong binding affinity for TP53, a pivotal tumor suppressor gene encoding the p53 protein, which played a fundamental role in cell cycle regulation and tumor suppression (Ter Huurne et al., 2020). When DNA damage occurs, p53 facilitated either DNA repair or apoptosis initiation to prevent malignant transformation. The high binding affinity between ART and TP53 suggested that ART might exert its regulatory effects on BLCA by modulating cell cycle processes. Furthermore, ART exhibited strong interactions with AKT1, a key molecule in the PI3K/AKT/mTOR signaling pathway, which was widely activated in various malignancies and promotes tumor cell survival and invasive behaviors (Yu et al., 2022). These findings suggested that ART might exert anti-BLCA effects by disrupting this signaling pathway, thereby inhibiting tumor cell survival and malignant progression.

By integrating network pharmacology and molecular docking techniques, this research preliminarily identified multiple core targets and regulatory pathways through which ART might exert its effects in BLCA. These key targets not only play essential roles in tumorigenesis and progression but may also be closely associated with the unique biological characteristics of BLCA, providing valuable theoretical insights into the potential anti-BLCA mechanisms of ART. In the next part, we began to focus on validating these predictions through experiments *in vitro* and *in vivo*, and further elucidating the underlying molecular regulatory mechanisms.

3.3 ART inhibited BLCA proliferation and migration

The chemical structure of ART was shown in Figure 3A. According to network pharmacology analysis, ART exhibited significant anti-tumor properties against BLCA. Initial evaluations of its efficacy were carried out using MTT, colony formation, wound healing and cell migration assays.

The effect of ART on BLCA cell growth was evaluated by treating cells with varying ART concentrations for 24 h and assessing viability with the MTT assay. The results showed that ART caused a dose-dependent decrease in cell viability, with

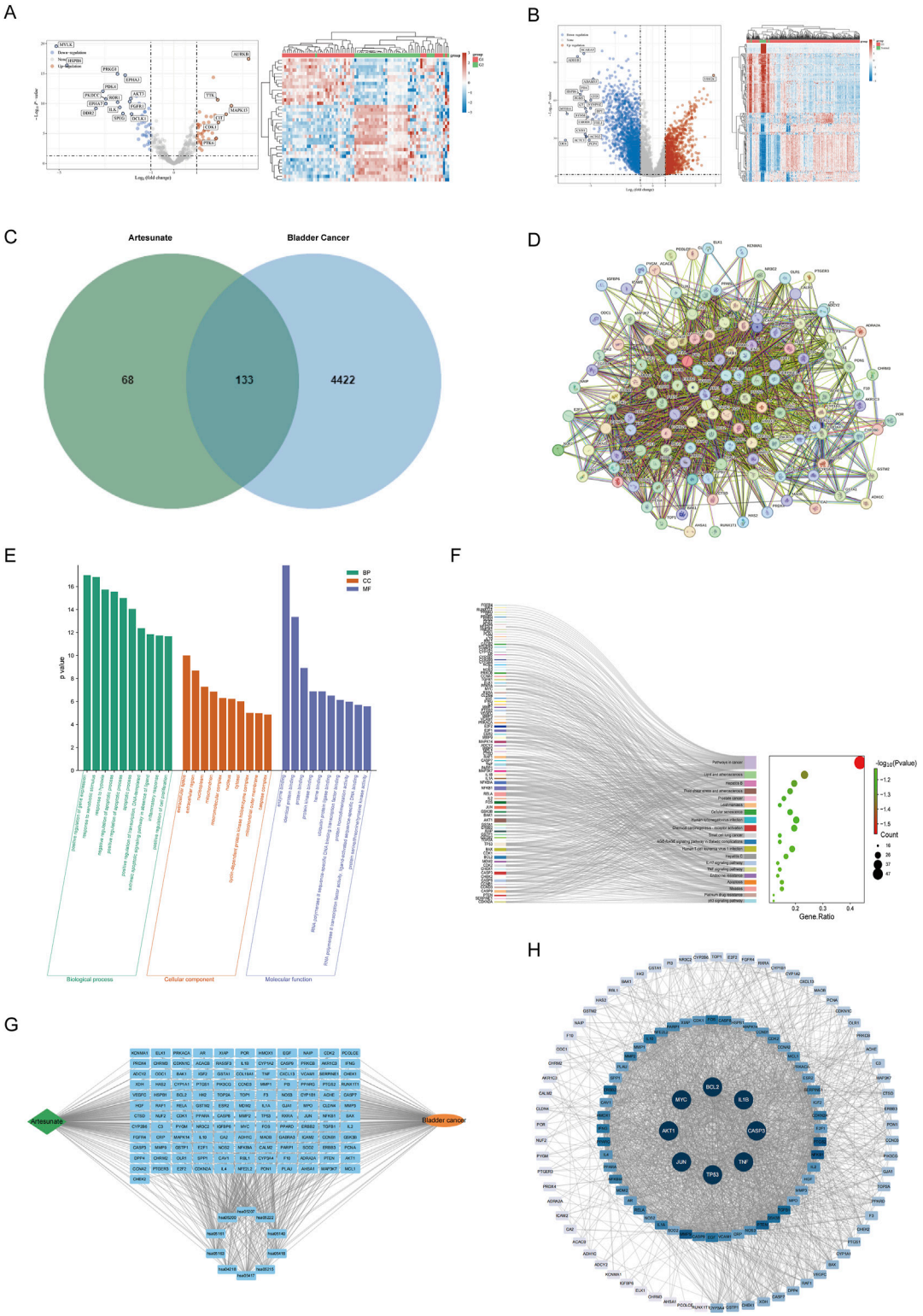

FIGURE 1
The potential targets of ART for treating BLCA. **(A)** Using data from the GEO database, a volcano plot and detailed expression profiles were generated to illustrate the DEGs between tumor tissues and adjacent normal tissues in BLCA. **(B)** Using data from the TCGA database, a volcano plot and detailed expression profiles were generated to illustrate the DEGs between tumor tissues and adjacent normal tissues in BLCA. **(C)** The Venn diagram of the intersecting targets of ART in BLCA. **(D)** PPI network based on STRING database analysis. **(E)** The Gene Ontology (GO) enrichment analysis identified the top 10 most significantly enriched terms in Cellular Component (CC), Biological Process (BP) and Molecular Function (MF) categories. **(F)** Top 20 enriched KEGG pathways. **(G)** Disease-Drug-Pathway-Targets network. **(H)** The core targets were presented in the form of a PPI network.

IC50 values of 53.8 μM for UMUC3 cells and 109.5 μM for T24 cells (Figure 3B). Additionally, colony formation assays confirmed that ART reduced the ability of BLCA cells to form colonies in a dose-dependent manner (Figure 3C).

Controlling tumor migration is vital for mitigating its aggressive behavior. The wound healing and cell migration assays showed that ART effectively reduced the migration of T24 and UMUC3 cells in a dose-dependent manner (Figures 3D,E).

3.4 ART induced BLCA apoptosis

Flow cytometry analysis revealed a substantial increase in apoptosis levels in BLCA cells with higher concentrations of ART (Figure 4A). WB experiments indicated that ART treatment reduced the expression of BCL-2 and increased the expression of Cleaved-Caspase 3/Caspase 3 in BLCA cells (Figure 4B). Cleaved-Caspase 3, a pivotal executioner of apoptosis, targets and cleaves various cellular substrates, ultimately driving cell death. Based on this, it can be strongly inferred that ART exerted its inhibitory effect on BLCA by inducing apoptosis via the Caspase pathway.

3.5 ART arrested BLCA cell cycle

Molecular docking simulation showed that ART bound strongly with p53 with a parameter of −8.2 kcal/mol. Given that p53 can halt the cell cycle at the G1 phase, we investigated whether ART had a similar effect on BLCA cells. After 24 h of ART treatment, flow cytometry revealed an increased proportion of cells in the G1 phase and a decreased proportion in the S phase, indicating that ART induced G1 phase arrest (Figure 5A).

Cyclin D-CDK4 and Cyclin E-CDK2 complexes are essential for regulating the transition from G1 to S phase. Cyclin D-CDK4 begins this transition by phosphorylating Rb protein early in G1, while Cyclin E-CDK2 completes it in late G1 and early S phase by further phosphorylating Rb and starting DNA replication. WB experiments showed that ART decreased the expression levels of CDK4, CDK2, Cyclin E1 and Cyclin D1 in BLCA cells in a dose-dependent manner (Figure 5B). Additionally, higher concentrations of ART led to increased levels of p53 protein, indicating that ART induced cell cycle arrest.

The findings indicated that ART affected cell cycle regulation in BLCA cells by blocking the transition from G1 to S phase, thereby contributing to its anti-BLCA effects.

3.6 ART inhibited the PI3K/AKT/mTOR signaling pathway in BLCA

The network pharmacology and molecular docking results indicated a strong interaction between ART and AKT. To assess whether ART disrupted the AKT signaling pathway, WB experiments were performed to reveal that ART treatment significantly reduced the levels of p-PI3K/PI3K, p-AKT/AKT and p-mTOR/mTOR compared to the control group (Figures 6A,B).

In summary, ART inhibited the activity of its corresponding signaling pathways by significantly reducing the phosphorylation levels of key proteins such as PI3K, AKT and mTOR in BLCA cells. This reduction in phosphorylation dampened the activity of the pathway, which was crucial for cell survival and proliferation, thereby potentially inhibiting cancer progression.

3.7 ART effectively exerted its inhibitory effects on BLCA *in vivo*

Studies *in vitro* unequivocally demonstrated the potent inhibitory effect of ART on BLCA cells. To further substantiate the pharmacological efficacy of ART, complementary experiments *in vivo* were conducted. As depicted in Figure 7A, a subcutaneous tumor model was established in nude mice, followed by intraperitoneal ART administration 7 days post-inoculation. Tumor size and weight were subsequently measured after 15 days of treatment. As illustrated in Figures 7B,C, the ART group displayed significant differences in tumor size and weight relative to the control group, suggesting that ART effectively suppressed further tumor growth. Moreover, no significant differences in body weight were observed between the two groups. IHC staining of subcutaneous tumors in nude mice revealed that the expression of Ki67, a proliferation marker, was significantly reduced in the ART group compared to the control group (Figure 7D). Furthermore, after harvesting the internal organs from both groups of nude mice and performing HE staining, no significant damage to the organs was observed in either group (Figure 7E). Additionally, no significant differences in body weight were noted between the two groups, suggesting that ART has minimal toxicity and side effects, with favorable drug safety.

4 Discussion

NMIBC is characterized by a high recurrence rate, with a subset of patients potentially progressing to MIBC or metastatic BLCA, thereby complicating treatment strategies (van Rhijn et al., 2009). At present, the management of BLCA predominantly relies on surgical resection, intravesical chemotherapy and immunotherapy (Patel et al., 2020). However, radical cystectomy can substantially impair a patient's quality of life (Clements et al., 2022), while intravesical chemotherapy and immunotherapy are hindered by challenges such as drug resistance and adverse side effects, which limited their long-term efficacy (Han et al., 2020; Martins et al., 2019).

Artemisia annua, a traditional Chinese medicinal herb, had its main active component, artemisinin, widely used for its anti-malarial properties (Efferth, 2017). Recent studies have shown that both artemisinin and its semi-synthetic derivative, ART, held considerable promise for cancer treatment. ART, with its improved water solubility and bioavailability over artemisinin, has been demonstrated to exert anti-tumor effects by inducing apoptosis and inhibiting choroidal melanoma through angiogenesis suppression (Efferth et al., 2001; Kelter et al., 2007; Geng et al., 2021). The therapeutic effects and mechanisms of ART in BLCA required further investigation. Network pharmacology was an innovative approach that integrated systems biology with multi-dimensional data integration techniques. This methodology

TABLE 1 Detailed information on ART binding to core targets.

Targets	Binding energy (kcal/mol)	Hydrogen bond sites	Hydrogen bond length (Å)
AKT1	−7.0	GLY-16, ARG-15	2.2Å; 2.3Å, 2.8Å, 2.3Å
BCL-2	−6.7	GLU-113, LYS-24; ARG-28; ARG-70	2.6Å; 2.2Å; 1.9Å; 2.8Å
Caspase3	−7.1	ASN-208; TRP-214; PHE-250	2.3Å, 2.7Å, 2.1Å; 2.4Å; 2.1Å, 2.3Å, 2.5Å
IL1B	−6.8	GLU-64; LYS-65	2.4Å; 2.7Å
JUN	−7.0	LYS-122; ASN-175; LYS-49	1.9Å; 2.4Å; 2.6Å
MYC	−8.0	SER-91; ILE-90	2.5Å; 2.5Å
TNF	−6.7	ASN-19; ARG-31	2.6Å; 2.9Å
TP53	−8.2	ARG-1597; ASN-1594	2.5Å, 2.8Å; 2.0Å, 2.4Å

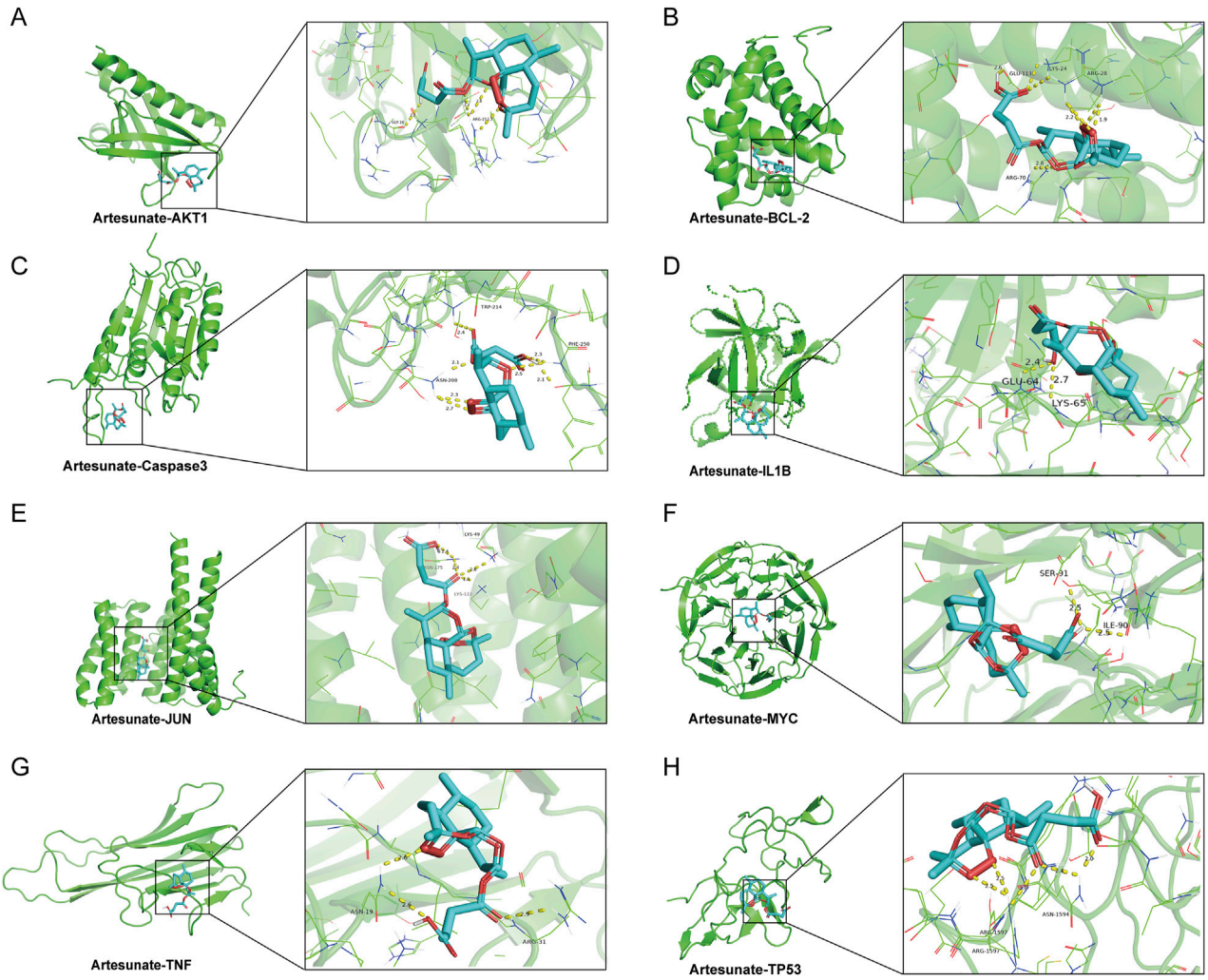

FIGURE 2
The patterns of molecular docking. **(A)** ART-AKT1. **(B)** ART-BCL-2. **(C)** ART-Caspase 3. **(D)** ART-IL1B. **(E)** ART-JUN. **(F)** ART-MYC. **(G)** ART-TNF. **(H)** ART-TP53.

facilitated the identification of various active components in traditional Chinese medicine and their potential targets. By constructing comprehensive drug-target-disease networks, network pharmacology systematically elucidated the intricate relationships between traditional Chinese medicine components and disease-associated targets. Molecular docking simulation was

10.3389/fphar.2025.1584502

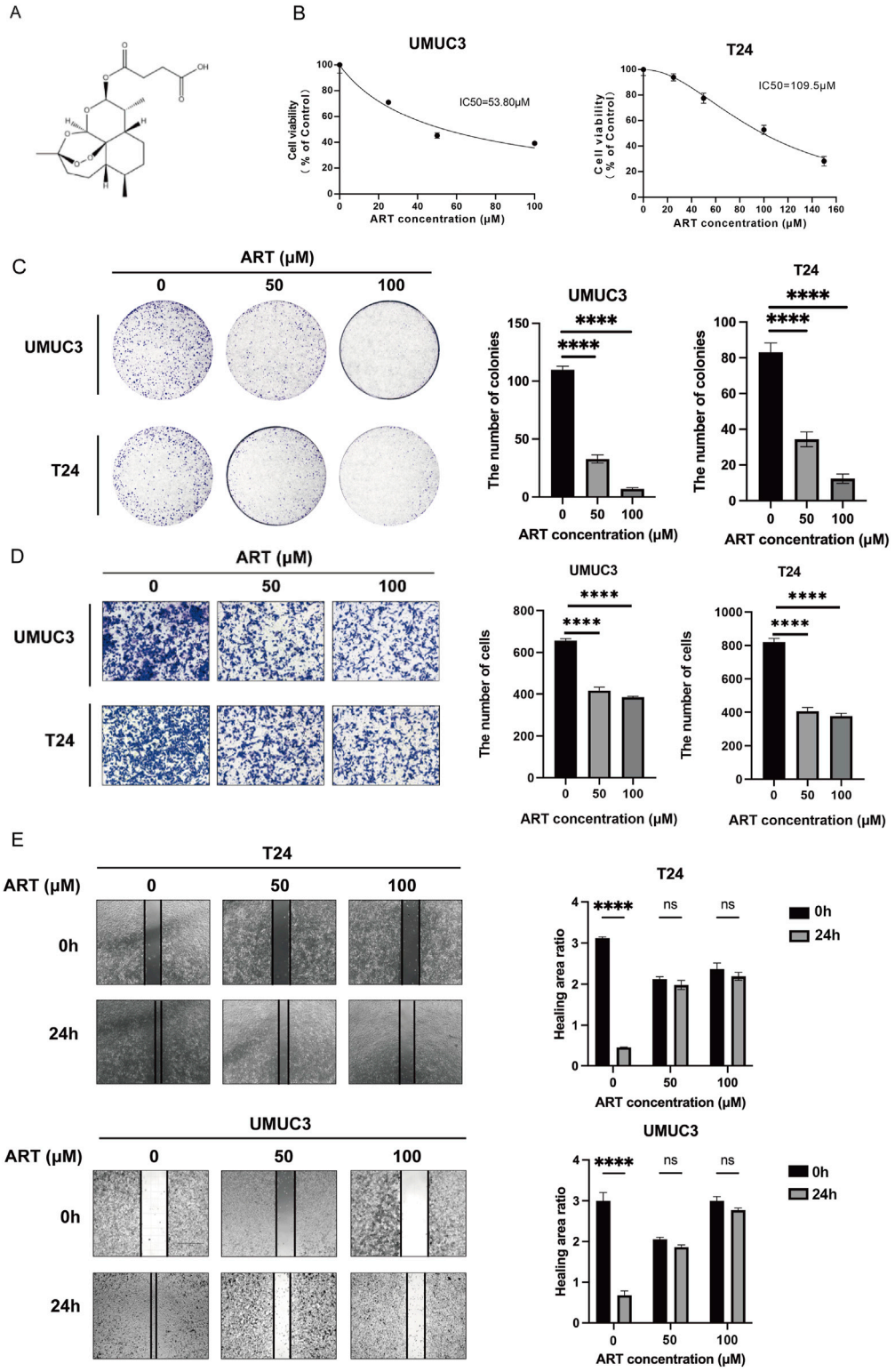

FIGURE 3
ART inhibited BLCA cells proliferation and migration. **(A)** The chemical structure of ART. **(B)** The MTT assays were used to measure the viability of UMUC3 and T24 cells. **(C)** ART reduced colony formation in UMUC3 and T24 cells in a dose-dependent manner. **(D)** ART decreased cell migration in both T24 and UMUC3 cells in a dose-dependent manner. **(E)** The wound healing assay assessed migration of UMUC3 and T24 cells after 24-h treatment with ART at concentrations of 0, 50 and 100 μM.

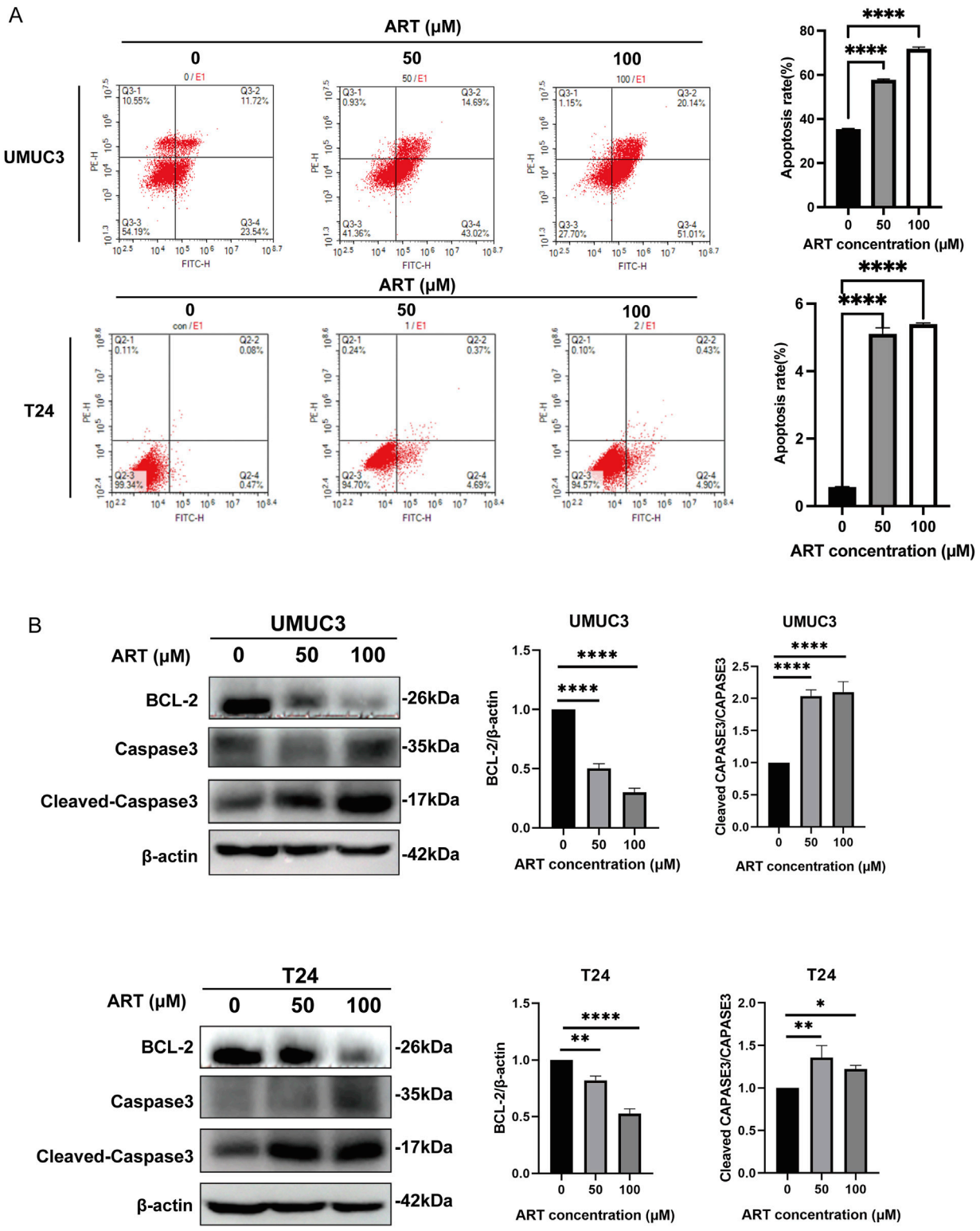

FIGURE 4
ART induced BLCA apoptosis. **(A)** The effects of ART treatment on apoptosis in UMUC3 and T24 cell lines were assessed through FACS analysis with Annexin V-FITC and PI staining. **(B)** Apoptosis-related proteins were examined via WB experiments.

a computational technique used to predict the binding modes and interaction strengths between drug molecules and proteins. Using bioinformatics databases, this research identified potential core targets for ART in the treatment of BLCA. Molecular docking simulation effectively demonstrated the binding affinity and interaction sites between ART and its target genes. These

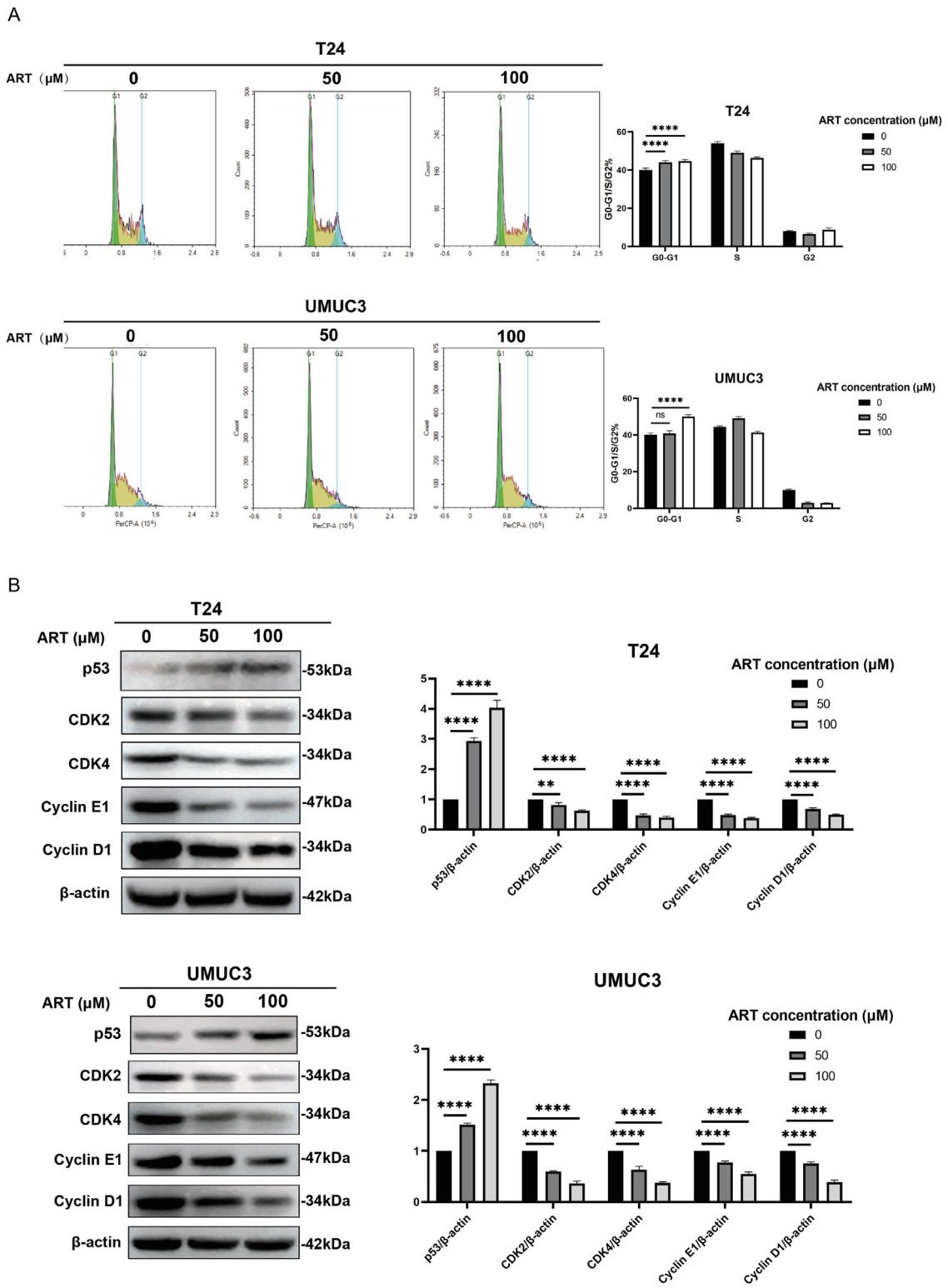

FIGURE 5
ART induced BLCA cell cycle arrest. **(A)** ART caused G1 phase arrest in T24 and UMUC3 cells, as shown by PI staining and flow cytometry. **(B)** WB experiments were used to measure the levels of proteins involved in cell cycle arrest.

simulations provided detailed insights into how ART interacted with these key proteins, revealing potential binding sites and the strength of these interactions, which were crucial for understanding its therapeutic effects. These predictions were subsequently validated through a series of experiments, providing insights into the mechanisms by which ART exerted its anti-BLCA effects. These

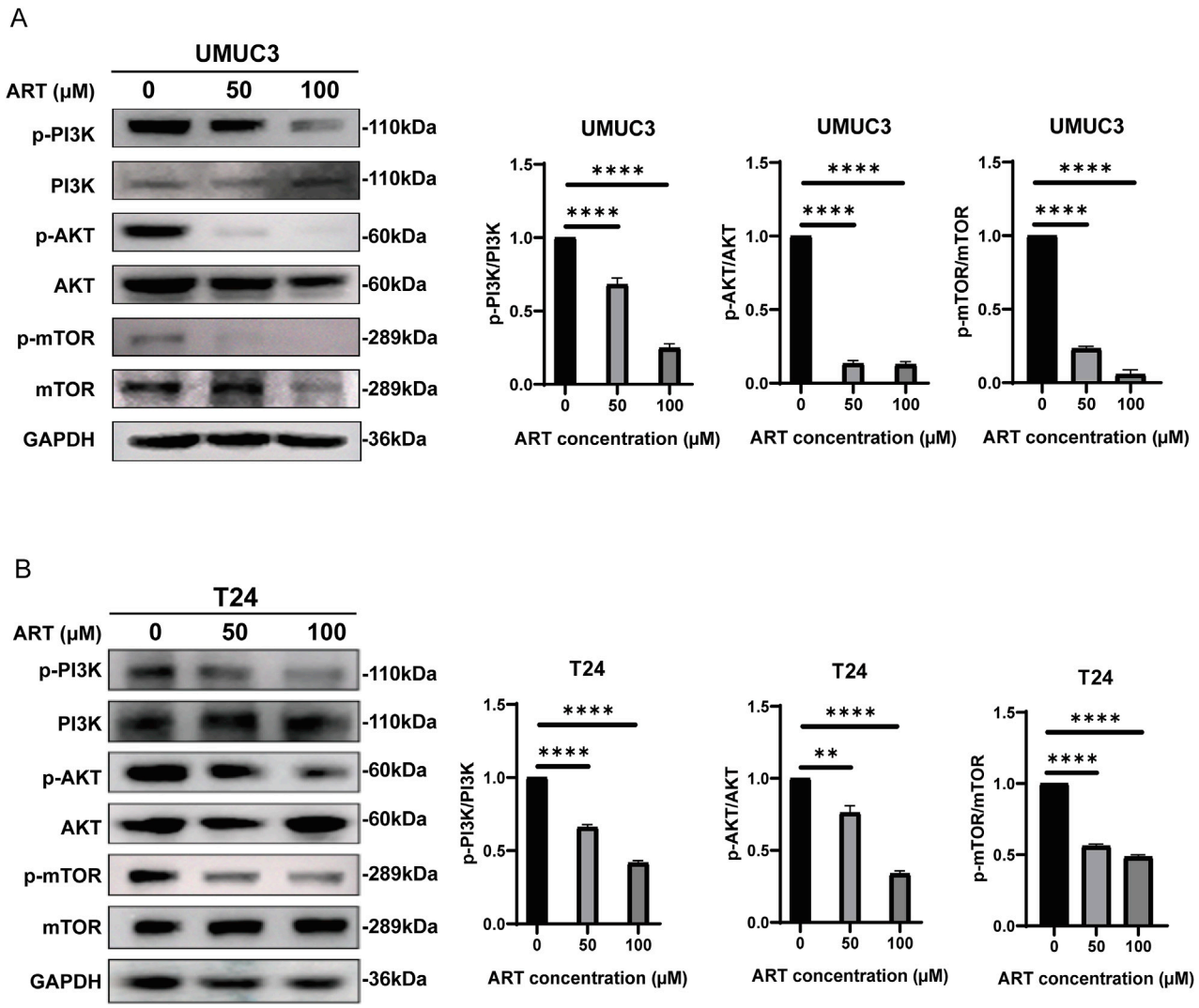

FIGURE 6
ART inhibited BLCA by targeting the PI3K/AKT/mTOR pathway. **(A,B)** WB were employed to assess the expression levels of PI3K, AKT and mTOR in BLCA cells treated with various concentrations of ART over a 24-h period.

findings revealed that ART exerted its anti-tumor effects through various mechanisms, including the induction of apoptosis, the disruption of cell cycle progression and the inhibition of the PI3K/AKT/mTOR signaling pathway.

In this study, molecular docking simulations revealed that ART formed a significant interaction with the apoptosis-related protein BCL-2, underscoring its potential role in regulating apoptotic pathways through this target. BCL-2 is an anti-apoptotic protein that plays a crucial role in cell survival by inhibiting apoptosis. It achieves this by preventing the release of cytochrome c from the mitochondria, which is a key step in the apoptotic cascade. By blocking this release, BCL-2 helps maintain cell integrity and viability, making it a critical factor in regulating programmed cell death. By blocking this release, BCL-2 inhibited the activation of caspases, which are critical executors of apoptosis (Ashkenazi et al., 2017). Based on flow cytometry analysis, it was evident that apoptosis levels in BLCA cells increased significantly with higher concentrations of ART. WB experiments revealed that ART reduced BCL-2 protein expression in BLCA cells, suggesting that ART promoted apoptosis by diminishing anti-apoptotic signaling. In contrast, Cleaved-Caspase 3 serves as a pivotal executioner in the apoptosis process. Once activated, this enzyme will initiate the cell death program by cleaving a range of cellular substrates. These cleavages lead to the dismantling of crucial cellular components, ultimately resulting in programmed cell death. The activation and function of Cleaved-Caspase 3 are essential for orchestrating the final stages of apoptosis, making it a key player in regulating cellular turnover and eliminating damaged cells. After ART treatment, the observed rise in Cleaved-Caspase 3 expression provided additional evidence that ART triggered apoptosis via the Caspase pathway. These findings suggested that the primary mechanism through which ART exerted its anti-tumor effects on BLCA cells is by inducing apoptosis.

Through network pharmacology analysis, this research identified that ART might exert its anti-BLCA effects by targeting the TP53 signaling pathway. Molecular docking simulations further

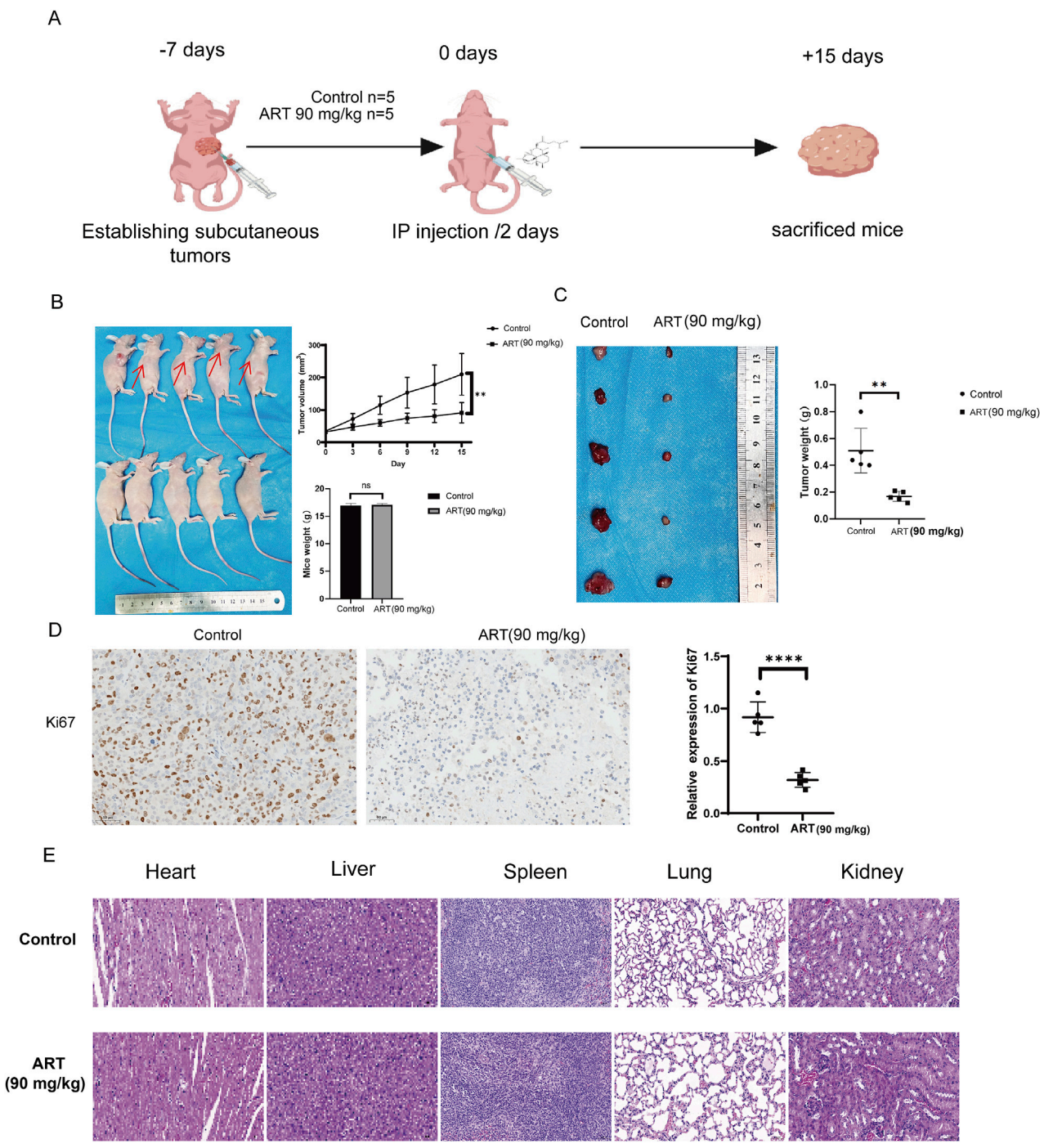

FIGURE 7
Assessment *in vivo* of the anti-tumor efficacy of ART in BLCA. **(A)** Six-week-old female nude mice were subcutaneously injected with 1×10^7 T24 cells. One week later, the experimental group was intraperitoneally administered ART at a dose of 90 mg/kg, while the control group received an equivalent volume of saline. Injections were administered every 2 days, and tumor volume and body weight were monitored every 3 days. After 15 days of treatment, the mice were euthanized, and tumor volume and weight were subsequently assessed. The diagram was created with BioGDP.com (Jiang et al., 2025). **(B)** Tumor volume growth trajectory and body weight changes in nude mice. **(C)** Tumor size and mass in subcutaneously implanted nude mice. **(D)** Ki67 staining of subcutaneous tumors in nude mice. **(E)** HE staining of internal organs from the control and treatment groups of mice.

confirmed that ART can effectively bind to the TP53 protein, suggesting that ART may activate this signaling pathway by directly acting on TP53. The TP53 gene encodes the p53 protein, a crucial tumor suppressor that primarily regulates cell cycle arrest, repairs DNA damage or initiates apoptotic mechanisms to prevent the proliferation of damaged cells. This function helps maintain genomic stability and prevents the accumulation of mutations. Under normal conditions, when DNA damage occurs, p53 is activated and functions as a transcription factor to regulate multiple target genes, thereby determining cell fate. If the damage

is repairable, p53 induces cell cycle arrest, allowing sufficient time for DNA repair. However, if the damage is irreversible, p53 triggers apoptosis, promoting the clearance of damaged cells and preventing their proliferation (Wang et al., 2023). Additionally, p53 regulates the cell cycle by upregulating the expression of p21, a key checkpoint regulator. p21 inhibits the kinase activity of CDK4/6-CyclinD1 and CDK2-CyclinE complexes by directly binding to them, thereby preventing the transition from the G1 phase to the DNA synthesis phase (Engeland, 2022). This results in G0/G1 phase arrest, inhibiting cell proliferation and allowing sufficient time for DNA repair or other cellular responses. The G0/G1 phase is the initial stage of the cell cycle, during which cells grow, synthesize RNA and produce essential proteins for DNA replication. Therefore, upregulation of p21 not only effectively halts cell cycle progression but also ensures that cells have sufficient time to repair genomic damage, preventing the expansion and accumulation of mutated cells. Further experimental results confirmed that ART induced G1 phase cell cycle arrest in BLCA cells. Flow cytometry analysis showed a significant increase in the proportion of BLCA cells in the G1 phase after ART treatment, indicating that ART effectively blocked the transition from the G1 to the S phase. Additionally, WB experiments demonstrated that ART significantly reduced the expression of G1 phase markers CDK2 and CDK4 while increasing p53 expression, suggesting that ART promoted BLCA cell cycle arrest by activating the p53 pathway. CDK2 and CDK4 are key regulators of cell cycle progression and their activity are controlled by p53. Under ART treatment, the reduced expression levels of CDK2 and CDK4 further confirmed that ART inhibited these critical cell cycle proteins, leading to G1 phase arrest and effectively suppressing excessive proliferation of BLCA cells. In conclusion, this study demonstrated that ART exerted its anti-cancer effects by activating the p53 signaling pathway and inducing G1 phase arrest in BLCA.

In addition, this research utilized network pharmacology and molecular docking to identify that ART might act on AKT1, with a strong binding affinity for AKT1. It was hypothesized that ART directly bound to AKT1, thereby inhibiting its activity and exerting an anti-cancer effect in BLCA. The PI3K/AKT/mTOR signaling pathway is a core regulatory pathway involved in the malignant behavior of tumor cells, playing a critical role in tumor initiation and progression (Peng et al., 2022). Previous studies have shown that this pathway mediates various pro-cancer biological effects in tumor cells, primarily including the following aspects: (1) Promotion of cell cycle progression—by regulating key proteins involved in the G1/S phase transition, accelerating the progression of the cell cycle and thus promoting cell proliferation; (2) Inhibition of apoptosis—by suppressing both mitochondrial-mediated intrinsic apoptosis and death receptor-mediated extrinsic apoptosis signals, enhancing tumor cell survival; (3) Promotion of angiogenesis—by upregulating VEGF expression, promoting the survival, proliferation and migration of endothelial cells, inhibiting the expression of angiogenesis inhibitors and accelerating the formation of new blood vessels to support tumor growth (Yu et al., 2022; Deng et al., 2024). The PI3K/AKT/mTOR signaling pathway is a core regulatory axis in cell growth, proliferation, survival and metabolism, widely involved in the development and progression of various cancers. The activation of this pathway is usually triggered by the binding of growth factors or cytokines to their receptors (such as EGFR, PDGFR), which then activate PI3K to generate PIP3 and activate AKT. Activated AKT not only promotes the expression of cyclins (such as Cyclin D1) but also inhibits apoptosis-related proteins (such as BAX, FOXO), while activating mTOR to enhance cell proliferation and survival. As a downstream effector of this pathway, mTOR not only promotes protein synthesis and metabolic reprogramming but also enhances tumor cell tolerance and invasiveness by regulating HIF-1α (Fontana et al., 2024; Duan et al., 2018; Chen et al., 2024). Given the pivotal role of the PI3K/AKT/mTOR signaling pathway in cancer biology, inhibiting this pathway has become a key strategy in anti-cancer therapy. Further experimental validation indicated that ART could inhibit the phosphorylation activity of the PI3K/AKT/mTOR signaling pathway in BLCA cells, effectively suppressing tumor proliferation and survival. Experiments *in vivo* demonstrated that ART significantly delayed the growth of subcutaneous tumors in nude mice, further highlighting its potent anti-tumor effects through inhibition of the PI3K/AKT/mTOR signaling pathway. Moreover, ART not only effectively inhibited tumor progression but also showed favorable safety, indicating its potential as a promising therapeutic drug. As an inhibitor of the PI3K/AKT/mTOR signaling pathway, ART represents a promising therapeutic strategy that targets key mechanisms of tumor growth and survival. Future studies will explore the combination of ART with other therapeutic drugs to evaluate its potential synergistic effects, thereby further enhancing its efficacy and expanding its clinical applications.

In this research, it was also found that MYC might play an important role in the anti-cancer effect of ART on BLCA, and ART had a strong binding affinity for MYC. MYC is an oncogene belonging to the transcription factor family, mainly regulating key biological processes such as cell proliferation, metabolism, apoptosis and differentiation. The MYC family includes c-MYC, N-MYC and L-MYC, with c-MYC being the most extensively studied member. The expression regulation of the MYC is highly complex, mainly involving interactions with other transcription factors and regulatory factors to regulate the transcription of target genes, thereby participating in multiple physiological processes of cells. In normal cells, MYC expression typically supports cell growth, proliferation and differentiation. However, in tumor cells, the overexpression or uncontrolled activation of MYC often drives tumorigenesis and progression. The role of MYC in tumors manifests in several aspects, including promoting cell proliferation, metabolic reprogramming, inhibiting apoptosis, promoting genomic instability, modulating the tumor microenvironment and cross-regulating with other signaling pathways (Krenz et al., 2024). MYC-targeted WDR4 promoted proliferation, metastasis and sorafenib resistance by inducing CCNB1 translation in hepatocellular carcinoma (Xia et al., 2021). Therefore, MYC is not only a key driver of tumorigenesis but also a potential therapeutic target. Studies have shown that inhibiting MYC expression has significant anticancer effects in tumor treatment. Among these, the potential of natural compounds in inhibiting MYC expression has gradually gained attention. Licoflavone B suppressed myeloma growth by inhibiting MYC (Liu et al., 2022). Cryptotanshinone inhibited ovarian tumor growth and metastasis by degrading c-Myc and attenuating the FAK signaling pathway (Guo et al., 2022). Further research has found that ART inhibited aerobic glycolysis by suppressing c-Myc, thereby

exerting anti-cancer effects in non-small cell lung cancer (Zhang et al., 2022). Thus, the application of natural compounds may emerge as a new direction for MYC-targeted therapy. Future research will focus on exploring how ART exerted its anti-cancer effects in BLCA through targeting the MYC, which will help better understand ART's anti-cancer mechanism and provide a theoretical basis for developing new cancer treatment strategies.

5 Conclusion

In summary, this study combined network pharmacology and molecular docking to identify key targets of ART in BLCA and validated its therapeutic effects through experiments *in vitro* and *in vivo*. These findings provided a multi-dimensional mechanistic intervention strategy for the treatment of BLCA and offer important theoretical support for the development of targeted therapeutic strategies, laying the foundation for the further expansion of traditional Chinese medicine applications in BLCA treatment.

Data availability statement

The original contributions presented in the study are included in the article/Supplementary Material, further inquiries can be directed to the corresponding authors.

Ethics statement

Ethical approval was not required for the studies on humans in accordance with the local legislation and institutional requirements because only commercially available established cell lines were used. The animal study was approved by Qingdao University Experimental Animal Welfare Ethics Committee Approval Document. The study was conducted in accordance with the local legislation and institutional requirements.

Author contributions

YY: Investigation, Methodology, Software, Visualization, Writing – original draft. GC: Data curation, Writing – original draft. QM: Formal Analysis, Writing – original draft. ZL: Visualization, Writing – original draft. YL: Funding acquisition, Supervision, Writing – review and editing. HN: Funding acquisition, Supervision, Writing – review and editing.

Funding

The author(s) declare that financial support was received for the research and/or publication of this article. This study was funded by the National Natural Science Foundation of China (82071750, 81772713), the Taishan Scholar Program of Shandong Province (tstp20221165) and Medical Health Science and Technology Fund of Shandong Province (202404050883).

Acknowledgments

We would like to express our gratitude to the researchers and teams involved in the GSE27448, GSE130598, GSE121711, GSE130598 and TCGA datasets for their contributions in specimen collection and their generous sharing of data with the scientific community.

Conflict of interest

The authors declare that the research was conducted in the absence of any commercial or financial relationships that could be construed as a potential conflict of interest.

Generative AI statement

The author(s) declare that no Generative AI was used in the creation of this manuscript.

Publisher's note

All claims expressed in this article are solely those of the authors and do not necessarily represent those of their affiliated organizations, or those of the publisher, the editors and the reviewers. Any product that may be evaluated in this article, or claim that may be made by its manufacturer, is not guaranteed or endorsed by the publisher.

Supplementary material

The Supplementary Material for this article can be found online at: https://www.frontiersin.org/articles/10.3389/fphar.2025.1584502/full#supplementary-material

References

Ashkenazi, A., Fairbrother, W. J., Leverson, J. D., and Souers, A. J. (2017). From basic apoptosis discoveries to advanced selective BCL-2 family inhibitors. *Nat. Rev. Drug Discov.* 16, 273–284. doi:10.1038/nrd.2016.253

Chen, S., Liao, J., Li, J., and Wang, S. (2024). GPC2 promotes prostate cancer progression via MDK-mediated activation of PI3K/AKT signaling pathway. *Funct. Integr. Genomics* 24, 127. doi:10.1007/s10142-024-01406-y

Chen, S. Y., Chao, C. N., Huang, H. Y., Zhao, P. W., and Fang, C. Y. (2023). Artesunate exhibits synergy with cisplatin and cytotoxicity for upper tract and bladder urothelial carcinoma cells. *Anticancer Res.* 43, 1175–1184. doi:10.21873/anticanres.16263

Clements, M. B., Atkinson, T. M., Dalbagni, G. M., Li, Y., Vickers, A. J., Herr, H. W., et al. (2022). Health-related quality of life for patients undergoing radical cystectomy: results of a large prospective cohort. *Eur. Urol.* 81, 294–304. doi:10.1016/j.eururo.2021.09.018

Deng, Z., Qing, Q., and Huang, B. (2024). A bibliometric analysis of the application of the PI3K-AKT-mTOR signaling pathway in cancer. *Naunyn Schmiedeb. Arch. Pharmacol.* 397, 7255–7272. doi:10.1007/s00210-024-03112-9

Duan, S., Huang, W., Liu, X., Liu, X., Chen, N., Xu, Q., et al. (2018). IMPDH2 promotes colorectal cancer progression through activation of the PI3K/

AKT/mTOR and PI3K/AKT/FOXO1 signaling pathways. *J. Exp. Clin. Cancer Res.* 37, 304. doi:10.1186/s13046-018-0980-3

Efferth, T. (2017). From ancient herb to modern drug: artemisia annua and artemisinin for cancer therapy. *Semin. Cancer Biol.* 46, 65–83. doi:10.1016/j.semcancer.2017.02.009

Efferth, T., Dunstan, H., Sauerbrey, A., Miyachi, H., and Chitambar, C. R. (2001). The anti-malarial artesunate is also active against cancer. *Int. J. Oncol.* 18, 767–773. doi:10.3892/ijo.18.4.767

Engeland, K. (2022). Cell cycle regulation: p53-p21-RB signaling. *Cell Death Differ.* 29, 946–960. doi:10.1038/s41418-022-00988-z

Fei, Z., Gu, W., Xie, R., Su, H., and Jiang, Y. (2018). Artesunate enhances radiosensitivity of esophageal cancer cells by inhibiting the repair of DNA damage. *J. Pharmacol. Sci.* 138, 131–137. doi:10.1016/j.jphs.2018.09.011

Fontana, F., Giannitti, G., Marchesi, S., and Limonta, P. (2024). The PI3K/Akt pathway and glucose metabolism: a dangerous liaison in cancer. *Int. J. Biol. Sci.* 20, 3113–3125. doi:10.7150/ijbs.89942

Ge, J. C., Qian, Q., Gao, Y. H., Zhang, Y. F., Li, Y. X., Wang, X., et al. (2023). Toxic effects of Tripterygium glycoside tablets on the reproductive system of male rats by metabolomics, cytotoxicity, and molecular docking. *Phytomedicine* 114, 154813. doi:10.1016/j.phymed.2023.154813

Geng, B., Zhu, Y., Yuan, Y., Bai, J., Dou, Z., Sui, A., et al. (2021). Artesunate suppresses choroidal melanoma vasculogenic mimicry formation and angiogenesis via the Wnt/CaMKII signaling Axis. *Front. Oncol.* 11, 714646. doi:10.3389/fonc.2021.714646

Guo, H., Zhang, W., Wang, J., Zhao, G., Wang, Y., Zhu, B. M., et al. (2022). Cryptotanshinone inhibits ovarian tumor growth and metastasis by degrading c-Myc and attenuating the FAK signaling pathway. *Front. Cell Dev. Biol.* 10, 959518. doi:10.3389/fcell.2022.959518

Han, J., Gu, X., Li, Y., and Wu, Q. (2020). Mechanisms of BCG in the treatment of bladder cancer-current understanding and the prospect. *Biomed. Pharmacother.* 129, 110393. doi:10.1016/j.biopha.2020.110393

Hermans, T. J. N. V., van der Heijden, C. S., Schmitz-Draeger, M. S., Kassouf, B. J., WassimSeiler, R. K., Grivas, A. M., et al. (2018). Neoadjuvant treatment for muscle-invasive bladder cancer: the past, the present, and the future. *Urol. Oncol.* 36, 413–422. doi:10.1016/j.urolonc.2017.10.014

Iqbal, W., Alkarim, S., Kamal, T., Choudhry, H., Sabir, J., Bora, R. S., et al. (2019). Rhazyaminine from *Rhazya stricta* inhibits metastasis and induces apoptosis by downregulating bcl-2 gene in MCF7 cell line. *Integr. Cancer Ther.* 18, 1534735418809901. doi:10.1177/1534735418809901

Jiang, S., Li, H., Zhang, L., Mu, W., Zhang, Y., Chen, T., et al. (2025). Generic Diagramming Platform (GDP): a comprehensive database of high-quality biomedical graphics. *Nucleic Acids Res.* 53, D1670–d1676. doi:10.1093/nar/gkae973

Kelter, G., Steinbach, D., Konkimalla, V. B., Tahara, T., Taketani, S., Fiebig, H. H., et al. (2007). Role of transferrin receptor and the ABC transporters ABCB6 and ABCB7 for resistance and differentiation of tumor cells towards artesunate. *PLoS One* 2, e798. doi:10.1371/journal.pone.0000798

Krenz, B., Lee, J., Kannan, T., and Eilers, M. (2024). Immune evasion: an imperative and consequence of MYC deregulation. *Mol. Oncol.* 18, 2338–2355. doi:10.1002/1878-0261.13695

Li, J., Shan, K., Huang, W., Su, Q., Qi, Y., Zhang, Z., et al. (2024). The combination treatment of RC48 and STAT3 inhibitor acts as a promising therapeutic strategy for basal bladder cancer. *Front. Immunol.* 15, 1432586. doi:10.3389/fimmu.2024.1432586

Liu, L., Geng, X., Zhang, J., Li, S., and Gao, J. (2022). Structure-based discovery of Licoflavone B and Ginkgetin targeting c-Myc G-quadruplex to suppress c-Myc transcription and myeloma growth. *Chem. Biol. Drug Des.* 100, 525–533. doi:10.1111/cbdd.14064

Martins, F., Sofiya, L., Sykiotis, G. P., Lamine, F., Maillard, M., Fraga, M., et al. (2019). Adverse effects of immune-checkpoint inhibitors: epidemiology, management and surveillance. *Nat. Rev. Clin. Oncol.* 16, 563–580. doi:10.1038/s41571-019-0218-0

Patel, V. G., Oh, W. K., and Galsky, M. D. (2020). Treatment of muscle-invasive and advanced bladder cancer in 2020. *CA Cancer J. Clin.* 70, 404–423. doi:10.3322/caac.21631

Peng, Y., Wang, Y., Zhou, C., Mei, W., and Zeng, C. (2022). PI3K/Akt/mTOR pathway and its role in cancer therapeutics: are we making headway? *Front. Oncol.* 12, 819128. doi:10.3389/fonc.2022.819128

Siegel, R. L., Giaquinto, A. N., and Jemal, A. (2024). Cancer statistics. *CA Cancer J. Clin.* 74, 12–49. doi:10.3322/caac.21820

Ter Huurne, M., Peng, T., Yi, G., van Mierlo, G., Marks, H., and Stunnenberg, H. G. (2020). Critical role for P53 in regulating the cell cycle of ground state embryonic stem cells. *Stem Cell Rep.* 14, 175–183. doi:10.1016/j.stemcr.2020.01.001

Trimble, C. L., Levinson, K., Maldonado, L., Donovan, M. J., Clark, K. T., Fu, J., et al. (2020). A first-in-human proof-of-concept trial of intravaginal artesunate to treat cervical intraepithelial neoplasia 2/3 (CIN2/3). *Gynecol. Oncol.* 157, 188–194. doi:10.1016/j.ygyno.2019.12.035

van Rhijn, B. W., Burger, M., Lotan, Y., Solsona, E., Stief, C. G., Sylvester, R. J., et al. (2009). Recurrence and progression of disease in non-muscle-invasive bladder cancer: from epidemiology to treatment strategy. *Eur. Urol.* 56, 430–442. doi:10.1016/j.eururo.2009.06.028

von Hagens, C., Walter-Sack, I., Goeckenjan, M., Storch-Hagenlocher, B., Sertel, S., Elsässer, M., et al. (2019). Long-term add-on therapy (compassionate use) with oral artesunate in patients with metastatic breast cancer after participating in a phase I study (ARTIC M33/2). *Phytomedicine* 54, 140–148. doi:10.1016/j.phymed.2018.09.178

Wang, H., Guo, M., Wei, H., and Chen, Y. (2023). Targeting p53 pathways: mechanisms, structures, and advances in therapy. *Signal Transduct. Target Ther.* 8, 92. doi:10.1038/s41392-023-01347-1

Witjes, J. A., Bruins, H. M., Cathomas, R., Compérat, E. M., Cowan, N. C., Gakis, G., et al. (2021). European association of Urology guidelines on muscle-invasive and metastatic bladder cancer: summary of the 2020 guidelines. *Eur. Urol.* 79, 82–104. doi:10.1016/j.eururo.2020.03.055

Xia, P., Zhang, H., Xu, K., Jiang, X., Gao, M., Wang, G., et al. (2021). MYC-targeted WDR4 promotes proliferation, metastasis, and sorafenib resistance by inducing CCNB1 translation in hepatocellular carcinoma. *Cell Death Dis.* 12, 691. doi:10.1038/s41419-021-03973-5

Xiao, Q., Yang, L., Hu, H., and Ke, Y. (2020). Artesunate targets oral tongue squamous cell carcinoma via mitochondrial dysfunction-dependent oxidative damage and Akt/AMPK/mTOR inhibition. *J. Bioenerg. Biomembr.* 52, 113–121. doi:10.1007/s10863-020-09823-x

Yang, Q., Li, S., Fu, Z., Lin, B., Zhou, Z., Wang, Z., et al. (2017). Shikonin promotes adriamycin-induced apoptosis by upregulating caspase-3 and caspase-8 in osteosarcoma. *Mol. Med. Rep.* 16, 1347–1352. doi:10.3892/mmr.2017.6729

Yao, J., Huang, M., Shen, Q., Ding, M., Yu, S., Guo, Y., et al. (2022). c-Myc-PD-L1 Axis sustained gemcitabine-resistance in pancreatic cancer. *Front. Pharmacol.* 13, 851512. doi:10.3389/fphar.2022.851512

Yu, L., Wei, J., and Liu, P. (2022). Attacking the PI3K/Akt/mTOR signaling pathway for targeted therapeutic treatment in human cancer. *Semin. Cancer Biol.* 85, 69–94. doi:10.1016/j.semcancer.2021.06.019

Zhang, Q., Yi, H., Yao, H., Lu, L., He, G., Wu, M., et al. (2021). Artemisinin derivatives inhibit non-small cell lung cancer cells through induction of ROS-dependent apoptosis/ferroptosis. *J. Cancer* 12, 4075–4085. doi:10.7150/jca.57054

Zhang, Y., Wang, Y., Li, Y., Huang, C., Xiao, X., Zhong, Z., et al. (2022). Dihydroartemisinin and artesunate inhibit aerobic glycolysis via suppressing c-Myc signaling in non-small cell lung cancer. *Biochem. Pharmacol.* 198, 114941. doi:10.1016/j.bcp.2022.114941

Zhao, L., Zhang, H., Li, N., Chen, J., Xu, H., Wang, Y., et al. (2023). Network pharmacology, a promising approach to reveal the pharmacology mechanism of Chinese medicine formula. *J. Ethnopharmacol.* 309, 116306. doi:10.1016/j.jep.2023.116306

Zhou, X., Chen, Y., Wang, F., Wu, H., Zhang, Y., Liu, J., et al. (2020). Artesunate induces autophagy dependent apoptosis through upregulating ROS and activating AMPK-mTOR-ULK1 axis in human bladder cancer cells. *Chem. Biol. Interact.* 331, 109273. doi:10.1016/j.cbi.2020.109273

frontiers | Frontiers in Pharmacology

TYPE Original Research
PUBLISHED 22 April 2025
DOI 10.3389/fphar.2025.1585862

OPEN ACCESS

EDITED BY
Lei Yin,
Shanghai Jiaotong University School of Medicine, China

REVIEWED BY
Prabhakar Mujagond,
Southern Medical University, China
Yi Heng Li,
Longgang Central Hospital, China

*CORRESPONDENCE
Xuefan Zeng,
zxfcqmu@163.com
Lijun Li,
15200508632@163.com

RECEIVED 01 March 2025
ACCEPTED 04 April 2025
PUBLISHED 22 April 2025

CITATION
Li L, Bai J, Wen X and Zeng X (2025) Adverse reactions of four multi-targeted tyrosine kinase inhibitors: a descriptive analysis of the WHO-VigiAccess database.
Front. Pharmacol. 16:1585862.
doi: 10.3389/fphar.2025.1585862

Adverse reactions of four multi-targeted tyrosine kinase inhibitors: a descriptive analysis of the WHO-VigiAccess database

Lijun Li[1,2,3]*, Jiayu Bai[4], Xuelong Wen[5] and Xuefan Zeng[6]*

[1]Department of Pharmacy, The Second Affiliated Hospital, University of South China, Hengyang, Hunan, China, [2]Hengyang Medical School, University of South China, Hengyang, Hunan, China, [3]Hunan Provincial Key Clinical Laboratory of Basic and Clinical Pharmacological Research of Gastrointestinal Cancer, the Second Affiliated Hospital, University of South China, Hengyang, Hunan, China, [4]Department of rehabilitation medicine, The First Affiliated Hospital of Dalian Medical University, Dalian, Liaoning, China, [5]Wuxi School of Medicine, Jiangnan University, Wuxi, Jiangsu, China, [6]Chongqing Medical University, Chongqing, China

Background: The introduction of multi-targeted tyrosine kinase inhibitors (MTKIs) such as axitinib, lenvatinib, sorafenib, and sunitinib has greatly broadened the available treatment options for Renal Cell Carcinoma (RCC). The study aims to compare the nature of the adverse reactions associated with these four MTKIs to identify which medication poses the least risk for personalized patient management, thus enabling more accurate clinical drug oversight.

Methods: Employing a retrospective descriptive analysis methodology, this research concentrated on four commercially available MTKIs. Reports pertaining to these medications were sourced from the WHO-VigiAccess database. The data gathering process involved collecting comprehensive information on various parameters, such as age demographics, gender, and the geographical distribution of patients associated with the ADR reports. Furthermore, the study explored disease systems and symptoms that were documented alongside the adverse reactions, as outlined in the annual ADR reports produced by the WHO. To assess the relationship between these four MTKIs and the linked AEs, both the Proportional Reporting Ratio (PRR) and the Reported Odds Ratio (ROR) were utilized.

Results: At the time of the search, a total of 123,818 AEs associated with the four MTKIs had been documented in the VigiAccess database. The common ADRs for these four MTKIs include diarrhoea, fatigue, death, hypertension, nausea, asthenia, weight decreased, and vomiting. Gastrointestinal disorders and general disorders and administration site conditions emerged as the SOCs with the highest number of adverse signals, both ranking first in terms of frequency. The elevated ROR (1.08) and PRR (1.06) values associated with gastrointestinal disorders in patients treated with sorafenib suggest a higher incidence of such adverse events compared to those observed with axitinib, lenvatinib, and sunitinib.

Conclusion: Recent comparative observational research suggests that the ADR reports submitted to the WHO and the FDA for these medications highlight both common and specific ADRs. It is essential for clinical practitioners to develop

personalized treatment strategies that consider the adverse effects linked to different medications, alongside the unique circumstances of their patients, thus encouraging the responsible use of these MTKIs.

KEYWORDS

MTKIs, renal cell carcinoma, adverse drug reactions, WHO-Vigiaccess, ROR

Introduction

Renal Cell Carcinoma (RCC) stands out as the most prevalent malignant tumor affecting the kidneys, representing over 90% of all renal cancers. This type of cancer arises from the epithelial cells found within the renal tubules and showcases considerable heterogeneity, alongside a notable resistance to standard chemotherapy and radiotherapy treatments (Hsieh et al., 2017). The underlying mechanisms of RCC are complex, with the overproduction of Vascular Endothelial Growth Factor (VEGF) and Vascular Endothelial Growth Factor Receptor (VEGFR) playing a pivotal role in the processes of tumor angiogenesis and development. Remarkably, around 25% of patients diagnosed with RCC present with either locally advanced or metastatic disease, and between 20% and 40% of individuals with localized primary tumors will ultimately experience the spread of metastases. Given the frequently asymptomatic progression and the unfavorable outlook linked to advanced or metastatic RCC, the range of treatment options remains quite limited. Among the various subtypes of RCC, Clear Cell Renal Cell Carcinoma (ccRCC) is the most common, representing approximately 70%–80% of all RCC instances. ccRCC is distinguished by significant vascularization, and its development is closely linked to hereditary von Hippel-Lindau (VHL) disease. In ccRCC specifically, the loss of function of the VHL tumor suppressor gene leads to the excessive buildup of Hypoxia-Inducible Factor (HIF) (Sato et al., 2013). Under normal physiological circumstances, HIF serves as a transcription factor that enhances the expression of multiple pro-angiogenic factors, such as VEGF and Platelet-Derived Growth Factor (PDGF) (Chen et al., 2023). As a result, in most ccRCC cases, dysregulation of signaling pathways caused by mutations in the VHL gene facilitates angiogenesis, as well as the survival, proliferation, and differentiation of cancerous cells. The introduction of Multi-Targeted Tyrosine Kinase Inhibitors (MTKIs) has brought about a significant change in the treatment approach for RCC. MTKIs function by targeting an array of protein kinases, such as the VEGFR, PDGFR, and the Stem Cell Factor Receptor (c-KIT) (Faivre et al., 2007). Presently, commonly utilized MTKIs include axitinib, lenvatinib, sorafenib, and sunitinib, all of which have demonstrated considerable clinical effectiveness in the management of advanced or metastatic RCC. By inhibiting the activities of VEGFR, PDGFR, and other associated kinases, these agents promote their antitumor effects, hindering tumor angiogenesis and growth while triggering apoptosis (Bahadoram et al., 2022). As a result, they offer novel therapeutic avenues for patients facing advanced RCC. Despite the thoroughness of pre-marketing clinical trials, the safety of these medications remains partially undefined based on data from pre-authorization studies, as these trials are performed in controlled conditions that differ from everyday practice (Gagliardi et al., 2022). Four MTKIs have been available on the market for a considerable period, catering to a wide range of patients and serving various purposes. Consequently, it is crucial and informative to perform safety research by utilizing extensive real-world data. Therefore, a more thorough characterization of the ADRs associated with these MTKIs is necessary, utilizing spontaneous reports gathered from pharmacovigilance databases. It is important to highlight that comparative studies addressing the similarities and differences in ADRs induced by these medications are notably lacking. Since 2015, the data stored in VigiBase has been accessible to the public through VigiAccess (Watson et al., 2018; Habarugira and Figueras, 2021). The VigiAccess database facilitates searches using the trade names of drugs, while also identifying the active ingredients and presenting the corresponding results of ADR reports. This research primarily focuses on four MTKIs: axitinib, lenvatinib, sorafenib, and sunitinib. Clinicians often need to tailor treatment options based on the potential risk of AEs for each patient. To assess the occurrence of adverse reactions associated with these MTKIs, we conducted a descriptive study that analyzed spontaneously reported adverse reactions in the VigiAccess database and compared the rates of adverse reactions linked to these four MTKIs. Furthermore, we employed the Proportional Reporting Ratio (PRR) and the Reported Odds Ratio (ROR) to evaluate the relationship between these four MTKIs and the associated AEs.

Materials and methods

Drug sample

Table 1 presents the four MTKIs that we have studied and are currently available for clinical use. Axitinib is a potent and selective second-generation VEGFR inhibitor that targets VEGFR-1, VEGFR-2, and VEGFR-3, while exhibiting a weaker inhibitory effect on PDGFR. It is primarily utilized as a second-line treatment for advanced RCC (Schmidt et al., 2018). In the AXIS Phase III clinical trial, axitinib significantly extended the progression-free survival (PFS) of patients, achieving a median PFS of 6.7 months. Lenvatinib targets multiple receptor tyrosine kinases, including VEGFR, FGFR, and PDGFR, thereby inhibiting tumor angiogenesis and cell proliferation by blocking these targets. It is widely employed in the treatment of RCC, thyroid cancer, and hepatocellular carcinoma (Romero, 2019). In 2015, lenvatinib received FDA approval for the second-line treatment of advanced RCC. Based on Phase II clinical trial data, the median PFS for the lenvatinib combination therapy group reached 14.6 months, significantly surpassing that of the monotherapy group (Motzer et al., 2015). Sorafenib is the first MTKI approved for advanced RCC, targeting VEGFR, PDGFR, and RAF kinase. In 2005, sorafenib received FDA approval based on the results of the Phase III

TABLE 1 General information of four MTKIs.

Active ingredients	Brand names	Chemical formula	Drug targets	Main conditions	The earliest year on the market
Axitinib	Inlyta, Axinix	$C_{22}H_{18}N_4OS$	VEGFR and PDGFR	Renal cell carcinoma, Pancreatic cancer	2012
Lenvatinib	Lenvima	$C_{22}H_{23}ClN_4O_7S$	VEGFR, FGFR, PDGFR, RET	Thyroid cancer, Renal cell carcinoma, Hepatocellular carcinoma	2015
Sorafenib	Nexavar	$C_{28}H_{24}ClF_3N_4O_6S$	VEGFR, PDGFR, RAF	Renal cell carcinoma, Hepatocellular carcinoma, Thyroid cancer	2005
Sunitinib	Sutent	$C_{26}H_{33}FN_4O_7$	VEGFR, PDGFR, KIT and FLT3	Renal cell carcinoma, Gastrointestinal stromal tumor, Pancreatic cancer	2006

TARGET trial, which demonstrated that the median PFS for the sorafenib group was 5.5 months, significantly longer than the 2.8 months observed in the placebo group, with a disease control rate of 84%. Although subsequent drugs have surpassed sorafenib in certain metrics, it remains a crucial option for the treatment of advanced renal cancer (Wilhelm et al., 2006). Sunitinib is an oral MTKI primarily targeting VEGFR, PDGFR, KIT, and FLT3. In 2006, sunitinib received FDA approval for the first-line treatment of advanced RCC. Key Phase III trials indicated that the median PFS for the sunitinib group was 11 months, significantly better than the 5 months reported for the interferon-α group. Due to its inhibitory effect on KIT, sunitinib is also approved for the second-line treatment of gastrointestinal stromal tumors (Moran et al., 2019).

Data sources

The WHO-VigiAccess database was searched on 17 February 2025, to gather all documented AEs that occurred following the introduction of four MTKIs. The access URL is https://www.vigiaccess.org. All pharmaceutical agents under study were identified using their generic names. Data collection spanned different age ranges, genders, years of reporting, and geographic regions, as detailed by WHO-VigiAccess. Descriptive statistics were computed utilizing Excel 2021.

WHO-VigiAccess serves as an open-access portal to the PIDM database, facilitating the retrieval of safety reports concerning medicinal products provided by the UMC. The evaluation was based on system organ class (SOC) and preferred terms (PTs) as defined by the Medical Dictionary for Regulatory Activities (MedDRA). As a result, records for each MTKI were gathered, and all distinct AEs noted at the MedDRA SOC and PT levels were pinpointed to outline the range of toxicities. The reporting terms employed in MedDRA were compiled from various dictionaries, including the WHO Adverse Reaction Terminology (WHO-ART) and others (Sultana et al., 2020). In total, 27 items were classified by SOC. This research concentrated on the PTs, which represent the extent of publicly available information in the VigiBase database via WHO-VigiAccess. To assess the outcomes of the identified safety signals, we organized them using outcome codes, culminating in three essential categories: death, hospitalization, and major events, which encompass life-threatening occurrences, disabilities, and congenital anomalies.

Disproportionality analysis

In order to evaluate the possible association between axitinib, lenvatinib, sorafenib, and sunitinib with AEs under gastrointestinal disorders, we used two methods for disproportionate analysis: ROR and PRR. ROR is mainly used to measure the imbalanced probability of reporting AEs for specific drugs compared with other drugs.

The calculation formula was:

$$ROR = \frac{a \times d}{b \times c}$$

(a) refers to the quantity of reports for particular drugs and particular AEs, (b) represents the quantity of reports for specific drugs and other AEs, (c) refers to the number of reports on other drugs and specific AEs, (d) represents the number of reports on other drugs and other AEs. PRR refers to the proportion of spontaneous reports of a specific drug associated with a specific adverse outcome divided by the corresponding proportion of other drugs. The calculation formula was:

$$PRR = \frac{a \times (c + d)}{c \times (a + b)}$$

Both ROR and PRR require that at least 5 cases ($a \geq 5$) of particular drug and AEs to consider the calculated results valid. If ROR ≥2 and the lower limit of the 95% confidence interval (CI) ≥ 1, the signal is considered disproportionate, indicating that there may be a safety problem. These criteria ensure that the observed disproportion is not due to random variation (Montastruc et al., 2011). In our analysis, we systematically evaluate the ratio of ADRs reports of using four MTKIs in gastrointestinal disorders. The analysis results help to provide guidance for the correct use of drugs.

Statistical analysis

A retrospective quantitative approach was adopted for this study. Descriptive analysis was conducted using Excel to evaluate the characteristics of individuals who experienced adverse reactions to the four MTKIs. The rate of ADR reporting for each MTKI was determined by dividing the number of ADR symptoms associated with that specific drug by the total number of ADR reports. The common ADRs linked to each medication were identified as those symptoms corresponding to the top 20 ADR report rates. The reported ADR symptoms for each drug were calculated, followed

TABLE 2 Characteristics of ADR reports of four MTKIs.

Categories	Axitinib	Lenvatinib	Sorafenib	Sunitinib
Number of ADR reports	18,257	28,819	35,009	41,733
Female	4,955 (27.14%)	15,408 (53.46%)	9,297 (26.56%)	13,621 (32.64%)
Male	12,098 (66.26%)	12,703 (44.08%)	23,606 (67.43%)	25,078 (60.09%)
Unknown	1,204 (6.59%)	708 (2.46%)	2,106 (6.02%)	3,034 (7.27%)
0–27 days	3 (0.02%)	1 (0.01%)	13 (0.04%)	5 (0.01%)
28 days to 23 months	2 (0.01%)	1 (0.01%)	15 (0.04%)	1 (0.01%)
2–11 years	7 (0.04%)	13 (0.05%)	135 (0.39%)	19 (0.05%)
12–17 years	14 (0.08%)	44 (0.15%)	175 (0.50%)	58 (0.14%)
18–44 years	487 (2.67%)	800 (2.78%)	2,079 (5.94%)	1,790 (4.29%)
45–64 years	6,186 (33.88%)	7,488 (25.98%)	12,580 (35.93%)	13,359 (32.01%)
65–74 years	5,195 (28.45%)	7,137 (24.76%)	8,523 (24.35%)	10,544 (25.27%)
≥75 years	2,835 (15.53%)	4,125 (14.31%)	4,672 (13.35%)	5,190 (12.44%)
Unknown	3,528 (19.32%)	9,210 (31.96%)	6,817 (19.47%)	10,767 (25.80%)
Americas	11,689 (64.02%)	11,888 (41.25%)	12,420 (35.48%)	23,756 (56.92%)
Asia	3,313 (18.15%)	13,205 (45.82%)	14,021 (40.05%)	6,897 (16.53%)
Europe	3,135 (17.17%)	3,391 (11.77%)	8,239 (23.53%)	10,174 (24.38%)
Oceania	18 (0.10%)	295 (1.02%)	205 (0.59%)	357 (0.86%)
Africa	102 (0.56%)	40 (0.14%)	124 (0.35%)	549 (1.32%)
2025	195 (1.07%)	528 (1.83%)	127 (0.36%)	64 (0.15%)
2024	2,309 (12.65%)	7,706 (26.74%)	1,331 (3.80%)	984 (2.36%)
2023	1,922 (10.53%)	6,330 (21.96%)	2,019 (5.77%)	1,423 (3.41%)
2022	2,916 (15.97%)	4,468 (15.50%)	1,497 (4.28%)	2,472 (5.92%)
2021	2,276 (12.47%)	2,573 (8.93%)	1,399 (4.00%)	1,926 (4.62%)
2020	1,826 (10.00%)	2,169 (7.53%)	1,739 (4.97%)	2,046 (4.90%)
2019	993 (5.44%)	2,489 (8.64%)	2,053 (5.86%)	3,121 (7.48%)
2018	960 (5.26%)	1,228 (4.26%)	2,374 (6.78%)	3,785 (9.07%)
2017	692 (3.79%)	819 (2.84%)	4,033 (11.52%)	3,717 (8.91%)
2016	897 (4.91%)	423 (1.47%)	2,723 (7.78%)	3,272 (7.84%)
2015	1,486 (8.14%)	83 (0.29%)	3,333 (9.52%)	4,447 (10.66%)
before 2014	1,785 (9.78%)	3 (0.01%)	12,381 (35.37%)	14,476 (34.69%)

by a descriptive comparative analysis. Frequencies and percentages were utilized to classify the descriptive variables.

Results

Description of the studied cases

The initial documentation regarding adverse reactions to axitinib, lenvatinib, sorafenib, and sunitinib was first noted in the WHO-VigiAccess database during the years 2003, 2004, 2008, and 2013, respectively. By 2025, the WHO had gathered a cumulative total of 18,257, 28,819, 35,009, and 41,733 reports of ADRs linked to these four MTKIs, summing up to an overall total of 123,818 reports. Within these 123,818 ADR reports associated with the four MTKIs, as illustrated in Table 2, there were 7,052 cases in which the sex of the subjects was not specified. Importantly, the amount of ADR reports from males (73,485) significantly surpassed that from females (43,281), resulting in a male-to-female ratio of 1.70:1, highlighting a notable difference. When excluding reports that did not include age information, the age group most frequently reporting incidents was predominantly individuals aged 45–64 years. Additionally, most AEs were noted from the Americas, constituting 48.26% of the overall total. More

10.3389/fphar.2025.1585862

TABLE 3 ADR number and report rate of 27 SOCs of four MTKIs.

System organ classes	Axitinib (N = 18,257)	Lenvatinib (N = 28,819)	Sorafenib (N = 35,009)	Sunitinib (N = 41,733)
Blood and lymphatic system disorders	402 (2.20%)	1,265 (4.39%)	2,475 (7.07%)	5,785 (13.86%)
Cardiac disorders	859 (4.71%)	1,514 (5.25%)	1,612 (4.60%)	2,401 (5.75%)
Congenital, familial and genetic disorders	7 (0.04%)	9 (0.03%)	33 (0.09%)	38 (0.09%)
Ear and labyrinth disorders	176 (0.96%)	134 (0.46%)	298 (0.85%)	347 (0.83%)
Endocrine disorders	859 (4.71%)	2,187 (7.59%)	176 (0.50%)	1,584 (3.80%)
Eye disorders	382 (2.09%)	433 (1.50%)	573 (1.64%)	1,436 (3.44%)
Gastrointestinal disorders	8,560 (46.89%)	15,896 (55.16%)	21,436 (61.23%)	26,444 (63.36%)
General disorders and administration site conditions	8,982 (49.20%)	10,963 (38.04%)	15,701 (44.85%)	25,495 (61.09%)
Hepatobiliary disorders	675 (3.70%)	1,533 (5.32%)	2,311 (6.60%)	1,649 (3.95%)
Immune system disorders	157 (0.86%)	250 (0.87%)	289 (0.83%)	380 (0.91%)
Infections and infestations	1,293 (7.08%)	2,763 (9.59%)	3,169 (9.05%)	4,224 (10.12%)
Injury, poisoning and procedural complications	3,015 (16.51%)	2,660 (9.23%)	4,508 (12.88%)	4,901 (11.74%)
Investigations	3,825 (20.95%)	8,197 (28.44%)	7,164 (20.46%)	11,857 (28.41%)
Metabolism and nutrition disorders	1,985 (10.87%)	4,976 (17.27%)	4,688 (13.39%)	5,480 (13.13%)
Musculoskeletal and connective tissue disorders	2,180 (11.94%)	3,729 (12.94%)	4,954 (14.15%)	5,496 (13.17%)
Neoplasms benign, malignant and unspecified (incl cysts and polyps)	3,058 (16.75%)	3,052 (10.59%)	5,182 (14.80%)	8,206 (19.66%)
Nervous system disorders	3,391 (18.57%)	5,724 (19.86%)	5,651 (16.14%)	9,373 (22.46%)
Pregnancy, puerperium and perinatal conditions	2 (0.01%)	3 (0.01%)	6 (0.02%)	24 (0.06%)
Psychiatric disorders	858 (4.70%)	1,385 (4.81%)	1,936 (5.53%)	2,482 (5.95%)
Renal and urinary disorders	1,077 (5.90%)	2,294 (7.96%)	1,392 (3.98%)	3,028 (7.26%)
Reproductive system and breast disorders	123 (0.67%)	281 (0.98%)	476 (1.36%)	567 (1.36%)
Respiratory, thoracic and mediastinal disorders	3,220 (17.64%)	4,646 (16.12%)	4,960 (14.17%)	5,979 (14.33%)
Skin and subcutaneous tissue disorders	2,380 (13.04%)	3,459 (12.00%)	16,034 (45.80%)	9,798 (23.48%)
Social circumstances	73 (0.40%)	119 (0.41%)	198 (0.57%)	187 (0.45%)
Surgical and medical procedures	637 (3.49%)	512 (1.78%)	952 (2.72%)	492 (1.18%)
Vascular disorders	2,247 (12.31%)	4,151 (14.40%)	2,741 (7.83%)	4,543 (10.89%)
Product issues	44 (0.24%)	58 (0.20%)	79 (0.23%)	77 (0.18%)

information about the reporting years for each medication analyzed can be found in Table 2.

Distribution of 20 SOCs of four MTKIs

Table 3 presents the reporting frequencies of 27 SOCs associated with four MTKIs. Axitinib exhibited elevated rates of adverse reactions in the categories of respiratory, thoracic, and mediastinal disorders, as well as in injury, poisoning, and procedural complications, when compared to the other three agents. Lenvatinib demonstrated higher adverse reaction rates in endocrine disorders, metabolic and nutritional disorders, renal and urinary disorders, and vascular disorders. Sorafenib showed increased rates of adverse reactions in hepatobiliary disorders and musculoskeletal and connective tissue disorders. Notably, the incidence of skin and subcutaneous tissue disorders was significantly higher for sorafenib than for the other agents. Sunitinib exhibited elevated adverse reaction rates across multiple SOC categories, including blood and lymphatic system disorders, gastrointestinal disorders, general disorders and administration site conditions, benign, malignant, and unspecified neoplasms (including cysts and polyps), nervous system disorders, and psychiatric disorders. Furthermore, the rates of ADRs exceeding 10% in the SOC were 11 for axitinib, 10 for lenvatinib, 10 for sorafenib, and 13 for sunitinib.

TABLE 4 Disproportionality analysis based on gastrointestinal disorders.

Drugs	ROR (95%CI)	PRR (95%CI)
Axitinib	0.86 (0.84–0.89)	0.89 (0.87–0.91)
Lenvatinib	1.04 (1.02–1.06)	1.03 (1.02–1.05)
Sorafenib	1.08 (1.06–1.10)	1.06 (1.05–1.08)
Sunitinib	0.97 (0.96–0.99)	0.97 (0.98–0.99)

Disproportionality analysis based on gastrointestinal disorders

By observing and comparing the SOC distribution of four MTKIs, we found that these MTKIs exhibited the highest reported rates of adverse reactions under the categories of gastrointestinal disorders. To further compare these four medications, we conducted a disproportionate analysis using the ROR and PRR methods. Table 4 presents the results of this analysis, indicating the following ROR values for the four drugs: axitinib: 0.86 (0.84–0.89), lenvatinib: 1.04 (1.02–1.06), sorafenib: 1.08 (1.06–1.10), and sunitinib: 0.97 (0.96–0.99). Additionally, the PRR values for the four drugs were as follows: axitinib: 0.89 (0.87–0.91), lenvatinib: 1.03 (1.02–1.05), sorafenib: 1.06 (1.05–1.08), and sunitinib: 0.97 (0.98–0.99). These findings suggest that among the four MTKIs, axitinib had the lowest reported proportion of gastrointestinal disorders, whereas sorafenib exhibited a slightly higher reported proportion in comparison to the other drugs.

Most common ADRs of four MTKIs

Table 5 presents the 20 most frequently reported ADRs associated with the four MTKIs. The manifestations listed are preferred terms categorized within the SOC. Common ADRs for the four MTKIs include diarrhea, fatigue, death, hypertension, nausea, asthenia, weight loss, and vomiting. Among axitinib and sunitinib, death and disease progression are among the most frequently reported ADRs. Additionally, dysphonia and hypothyroidism warrant particular attention for both axitinib and lenvatinib. Furthermore, lenvatinib is associated with specific ADRs, including dehydration, arthralgia, and constipation. The reporting rates of rash and hepatocellular carcinoma for sorafenib are significantly higher than those for the other drugs. Sunitinib exhibits more pronounced hematological toxicity, primarily manifesting as thrombocytopenia, and may also lead to dysgeusia.

Serious AEs of four MTKIs

Through WHO-VigiAccess, we can identify significant AEs associated with four MTKIs, including life-threatening occurrences, disabilities, and congenital malformations. The proportions of serious adverse reactions reported for axitinib, lenvatinib, sorafenib, and sunitinib were 9.74%, 3.02%, 6.63%, and 7.95%, respectively (Figure 1).

The same and different points of common ADRs of four MTKIs

By examining the top 20 ADRs associated with each MTKI within the SOCs, a cumulative total of 163 identical signals was identified across the four MTKIs. All overlapping signals are detailed in Table 6. Gastrointestinal disorders and general disorders and administration site conditions emerged as the SOCs with the highest number of adverse signals, both ranking first in terms of frequency. For gastrointestinal disorders, the five most frequently reported reactions were flatulence, stomatitis, haematemesis, dry mouth, and oral pain. Meanwhile, for general disorders and administration site conditions, the top five reactions included condition aggravated, mucosal inflammation, pyrexia, disease progression, and oedema.

Notably, when comparing the top 20 ADRs for each MTKI drug in the SOCs, each MTKI exhibited distinct PTs of ADRs in the following categories: general disorders and administration site conditions, investigations, and vascular disorders (Table 7). The number of unique symptoms reported for axitinib, lenvatinib, sorafenib, and sunitinib was 24, 25, 35, and 22, respectively.

Discussion

In the treatment of RCC, axitinib, lenvatinib, sorafenib, and sunitinib have demonstrated significant clinical benefits. However, these MTKIs are also associated with a range of ADRs that can often be dose-limiting. By targeting not only the VEGFR but also other receptors such as the PDGFR and FGFR, these agents may induce hypertension, fatigue, gastrointestinal disturbances, and cardiovascular toxicities. Such ADRs can significantly affect patients' quality of life, treatment adherence, and overall therapeutic outcomes (Shu et al., 2022; Zhang et al., 2024). Therefore, a systematic evaluation of their safety profiles is essential to optimize patient care and to address the ongoing challenge of rationally selecting the most appropriate MTKIs for RCC in clinical practice.

The Spontaneous Reporting System (SRS) serves an essential role in pharmacovigilance, facilitating the assessment of the safety of suspected AEs due to inherent limitations associated with clinical trials. Such limitations encompass stringent trial design, strict enrollment criteria, relatively small sample sizes, and short follow-up durations. Furthermore, data derived from clinical trials may not accurately represent real-world contexts, where variations in patient demographics and comorbidities can be significant. The SRS is crucial for detecting safety signals. Research related to the safety signals of numerous medications primarily relies on three major databases: the EudraVigilance Data Analysis System (EVDAS), the FDA Adverse Event Reporting System (FAERS), and WHO-VigiBase® (Vogel et al., 2020). In 2015, the WHO launched WHO-VigiAccess, a platform that grants public access to the data compiled in VigiBase®, which is the WHO's comprehensive repository of documented potential adverse effects linked to medicinal products. By analyzing information from the WHO-VigiAccess database, one can reveal previously unidentified connections between medications and AEs, as well as validate certain established clinical correlations (Yamoah

10.3389/fphar.2025.1585862

TABLE 5 Top 20 ADRs of four MTKIs.

Axitinib (N = 18,257)		Lenvatinib (N = 28,819)		Sorafenib (N = 35,009)		Sunitinib (N = 41,733)	
ADR	Report rate %	ADR	Report rate %	ADR	Report rate %	ADR	Report rate %
Diarrhoea	15.05%	Diarrhoea	12.02%	Diarrhoea	15.72%	Diarrhoea	11.89%
Fatigue	10.73%	Fatigue	10.34%	Rash	8.43%	Fatigue	10.48%
Death	9.00%	Hypertension	9.42%	Fatigue	7.83%	Nausea	7.65%
Hypertension	8.73%	Decreased appetite	8.20%	Decreased appetite	7.20%	Death	7.59%
Neoplasm progression	8.21%	Malignant neoplasm progression	7.35%	Nausea	6.40%	Neoplasm progression	7.52%
Off label use	6.48%	Nausea	7.10%	Off label use	6.27%	Disease progression	7.43%
Disease progression	6.04%	Blood pressure increased	6.34%	Asthenia	5.64%	Asthenia	6.20%
Nausea	5.70%	Vomiting	5.65%	Death	5.41%	Hypertension	6.04%
Dysphonia	5.58%	Asthenia	5.55%	Hepatocellular carcinoma	5.22%	Decreased appetite	5.61%
Decreased appetite	5.46%	Weight decreased	4.66%	Pain in extremity	4.67%	Vomiting	5.22%
Blood pressure increased	4.48%	Hypothyroidism	4.55%	Abdominal pain	4.58%	Stomatitis	4.10%
Asthenia	4.17%	Dehydration	3.97%	Alopecia	4.31%	Thrombocytopenia	3.99%
Weight decreased	4.06%	Headache	3.90%	Vomiting	4.30%	Dysgeusia	3.75%
Stomatitis	3.08%	Rash	3.08%	Pruritus	4.08%	Malaise	3.68%
Headache	3.05%	Stomatitis	2.89%	Weight decreased	4.04%	Weight decreased	3.41%
Vomiting	2.91%	Arthralgia	2.78%	Hypertension	3.95%	Platelet count decreased	3.19%
Hypothyroidism	2.56%	Constipation	2.58%	Blister	3.63%	Pain in extremity	3.10%
Malaise	2.55%	Dysphonia	2.53%	Pyrexia	3.26%	Blood pressure increased	3.04%
Rash	2.49%	Abdominal pain	2.49%	Skin exfoliation	2.87%	Anaemia	2.86%
Pain	2.46%	Death	2.38%	Pain	2.86%	Pain	2.79%

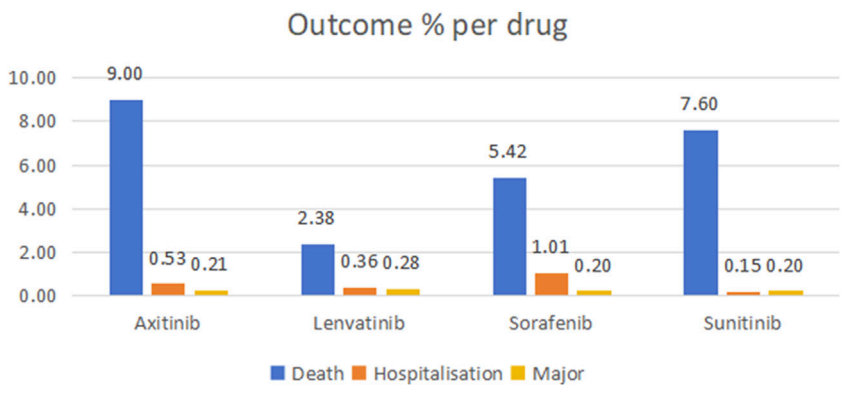

FIGURE 1
Outcomes for serious adverse events associated with four TIKs at the level of preferred terms (major events comprising life-threatening incidents, disabilities, and congenital anomalies).

TABLE 6 Same ADRs between four MTKIs.

System organ classes	ADRS	Signal N
Blood and lymphatic system disorders	Anaemia, Thrombocytopenia	2
Cardiac disorders	Cardiac failure, Palpitations, Cardiac failure congestive, Atrial fibrillation, Cardiac disorder, Myocardial infarction	6
Endocrine disorders	Hypothyroidism	1
Eye disorders	Visual impairment, Vision blurred	2
Gastrointestinal disorders	Flatulence, Stomatitis, Haematemesis, Dry mouth, Oral pain, Mouth ulceration, Pancreatitis, Gastrointestinal haemorrhage, Abdominal pain, Haematochezia, Dyspepsia, Nausea, Abdominal distension, Diarrhoea, Constipation, Vomiting, Abdominal pain upper, Abdominal discomfort, Dysphagia, Glossodynia, Gastrointestinal disorder	21
General disorders and administration site conditions	Condition aggravated, Mucosal inflammation, Pyrexia, Disease progression, Oedema, Drug ineffective, Oedema peripheral, Feeling abnormal, Malaise, Gait inability, Chest pain, Chills, General physical health deterioration, Peripheral swelling, Fatigue, Gait disturbance, Drug intolerance, Swelling, Pain, Asthenia, Death	21
Hepatobiliary disorders	Liver disorder, Hepatic function abnormal	2
Immune system disorders	Hypersensitivity	1
Infections and infestations	Urinary tract infection, Pneumonia, Nasopharyngitis, Sepsis, Infection	5
Injury, poisoning and procedural complications	Fall, Product dose omission issue, Product use in unapproved indication, Contusion, Toxicity to various agents, Off label use, Product use issue	7
Investigations	Blood creatinine increased, Haemoglobin decreased, Weight increased, Heart rate increased, White blood cell count decreased, Weight decreased, Blood pressure increased, Alanine aminotransferase increased, Hepatic enzyme increased, Blood bilirubin increased, Aspartate aminotransferase increased, Blood glucose increased, Blood potassium decreased, Platelet count decreased	14
Metabolism and nutrition disorders	Feeding disorder, Dehydration, Hyperkalaemia, Decreased appetite, Hypophagia, Hyponatraemia	6
Musculoskeletal and connective tissue disorders	Back pain, Joint swelling, Myalgia, Arthralgia, Muscular weakness, Muscle spasms, Musculoskeletal pain, Bone pain, Pain in extremity	9
Skin and subcutaneous tissue disorders	Alopecia, Skin exfoliation, Dry skin, Pruritus, Blister, Erythema, Acne, Skin discolouration, Skin disorder, Rash, Skin ulcer, Urticaria, Hyperkeratosis	13
Neoplasms benign, malignant and unspecified (incl cysts and polyps)	Renal cell carcinoma, Renal cancer, Malignant neoplasm progression	3
Nervous system disorders	Balance disorder, Burning sensation, Memory impairment, Cerebral haemorrhage, Somnolence, Lethargy, Tremor, Headache, Dizziness, Seizure, Speech disorder, Neuropathy peripheral, Loss of consciousness, Ageusia, Cerebrovascular accident, Hypoaesthesia, Syncope, Paraesthesia, Dysgeusia	18
Psychiatric disorders	Insomnia, Anxiety, Confusional state, Eating disorder, Depression	5
Renal and urinary disorders	Proteinuria, Renal failure, Acute kidney injury, Renal impairment, Haematuria	10
Respiratory, thoracic and mediastinal disorders	Cough, Epistaxis, Haemoptysis, Pleural effusion, Dysphonia, Interstitial lung disease, Pulmonary oedema, Oropharyngeal pain, Pulmonary embolism, Dyspnoea	10
Social circumstances	Loss of personal independence in daily activities	1
Vascular disorders	Deep vein thrombosis, Haemorrhage, Hypertension, Thrombosis, Blood pressure fluctuation, Hypotension	6

et al., 2022). This research intends to assess the post-market AEs associated with four MTKIs using the WHO-VigiAccess database.

According to data from WHO-VigiAccess, 48.26% of AEs related to these four MTKIs were reported from the Americas, with only 815 report of AEs originating from Africa. Prior research has highlighted a significant issue with the low reporting rates of AEs in both Africa and Oceania (Alawadhi et al., 2012; Gidudu et al., 2020). The incidence of RCC is higher in regions with elevated income levels, likely due to improved access to medical resources and the increased prevalence of imaging diagnostics. In South Africa, the limited understanding of biopharmaceuticals among healthcare workers, coupled with high costs and complex procurement procedures, further exacerbates the barriers to the utilization of these medications (Hajjaj-Hassouni et al., 2012; Martelli et al., 2017; Kvamme et al., 2020). The African region has been noted for having the lowest incidence of reported AEs, which could be linked to insufficient social mobilization, restricted access to AE reporting mechanisms, and low levels of information system coverage. The number of ADR reports from men (73,485) significantly exceeded that of women (43,281), yielding a male-to-

TABLE 7 Different ADRs between four MTKIs.

System organ classes	Axitinib	Lenvatinib	Sorafenib	Sunitinib
Blood and lymphatic system disorders	Polycythaemia			Disseminated intravascular coagulation
Cardiac disorders		Cardiomyopathy	Tachycardia	Bradycardia, Pericardial effusion
Eye disorders				Lacrimation increased, Eye swelling, Eyelid oedema, Periorbital oedema
Gastrointestinal disorders	Tongue discomfort, Glossitis, Swollen tongue	Large intestine perforation, Intestinal obstruction, Intestinal perforation	Melaena, Pancreatitis acute, Faeces discoloured, Gastritis, Oesophageal varices haemorrhage	
General disorders and administration site conditions	Therapy partial responder	Decreased activity	Feeling hot, Unevaluable event, Adverse drug reaction	Multiple organ dysfunction syndrome, Face oedema
Hepatobiliary disorders	Hypertransaminasaemia, Hepatic cytolysis	Cholangitis, Gallbladder disorder, Cholecystitis acute	Hepatic cirrhosis, Hepatic pain	
Immune system disorders	Drug hypersensitivity			Decreased immune responsiveness
Infections and infestations	Candida infection	Cystitis, Septic shock	Gastroenteritis	
Injury, poisoning and procedural complications	Product dose omission in error, Wound, Intentional product use issue, Infusion related reaction, Product prescribing error	Incorrect dose administered		
Investigations	Laboratory test abnormal	Heart rate decreased, Blood magnesium decreased, Blood calcium decreased	Lipase increased, Blood alkaline phosphatase increased, Body temperature increased, Alpha 1 foetoprotein increased	Full blood count abnormal, Red blood cell count decreased, Full blood count decreased, Blood urea increased, Ejection fraction decreased
Metabolism and nutrition disorders		Tumour lysis syndrome, Electrolyte imbalance, Type 1 diabetes mellitus	Fluid intake reduced, Hypophosphataemia	
Musculoskeletal and connective tissue disorders		Fistula	Flank pain	Pain in jaw
Skin and subcutaneous tissue disorders	Night sweats		Dermatitis bullous, Rash papular, Palmoplantar keratoderma, Dermatitis, Rash erythematous, Drug eruption, Skin burning sensation	Hair colour changes, Yellow skin
Neoplasms benign, malignant and unspecified (incl cysts and polyps)		Cancer pain	Hepatocellular carcinoma, Metastases to bone, Acute myeloid leukaemia, Hepatic cancer, Thyroid cancer, Metastasis, Metastases to central nervous system, Metastases to lung	Gastrointestinal stromal tumour
Nervous system disorders	Cognitive disorder, Dysstasia, Movement disorder	Altered state of consciousness, Migraine		
Psychiatric disorders		Delirium, Hallucination		Mental status changes
Renal and urinary disorders				Chronic kidney disease
Reproductive system and breast disorders		Vaginal haemorrhage		
Respiratory, thoracic and mediastinal disorders	Throat irritation, Rhinorrhoea			

(Continued on following page)

TABLE 7 (*Continued*) Different ADRs between four MTKIs.

System organ classes	Axitinib	Lenvatinib	Sorafenib	Sunitinib
Surgical and medical procedures	Hospice care, Therapy interrupted, Nephrectomy			
Vascular disorders	Polycythaemia	Internal haemorrhage	Flushing	Pallor

female ratio of 1.70:1. When excluding reports lacking information on age, the demographic groups with the highest rates of reported incidents were primarily those aged 45–64 years. This is consistent with epidemiological findings that RCC incidence is approximately twice as high in men compared to women, likely due to differences in sex hormones, gender-specific tumor microenvironments, and lifestyle factors. RCC is predominantly diagnosed in individuals aged 50–80 years (Capitanio et al., 2019). When analyzing the adverse reactions associated with these four MTKIs across different age groups, the lack of age data for 30,322 cases (24.49%) will inevitably impact the accuracy of our conclusions.

An AE reporting rate of ≥1% is typically regarded as common (Chen et al., 2019). The serious AEs associated with the four MTKIs—axitinib, lenvatinib, sorafenib, and sunitinib—include life-threatening events, disabilities, and congenital malformations. The mortality rates associated with these drugs are 9% for axitinib, 2.38% for lenvatinib, 5.42% for sorafenib, and 7.60% for sunitinib. Furthermore, sorafenib has a hospitalization rate of 1.01%. The most frequently reported ADRs for all four MTKIs include diarrhea, fatigue, death, hypertension, nausea, asthenia, weight loss, and vomiting. Notably, these four MTKIs exhibited the highest reported rates of adverse reactions within the gastrointestinal disorders category. An analysis of the ROR and PRR indicated that axitinib had the lowest reported proportion of gastrointestinal disorders, whereas sorafenib had a slightly higher reported proportion compared to the other drugs.

The adverse reaction most frequently encountered with the four MTKIs is diarrhea, which can significantly diminish treatment effectiveness and patient adherence, negatively impacting long-term outcomes for cancer patients, and in extreme cases, may even pose a threat to life (Keefe and Anthony, 2008). Diarrhea generally arises early in the treatment timeline, particularly during the initial month. The intensity of this condition is closely tied to the medication type and dosage. MTKIs can disrupt the blood supply to the intestinal lining by blocking the VEGFR, resulting in ischemia and hypoxia of the intestinal mucosa, which may trigger diarrhea. Additionally, patients on MTKIs therapy often develop submucosal fat accumulation in the gastrointestinal region, potentially linked to intestinal lymphangiectasia, which can exacerbate malabsorption and diarrhea (Liu et al., 2024). Managing diarrhea primarily depends on empirical symptomatic treatments, and educating patients is pivotal. It is vital for healthcare providers to discuss the possible side effects of MTKIs therapy with patients before starting treatment and to evaluate whether diarrhea is caused by MTKIs therapy during treatment. For those experiencing diarrhea, it is usually necessary to reduce or pause MTKIs therapy, and hospitalization may be considered if required. After diarrhea subsides, decisions regarding the resumption of treatment and dosage adjustments should be made based on the patient's clinical situation. Regarding therapeutic options, probiotics and fecal microbiota transplantation might be utilized to adjust the gut microbiota and ease diarrhea (Ianiro et al., 2020). It is crucial to distinguish MTKI-induced diarrhea from infectious diarrhea and chemotherapy-related diarrhea, managing each case individually according to the severity and related complications (Benson et al., 2004).

MTKIs have the potential to cause hypertension in the management of RCC. This is likely due to the suppression of nitric oxide and prostacyclin synthesis that occurs when MTKIs inhibit VEGFR, resulting in the contraction of vascular smooth muscle. Moreover, another possible reason for hypertension associated with MTKIs is capillary rarefaction. This condition involves decreased vascular density, which heightens vascular resistance and, in turn, raises blood pressure (Hasinoff and Patel, 2010). It is essential for hypertensive patients, especially older adults with elevated baseline blood pressure, to establish effective blood pressure management before starting MTKI treatment. Patients who experience hypertension during therapy should follow standard protocols for hypertension management. Should blood pressure rise to alarmingly high levels, it is recommended to modify the MTKI dosage or pause the treatment. Studies suggest that the likelihood of hypertension may correlate with the dose of MTKIs, and hypertension itself could act as an important biomarker related to the effectiveness of the treatment (Ravaud and Sire, 2009). For instance, research utilizing real-world data from Japan demonstrated that patients with hypertension receiving MTKIs for RCC experienced enhanced overall survival (OS) and PFS over a 24-week period (Akaza et al., 2015). Furthermore, hypertension that develops during therapy is acknowledged as a standalone biomarker for the efficacy of sunitinib (Donskov et al., 2015). While axitinib and lenvatinib tend to show a greater frequency of hypertension compared to sunitinib, they typically pose a lower risk of cardiovascular issues. A thorough cardiovascular risk evaluation should be carried out before beginning MTKIs therapy, alongside consistent monitoring of blood pressure and potential cardiotoxic effects during the initial treatment phase (Bæk Møller et al., 2019).

Hypothyroidism might be linked to the suppression of the VEGFR, leading to the deterioration of capillary networks within the thyroid and a subsequent decrease in blood flow to thyroid cells as a result of the blockade of VEGFR (Liao et al., 2021). In addition, it can negatively influence thyroid function by lowering iodine absorption and inhibiting the activity of thyroid peroxidase. The onset of hypothyroidism usually takes time to manifest and may continue even after treatment has stopped (Wu and Huang, 2020). Consequently, during the early phases of treatment, it is advisable to closely monitor thyroid function and to inform patients about associated symptoms to allow for quick detection and treatment

of thyroid-related issues. The clinical studies have verified that hypothyroidism among patients with RCC undergoing therapies like sunitinib or sorafenib acts as a favorable indicator of treatment success (Schmidinger et al., 2011; Baldazzi et al., 2012). Moreover, the emergence of skin rash is seen as a sign of increased effectiveness, with its side effects thought to relate to cross-activity among different kinases (Liu et al., 2013; Massey et al., 2015). Research has indicated that thoughtfully adjusting the medication dosage can substantially reduce adverse reactions while preserving therapeutic effectiveness. MTKIs hinder angiogenesis and disrupt the Wnt/β-catenin signaling pathway, affecting the differentiation of oral mucosal epithelial cells, preventing the regeneration of taste bud cells, and impairing nerve repair, which may result in conditions like stomatitiss, dry mouth, and dysgeusia (Boers-Doets et al., 2012; Epstein and Barasch, 2010; Naik et al., 2009). The inhibition of VEGF, recognized as a neurotrophic factor, could disrupt the conduction of taste nerves, while the broad inhibitory actions of these agents might further compromise olfactory capabilities (Carmeliet et al., 2013). Sunitinib has shown a notable association with dysgeusia, although the direct causal links remain ambiguous in current research.

These MTKIs are transported to the liver and metabolized by CYP3A4. So, avoid combining them with drugs that affect CYP3A4 activity. These drugs may alter the plasma concentrations of MTKIs, impacting efficacy or increasing toxicity (Bæk Møller et al., 2019; Wang et al., 2016). Also, a comprehensive, multidisciplinary approach can better manage MTKI - related drug ADRs, enhancing patients" treatment experience and prognosis. Implementing regular multidisciplinary meetings to share patient information and discuss complex cases, utilizing a shared electronic health records system for real-time access to the latest patient data, jointly developing and carrying out patient education programs to ensure patients fully understand their treatment and potential ADRs, and collaborating on research projects to assess the effectiveness of management strategies and promote improvements in clinical practice.

The WHO-VigiAccess database, which operates on a voluntary basis for AE reporting, presents several challenges that hinder its ability to deliver a complete and thorough count of AEs. The database may not contain all the necessary information regarding reported incidents, which underscores the importance of enhancing the transparency of reporting practices. By improving the clarity and accessibility of the data provided to the public, stakeholders can engage in more effective screening for potential connections between pharmaceuticals and adverse reactions. This would also help prevent misguidance that could arise from incomplete or unclear information. The reliance on a spontaneous reporting system carries significant inherent limitations, primarily due to various biases that can affect the reporting process. These include notoriety bias, wherein more well-known drugs may receive disproportionate attention, selection bias, which can skew the data towards certain demographics, and under-reporting, which typically results in significant gaps in data collection (Faillie, 2019).

Conclusion

Our research indicates that the adverse reaction reports submitted to the WHO and the FDA for these drugs highlight both common and specific adverse reactions. Clinicians must develop personalized treatment strategies that consider the adverse reactions associated with different drugs, as well as the unique circumstances of each patient, thereby encouraging the responsible use of these MTKIs.

Data availability statement

The original contributions presented in the study are included in the article/supplementary material, further inquiries can be directed to the corresponding authors.

Ethics statement

Ethical approval was not required for the study involving humans in accordance with the local legislation and institutional requirements. Written informed consent to participate in this study was not required from the participants or the participants' legal guardians/next of kin in accordance with the national legislation and the institutional requirements.

Author contributions

LJL: Writing – original draft, Writing – review and editing. JB: Writing – original draft, Writing – review and editing. XW: Writing – original draft, Writing – review and editing. XZ: Writing – original draft, Writing – review and editing.

Funding

The author(s) declare that financial support was received for the research and/or publication of this article. This work was supported by grants from the Hunan Natural Science Foundation Youth Foundation (2022JJ40388).

Acknowledgments

We sincerely appreciate the significant contributions made by all the authors towards this study, their invaluable efforts have been instrumental in its success. LJL serves as both the first author and the last corresponding author of this article.

Conflict of interest

The authors declare that the research was conducted in the absence of any commercial or financial relationships that could be construed as a potential conflict of interest.

Generative AI statement

The authors declare that no Generative AI was used in the creation of this manuscript.

Publisher's note

References

Akaza, H., Naito, S., Ueno, N., Aoki, K., Houzawa, H., Pitman, L. S., et al. (2015). Real-world use of sunitinib in Japanese patients with advanced renal cell carcinoma: efficacy, safety and biomarker analyses in 1689 consecutive patients. *Jpn. J. Clin. Oncol.* 45 (6), 576–583. doi:10.1093/jjco/hyv045

Alawadhi, A., Alawneh, K., and Alzahrani, Z. A. (2012). The effect of neutralizing antibodies on the sustainable efficacy of biologic therapies: what's in it for African and Middle Eastern rheumatologists. *Clin. Rheumatol.* 31 (9), 1281–1287. doi:10.1007/s10067-012-2040-2

Bahadoram, S., Davoodi, M., Hassanzadeh, S., Bahadoram, M., Barahman, M., and Mafakher, L. (2022). Renal cell carcinoma: an overview of the epidemiology, diagnosis, and treatment. *G. Ital. Nefrol.* 39 (3), 2022-vol3.

Bæk Møller, N., Budolfsen, C., Grimm, D., Krüger, M., Infanger, M., Wehland, M., et al. (2019). Drug-induced hypertension caused by multikinase inhibitors (sorafenib, sunitinib, lenvatinib and axitinib) in renal cell carcinoma treatment. *Int. J. Mol. Sci.* 20 (19), 4712. doi:10.3390/ijms20194712

Baldazzi, V., Tassi, R., Lapini, A., Santomaggio, C., Carini, M., and Mazzanti, R. (2012). The impact of sunitinib-induced hypothyroidism on progression-free survival of metastatic renal cancer patients: a prospective single-center study. *Urol. Oncol.* 30 (5), 704–710. doi:10.1016/j.urolonc.2010.07.015

Benson, A. B., 3rd, Ajani, J. A., Catalano, R. B., Engelking, C., Kornblau, S. M., Martenson, J. A., Jr., et al. (2004). Recommended guidelines for the treatment of cancer treatment-induced diarrhea. *J. Clin. Oncol.* 22 (14), 2918–2926. doi:10.1200/JCO.2004.04.132

Boers-Doets, C. B., Epstein, J. B., Raber-Durlacher, J. E., Ouwerkerk, J., Logan, R. M., Brakenhoff, J. A., et al. (2012). Oral adverse events associated with tyrosine kinase and mammalian target of rapamycin inhibitors in renal cell carcinoma: a structured literature review. *Oncol.* 17 (1), 135–144. doi:10.1634/theoncologist.2011-0111

Capitanio, U., Bensalah, K., Bex, A., Boorjian, S. A., Bray, F., Coleman, J., et al. (2019). Epidemiology of renal cell carcinoma. *Eur. Urol.* 75 (1), 74–84. doi:10.1016/j.eururo.2018.08.036

Carmeliet, P., Ruiz de Almodovar, C., and Carmen, R. D. A. (2013). VEGF ligands and receptors: implications in neurodevelopment and neurodegeneration. *Cell. Mol. Life Sci.* 70 (10), 1763–1778. doi:10.1007/s00018-013-1283-7

Chen, C., Borrego, M. E., Roberts, M. H., and Raisch, D. W. (2019). Comparison of post-marketing surveillance approaches regarding infections related to tumor necrosis factor inhibitors (TNFi's) used in treatment of autoimmune diseases. *Expert Opin. Drug Saf.* 18 (8), 733–744. doi:10.1080/14740338.2019.1630063

Chen, Y. W., Wang, L., Panian, J., Dhanji, S., Derweesh, I., Rose, B., et al. (2023). Treatment landscape of renal cell carcinoma. *Curr. Treat. Options Oncol.* 24 (12), 1889–1916. doi:10.1007/s11864-023-01161-5

Donskov, F., Michaelson, M. D., Puzanov, I., Davis, M. P., Bjarnason, G. A., Motzer, R. J., et al. (2015). Sunitinib-associated hypertension and neutropenia as efficacy biomarkers in metastatic renal cell carcinoma patients. *Br. J. Cancer* 113 (11), 1571–1580. doi:10.1038/bjc.2015.368

Epstein, J. B., and Barasch, A. (2010). Taste disorders in cancer patients: pathogenesis, and approach to assessment and management. *Oral Oncol.* 46 (2), 77–81. doi:10.1016/j.oraloncology.2009.11.008

Faillie, J. L. (2019). Case-non-case studies: principle, methods, bias and interpretation. *Therapie* 74 (2), 225–232. doi:10.1016/j.therap.2019.01.006

Faivre, S., Demetri, G., Sargent, W., and Raymond, E. (2007). Molecular basis for sunitinib efficacy and future clinical development. *Nat. Rev. Drug Discov.* 6 (9), 734–745. doi:10.1038/nrd2380

Gagliardi, A., Iaquinta, F. S., Grembiale, R. D., De Sarro, C., Fabiano, A., Fraija, D., et al. (2022). Real-world safety profile of biologics used in rheumatology: a six-year observational pharmacovigilance study in the calabria region. *Pharmaceutics* 14 (11), 2328. doi:10.3390/pharmaceutics14112328

Gidudu, J. F., Shaum, A., Dodoo, A., Bosomprah, S., Bonsu, G., Amponsa-Achiano, K., et al. (2020). Barriers to healthcare workers reporting adverse events following immunization in four regions of Ghana. *Vaccine* 38 (5), 1009–1014. doi:10.1016/j.vaccine.2019.11.050

Habarugira, J. M. V., and Figueras, A. (2021). Pharmacovigilance network as an additional tool for the surveillance of antimicrobial resistance. *Pharmacoepidemiol. Drug Saf.* 30 (8), 1123–1131. doi:10.1002/pds.5249

Hajjaj-Hassouni, N., Al-Badi, M., Al-Heresh, A., Al-Emadi, S., El Bawendi, A., El Garf, A., et al. (2012). The practical value of biologics registries in Africa and Middle East: challenges and opportunities. *Clin. Rheumatol.* 31 (3), 407–416. doi:10.1007/s10067-011-1918-8

Hasinoff, B. B., and Patel, D. (2010). Mechanisms of myocyte cytotoxicity induced by the multikinase inhibitor sorafenib. *Cardiovasc. Toxicol.* 10 (1), 1–8. doi:10.1007/s12012-009-9056-0

Hsieh, J. J., Purdue, M. P., Signoretti, S., Swanton, C., Albiges, L., Schmidinger, M., et al. (2017). Renal cell carcinoma. *Nat. Rev. Dis. Prim.* 3, 17009. doi:10.1038/nrdp.2017.9

Ianiro, G., Rossi, E., Thomas, A. M., Schinzari, G., Masucci, L., Quaranta, G., et al. (2020). Faecal microbiota transplantation for the treatment of diarrhoea induced by tyrosine-kinase inhibitors in patients with metastatic renal cell carcinoma. *Nat. Commun.* 11 (1), 4333. doi:10.1038/s41467-020-18127-y

Keefe, D., and Anthony, L. (2008). Tyrosine kinase inhibitors and gut toxicity: a new era in supportive care. *Curr. Opin. Support. Palliat. Care* 2 (1), 19–21. doi:10.1097/SPC.0b013e3282f5273f

Kvamme, M. K., Lie, E., Uhlig, T., Moger, T. A., Kvien, T. K., and Kristiansen, I. S. (2020). Cost-effectiveness of TNF inhibitors vs synthetic disease-modifying antirheumatic drugs in patients with rheumatoid arthritis: a Markov model study based on two longitudinal observational studies. *Rheumatol. Oxf. Engl.* 59 (4), 917. doi:10.1093/rheumatology/kez609

Liao, X., Liu, Z., and Song, H. (2021). Thyroid dysfunction related to vascular endothelial growth factor receptor tyrosine kinase inhibitors: a real-world study based on FAERS. *J. Clin. Pharm. Ther.* 46 (5), 1418–1425. doi:10.1111/jcpt.13472

Liu, H. B., Wu, Y., Lv, T. F., Yao, Y. W., Xiao, Y. Y., Yuan, D. M., et al. (2013). Skin rash could predict the response to EGFR tyrosine kinase inhibitor and the prognosis for patients with non-small cell lung cancer: a systematic review and meta-analysis. *PloS One* 8 (1), e55128. doi:10.1371/journal.pone.0055128

Liu, J., Yan, S., Du, J., Teng, L., Yang, R., Xu, P., et al. (2024). Mechanism and treatment of diarrhea associated with tyrosine kinase inhibitors. *Heliyon* 10 (6), e27531. doi:10.1016/j.heliyon.2024.e27531

Martelli, L., Olivera, P., Roblin, X., Attar, A., and Peyrin-Biroulet, L. (2017). Cost-effectiveness of drug monitoring of anti-TNF therapy in inflammatory bowel disease and rheumatoid arthritis: a systematic review. *J. Gastroenterol.* 52 (1), 19–25. doi:10.1007/s00535-016-1266-1

Massey, P. R., Okman, J. S., Wilkerson, J., and Cowen, E. W. (2015). Tyrosine kinase inhibitors directed against the vascular endothelial growth factor receptor (VEGFR) have distinct cutaneous toxicity profiles: a meta-analysis and review of the literature. *Support. Care Cancer* 23 (6), 1827–1835. doi:10.1007/s00520-014-2520-9

Montastruc, J. L., Sommet, A., Bagheri, H., and Lapeyre-Mestre, M. (2011). Benefits and strengths of the disproportionality analysis for identification of adverse drug reactions in a pharmacovigilance database. *Br. J. Clin. Pharmacol.* 72 (6), 905–908. doi:10.1111/j.1365-2125.2011.04037.x

Moran, M., Nickens, D., Adcock, K., Bennetts, M., Desscan, A., Charnley, N., et al. (2019). Sunitinib for metastatic renal cell carcinoma: a systematic review and meta-analysis of real-world and clinical trials data. *Target. Oncol.* 14 (4), 405–416. doi:10.1007/s11523-019-00653-5

Motzer, R. J., Hutson, T. E., Glen, H., Michaelson, M. D., Molina, A., Eisen, T., et al. (2015). Lenvatinib, everolimus, and the combination in patients with metastatic renal cell carcinoma: a randomised, phase 2, open-label, multicentre trial. *Lancet Oncol.* 16 (15), 1473–1482. doi:10.1016/S1470-2045(15)00290-9

Naik, S., Dothager, R. S., Marasa, J., Lewis, C. L., and Piwnica-Worms, D. (2009). Vascular endothelial growth factor receptor-1 is synthetic lethal to aberrant {beta}-Catenin activation in colon cancer. *Clin. Cancer Res.* 15 (24), 7529–7537. doi:10.1158/1078-0432.CCR-09-0336

Ravaud, A., and Sire, M. (2009). Arterial hypertension and clinical benefit of sunitinib, sorafenib and bevacizumab in first and second-line treatment of metastatic renal cell cancer. *Ann. Oncol.* 20 (5), 966–967. doi:10.1093/annonc/mdp201

Romero, D. (2019). Axitinib-ICIs boost the RCC armamentarium. *Nat. Rev. Clin. Oncol.* 16 (4), 207. doi:10.1038/s41571-019-0193-5

Sato, Y., Yoshizato, T., Shiraishi, Y., Maekawa, S., Okuno, Y., Kamura, T., et al. (2013). Integrated molecular analysis of clear-cell renal cell carcinoma. *Nat. Genet.* 45 (8), 860–867. doi:10.1038/ng.2699

Schmidinger, M., Vogl, U. M., Bojic, M., Lamm, W., Heinzl, H., Haitel, A., et al. (2011). Hypothyroidism in patients with renal cell carcinoma: blessing or curse? *Cancer* 117 (3), 534–544. doi:10.1002/cncr.25422

Schmidt, D., Rodat, T., Heintze, L., Weber, J., Horbert, R., Girreser, U., et al. (2018). Axitinib: a photoswitchable approved tyrosine kinase inhibitor. *ChemMedChem* 13 (22), 2415–2426. doi:10.1002/cmdc.201800531

Shu, Y., Ding, Y., Dai, B., and Zhang, Q. (2022). A real-world pharmacovigilance study of axitinib: data mining of the public version of FDA adverse event reporting system. *Expert Opin. Drug Saf.* 21 (4), 563–572. doi:10.1080/14740338.2022.2016696

Sultana, J., Scondotto, G., Cutroneo, P. M., Morgante, F., and Trifirò, G. (2020). Intravitreal anti-VEGF drugs and signals of dementia and Parkinson-like events: analysis of the VigiBase database of spontaneous reports. *Front. Pharmacol.* 11, 315. doi:10.3389/fphar.2020.00315

Vogel, U., van Stekelenborg, J., Dreyfus, B., Garg, A., Habib, M., Hosain, R., et al. (2020). Investigating overlap in signals from EVDAS, FAERS, and VigiBase(®). *Drug Saf.* 43 (4), 351–362. doi:10.1007/s40264-019-00899-y

Wang, X., Zhang, X., Huang, X., Li, Y., Wu, M., and Liu, J. (2016). The drug-drug interaction of sorafenib mediated by P-glycoprotein and CYP3A4. *Xenobiotica* 46 (7), 651–658. doi:10.3109/00498254.2015.1109160

Watson, S., Chandler, R. E., Taavola, H., Härmark, L., Grundmark, B., Zekarias, A., et al. (2018). Safety concerns reported by patients identified in a collaborative signal detection workshop using VigiBase: results and reflections from lareb and uppsala monitoring centre. *Drug Saf.* 41 (2), 203–212. doi:10.1007/s40264-017-0594-2

Wilhelm, S., Carter, C., Lynch, M., Lowinger, T., Dumas, J., Smith, R. A., et al. (2006). Discovery and development of sorafenib: a multikinase inhibitor for treating cancer. *Nat. Rev. Drug Discov.* 5 (10), 835–844. doi:10.1038/nrd2130

Wu, J., and Huang, H. (2020). Acquired hypothyroidism in patients with metastatic renal cell carcinoma treated with tyrosine kinase inhibitors. *Drug Des. Dev. Ther.* 14, 3977–3982. doi:10.2147/DDDT.S270210

Yamoah, P., Mensah, K. B., Attakorah, J., Padayachee, N., Oosthuizen, F., and Bangalee, V. (2022). Adverse events following immunization associated with coronavirus disease 2019 (COVID-19) vaccines: a descriptive analysis from VigiAccess. *Hum. Vaccin. Immunother.* 18 (6), 2109365. doi:10.1080/21645515.2022.2109365

Zhang, X., Ren, X., Zhu, T., Zheng, W., Shen, C., and Lu, C. (2024). A real-world pharmacovigilance study of FDA adverse event reporting system (FAERS) events for sunitinib. *Front. Pharmacol.* 15, 1407709. doi:10.3389/fphar.2024.1407709

frontiers | Frontiers in Pharmacology

TYPE Original Research
PUBLISHED 27 May 2025
DOI 10.3389/fphar.2025.1618898

OPEN ACCESS

EDITED BY
Lei Yin,
Shanghai Jiaotong University School of Medicine, China

REVIEWED BY
Chunhua Lin,
Yantai Yuhuangding Hospital, China
Shouzhen Chen,
Shandong University, China

*CORRESPONDENCE
Sentai Ding,
dingsentai@126.com

RECEIVED 27 April 2025
ACCEPTED 14 May 2025
PUBLISHED 27 May 2025

CITATION
Cui J, Xu P, Guo C, Guan Y, Zhu K and Ding S (2025) Efficacy and safety of Tislelizumab combined with Axitinib as first-line treatment for intermediate- and high-risk metastatic clear-cell renal cell carcinoma.
Front. Pharmacol. 16:1618898.
doi: 10.3389/fphar.2025.1618898

Efficacy and safety of Tislelizumab combined with Axitinib as first-line treatment for intermediate- and high-risk metastatic clear-cell renal cell carcinoma

Jie Cui[1], Pengyong Xu[1], Changying Guo[1,2], Yong Guan[1,2], Kejia Zhu[1,2] and Sentai Ding[1,2]*

[1]Department of Urology, Yantai Penglai People's Hospital, Yantai, China, [2]Department of Urology, Shandong Provincial Hospital Affiliated to Shandong First Medical University, Jinan, China

Objective: To evaluate the efficacy and safety of Tislelizumab combined with Axitinib in the treatment of intermediate-high risk metastatic clear-cell renal cell carcinoma (ccRCC).

Methods: From September 2021 to June 2023, a total of 20 untreated patients with intermediate-high risk metastatic advanced ccRCC from Shandong Provincial Hospital were included in the study. Clinical characteristics and efficacy were analyzed, and adverse events (AEs) were summarized. All patients received Tislelizumab (200 mg every 3 weeks) and Axitinib (5 mg twice daily bid) until disease progression or intolerable toxicity occurred. The primary endpoint was objective response rate (ORR), and secondary endpoints included disease control rate (DCR), progression-free survival (PFS), overall survival (OS), and incidence of adverse reactions (AEs).

Results: The median follow-up time was 19.0 months (range, 9.2–24.4 months), and the median treatment cycle was 16 (range, 2–16). Partial response was observed in 14 patients (70%), stable disease in 2 patients (10%), and disease progression in 4 patient (20%). The overall ORR was 70.0%, and the DCR was 80.0%. The 1-year OS rate was 100%. The incidence of any grade AEs was 85% (17/20), and the incidence of grade 3–4 AEs was 15% (3/20). Common AEs included gastrointestinal reactions (60%, 12/20), rash (40%, 8/20), and hypertension (30%, 6/20).

Conclusion: Tislelizumab combined with Axitinib as first-line treatment for intermediate-high risk metastatic ccRCC showed significant efficacy and manageable safety.

KEYWORDS

clear-cell renal cell carcinoma, tislelizumab, axitinib, first-line treatment, immunotherapy

1 Introduction

Renal cell carcinoma (RCC) is one of the most common malignancies of the urinary system, accounting for approximately 3%–5% of newly diagnosed cancer cases (Capitanio et al., 2019). Surgery is the primary treatment for early-stage RCC; however, due to its insidious symptoms, 20%–30% of patients present with distant metastases at the time of initial diagnosis, rendering them ineligible for surgical intervention. Additionally, about 30%–40% of patients who undergo radical surgery will experience a recurrence of metastatic disease (Bahadoram et al., 2022). Once metastasis occurs, the 5-year survival rate for these patients is approximately 10% (Siegel et al., 2022). Although first-line targeted therapies that inhibit TKI(Tyrosine Kinase Inhibitors),including epidermal growth factor receptor (EGFR),vascular endothelial growth factor receptors (VEGFRs),platelet-derived growth factor receptor (PDGFR), fibroblast growth factor receptor (FGFR), KIT,etc., such as sunitinib, axitinib, and pazopanib, have significantly improved the prognosis of patients with advanced RCC, most patients who receive long-term monotherapy with TKI and then followed by VEGFR inhibitors axitinib or Everolimus etc., and eventually develop resistance, failing to achieve a sustained clinical response (Bergers and Hanahan, 2008; Padala et al., 2020).

Multiple studies have shown that adding anti-programmed death receptor-1 (PD-1)/ programmed death receptor ligand 1 (PD-L1) monoclonal antibodies to VEGFR inhibitors exhibits synergistic antitumor activity, significantly improving the efficacy of first-line treatment for advanced RCC (Motzer et al., 2019; Rini et al., 2019a; Powles et al., 2020). Large clinical studies have demonstrated that the objective response rate (ORR) of pembrolizumab combined with axitinib as first-line treatment for advanced RCC is 59.3%, with a progression-free survival (PFS) of 15.4 months (Powles et al., 2020). Consequently, the National Comprehensive Cancer Network (NCCN), the European Association of Urology (EAU), and the Chinese Society of Clinical Oncology (CSCO) guidelines for the diagnosis and treatment of renal cancer have recommended immunotherapy combined with axitinib as a first-line treatment option for advanced RCC. Besides pembrolizumab, clinical studies of other PD-1/PD-L1 inhibitors (such as avelumab, toripalimab, etc.) combined with axitinib have also further validated the efficacy of these targeted immunotherapy combinations (Yan et al., 2024; Choueiri et al., 2025). However, the options for first-line treatment of advanced metastatic RCC with immunotherapy combined with axitinib remain limited.

Tislelizumab is a humanized anti-PD-1 IgG4 monoclonal antibody with a modified Fc region designed to minimize binding to macrophage Fcγ receptors (FcγR). This modification effectively avoids antibody-dependent cellular phagocytosis (ADCP), a potential mechanism for T-cell clearance and resistance to anti-PD-1 antibodies. Additionally, Tislelizumab exhibits a different binding mode compared to other immune checkpoint inhibitors, resulting in superior affinity—approximately 100 times higher than Pembrolizumab and 50 times higher than Nivolumab (Feng et al., 2019; Lee and Keam, 2020; Lee et al., 2020). In 2020, Tislelizumab was approved by the National Medical Products Administration (NMPA) for the treatment of advanced urothelial carcinoma, making it the first immune checkpoint inhibitor approved for a urological cancer indication in China (Ding et al., 2025). Previous studies have shown that the combination of Axitinib and Tislelizumab significantly improves efficacy compared to Axitinib monotherapy (ORR, 59.1% vs. 40.7%; DCR, 81.8% vs. 66.7%) (Wang et al., 2022). Another study investigating the efficacy of Axitinib combined with Tislelizumab in advanced RCC reported an ORR of 50%, with one patient achieving complete response (CR) (Wu C et al., 2021). Therefore, this real-world observational study aims to analyze the efficacy and safety of Tislelizumab combined with Axitinib as first-line treatment in patients with metastatic RCC treated at Shandong Provincial Hospital.

2 Materials and methods

2.1 Data collection

This study included 20 patients with intermediate-high risk metastatic advanced ccRCC from Shandong Provincial Hospital between September 2021 and June 2023.

2.2 Inclusion criteria

(1)Histopathologically confirmed recurrent or metastatic advanced clear cell renal carcinoma. (2) Patients aged 18–75 years. (3) No prior treatment with targeted therapy or immune checkpoint inhibitors. (4) At least one measurable target lesion at enrollment according to RECIST Version 1.1. (5) All acute toxicities from previous anti-tumor treatments resolved to grade 0–1 or to the levels specified in the inclusion/exclusion criteria (except for alopecia and other toxicities deemed not to pose a safety risk by the investigator) according to NCI CTCAE Version 5.0. (6) Expected survival time ≥12 weeks. (7) Karnofsky Performance Status (KPS) score >60, Eastern Cooperative Oncology Group (ECOG) performance status score of 0–2. (8) Adequate organ function, including absolute neutrophil count ≥1.5 × 10⁹/L, platelets ≥80 × 10⁹/L, hemoglobin ≥9.0 g/dL; total bilirubin ≤1.5×upper limit of normal (ULN), alanine aminotransferase (ALT) and aspartate aminotransferase (AST) ≤2.5×ULN (≤5×ULN for patients with liver metastases); serum creatinine ≤1.25×ULN or creatinine clearance rate ≥60 mL/min.

2.3 Treatment protocol

All patients received intravenous Tislelizumab 200 mg every 3 weeks and oral Axitinib (5 mg orally twice daily) until disease progression or intolerable toxicity occurred. The primary endpoint was objective response rate (ORR), and secondary endpoints included disease control rate (DCR), progression-free survival (PFS), overall survival (OS), and incidence of adverse events (AEs).

TABLE 1 Baseline characteristics.

Characteristic	patients
Age,Median (range) — yr	60.2 (33.5–82.3)
Male sex — no. (%)	16 (80.0)
ECOG,no. (%)	
0–1	14 (70.0)
2	6 (30.0)
IMDC prognostic risk, no. (%)	
Intermediate	15 (75.0)
Poor	5 (25.0)
Stage, no. (%)	
III	7 (35.0)
IV	13 (65.0)
Sites of metastasis — no. (%)	
Lung	9 (45.0)
Bone	5 (25.0)
Lymph node	5 (25.0)
pancreas	1 (5.0)
omentum	1 (5.0)
brain	1 (5.0)
Liver	1 (5.0)

ECOG, eastern cooperative oncology group; IMDC, international metastatic renal cell carcinoma database consortium.

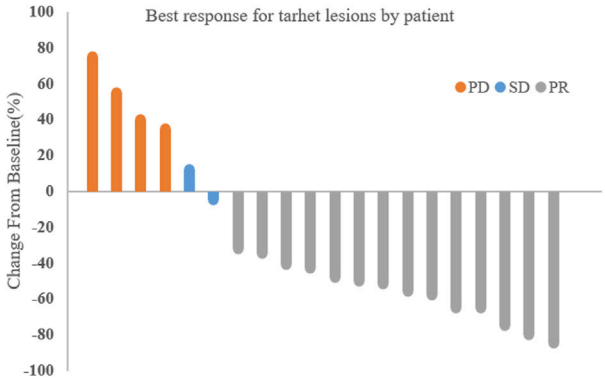

FIGURE 1
Best response for target lesions by patient.

2.4 Efficacy and adverse event evaluation

Efficacy was evaluated using CT or MRI imaging before treatment and every 6 weeks after the start of treatment, according to RECIST Version 1.1. Adverse events were graded according to NCI CTCAE Version 5.0.

2.5 Statistical analysis

Statistical analyses were performed using SPSS 16.0 software. Categorical data were expressed as numbers or percentages. Continuous data (e.g., age) were expressed as median (range). The correlation between gene mutations and PD-L1 status with treatment efficacy was analyzed using Fisher's exact test. Survival curves were generated using the Kaplan-Meier method, and survival times were expressed as median with 95% confidence intervals (CI). A two-sided P-value ≤0.05 was considered statistically significant.

3 Results

3.1 Clinical data

A total of 20 patients were included in this study, comprising 16 males (80%) and 4 females (20%), with a median age of 60.2 years (range, 33.5–82.3 years). Among them, 14 patients (70%) had an ECOG performance status score of 0–1, and 6 patients (30%) had a score of 2. According to IMDC risk stratification, 15 patients (75%) were classified as intermediate risk, and 5 patients (25%) as high risk. Tumor staging revealed 7 patients (35%) with stage III and 13 patients (65%) with stage IV disease. The most common sites of metastasis were the lungs (9 patients, 45%), bones (5 patients, 25%), lymph nodes (5 patients, 25%), and other sites (4 patients, including the pancreas, omentum, liver and brain). The baseline characteristics of all patients are shown in Table 1.

3.2 Efficacy analysis

The median treatment cycle was 16 cycles (range, 2–16), and the median follow-up time was 19.0 months (range, 9.2–24.4 months). All 20 patients were evaluable for efficacy (Figure 1). Among them, 14 patients (70%) achieved partial response (PR), 2 patients (10%) had stable disease (SD), and 4 patients (20%) experienced disease progression (PD). The overall objective response rate (ORR) was 70% (95% CI, 48.9%–84.8%), and the disease control rate (DCR) was 80% (95% CI, 58.4%–91.9%).

3.3 Gene mutations and PD-L1 status

Using capture-based NGS sequencing (Illumina Hiseq4000), the most common mutations identified in the patients of this study were VHL (40%), BAP1 (25%), and TP53 (25%). The current data did not reveal a significant correlation between VHL mutation status and ORR ($p = 0.37$). Immunohistochemical analysis was conducted utilizing the 22C3 antibody, where a Combined Positive Score (CPS) greater than 1 was used as the threshold to determine PD-L1 positivity. In this study, the PD-L1 positivity rate was 40% (8/20). Fisher's exact test analysis showed no correlation between PD-L1 status and ORR ($p = 0.67$). The PD-L1 and gene mutation status of all patients are shown in Table 2. PD-L1 staining image of PD-L1 protein expression level detection are shown in Figure 2.

3.4 Adverse events

Among the 20 patients, the incidence of any grade adverse events (AEs) was 85% (17/20). Most AEs were grade 1–2, with

TABLE 2 PD-L1 and gene mutation status.

No.	PD-L1 (+/−); CPS	Gene mutations
1	(−); 0	VHL S80R、BAP1
2	(+); 5	ARID1A c.4101 + 1G>A、VHL W117S、MET、BAP1
3	(−); 0	MAP2K2 F57L、NONO-TFE3 (N3::T7)、BAP1
4	(+); 60	CDKN2A A36fs、TP53 P75fs、TP53 V157F、BAP1
5	(−); 0	BAP1 S482fs
6	(−); 0	PTEN PIK3CA
7	(+); 20	VHL CHEK1 TP53
8	(−); 0	POLD1、TP53
9	(+); 20	FGFR1、ARID1A
10	(−); 0	VHL H115N
11	(−); 0	MTOR R2368Q
12	(+); 5	TP53 G266R
13	(−); 0	VHL E55Vfs*77
14	(−); 0.1	PIK3CA E707K、TSC1 R37C
15	(−); 0	PIK3CA H1047R、KRAS G12V、TP53 R273C、VHL V130Lfs*29
16	(−); 0	MTOR S2215F、FGFR3 E157K、ATRX D1916N
17	(−); 0	TSC1 R509*、VHL F76Sfs*83
18	(+); 8	TP53 H179R、VHL C162Afs*8
19	(+); 55	ATM Q1531*
20	(+); 1	CCND1 E280V、VHL I206Nfs*50

PD-L1, programmed death receptor ligand 1; CPS, Combined Positive Score; +:PD-L1, positive; -:PD-L1, negative.

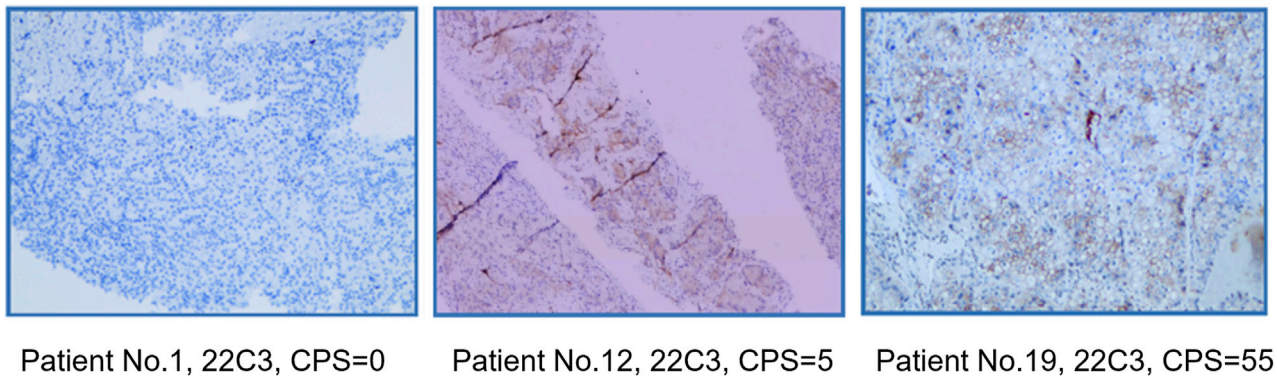

FIGURE 2
PD-L1 staining image of PD-L1 protein expression level detection.

common AEs including diarrhea (60%, 12/20), rash (40%, 8/20), pruritus (30%, 6/20), hypertension (30%, 6/20), and decreased appetite (15%, 3/20). The incidence of grade ≥3 AEs was 15% (3/20). Specifically, One patient was classified as having grade 3 hypertension and required two antihypertensive medications to maintain normal blood pressure levels. Another patient experienced grade 3 skin adverse reactions, leading to permanent discontinuation of the medication and subsequent treatment at a dermatology hospital. A third patient developed grade 3 liver function impairment and grade 3 thrombocytopenia

5 days after the first administration of Tislelizumab. The patient's aspartate aminotransferase levels peaked at 288 U/L, and platelet count dropped to a minimum of 46 x 109/L, resulting in disseminated intravascular coagulation. The patient was admitted to the intensive care unit for treatment, including methylprednisolone pulse therapy. Three days later, the adverse reactions reduced to grade 1. It was decided to suspend Tislelizumab and continue with Pazopanib targeted therapy.

4 Discussion

This study is the first report on the efficacy and safety of Tislelizumab combined with Axitinib as first-line treatment for Chinese patients with intermediate-high risk metastatic RCC. The results showed that the 20 patients had favorable tumor response and safety profiles, with an ORR of 70%, a DCR of 80%.

Compared to previous trials involving unselected patient populations, this real-world study focused on a higher-risk population, with all enrolled patients being classified as intermediate-high risk according to IMDC stratification (100% vs. 68%–80%) (Motzer et al., 2018; Motzer et al., 2019; Rini et al., 2019a; Rini et al., 2019b; Choueiri et al., 2021; Motzer et al., 2021; Yan et al., 2024). In this study, treatment-naive metastatic RCC patients receiving the combination of Axitinib and Tislelizumab demonstrated significantly higher ORR values compared to most similar treatment regimens (70% vs. 37.0%–59.3%) (Motzer et al., 2019; Rini et al., 2019a; Yan et al., 2024), confirming its efficacy as a first-line treatment for metastatic RCC. Additionally, due to the short follow-up period, the PFS and OS data are not yet mature. Despite the significant efficacy observed, the results of cross-comparisons should be interpreted with caution; furthermore, due to the small sample size and study design limitations, larger phase III trials are needed to validate the efficacy of this combination therapy.

In terms of safety, Tislelizumab combined with Axitinib was well-tolerated. The incidence of any grade AEs in this study was 94.1%, with common events such as gastrointestinal reactions, skin reactions, and hypertension, which were generally tolerable and manageable, resolving quickly after symptomatic treatment. Additionally, the incidence of grade ≥3 AEs was 17.6%, including hypertension, skin reactions, and liver toxicity, which were successfully controlled through necessary dose reductions or treatment interruptions. Hypertension was one of the most common AEs in this study, as well as a typical treatment-related toxicity in other immunotherapy combined with Axitinib regimens. Compared to safety data reported abroad, the incidence of any grade (35.3% vs. 49.5%) and grade ≥3 (5.9% vs. 25.6%) hypertension in this study was lower (Rini et al., 2019a). Overall, Tislelizumab combined with Axitinib was well-tolerated by most patients.

In this study, no significant correlation was observed between PD-L1 positivity (40%) and ORR ($p = 0.67$). Another RENOTORCH study of axitinib in combination with teraplizumab included patients with intermediate- to high-risk advanced renal cancer, with an ORR of 58.54% (24/41) for the combination in 24 high-risk patients assessed by an independent review committee, but no data on PD-L1 status and efficacy (Yan et al., 2024). The synergistic effect of axitinib with immunotherapy has been demonstrated to enhance T-cell infiltration in tumours, thereby partially counteracting immunosuppression in PD-L1-negative patients (Atkins MB, et al., 2018). Kidney cancer develops in 25%–45% of VHL patients and is uniformly clear cell, bilateral, and multifocal (Schmidt and Linehan, 2016). In this study, the VHL mutation rate was found to be 40% in the cohort of high-risk patients. No significant association was identified between VHL mutation status and objective response rate ($p = 0.37$). Furthermore, it was hypothesised that genomic complexity (e.g., chromosomal copy number variation, epigenetic remodelling) in high-risk populations may mask the predictive value of a single gene (e.g., VHL). It is noteworthy that, although VHL mutation status was not significantly associated with ORR ($p = 0.37$), BAP1/TP53 co-mutations (10% of this cohort) may be associated with poorer treatment response.

This study also has some limitations: (1) The follow-up period was short, and survival indicators are not yet complete, requiring further exploration of the long-term survival outcomes and safety of Tislelizumab combined with Axitinib; (2) Due to the study design and sample size limitations, all interpretations of the results are preliminary, and larger trials are needed in the future to further validate the clinical practice value of this combination regimen.

In summary, this real-world prospective study demonstrates that Tislelizumab combined with Axitinib as first-line treatment for intermediate-high risk metastatic RCC is effective and safe. This study suggests that this combination regimen is a feasible treatment strategy for intermediate-high risk metastatic RCC.

Data availability statement

The original contributions presented in the study are included in the article/supplementary material, further inquiries can be directed to the corresponding author.

Ethics statement

The studies involving humans were approved by Shandong Provincial Hospital Medical Ethics Committee (2021-370). The studies were conducted in accordance with the local legislation and institutional requirements. The participants provided their written informed consent to participate in this study.

Author contributions

JC: Writing – original draft, Validation, Conceptualization. PX: Validation, Investigation, Writing – review and editing. CG: Writing – review and editing, Project administration. YG: Writing – review and editing, Project administration. KZ: Writing – original draft. SD: Writing – review and editing, Funding acquisition, Supervision, Resources, Conceptualization.

Funding

The author(s) declare that financial support was received for the research and/or publication of this article. This study was funded by Shandong Provincial Natural Science Foundation (grant nos. ZR2021QH313, ZR2023LZL005).

Conflict of interest

The authors declare that the research was conducted in the absence of any commercial or financial relationships that could be construed as a potential conflict of interest.

Generative AI statement

The author(s) declare that no Generative AI was used in the creation of this manuscript.

Publisher's note

All claims expressed in this article are solely those of the authors and do not necessarily represent those of their affiliated organizations, or those of the publisher, the editors and the reviewers. Any product that may be evaluated in this article, or claim that may be made by its manufacturer, is not guaranteed or endorsed by the publisher.

References

Atkins, M. B., Plimack, E. R., Puzanov, I., Fishman, M. N., McDermott, D. F., Cho, D. C., et al. (2018). Axitinib in combination with pembrolizumab in patients with advanced renal cell cancer: a non-randomised, open-label, dose-finding, and dose-expansion phase 1b trial. *Lancet Oncol.* 19, 405–415. doi:10.1016/S1470-2045(18)30081-0

Bahadoram, S., Davoodi, M., Hassanzadeh, S., Bahadoram, M., Barahman, M., and Mafakher, L. (2022). Renal cell carcinoma: an overview of the epidemiology, diagnosis, and treatment. *G. Ital. Nefrol.* 39 (3), 2022.

Bergers, G., and Hanahan, D. (2008). Modes of resistance to anti-angiogenic therapy. *Nat. Rev. Cancer* 8 (8), 592–603. doi:10.1038/nrc2442

Capitanio, U., Bensalah, K., Bex, A., Boorjian, S. A., Bray, F., Coleman, J., et al. (2019). Epidemiology of renal cell carcinoma. *Eur. Urol.* 75 (1), 74–84. doi:10.1016/j.eururo.2018.08.036

Choueiri, T. K., Penkov, K., Uemura, H., Campbell, M. T., Pal, S., Kollmannsberger, C., et al. (2025). Avelumab + axitinib versus sunitinib as first-line treatment for patients with advanced renal cell carcinoma: final analysis of the phase III JAVELIN Renal 101 trial. *Ann. Oncol.* 36 (4), 387–392. doi:10.1016/j.annonc.2024.12.008

Choueiri, T. K., Powles, T., Burotto, M., Escudier, B., Bourlon, M. T., Zurawski, B., et al. (2021). Nivolumab plus Cabozantinib versus sunitinib for advanced renal-cell carcinoma. *N. Engl. J. Med.* 384 (9), 829–841. doi:10.1056/NEJMoa2026982

Ding, S., Wu, C., Cao, J., and Lyu, J. (2025). Immune checkpoint inhibitor therapy as a neoadjuvant treatment for muscle-invasive bladder carcinoma: a narrative review. *Curr. Urol.* 19 (1), 39–42. doi:10.1097/cu9.0000000000000263

Feng, Y., Hong, Y., Sun, H., Zhang, B., Wu, H., Li, K., et al. (2019). Abstract 2383: the molecular binding mechanism of tislelizumab, an investigational anti-PD-1 antibody, is differentiated from pembrolizumab and nivolumab. *Cancer Res.* 79 (13_Suppl. ment), 2383. doi:10.1158/1538-7445.am2019-2383

Lee, A., and Keam, S. J. (2020). Tislelizumab: first approval. *Drugs* 80 (6), 617–624. doi:10.1007/s40265-020-01286-z

Lee, S. H., Lee, H. T., Lim, H., Kim, Y., Park, U. B., and Heo, Y. S. (2020). Crystal structure of PD-1 in complex with an antibody-drug tislelizumab used in tumor immune checkpoint therapy. *Biochem. Biophys. Res. Commun.* 527 (1), 226–231. doi:10.1016/j.bbrc.2020.04.121

Motzer, R., Alekseev, B., Rha, S. Y., Porta, C., Eto, M., Powles, T., et al. (2021). Lenvatinib plus pembrolizumab or Everolimus for advanced renal cell carcinoma. *N. Engl. J. Med.* 384 (14), 1289–1300. doi:10.1056/NEJMoa2035716

Motzer, R. J., Penkov, K., Haanen, J., Rini, B., Albiges, L., Campbell, M. T., et al. (2019). Avelumab plus axitinib versus sunitinib for advanced renal-cell carcinoma. *N. Engl. J. Med.* 380 (12), 1103–1115. doi:10.1056/NEJMoa1816047

Motzer, R. J., Tannir, N. M., McDermott, D. F., Aren Frontera, O., Melichar, B., Choueiri, T. K., et al. (2018). Nivolumab plus Ipilimumab versus sunitinib in advanced renal-cell carcinoma. *N. Engl. J. Med.* 378 (14), 1277–1290. doi:10.1056/NEJMoa1712126

Padala, S. A., Barsouk, A., Thandra, K. C., Saginala, K., Mohammed, A., Vakiti, A., et al. (2020). Epidemiology of renal cell carcinoma. *World J. Oncol.* 11 (3), 79–87. doi:10.14740/wjon1279

Powles, T., Plimack, E. R., Soulieres, D., Waddell, T., Stus, V., Gafanov, R., et al. (2020). Pembrolizumab plus axitinib versus sunitinib monotherapy as first-line treatment of advanced renal cell carcinoma (KEYNOTE-426): extended follow-up from a randomised, open-label, phase 3 trial. *Lancet Oncol.* 21 (12), 1563–1573. doi:10.1016/S1470-2045(20)30436-8

Rini, B. I., Plimack, E. R., Stus, V., Gafanov, R., Hawkins, R., Nosov, D., et al. (2019a). Pembrolizumab plus axitinib versus sunitinib for advanced renal-cell carcinoma. *N. Engl. J. Med.* 380 (12), 1116–1127. doi:10.1056/NEJMoa1816714

Rini, B. I., Powles, T., Atkins, M. B., Escudier, B., McDermott, D. F., Suarez, C., et al. (2019b). Atezolizumab plus bevacizumab versus sunitinib in patients with previously untreated metastatic renal cell carcinoma (IMmotion151): a multicentre, open-label, phase 3, randomised controlled trial. *Lancet* 393 (10189), 2404–2415. doi:10.1016/S0140-6736(19)30723-8

Schmidt, L. S., and Linehan, W. M. (2016). Genetic predisposition to kidney cancer. *Semin. Oncol.* 43, 566–574. doi:10.1053/j.seminoncol.2016.09.001

Siegel, R. L., Miller, K. D., Fuchs, H. E., and Jemal, A. (2022). Cancer statistics, 2022. *CA Cancer J. Clin.* 72 (1), 7–33. doi:10.3322/caac.21708

Wang, Z., Chen, J., Li, Q., Li, N., Yu, J., and Liu, F. (2022). The effects of axitinib plus tislelizumab in the treatment of advanced renal cell carcinoma. *J. Oncol.* 2022, 2700166. doi:10.1155/2022/2700166

Wu, C., Huang, Z., Wu, B., Zhang, W., Chen, X., Lv, L., et al. (2021). Efficacy of axitinib combined with tislelizumab in patients with advanced renal cell carcinoma who failed first-line targeted therapy. *Chin. J. Clin. Pharmacol.* 37 (12), 1501–1504.

Yan, X. Q., Ye, M. J., Zou, Q., Chen, P., He, Z. S., Wu, B., et al. (2024). Toripalimab plus axitinib versus sunitinib as first-line treatment for advanced renal cell carcinoma: RENOTORCH, a randomized, open-label, phase III study. *Ann. Oncol.* 35 (2), 190–199. doi:10.1016/j.annonc.2023.09.3108

frontiers | Frontiers in Genetics

TYPE Original Research
PUBLISHED 17 July 2025
DOI 10.3389/fgene.2025.1592779

OPEN ACCESS

EDITED BY
Jialin Meng,
University of Science and Technology of China, China

REVIEWED BY
Shengfeng Zheng,
Fudan University, China
Yinjie Su,
Zhejiang Chinese Medical University, China

*CORRESPONDENCE
Yufei Gu,
urethra@163.com

RECEIVED 13 March 2025
ACCEPTED 08 July 2025
PUBLISHED 17 July 2025

CITATION
Hua B, Yang Q, Song S, Li W, Xu B and Gu Y (2025) Exploring the prognostic significance and therapeutic potential of SUCLG2 in prostate cancer.
Front. Genet. 16:1592779.
doi: 10.3389/fgene.2025.1592779

Exploring the prognostic significance and therapeutic potential of SUCLG2 in prostate cancer

Bao Hua, Qing Yang, Shangqing Song, Wenfeng Li, Bin Xu and Yufei Gu*

Department of Urology, School of Medicine, Shanghai Ninth People's Hospital, Shanghai Jiao Tong University, Shanghai, China

Background: Prostate cancer (PCa), a highly heterogeneous cancer with a complex molecular pathogenesis, is a leading cause of cancer-related mortality among men globally. The present study presents a lipid metabolism-based risk model for PCa and explores the role of succinyl-CoA ligase GDP-forming subunit beta (SUCLG2), a potential marker and therapeutic target in PCa involved in lipid metabolism and cancer progression, from the perspective of developing effective diagnostic and therapeutic strategies.

Methods: High-throughput RNA sequencing and single-cell RNA sequencing were used to investigate the expression and functional relevance of SUCLG2 in PCa. We analyzed 497 PCa samples from The Cancer Genome Atlas and conducted a comprehensive bioinformatics analysis, including univariate Cox proportional hazards regression, least absolute shrinkage and selection operator regression, and gene set enrichment analysis. Furthermore, quantitative real-time polymerase chain reaction and immunofluorescence assays were performed to validate SUCLG2 expression in clinical samples and the prostate carcinoma epithelial cell line 22Rv1.

Results: Our findings revealed that lipid metabolism-related genes, including SUCLG2, have significant prognostic value, based on a 16-gene risk model constructed that accurately predicted PCa prognosis. In particular, SUCLG2 was significantly enriched in luminal and basal/intermediate cell subsets, highlighting its potential role in tumor progression and therapy resistance. Drug sensitivity analysis indicated that SUCLG2 expression is correlated with the efficacy of several chemotherapeutic agents, based on which strategies for personalized therapy in PCa treatment could be devised.

Conclusion: SUCLG2 plays a pivotal role in the metabolic reprogramming of PCa, thus offering new insights into its progression and potential therapeutic targets. Our study underscores the importance of metabolic pathways in PCa pathogenesis and paves the way for the development of targeted therapies, thus contributing to personalized medicine in PCa management.

KEYWORDS

prostate cancer, SUCLG2, lipid metabolism, single-cell RNA sequencing, personalized therapy

Introduction

Prostate cancer (PCa) remains one of the most prevalent malignancies affecting men worldwide, posing significant challenges in terms of diagnosis, treatment, and management (Wang et al., 2018). The disease exhibits a highly heterogeneous clinical course that is underscored by a complex pathogenesis involving a wide array of molecular alterations and a diverse tumor microenvironment (Chen et al., 2021; Sekhoacha et al., 2022). Recent advancements in high-throughput sequencing technologies, particularly RNA sequencing (RNA-seq) and single-cell RNA sequencing (scRNA-seq), have opened new avenues for exploring the molecular landscape of PCa at a hitherto unprecedented level of depth. Further, genomics and transcriptomics studies have unveiled various subtypes of PCa characterized by distinct mutations and aberrant transcriptional profiles, shedding light on the molecular diversity underpinning the disease (Chen et al., 2019; You et al., 2016; Zhao et al., 2017).

scRNA-seq technology allows for the simultaneous assessment of thousands of cells within a sample, thus revealing the extent of heterogeneity among tumor cells (Azizi et al., 2018; Tirosh et al., 2016). This technology has highlighted the pivotal roles of luminal and basal/intermediate cells in the development and progression of PCa. Luminal cells, often linked to the differentiated state of the prostate gland, are implicated in the majority of PCa cases and are pivotal in the disease's androgen-driven progression (You et al., 2016; Zhao et al., 2017). Conversely, basal/intermediate cells, with their stem-cell-like properties and capacity for self-renewal, are thought to contribute to tumor initiation, recurrence, and resistance to therapy, emphasizing the complexity of effectively targeting PCa (Parson et al., 2001).

With regard to the molecular mechanisms, similar to other cancers, PCa has been linked with metabolic dysregulation, and several metabolism-related markers have been associated with tumor growth, progression, and therapy resistance (Yang et al., 2024). Among the known markers, succinyl-coenzyme A (CoA) ligase GDP-forming subunit beta (SUCLG2), a significant player in the lipid metabolism pathway, has emerged as a potential prognostic marker and therapeutic target in PCa (Lin et al., 2020; Hu et al., 2023). SUCLG2 has been implicated in several key metabolic processes critical to cancer metabolism, including the tricarboxylic acid (TCA) cycle, and represents a link between altered metabolic pathways and tumor biology (Wu et al., 2020). Based on these previous findings, the current study aims to explore in more depth the expression and functional relevance of SUCLG2 within the PCa milieu and, thereby, shed light on the molecular mechanisms by which lipid metabolism-related genes influence PCa progression and identify potential avenues for targeted therapy.

Based on our molecular studies, we have constructed a risk prediction model comprising 16 genes related to lipid metabolism in PCa that shows high accuracy for identifying patients at risk of poor survival. This model could help guide the development of more effective, targeted treatment strategies that can improve patient outcomes in this complex disease landscape.

Materials and methods

Clinical samples

A total of 10 matched pairs of tumor and adjacent normal tissue samples were procured from patients with PCa who underwent surgery in 2021 at the Shanghai Ninth People's Hospital, Shanghai Jiao Tong University School of Medicine. Prior to sample collection, written informed consent was obtained from all the participating patients. The research protocol received the approval of the Institutional Ethical Review Board of the Shanghai Ninth People's Hospital, Shanghai Jiao Tong University School of Medicine, and was performed in compliance with the relevant ethical guidelines (approval no. SH9H-2021-A26-1).

Cell culture

The human prostate carcinoma epithelial cell line 22Rv1 was obtained from the cell bank of Fudan University. Cells were cultured in Dulbecco modified Eagle medium (Gibco, Grand Island, NY, United States) supplemented with 10% heat-inactivated fetal bovine serum (Gibco, Grand Island, NY, United States), 100 U/mL penicillin, and 100 μg/mL streptomycin (Gibco, Grand Island, NY, United States), in a humidified atmosphere containing 5% CO_2 and 95% air at 37°C.

Data collection

RNA sequencing data and clinical information for PCa samples were obtained from The Cancer Genome Atlas (TCGA) database (https://portal.gdc.cancer.gov) (Xu et al., 2023). A total of 497 prostate cancer samples were selected for further analysis. Samples with incomplete clinical information and normal tissue samples were excluded. A comprehensive list of 859 lipid metabolism-related genes was curated from "Reactome metabolism of lipids and lipoproteins," "Reactome phospholipid metabolism," "Hallmark fatty acid metabolism," and "KEGG glycerophospholipid metabolism" in the Molecular Signatures Database (MSigDB: https://www.gsea-msigdb.org/gsea/msigdb/index.jsp). This gene list served as the foundation for subsequent analyses. Immunohistochemical data for SUCLG2 expression in tissues were obtained from the Human Protein Atlas (https://www.proteinatlas.org).

Data preprocessing

To identify lipid metabolism genes with prognostic significance, univariate Cox proportional hazards regression analysis was performed on RNA-seq data, with a focus on the curated list of lipid metabolism genes. Genes with a p-value less than 0.05 were considered to have significant prognostic value. Least absolute shrinkage and selection operator (LASSO) regression analysis was employed to construct a risk model based on the prognostically significant genes identified with the R package "glmnet" (Xu et al., 2021). This method was chosen for its efficacy in handling high-dimensional data and its ability to enhance model predictability by imposing a penalty on the absolute size of the

coefficients. The following formula was used for calculating risk scores based on the expression levels of lipid metabolism-related genes: Risk score = ∑ni = ∑Coefi × xi, where xi stands for the expression level of gene i, and Coefi, for the regression coefficient. Based on the median risk score, the patients were divided into high- and low-risk groups.

Kaplan-Meier survival analysis was employed to evaluate the disparities in overall survival (OS), disease-free survival (DFS), and progression free survival (PFS) between the high- and low-risk groups. The precision of the risk model was gauged using receiver operating characteristic (ROC) curve analysis. Additionally, the expression profiles of the genes associated with lipid metabolism risk were depicted through heatmaps, utilizing the "pheatmap" package in R for visualization.

Single-cell RNA sequencing analysis

Single-cell RNA sequencing data from the included patients were downloaded from the GSE141445 dataset. The initial phase involved rigorous quality control measures to ensure the reliability of subsequent analyses. Cells were selected based on a set of predefined criteria aimed at excluding low-quality or ambiguous cells, thus refining the dataset for more accurate clustering and analysis. The criteria for inclusion were as follows: (1) expression of 200 to 5,218 distinct genes that can be used to capture a comprehensive, yet precise, transcriptomic profile; (2) mitochondrial gene expression under 20% to mitigate the influence of cellular stress or apoptosis, which might otherwise skew the findings; (3) a minimum transcript count threshold of 1,000 to filter out cells potentially compromised by inadequate RNA content, probably due to technical discrepancies.

Following quality control based on the above criteria, the "Seurat" package in R was utilized for data normalization, variance stabilization, and scaling. The dimensionality reduction techniques t-distributed Stochastic Neighbor Embedding (tSNE) and Uniform Manifold Approximation and Projection (UMAP) were employed to visualize the cellular landscapes and the distribution of the identified cell types, and thereby, provide insights into the complex architecture of PCa tissues at the single-cell level. A list of marker genes for different cell types was collected to annotate the cell clusters (Chen et al., 2021).

Functional enrichment analysis

Gene Ontology (GO) and Gene Set Enrichment Analysis (GSEA) were conducted using the "clusterProfiler" R package to identify the biological functions and pathways linked with the identified genes, with a focus on SUCLG2. This analysis aimed to illuminate the potential mechanisms by which these genes influence the progression of PCa.

Quantitative real-time polymerase chain reaction

For RNA extraction and qPCR analysis, total RNA was isolated from 10 matched pairs of tumor (PCa) and adjacent normal tissues utilizing the TRIzol reagent (Invitrogen, Carlsbad, CA, United States), with strict adherence to the manufacturer's guidelines. After extraction, the concentration of the retrieved RNA was determined, and this was followed by the synthesis of cDNA with the RevertAid First Strand cDNA Synthesis Kit (Takara Bio, Shiga, Japan), as per the kit's specifications. RNA was quantified in accordance with the protocol of the TRIzol reagent obtained from Invitrogen, and the extracted RNA was reverse-transcribed into cDNA using a dedicated reverse transcription kit. PCR amplification and detection were carried out in a 20 μL reaction volume utilizing the BIO-RAD fluorescent real-time PCR system. The sequences of the SUCLG2 primers were as follows:

Forward: 5′-TGTTGGTGGTGGTGCTACAG-3′,

Reverse: 5′-TCGTGTACCTTGTAACCGTACC-3′.

Immunofluorescence assay

A total of 1,000 cells of the prostate carcinoma epithelial cell line 22Rv1 were plated per well in a 24-well plate containing cell slides (NEST 801 010) and incubated for 24 h. Subsequently, the slides were rinsed thrice with phosphate-buffered saline (PBS) for 5 min each, and this was followed by fixation in 4% paraformaldehyde for 30 min. After fixation, the cells were washed three more times with PBS and then blocked with a solution containing 3% BSA and 0.2% Triton X-100 in PBS for 1 h at ambient temperature. The cells were then incubated overnight with primary rabbit anti-SUCLG2 antibodies (1:250, ab187996) and rinsed five times over a 15-min span using a wash buffer (containing 0.2% BSA and 0.05% Triton X-100 in PBS), after which they were incubated for 1 h with fluorescent-tagged secondary donkey anti-rabbit IgG (1:300, ab150068). This was followed with three rinses with the wash buffer, and then DAPI (0100–20, Southern Biotech) was applied for nuclear staining. Imaging was subsequently performed using a laser confocal microscope (ZEISS).

Drug sensitivity analysis

Drug sensitivity analysis was performed to explore the correlation between SUCLG2 expression and responsiveness to various chemotherapeutic agents, by utilizing the comprehensive drug sensitivity datasets available in the CellMiner database (https://discover.nci.nih.gov/cellminer/home.do). This segment of the study concentrated on identifying medications for which the half-maximal inhibitory concentration (IC50) values demonstrated a significant association with the expression levels of SUCLG2.

Pearson correlation coefficients were calculated to assess the strength and direction of the relationship between SUCLG2 expression and the IC50 values for each drug. Drugs exhibiting a statistically significant correlation ($p < 0.05$) were highlighted as potential candidates for targeted therapy of PCa based on altered SUCLG2 expression.

Statistical analysis

SPSS version 23.0 (SPSS Inc., Chicago, IL, United States) and R software for Windows version R-4.3.3 (The R Foundation for Statistical Computing, Vienna, Austria) were used for data analysis. P values <0.05 were considered to indicate statistical significance.

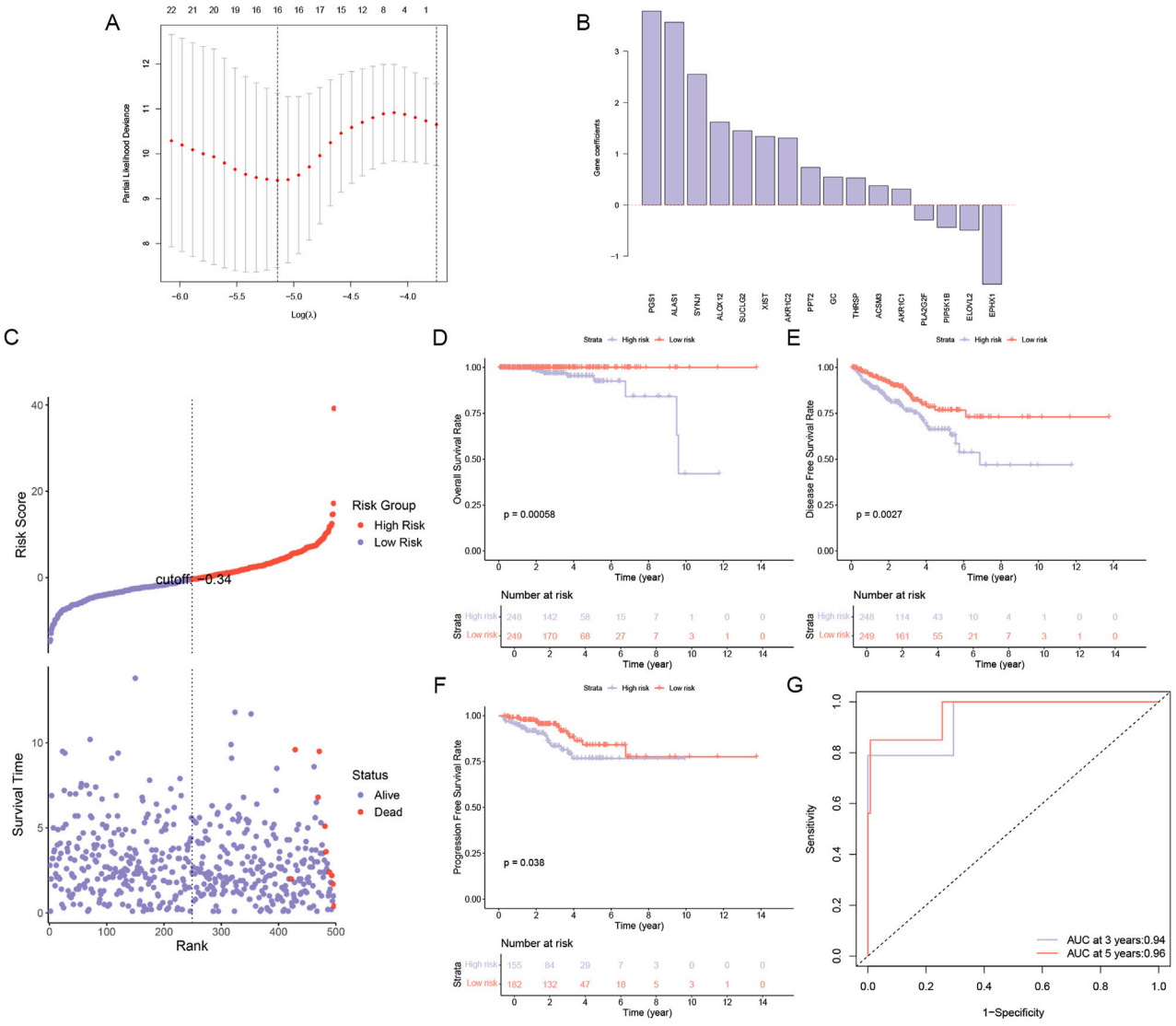

FIGURE 1
Construction and Validation of a Lipid Metabolism Gene Risk Model. **(A)** A LASSO regression model was constructed to identify 16 lipid metabolism-related genes associated with high risk in PCa. **(B)** Gene coefficients of genes related to the risk of PCa progression. **(C)** Risk score and survival time in high- and low-risk groups, **(D)** Overall survival analysis in high- and low-risk groups. **(E)** Disease-free survival analysis in high- and low-risk groups. **(F)** Progression-free survival analysis in high- and low-risk groups. **(G)** AUC curve for prediction accuracy.

Results

Construction and Validation of a risk model comprising lipid metabolism genes

In our quest to unravel the complex role of lipid metabolism in PCa, we embarked on a rigorous analysis of RNA-seq data from 497 PCa samples obtained from the TCGA database. By integrating these samples with a curated list of 859 lipid metabolism genes from the MSigDB database, we conducted a comprehensive univariate Cox regression analysis and identified 41 genes with significant prognostic value ($p < 0.05$). Leveraging the predictive power of these genes, we constructed a robust LASSO model that culminated in a 16-gene risk model that could accurately predict the prognosis of PCa (Figure 1A). As shown in Figure 1B, the gene coefficients represent the weight of the influence of each gene in the PCa sample. Based on the model, the cohort was divided into high-risk and low-risk groups with surgical precision, and a sharp contrast in mortality was observed between the two groups (Figure 1C). Survival analysis indicated that significantly better OS, DFS, and PFS were observed in the low-risk group (Figures 1D–F). Further, the ROC curve (Figure 1G) validated the accuracy of the model.

Clinical correlation and expression heatmap of the risk model comprising 16 lipid metabolism-related genes

We analyzed the correlation between the expression of the 16 lipid metabolism-related genes and clinicopathological

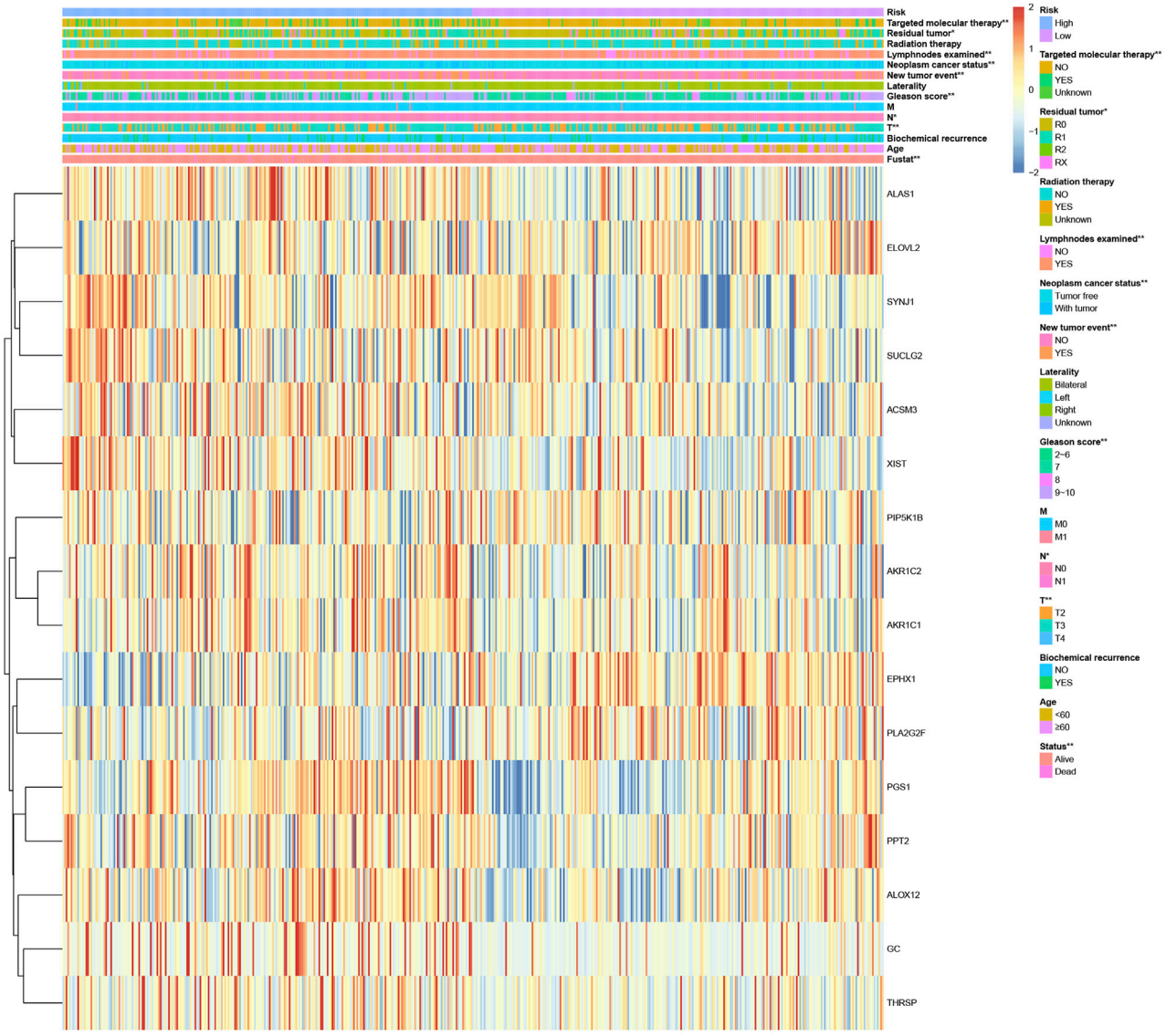

FIGURE 2
Clinical correlation and expression heatmap of the risk model comprising 16 lipid metabolism-related genes. *p < 0.05 and **p < 0.01.

characteristics (Figure 2), and the results showed that the expression of these 16 lipid metabolism-related genes was significantly correlated with clinical features such as T stage, N stage, Gleason score, new tumor event, neoplastic cancer status, number of lymph nodes examined, residual tumor, targeted molecular therapy, and survival status. In addition, SUCLG2, PPT2, PGS1, ALAS1, SYNJ1, ALOX12, ACSM3, THRSP, AKR1C1, AKR1C2, XIST, and GC were mainly expressed in the high-risk group. This implies that these 12 genes may be closely related to the poor prognosis of PCa.

Cellular heterogeneity based on single-cell RNA sequencing

To further investigate the cellular landscape of PCa, we employed single-cell RNA sequencing to dissect the heterogeneity of cell subsets. By analyzing 13 samples (12 sample of primary PCa and 1 sample of lymphocyte node metastasis) from 12 patients in the GSE141445 dataset, we screened and obtained 35,405 cells that were classified under 19 different cell clusters (Figure 3A). We used reported cell markers for detailed annotation of cell identity (Chen et al., 2021). In addition, tSNE and UMAP plots were drawn to observe the local characteristics and overall distribution of cell subsets (Figures 3B,C). Finally, we were able to confirm the presence and distribution of seven cell subsets, namely, luminal cells, basal/intermediate cells, T cells, endothelial cells, fibroblasts, monocytic cells, and mast cells.

Basal/intermediate and luminal cell subsets were found to express many of the identified lipid metabolism genes (Figure 3D). Except for GC and THRSP, the other high-risk lipid metabolism genes were broadly expressed across different cell subsets (Figure 3F). In particular, SUCLG2 was significantly enriched in the basal/intermediate and luminal cell subsets. This suggests that SUCLG2 may contribute to PCa progression via its activity in these two key epithelial cell populations (Figure 3G).

10.3389/fgene.2025.1592779

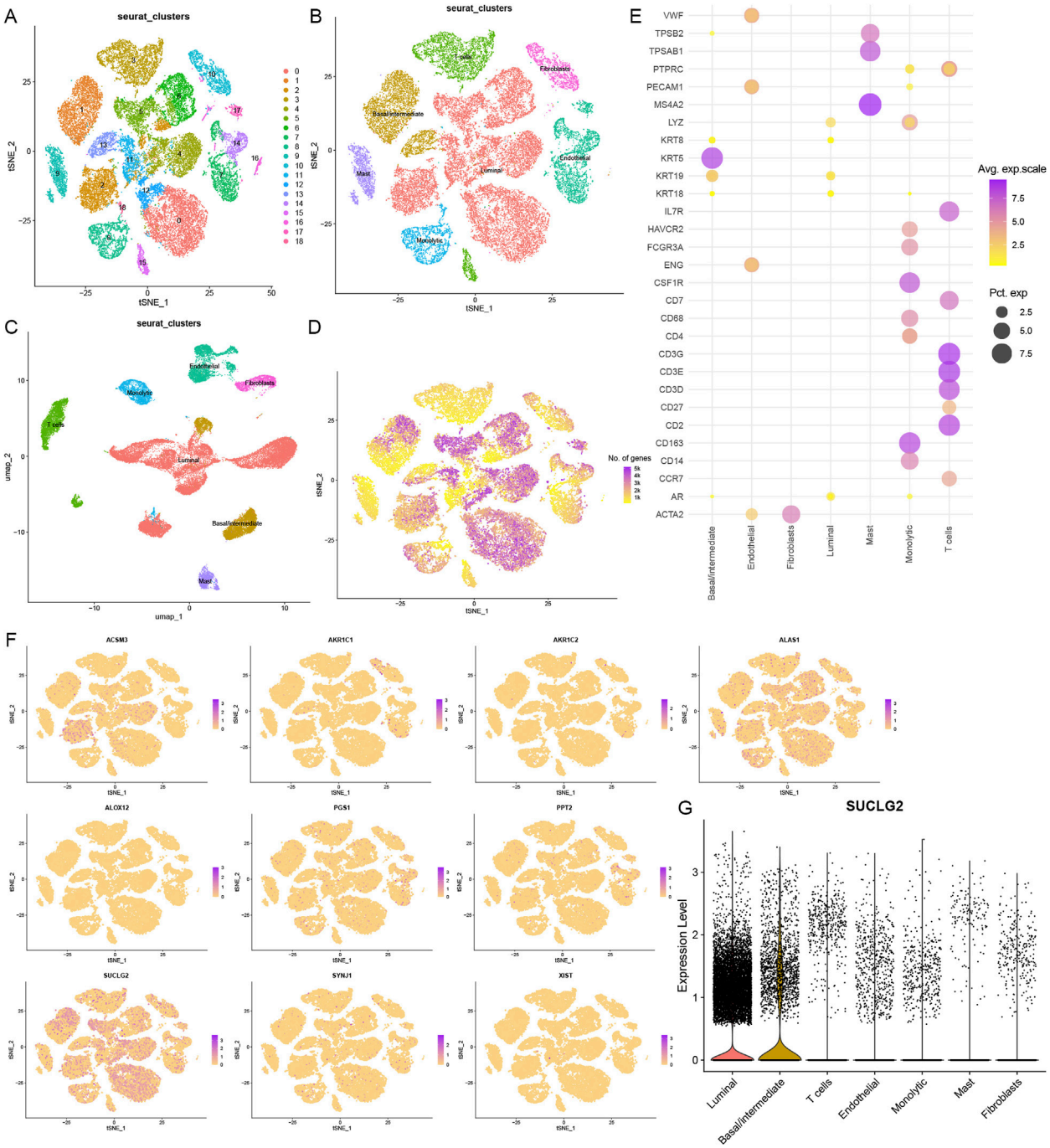

FIGURE 3
Cellular Heterogeneity based on Single-Cell RNA Sequencing. **(A)** A t-distributed stochastic neighbor embedding (tSNE) view of 35,405 single cells, color-coded by assigned cell clusters. **(B)** tSNE view of 7 cell subsets. **(C)** Uniform Manifold Approximation and Projection (UMAP) plot of 7 cell clusters. **(D)** tSNE view of all cells, color-coded by the number of genes detected in each cell. **(E)** Expression of marker genes for each cell type, where dot size and color represent the percentage of marker gene expression (pct. exp) and the averaged scaled expression (avg. exp. scale) value, respectively. **(F)** tSNE view of the expression of 10 lipid metabolism-related risk genes in 7 cell subsets. **(G)** Violin plot of SUCLG2 expression in 7 cell subsets.

Role of SUCLG2 in PCa based on functional enrichment analysis

To decipher the functional roles of SUCLG2 in PCa, we performed a comprehensive GO analysis on the 41 genes identified from the univariate Cox regression analysis and found that SUCLG2 played a significant role in multiple metabolic processes. This analysis pointed out SUCLG2's involvement in crucial metabolic pathways, including the acyl-CoA metabolic process, the thioester metabolic process, and purine metabolism, and the results were indicative of its central role in the metabolic reprogramming of PCa cells (Figure 4A).

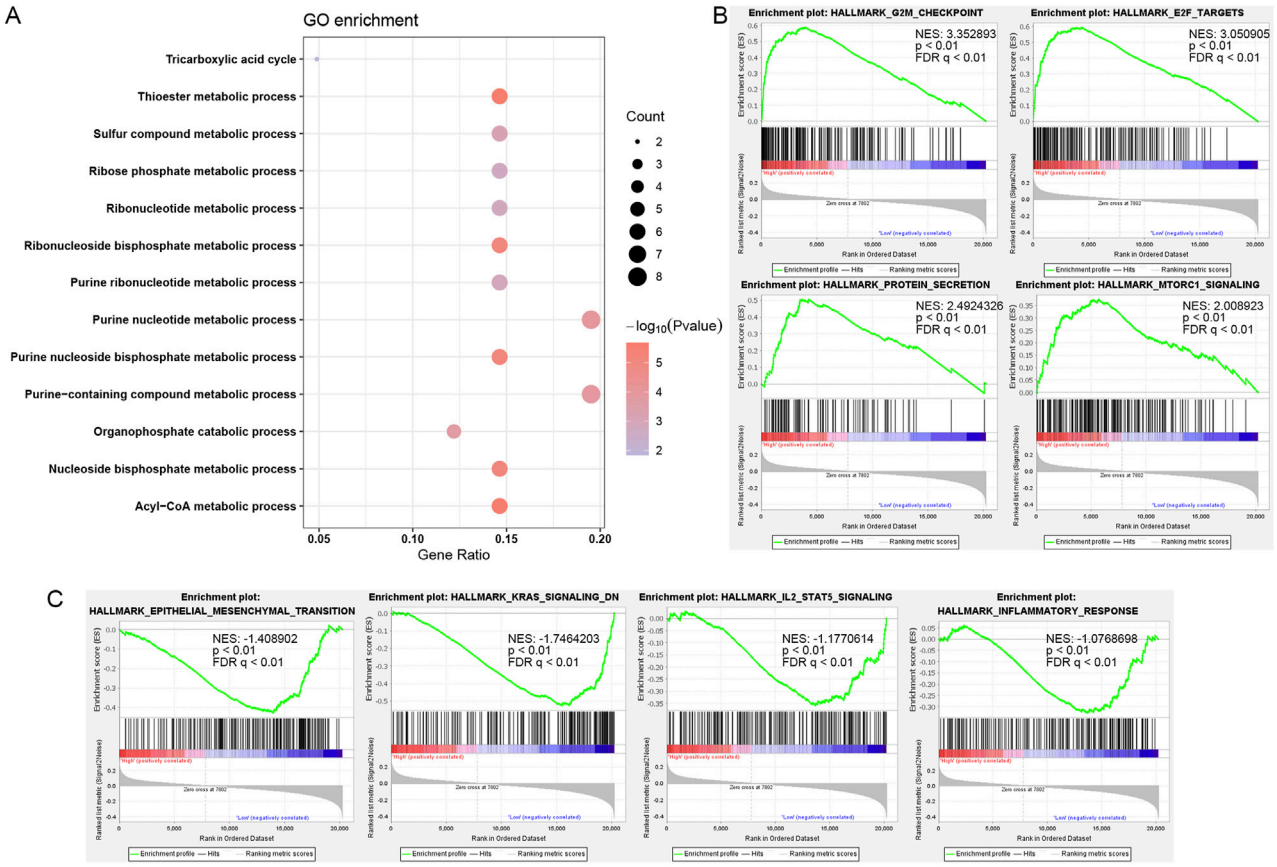

FIGURE 4
Role of SUCLG2 in PCa based on Functional Enrichment Analysis. **(A)** Gene Ontology (GO) enrichment for 41 lipid metabolism genes with significant prognostic value. **(B)** Gene Set Enrichment Analysis (GSEA) results related to high SUCLG2 expression. **(C)** GSEA results related to low expression of SUCLG2. NES, normalized enrichment score; FDR q, false discovery rate q value.

Subsequent GSEA further delineated the dichotomy in the biological pathways enriched among samples with high versus low SUCLG2 expression. That is, samples with elevated SUCLG2 levels were predominantly associated with cell cycle checkpoints and protein secretion pathways that were indicative of the potential mechanisms by which SUCLG2 may contribute to tumor aggressiveness (Figure 4B). Conversely, samples with lower SUCLG2 expression were enriched in pathways related to epithelial–mesenchymal transition and inflammatory responses, highlighting the multifaceted roles of SUCLG2 in tumor biology (Figure 4C).

The dual behavior of SUCLG2, associated with proliferative pathways at high expression and inflammatory/EMT pathways at low expression, may indicate a stage- or microenvironment-specific role. In early-stage tumors, SUCLG2 may promote biosynthetic and proliferative programs, while in inflamed or therapy-resistant settings, reduced SUCLG2 may shift the tumor state toward EMT and immune evasion.

Validation of SUCLG2 expression in PCa

To validate the differential expression of SUCLG2 in PCa, we conducted qPCR analysis to compare the mRNA expression of SUCLG2 in 10 pairs of tumor tissues and adjacent normal tissues. The results unequivocally confirmed higher expression levels of SUCLG2 in tumor tissues, reinforcing its relevance in PCa pathology (Figure 5A). Immunohistochemical data from The Human Protein Atlas further corroborated the elevated expression of SUCLG2 in PCa tissues, particularly within glandular epithelial cells, thus providing a histological perspective on its role in tumor biology (Figure 5B).

SUCLG2 is mainly involved in the transcription and translation of enzymes involved in the TCA cycle and energy metabolism in mitochondria, and accordingly, these enzymes are mainly expressed in the mitochondria of cells (Hu et al., 2023). Accordingly, immunofluorescence analysis of the PCa epithelial cell line 22Rv1 revealed the cytoplasmic localization of SUCLG2 and provided insights into its cellular function and potential mechanism of action in tumor progression (Figure 5C).

Drug sensitivity analysis

From the viewpoint of precisely tailoring PCa treatment to the needs of individual patients, our study ventured into the realm of pharmacogenomics to identify potential drugs that could serve as targeted therapies based on SUCLG2 expression levels. By delving

10.3389/fgene.2025.1592779

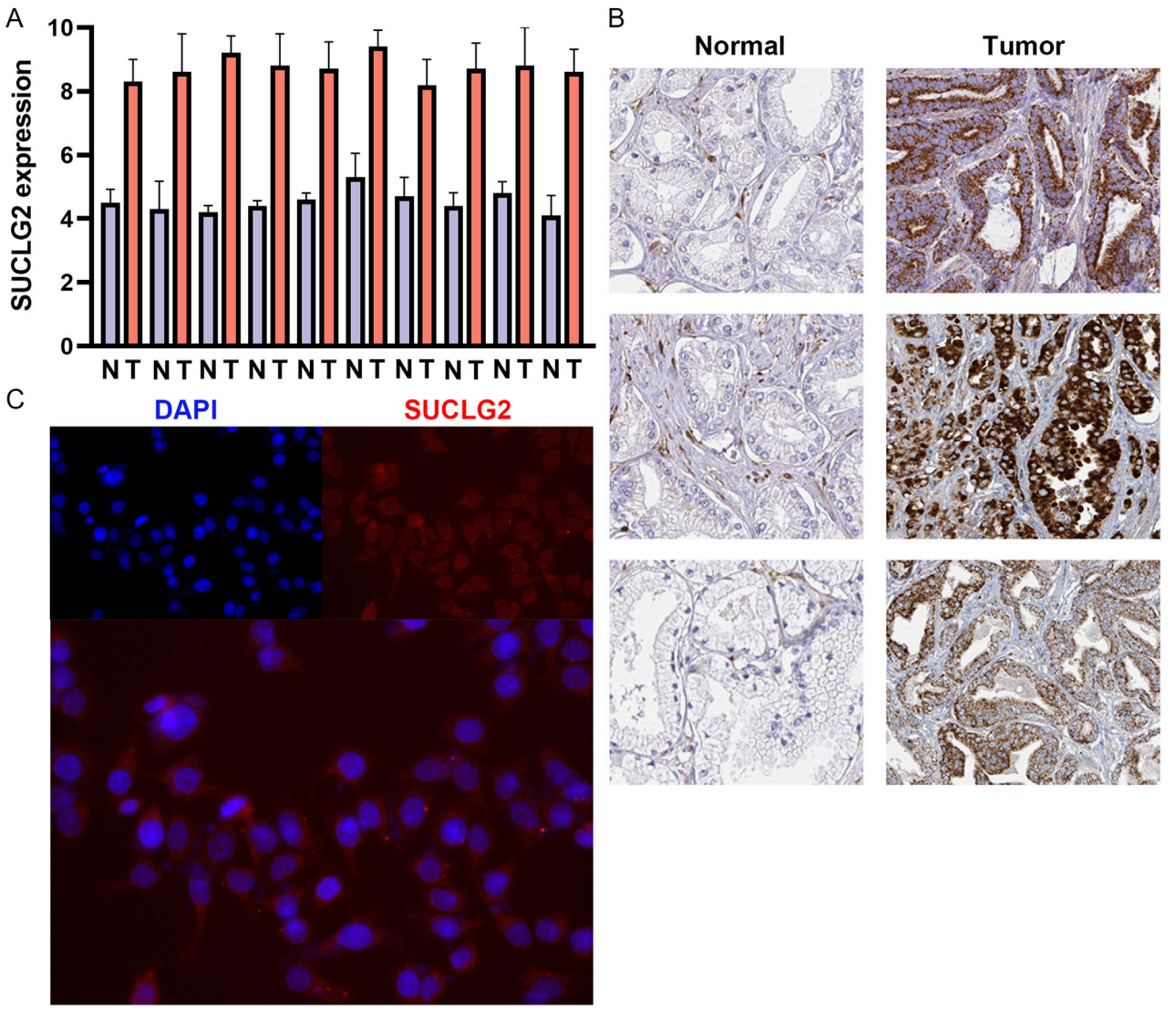

FIGURE 5
Validation of SUCLG2 Expression in PCa. **(A)** Quantitative real-time PCR analysis of 10 matched pairs of tumor and adjacent normal tissues. **(B)** Immunohistochemical data from the Human Protein Atlas dataset. **(C)** Immunofluorescence assay of SUCLG2 expression in the prostate carcinoma epithelial cell line 22Rv1.

into the comprehensive drug sensitivity data available in the Cellminer database, we meticulously analyzed and identified nine drugs that exhibited significant correlation with SUCLG2 expression levels in PCa cells.

Our analysis brought to light that the IC50 values of PD-0325901, RO-4987655, TAK-733, pimasertib, and RO-5126766 are positively correlated with SUCLG2 expression; thus, these drugs may exhibit increased efficacy in tumors with high SUCLG2 expression (Figure 6A) and may represent viable options for a more targeted and effective treatment strategy in patients with elevated levels of SUCLG2. Conversely, colchicine, docetaxel, GSK-461364, and lexibulin showed a negative correlation with SUCLG2 expression. Intriguingly, while colchicine, docetaxel, and GSK-461364 did not demonstrate significant differences in IC50 values between the high and low SUCLG2 expression groups, lexibulin displayed significantly higher IC50 values in the low expression group than in the high expression group (Figure 6B). This subtle relationship suggests that lexibulin, in particular, might be more suitable for patients with lower SUCLG2 levels and present a therapeutic avenue that could potentially protect patients from unnecessary toxicity while targeting the tumor more effectively.

Discussion

The present study intricately dissects the multifaceted landscape of PCa, delving deep into the lipid metabolism-related molecular mechanisms involved in its progression, specifically in terms of the role of SUCLG2. Through a risk model comprising 16 significant lipid metabolism genes as risk factors and comprehensive genomic and transcriptomic analyses coupled with functional assays, this research illuminates the prognostic significance of lipid metabolism

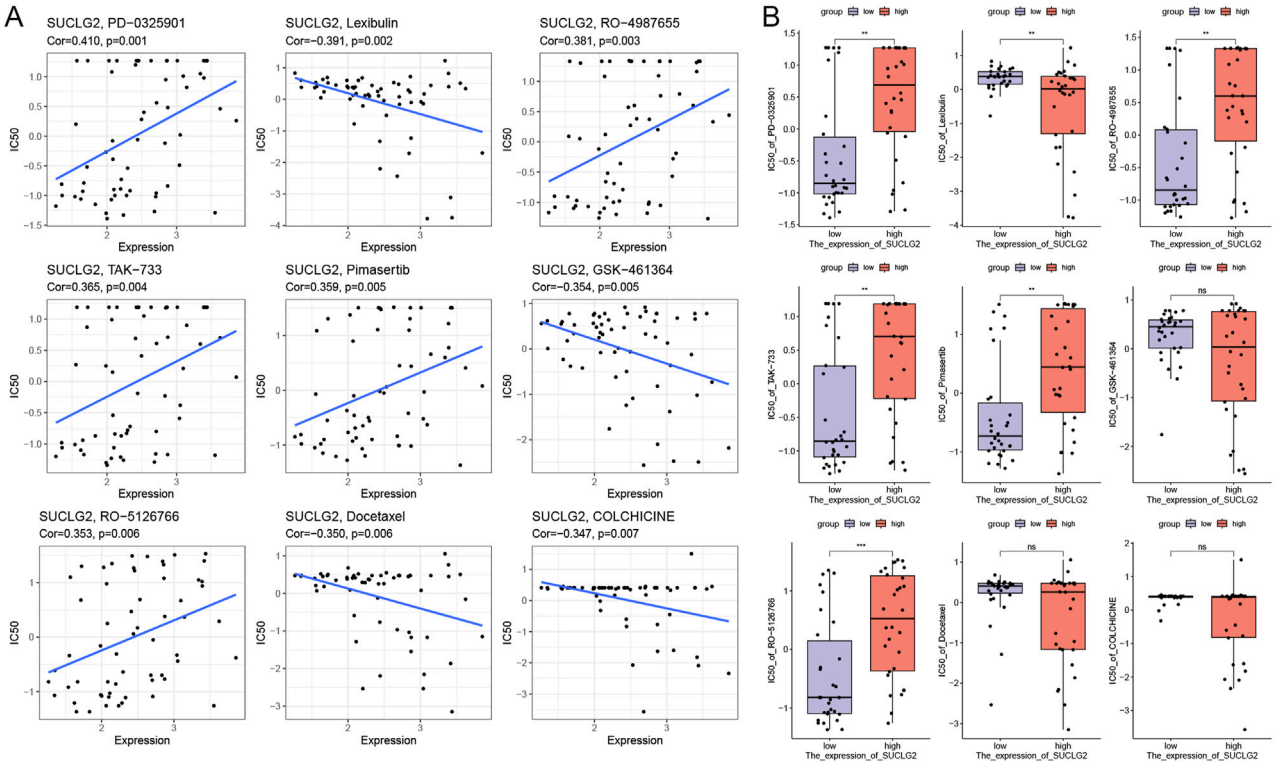

FIGURE 6
Results of Drug Sensitivity Analysis. **(A)** Correlation between gene expression and drug sensitivity for the top 9 drugs used for PCa treatment. **(B)** Relationship between gene expression and drug sensitivity in groups with high and low SUCLG2 expression. Cor, correlation coefficient; NS, not significant; **p < 0.01; ***p < 0.001.

genes in PCa and underscores SUCLG2's potential as a therapeutic target. Overall, our findings resonate with, and extend upon, the existing literature, affirming the complexity and heterogeneity of PCa pathogenesis and progression.

The novel 16 lipid metabolism-related gene risk model presented here holds the promise of transforming patient management by stratifying risk with hitherto unprecedented precision. The 16 lipid metabolism-related genes included in this model may be associated with the abnormal clinicopathological features of PCa patients, and in particular, 12 of them are more likely to lead to poor prognosis of PCa patients. This risk model not only highlights the prognostic potential of these genes in PCa but is also in alignment with previous studies advocating for the significance of metabolic pathways in cancer biology. Beyond prognostic prediction, the lipid metabolism-based risk model may also offer utility in identifying patients with aggressive disease features or in predicting treatment response, such as metabolic therapy or combination regimens. Future studies are warranted to validate the model's application in broader clinical contexts. In particular, studies have shown that alterations in lipid metabolism contribute to the development and progression of various cancers, including PCa, by supporting membrane biosynthesis, energy production, and signaling molecule generation (Martin-Perez et al., 2022; Currie et al., 2013; Bian et al., 2021). Further, it supports previous notions by demonstrating that dysregulated lipid metabolism is a hallmark of tumor growth and survival (Hopkins et al., 2018).

The pivotal role of SUCLG2 in PCa that emerged from our study is notable, positioning this gene as a key contributor to the metabolic reprogramming in PCa cells. Our findings are supported by Faubert et al. and Sun et al., who identified metabolic reprogramming as a critical factor in cancer progression, underscoring the importance of targeting metabolic pathways for cancer therapy (Faubert et al., 2020; Sun et al., 2022). The association between high SUCLG2 expression and aggressive PCa features, such as advanced tumor stage and poor prognosis, dovetails with recent discoveries in metabolic oncology. For instance, Wu et al. and Shen et al. reported that alterations in the TCA cycle enzymes, which SUCLG2 also contributes to, are indicative of a more malignant cancer phenotype, thus corroborating our observations (Wu et al., 2020; Shen et al., 2023).

The cellular heterogeneity within PCa significantly contributes to its diagnostic and therapeutic challenges. Particularly, the distinct roles of luminal and basal/intermediate cells in the disease's pathogenesis and progression have garnered considerable attention. Our study's findings, which emphasize the differential expression of SUCLG2 across these cellular subsets, offer novel insights into the metabolic reprogramming in PCa and its potential exploitation for therapeutic advances. Luminal cells, characterized by their expression of cytokeratin 8/18, are pivotal in the prostate gland's differentiated state and are implicated in the majority of PCa cases (Zhang et al., 2018; Dong et al., 2020). These cells are central to the androgen-driven progression of PCa, reflecting the dominant role of androgen receptors in the biology of these cells and, by extension, in the pathophysiology of PCa (Aurilio et al., 2020). Conversely, basal/intermediate cells, marked by cytokeratin 5/

14 expression, possess stem-cell-like properties, including the capacity for self-renewal and differentiation. These cells are hypothesized to contribute to tumor initiation, recurrence, and therapy resistance (Le Magnen et al., 2018). The distinct nature of these cellular compartments underscores the complexity of PCa and highlights the need for targeted therapeutic strategies that consider this cellular diversity.

Our analysis revealed that SUCLG2 is significantly enriched in both luminal and basal/intermediate cell subsets. This finding is critical, considering the enzyme's role in the TCA cycle and, by extension, in the metabolic landscape of PCa cells. The association of SUCLG2 with these cellular subsets suggests a link between metabolic processes and cellular differentiation states within the tumor microenvironment. Specifically, the elevated expression of SUCLG2 in luminal cells might contribute to the androgen-driven metabolic phenotype observed in the majority of PCa cases, potentially offering a mechanistic insight into the role of lipid metabolism in androgen receptor signaling (Butle et al., 2016). Moreover, the presence of SUCLG2 in basal/intermediate cells hints at the metabolic flexibility of these cells, which may underlie their role in tumor initiation and resistance to therapy. Thus, the stem-cell-like properties of basal/intermediate cells, coupled with their metabolic reprogramming mediated by SUCLG2, could provide a survival advantage under the selective pressures imposed by therapeutic interventions (Pfeiffer and Schalken, 2010). The enrichment of SUCLG2 in both luminal and basal/intermediate cell subsets may suggest context-dependent roles in prostate cancer biology. While luminal cells are typically associated with androgen signaling and differentiated tumor states, basal/intermediate cells are known for their stem-like, therapy-resistant features. The presence of SUCLG2 in both may indicate its involvement in both proliferative and adaptive metabolic programs, contributing to tumor heterogeneity and progression.

Overall, the functional analysis not only uncovers the diverse biological processes influenced by SUCLG2 but also underscores its potential as a pivotal player in the metabolic and proliferative aspects of PCa progression.

The drug sensitivity analysis conducted in this study not only furthers our understanding of the role of SUCLG2 in PCa but also opens up new avenues for personalized therapy. By correlating SUCLG2 expression levels with the efficacy of specific chemotherapeutic agents, we identify potential targeted therapies for PCa. Interestingly, the positive correlation between SUCLG2 expression and sensitivity to MEK inhibitors suggests that SUCLG2 may modulate or reflect MAPK pathway activity. While the mechanistic link remains to be fully elucidated, our findings raise the possibility that SUCLG2 could serve as an indirect marker for responsiveness to MAPK-targeted therapies in PCa. This approach mirrors the sentiments of Shemesh et al., who advocate for personalized medicine based on the molecular profiles of tumors to enhance treatment efficacy and minimize side effects (Shemesh et al., 2021). Through our comprehensive drug sensitivity analysis, we have not only illuminated the intricate connection between SUCLG2 expression and drug response in PCa but also identified specific drugs that could be leveraged for personalized treatment approaches. Specifically, our identification of drugs such as PD-0325901, RO-4987655, TAK-733, pimasertib, and RO-5126766, whose effectiveness may be heightened in PCa with elevated SUCLG2 expression, provides a promising foundation for future clinical trials and therapeutic strategies. Overall, the findings exemplify the potential of integrating molecular characteristics into therapeutic decision-making, heralding a new era of personalized medicine in the fight against PCa.

A notable limitation of our study is the reliance on computational and *in vitro* analyses to elucidate the role of SUCLG2 in PCa progression. While these approaches have provided valuable insights into the potential mechanisms by which SUCLG2 contributes to PCa, the complexity of cancer biology necessitates further validation through *in vivo* and *ex vivo* experiments. Specifically, the mechanistic role of SUCLG2 in PCa, especially in terms of its impact on tumor growth, metastasis, and response to therapy, remains to be fully elucidated. Future studies employing animal models and patient-derived tumor xenografts are essential to validate the therapeutic potential of targeting SUCLG2 in PCa. Additionally, exploring SUCLG2's interactions with the tumor microenvironment and its influence on cellular metabolism within the context of a living organism will offer a more comprehensive understanding of its role in cancer progression. These investigations will not only affirm the findings of our current study but also pave the way for translating these insights into clinical applications, potentially leading to more effective treatment strategies for PCa.

Conclusion

Our study emphasizes the intricate relationship between lipid metabolism and PCa progression, with SUCLG2 emerging as a significant prognostic marker and potential therapeutic target. By shedding light on the molecular mechanisms of PCa and identifying novel therapeutic avenues, this research contributes to the ongoing quest for more effective, personalized treatment strategies for PCa. As we move forward, the integration of metabolic profiling with clinical parameters promises to refine our approach to PCa management through therapies tailored to the unique molecular landscape of each patient's tumor.

Data availability statement

The datasets presented in this study can be found in online repositories. The names of the repository/repositories and accession number(s) can be found in the article/supplementary material.

Ethics statement

The studies involving humans were approved by the Institutional Ethical Review Board of the Shanghai Ninth People's Hospital, Shanghai Jiao Tong University School of Medicine. The studies were conducted in accordance with the local legislation and institutional requirements. The participants provided their written informed consent to participate in this study.

Author contributions

BH: Writing – original draft, Data curation, Methodology. QY: Data curation, Formal Analysis, Writing – original draft. SS: Investigation, Supervision, Writing – review and editing, Validation. WL: Writing – review and editing, Software, Conceptualization. BX: Formal Analysis, Writing – review and editing, Visualization, Conceptualization. YG: Writing – review and editing, Visualization, Project administration, Formal Analysis.

Funding

The author(s) declare that no financial support was received for the research and/or publication of this article.

Acknowledgments

The authors thank the Shanghai Ninth People's Hospital, Shanghai Jiao Tong University School of Medicine for their strong support of this study.

Conflict of interest

The authors declare that the research was conducted in the absence of any commercial or financial relationships that could be construed as a potential conflict of interest.

Generative AI statement

The author(s) declare that no Generative AI was used in the creation of this manuscript.

Publisher's note

All claims expressed in this article are solely those of the authors and do not necessarily represent those of their affiliated organizations, or those of the publisher, the editors and the reviewers. Any product that may be evaluated in this article, or claim that may be made by its manufacturer, is not guaranteed or endorsed by the publisher.

References

Aurilio, G., Cimadamore, A., Mazzucchelli, R., Lopez-Beltran, A., Verri, E., Scarpelli, M., et al. (2020). Androgen receptor signaling pathway in prostate cancer: from genetics to clinical applications. *Cells* 9 (12), 2653. doi:10.3390/cells9122653

Azizi, E., Carr, A. J., Plitas, G., Cornish, A. E., Konopacki, C., Prabhakaran, S., et al. (2018). Single-cell map of diverse immune phenotypes in the breast tumor microenvironment. *Cell* 174 (5), 1293–1308. doi:10.1016/j.cell.2018.05.060

Bian, X., Liu, R., Meng, Y., Xing, D., Xu, D., and Lu, Z. (2021). Lipid metabolism and cancer. *J. Exp. Med.* 218 (1), e20201606. doi:10.1084/jem.20201606

Butler, L. M., Centenera, M. M., and Swinnen, J. V. (2016). Androgen control of lipid metabolism in prostate cancer: novel insights and future applications. *Endocrine-related cancer* 23 (5), R219–R227. doi:10.1530/ERC-15-0556

Chen, S., Huang, V., Xu, X., Livingstone, J., Soares, F., Jeon, J., et al. (2019). Widespread and functional RNA circularization in localized prostate cancer. *Cell* 176 (4), 831–843. doi:10.1016/j.cell.2019.01.025

Chen, S., Zhu, G., Yang, Y., Wang, F., Xiao, Y.-T., Zhang, N., et al. (2021). Single-cell analysis reveals transcriptomic remodellings in distinct cell types that contribute to human prostate cancer progression. *Nat. Cell Biol.* 23 (1), 87–98. doi:10.1038/s41556-020-00613-6

Currie, E., Schulze, A., Zechner, R., Walther, T. C., and Farese, R. V., Jr. (2013). Cellular fatty acid metabolism and cancer. *Cell metab.* 18 (2), 153–161. doi:10.1016/j.cmet.2013.05.017

Dong, B., Miao, J., Wang, Y., Luo, W., Ji, Z., Lai, H., et al. (2020). Single-cell analysis supports a luminal-neuroendocrine transdifferentiation in human prostate cancer. *Commun. Biol.* 3 (1), 778. doi:10.1038/s42003-020-01476-1

Faubert, B., Solmonson, A., and DeBerardinis, R. J. (2020). Metabolic reprogramming and cancer progression. *Sci. (1979).* 368 (6487), eaaw5473. doi:10.1126/science.aaw5473

Hopkins, B. D., Pauli, C., Du, X., Wang, D. G., Li, X., Wu, D., et al. (2018). Suppression of insulin feedback enhances the efficacy of PI3K inhibitors. *Nature* 560 (7719), 499–503. doi:10.1038/s41586-018-0343-4

Hu, Q., Xu, J., Wang, L., Yuan, Y., Luo, R., Gan, M., et al. (2023). SUCLG2 regulates mitochondrial dysfunction through succinylation in lung adenocarcinoma. *Adv. Sci.* 10 (35), e2303535. doi:10.1002/advs.202303535

Le Magnen, C., Shen, M. M., and Abate-Shen, C. (2018). Lineage plasticity in cancer progression and treatment. *Annu. Rev. cancer Biol.* 2, 271–289. doi:10.1146/annurev-cancerbio-030617-050224

Lin, S. R., Wen, Y. C., Yeh, H. L., Jiang, K. C., Chen, W. H., Mokgautsi, N., et al. (2020). EGFR-upregulated LIFR promotes SUCLG2-dependent castration resistance and neuroendocrine differentiation of prostate cancer. *prostate cancer* 39 (44), 6757–6775. doi:10.1038/s41388-020-01468-9

Martin-Perez, M., Urdiroz-Urricelqui, U., Bigas, C., and Benitah, S. A. (2022). The role of lipids in cancer progression and metastasis. *Cell metab.* 34 (11), 1675–1699. doi:10.1016/j.cmet.2022.09.023

Parsons, J. K., Gage, W. R., Nelson, W. G., and De Marzo, A. M. (2001). p63 protein expression is rare in prostate adenocarcinoma: implications for cancer diagnosis and carcinogenesis. *Urology* 58 (4), 619–624. doi:10.1016/s0090-4295(01)01311-5

Pfeiffer, M. J., and Schalken, J. A. (2010). Stem cell characteristics in prostate cancer cell lines. *Eur. Urol.* 57 (2), 246–254. doi:10.1016/j.eururo.2009.01.015

Sekhoacha, M., Riet, K., Motloung, P., Gumenku, L., Adegoke, A., and Mashele, S. (2022). Prostate cancer review: Genetics, diagnosis, treatment options, and alternative approaches. *Molecules* 27 (17), 5730. doi:10.3390/molecules27175730

Shemesh, C. S., Hsu, J. C., Hosseini, I., Shen, B. Q., Rotte, A., Twomey, P., et al. (2021). Personalized cancer vaccines: clinical landscape, challenges, and opportunities. *Mol. Ther. J. Am. Soc. Gene Ther.* 29 (2), 555–570. doi:10.1016/j.ymthe.2020.09.038

Shen, T., Wang, H., Tang, B., Zhu, G., and Wang, X. (2023). The impact of RNA binding proteins and the associated long non-coding RNAs in the TCA cycle on cancer pathogenesis. *RNA Biol.* 20 (1), 223–234. doi:10.1080/15476286.2023.2216562

Sun, L., Zhang, H., and Gao, P. (2022). Metabolic reprogramming and epigenetic modifications on the path to cancer. *Protein Cell* 13 (12), 877–919. doi:10.1007/s13238-021-00846-7

Tirosh, I., Izar, B., Prakadan, S. M., Wadsworth, M. H., Treacy, D., Trombetta, J. J., et al. (2016). Dissecting the multicellular ecosystem of metastatic melanoma by single-cell RNA-seq. *Sci. (New York, NY)* 352 (6282), 189–196. doi:10.1126/science.aad0501

Wang, G., Zhao, D., Spring, D. J., and DePinho, R. A. (2018). Genetics and biology of prostate cancer. *Genes and Dev.* 32 (17-18), 1105–1140. doi:10.1101/gad.315739.118

Wu, B., Qiu, J., Zhao, T. V., Wang, Y., Maeda, T., Goronzy, I. N., et al. (2020). Succinyl-CoA ligase deficiency in pro-inflammatory and tissue-invasive T cells. *Cell metab.* 32 (6), 967–980. doi:10.1016/j.cmet.2020.10.025

Xu, X., Zhang, Y., Liao, C., Zhou, H., Wu, Y., and Zhang, W. (2023). Impact of ferroptosis-related risk genes on macrophage M1/M2 polarization and prognosis in glioblastoma. *Front. Cell. Neurosci.* 17, 1294029. doi:10.3389/fncel.2023.1294029

Xu, X., Zhou, E., Zheng, J., Zhang, C., Zou, Y., Lin, J., et al. (2021). Prognostic and predictive value of m6A "eraser" related gene signature in gastric cancer. *Front. Oncol.* 11, 631803. doi:10.3389/fonc.2021.631803

Yang, Y., Zhang, X., Cai, D., Zheng, X., Zhao, X., Zou, J. X., et al. (2024). Functional inversion of circadian regulator REV-ERBα leads to tumorigenic gene reprogramming. *Proc. Natl. Acad. Sci. U. S. A.* 121 (42), e2411321121. doi:10.1073/pnas.2411321121

You, S., Knudsen, B. S., Erho, N., Alshalalfa, M., Takhar, M., Al-Deen, A. H., et al. (2016). Integrated classification of prostate cancer reveals a novel luminal subtype with poor outcome. *Cancer Res.* 76 (17), 4948–4958. doi:10.1158/0008-5472.CAN-16-0902

Zhang, D., Zhao, S., Li, X., Kirk, J. S., and Tang, D. G. (2018). Prostate luminal progenitor cells in development and cancer. *Trends cancer* 4 (11), 769–783. doi:10.1016/j.trecan.2018.09.003

Zhao, S. G., Chang, S. L., Erho, N., Yu, M., Lehrer, J., Alshalalfa, M., et al. (2017). Associations of luminal and basal subtyping of prostate cancer with prognosis and response to androgen deprivation therapy. *JAMA Oncol.* 3 (12), 1663–1672. doi:10.1001/jamaoncol.2017.0751

frontiers | Frontiers in Pharmacology

TYPE Original Research
PUBLISHED 22 July 2025
DOI 10.3389/fphar.2025.1606914

OPEN ACCESS

EDITED BY
Lei Yin,
Shanghai Jiaotong University School of Medicine, China

REVIEWED BY
Soumya Basu,
Johns Hopkins University, United States
Minh Trong Quang,
Ho Chi Minh City Medicine and Pharmacy University, Vietnam

*CORRESPONDENCE
Emerson Isaac Arnold,
i_arnoldemerson@yahoo.com

RECEIVED 06 April 2025
ACCEPTED 30 June 2025
PUBLISHED 22 July 2025

CITATION
Chituri KK and Arnold EI (2025) Integrative genomic analysis identifies *DPP4* inhibition as a modulator of *FGF17* and *PDGFRA* downregulation and *PI3K/Akt* pathway suppression leading to apoptosis. *Front. Pharmacol.* 16:1606914. doi: 10.3389/fphar.2025.1606914

Integrative genomic analysis identifies *DPP4* inhibition as a modulator of *FGF17* and *PDGFRA* downregulation and *PI3K/Akt* pathway suppression leading to apoptosis

Kiran Kumar Chituri and Emerson Isaac Arnold *

Bioinformatics Programming Lab, Department of Bioscience, School of Bio Sciences and Technology, Vellore Institute of Technology, Vellore, Tamilnadu, India

Introduction: Prostate cancer (PCa) remains a significant global health challenge despite advancements in treatment strategies. There is a need to explore the molecular heterogeneity of PCa to facilitate the development of personalized treatment approaches. This study investigates the molecular heterogeneity of PCa by combining genomic and transcriptomic data using a systems biology approach.

Methods: By utilising whole-genome sequencing and differentially expressed genes from "The Cancer Genome Atlas Prostate Adenocarcinoma (TCGA-PRAD)" patient samples, we identified 357 intersecting genes. From protein-protein interaction network analysis, 22 hub genes were identified as critical regulators associated with PCa prognosis and pathogenesis. Furthermore, these hub genes were subjected to functional and pathway enrichment analysis via gene ontology (GO) and the Kyoto Encyclopaedia of Genes and Genomes (KEGG).

Results: Notably, the *PI3K/Akt* signalling pathway was significantly enriched with eight of these hub genes, with significant clinical relevance. Dipeptidyl Peptidase 4 (DPP4) emerged as a promising therapeutic target. Further, in vitro assays were performed to investigate and validate the molecular role of DPP4 through pharmacological inhibition using Linagliptin, a selective DPP4 inhibitor. Inhibition of DPP4 led to the induction of apoptosis, G1/S phase cell cycle arrest, and significant suppression of cell proliferation and migration in PC3 and DU145 cell lines.

Discussion: These experiments revealed novel downstream regulatory effects of DPP4, demonstrating that its inhibition results in the transcriptional downregulation of *FGF17, PDGFRA, COL4A1*, and *COL9A2*, thereby contributing to the inactivation of the *PI3K/Akt* signaling pathway. Collectively, these findings highlight DPP4 as a potential therapeutic target for the treatment of PCa.

KEYWORDS

Linagliptin, prostate cancer, apoptosis, mutation, *DPP4/CD26*, *PI3K/Akt* pathway, PC3, DU145

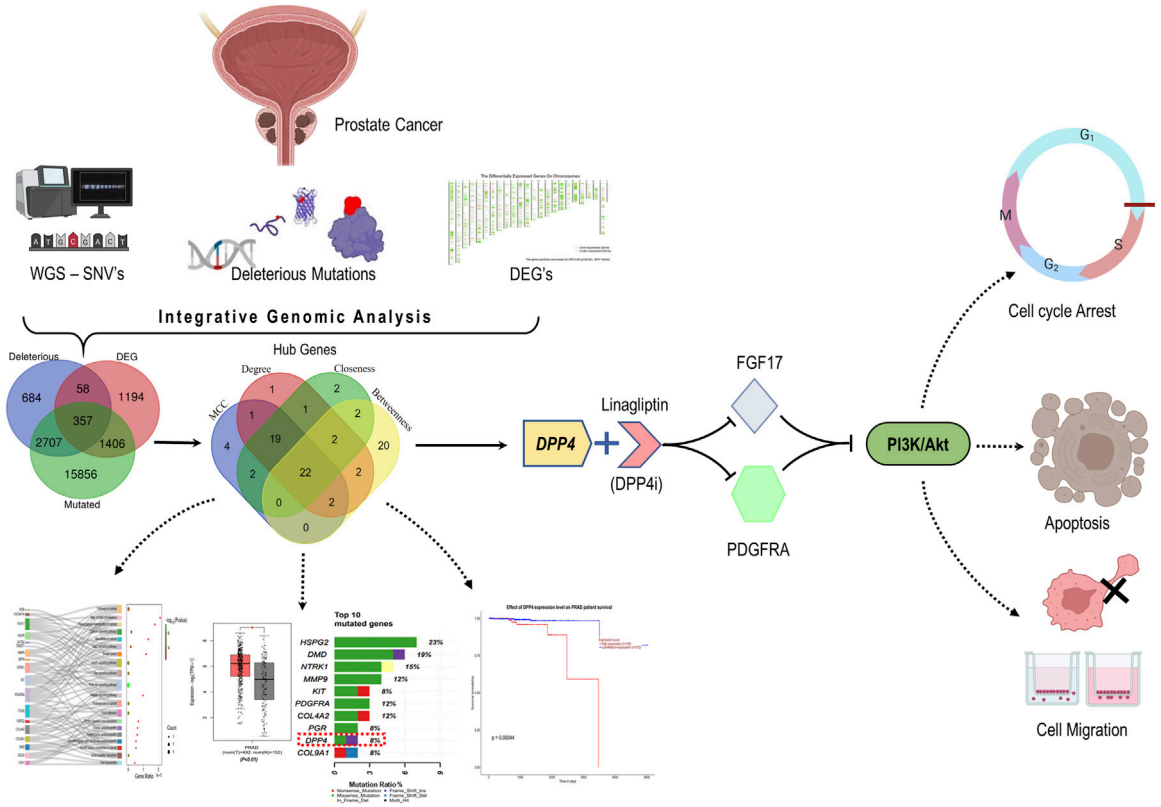

GRAPHICAL ABSTRACT

By integrative genomic analysis, DPP4 emerged as potential therapeutic target in PCa. Inhibiting DPP4 downregulates PDGFRA and FGF17 and induced cellular apoptosis, cell cycle arrest and hinders cell migration by disrupting the PI3K/Akt pathway.

1 Introduction

Prostate cancer (PCa) is a prevalent non-dermal heterogeneous malignancy among males that poses a significant health concern worldwide, and it remains the second leading cause of cancer-related deaths in men (Sekhoacha et al., 2022; Bhargavi et al., 2023). According to the American Cancer Society (ACS) report "Cancer Statistics 2023", there are an estimated 288,300 cases of PCa in the United States of America alone, accounting for 29% of all cancer types among males (Siegel et al., 2023). However, it is noteworthy that while a significant number of individuals may be diagnosed with PCa, only a minority of them will exhibit clinically relevant manifestations of the disease (Silberstein et al., 2013). Treatments available for PCa consist of surgery, radiation therapy, hormone therapy, chemotherapy, and targeted therapy. However, there is a pressing requirement for improved treatments, particularly for aggressive and treatment-resistant types of the condition. The emphasis should be on identifying and diagnosing PCa accurately, particularly in less developed nations where mortality rates are higher due to limited access to screening and better treatment alternatives (Sekhoacha et al., 2022; Wasim et al., 2023; Ferroni et al., 2019).

Advancements in genomics and precision medicine hold substantial promise for identifying novel therapeutic targets in PCa. Unique genetic alterations such as mutations in tumor suppressor genes and oncogenes can promote tumor progression and therapy resistance. Notably, the androgen receptor (AR) signaling pathway, a key driver of PCa, is tightly regulated by hormonal activity, particularly testosterone and dihydrotestosterone. Dysregulation of this pathway, often through AR gene amplification, mutations, or splice variants, leads to sustained AR activation even in the absence of androgens, contributing to castration-resistant prostate cancer (CRPC) (Ma et al., 2024; He et al., 2021; Chitluri and Emerson, 2024). Additionally, genetic alterations in pathways such as PTEN/PI3K/AKT, DNA damage repair (e.g., BRCA1/2), and TMPRSS2-ERG fusions further enhance tumor aggressiveness and confer resistance to conventional hormone therapies (Waarts et al., 2022; Berger and Mardis, 2018). Integrating hormonal context with genomic analysis is thus critical, as the crosstalk between androgen signaling and oncogenic mutations shapes disease trajectory and treatment response (Li et al., 2025; Wang et al., 2008). Understanding these interactions facilitates the development of targeted therapies such as AR inhibitors, PI3K inhibitors, and PARP inhibitors that disrupt key hormonal and genetic drivers of PCa progression (Antonarakis et al., 2020; Crumbaker et al., 2017).

Similarly, gene expression profiles can provide valuable information about the biological characteristics of a tumor (Creighton, 2023). Overexpression or under-expression of certain genes can indicate the presence of specific molecular subtypes of

cancer, each with distinct clinical behaviours and treatment responses. For instance, the overexpression of androgen receptor signaling pathways in metastatic PCa highlights the importance of androgen deprivation therapies (Hoang et al., 2017; Jillson et al., 2021). Nevertheless, some patients develop resistance to androgen deprivation therapy (ADT), resulting in poor prognosis and limited treatment choices (Maitland, 2021). However, as tumors evolve, they may alter their gene expression patterns to develop resistance to these therapies, necessitating the identification of new targets and the development of novel therapeutic approaches (Gatenby and Brown, 2020). We have conducted a comprehensive study to address this issue. Our study involved identifying mutated genes (MutGs), characterizing deleterious mutated genes (DMutGs) from NGS data and integrating differentially expressed genes (DEGs) retrieved from the GEPIA2 database. Additionally, we incorporated protein-protein interaction (PPI) networks, identified hub genes, predicted correlations between hub genes, and conducted Gene Ontology (GO) and Kyoto Encyclopaedia of Genes and Genomes (KEGG) pathway enrichment analyses. Furthermore, we evaluated immune cell infiltrates and performed survival analysis using large-scale DNA microarray and RNA-Seq data from GEO, TCGA, and other public databases to explore potential hub genes and biological pathways related to the occurrence, development, and prognosis of PCa. We identified 22 hub genes involved in PCa progression and metastasis, investigated them, identified potential therapeutic targets, and experimentally validated them.

2 Materials and methods

2.1 *In-silico*

2.1.1 Dataset download and single nucleotide variants (SNV's) identification from WGS

To conduct our study, we obtained the paired-end (PE) whole genome sequence (WGS) of a human adult male prostate tumor tissue in fasta format with the run SRA accession SRP250789 from the SRA database accessed on February 2023. We also obtained differentially expressed genes (DEGs) for prostate adenocarcinoma (PRAD), from the GEPIA2 database (Tang et al., 2019). These genes were selected based on specific criteria, including a $\log_2$FC > 1 and a q-value <0.01. To ensure the quality of the WGS reads, we subjected them to quality control and assessed the quality using FastQC. Any low-quality sequences were removed using Trimmomatic ILLUMINACLIP NexteraPE-PE for adapters, with MINLEN adopted to drop the reads below 25 bp length and SLIDINGWINDOW was invoked to remove the bases with a phred score below 20. The trimmed sequences were then aligned to the reference genome using Burrows-Wheeler aligner (BWA). Variants were detected using bcftools, and SNVs with a high-quality score of >100 were filtered.

2.1.2 Determining common genes

The polyphen2 tool (Adzhubei et al., 2013) (accessed on April 2023) was used to assess the ability to predict single nucleotide variants, identify mutated genes, and predict genomes with deleterious mutations. The analysis compared deleterious mutated genes (DMutGs) to mutated genes (MutGs) and differentially expressed genes (DEGs). This investigation led to the identification of specific genes with deleterious mutations and differential expression.

2.1.3 PPI networking and hub gene selection

STRING app (Szklarczyk et al., 2021) (accessed on May 2023) was used to investigate the interaction network in the common human gene set identified previously. Interaction pairs were combined with those that were experimentally verified so that an interaction scores greater than 0.4 was applied as the cut-off. Closely interacting genes were listed. We identified the top 50 hub genes based on the four topological methods: maximum clique centrality (MCC), degree, closeness, betweenness, and overlapping genes between such methods were selected.

2.1.4 Enrichment analysis

In addition, the Gene Ontology (GO) analysis with the help of R "clusterProfiler" was performed to investigate further functional roles played by the overlapped hub genes and the top cluster genes. The cellular component (CC), biological process (BP), and molecular functions (MF) involved with the presented genes were determined by GO enrichment analysis. Likewise, using ShinyGO (v.0.79) (Ge et al., 2020), KEGG analysis was performed to correlate the enriched biological pathways of the hubs with edge cut-off = 0.2 and FDR p-value cut-off = 0.05, followed by classification of signal pathways. This enabled us to identify some putative biological processes, signaling pathways and human disease pathways that would account for PCa pathogenesis and progression.

2.1.5 Kaplan-Meier overall survival (OS) analysis of hubs

To investigate the prognostic potential for identified hub genes, Kaplan-Meier curve analysis was performed to compare clinical outcomes based on the hub gene expressions associated with poor prognosis in PCa, highlighting their potential as prognostic biomarkers for identifying high-risk patients' overall outcomes in PCa patients. In the current study, Kaplan-Meier survival analysis with hazard ratio (HR) was performed using UALCAN (Chandrashekar et al., 2017) and GEPIA2.0 databases - TCGA prostate adenocarcinoma (PRAD) cohort (accessed on August 2023). The cohort population was stratified into high- and low-expression groups based on the median hub genes expression level, ensuring an unbiased and biologically relevant comparison. (log rank p-value<0.05, p (HR) < 0.05).

2.1.6 Tumor infiltration analysis

To further investigate the potential role of the identified hub genes in the tumor microenvironment, we evaluated the correlation between tumor-infiltrating immune cells across the TCGA-PRAD cohort and the expression levels of PCa hub genes using the TIMER2.0 database (accessed on September 2023) (Li et al., 2020). We used the Spearman's test (ρ) and a p-value of <0.05 was considered statistically significant. This analysis helped us to gain insights into the potential interactions between immune cells and the identified hub genes in PCa, which may provide new avenues for therapeutic interventions.

2.1.7 Estimating the expression of the hubs in correlation with DPP4

To check the expression of the other hub genes in comparison with DPP4, we used the Gene_Corr module, and the degree of correlation was established based on the "Spearman's rho" value. These analyses helped us to evaluate the potential impact of DPP4 expression on the expression of other hub genes in PCa and identify potential therapeutic targets.

2.2 *In-vitro*

2.2.1 Cell lines and reagents

DU145, PC3 and HEK293 were obtained from the National Center for Cell Sciences (NCCS, Pune). For cell culture, Dulbecco's Modified Eagle Medium, High Glucose (DMEM), Fetal Bovine Serum (FBS), Antibiotic Mixture (Streptomycin and penicillin) and Cell culture grade dimethyl sulfoxide (DMSO) were purchased from HI-Media laboratories, Mumbai. RT-PCR and cDNA conversion kits were obtained from Takara, Chennai. Other plastic materials, including Transwell migration plates, were purchased from Tarson, India. Linagliptin and doxorubicin were purchased from Sigma-Aldrich, India.

2.2.2 Cell maintenance and cell viability assay

DU145, PC3 and HEK293 cells were maintained in a humidified incubator set at 37°C and 5% CO2, using a complete medium including DMEM, 10% FBS, 100 IU/mL penicillin, and 100 μg/mL streptomycin. The media was changed every 2–3 days. Once the cells had achieved 80%–90% confluency, they were collected, and experimental procedures were carried out.

Cell viability was assessed by seeding cells at a density of 1×10^4 per well on a 96-well plate supplemented with complete medium and incubating them overnight in a humidifier incubator. The next day, the culture medium was withdrawn, and the cells were exposed to Linagliptin at varying concentrations for 24 h. Following the specified duration, the drug was removed, and 20 μL of MTT (5 mg/mL in PBS) was added to the well. The well was then incubated in the absence of light for 4 h. After 4 h, MTT was removed, and 100 μL of DMSO was added to the wells. The intensity of the formazan crystal was then quantified at 490 nm using a Microplate Reader from Bio-Tek, United States. Three repetitions of each analysis were conducted, and the cell viability was compared to that of the untreated control group. In this work, doxorubicin served as the positive control.

2.2.3 Morphological changes

PC3 and DU145 cells, exhibiting exponential growth, were collected and plated in 6-well plates at a density of 1×10^5 cells per well and incubated overnight. The cells were subsequently incubated for 24 h with Linagliptin (IC50), while cells treated with Doxorubicin were the positive control. Cell morphology was analyzed using an inverted microscope (MAGNUS 10J617).

2.2.4 Scratch assay

For this assay, PC3 and DU-145 cells were seeded at a density of 1×10^5 cells per well in a 6-well plate and incubated for 24 h. A scratch was created on the plates utilizing a 200 μL sterile pipette tip. The plate was washed with 1XPBS to eliminate cellular debris and subsequently treated with Linagliptin (IC50) for 24 h. Control cells were kept untreated, while doxorubicin (3.5 μM) was the positive control. Images were obtained at 0th and 24th-hour post-drug administration utilizing an inverted microscope (MAGNUS 10J617). Image closure was measured using ImageJ software and represented as %wound closure relative to the size at the 0th hour. The percentage of wound closure is calculated as follows:

$$\%\ \text{Would Closure} = \frac{(Original\ scratch\ width) - (new\ scratch\ width)}{Original\ scratch\ width} \times 100$$

2.2.5 Transwell migration assay

The impact of Linagliptin on the migration of PC3 and DU145 cells was further examined using a Transwell migration experiment in 6-well Corning Transwell cell culture inserts with an 8 μm pore size. Subsequently, following treatment with Linagliptin at IC50 concentration and Doxorubicin, the cells were trypsinized and re-suspended in serum-free media. Subsequently, 200 μL (1×10^5 cells) of the cell suspension was introduced into the upper compartment in serum-free media, while 1,000 μL of complete media was supplied to the lower chamber. Following 24 h of incubation, the non-migrated cells from the upper surface of the insert were eliminated using a sterile cotton swab. The migrating cells on the lower side were rinsed with PBS and fixed in 70% ethanol for 10 min. The cells were subsequently stained with 0.5% crystal violet for 20 min, followed by a PBS wash to eliminate excess stain. The quantity of migrating cells was enumerated in three distinct fields and captured using an inverted microscope (MAGNUS 10J617).

2.2.6 Cell cycle analysis and determining apoptosis using annexin V-FITC

PC3 and DU145 cells (1×10^5 cells/well) were treated with Linagliptin for 24 h alongside a control group without treatment. The cells were trypsinized and rinsed three times with 1X PBS before being fixed in 5 mL of 70% ice-cold ethanol for 24 h on ice. The cells were subsequently rinsed with PBS and subjected to a 10 μg/mL RNase A (Himedia, Mumbai, India) treatment at 37 °C for 30 min. The cells were stained with 50 μg/mL propidium iodide (Thermo Fisher Scientific, Bangalore, India) for 20 min in the dark. The outcomes were assessed using flow cytometry (CytoFLEX S, Beckman Coulter). Additionally, percentage of apoptosis was determined using annexin-V fluorescein isothiocyanate (FITC) and propidium iodide (PI) apoptosis detection kit (BD Biosciences) according to the manufacturer's instructions. Percentage of apoptotic cells (annexin+/PI+) was analysed by flow cytometry (CytoFLEX S, Beckman Coulter).

2.2.7 AO/EtBr staining

An EtBr and AO double staining test was conducted to evaluate Linagliptin's impact on cellular apoptosis in PC3 and DU145 cells. The cells were cultured on coverslips and treated with Linagliptin for 24 h. Untreated control cells were maintained, whereas Doxorubicin served as the positive control. Following incubation, a staining solution comprising AO (100 mg mL^{-1}) and EtBr (100 mg mL^{-1}) was administered to the cells, which were then incubated in darkness for 5 min. Using a fluorescent microscope, the cells were subsequently analysed for their staining pattern (Weswox Optik-FM 3000).

TABLE 1 Primers list.

Gene Name	Forward Primer (5′-3′)	Reverse Primer (5′-3′)
PIK3CA	GGTTGTCTGTCAATCGGTGACTGT	GAACTGCAGTGCACCTTTCAAGC
AKT1	TTCTGCAGCTATGCGCAATGTG	TGGCCAGCATACCATAGTGAGGTT
PTEN	*GGTTGCCACAAAGTGCCTCGTTTA*	*CAGGTAGAAGGCAACTCTGCCAAA*
FGF17	GTGTTCACGGAGATCGTGCTG	GAACTGCTTCTGCTTCTCGGC
PDGFRA	GACTTTCGCCAAAGTGGAGGAG	AGCCACCGTGAGTTCAGAACGC
COL4A1	TGTTGACGGCTTACCTGGAGAC	GGTAGACCAACTCCAGGCTCTC
COL9A2	TGGAGTGGAAGGACCAAGAGGA	GTGCTGATCTGTCGGTGCTCTA
Beta-Actin	AGTCCTGTGGCATCCACGAA	GATCCACACGGAGTACTTGC

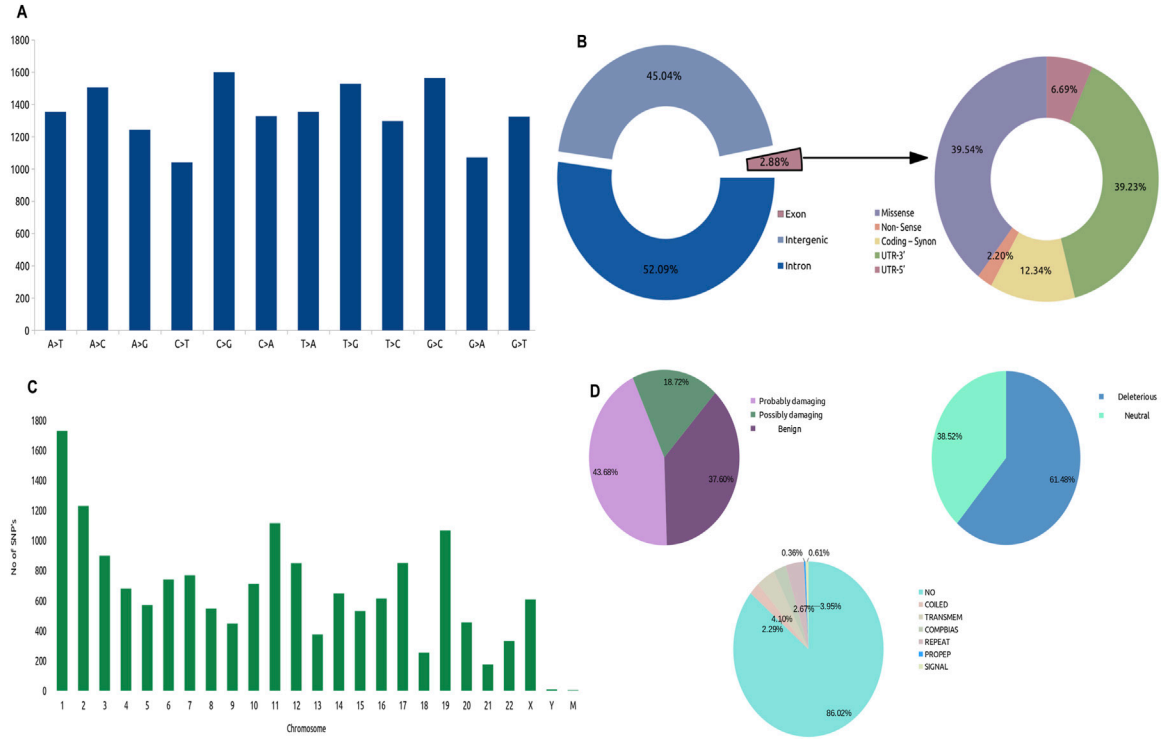

FIGURE 1
Distribution of SNV's in the Whole Genome Sequence (WGS), **(A)** Identified types of SNV's variations **(B)** Landscape of Missense mutations across Chromosomes, **(C)** Fractions of mutations across whole genome, **(D)** Types of exonic mutations: Characterization of Missense mutations, Left: Percentage of mutations that are probably damaging, possibly damaging and benign; Right: Percentage of mutations that are deleterious and neutral; Bottom: Location of mutations.

2.2.8 RNA isolation and RT-PCR

PC3 and DU145 cells (1×10^5 cells/well) were seeded in 6-well plates and treated with Linagliptin at IC50 concentration and Doxorubicin for 24 h. RT-PCR was employed to assess the mRNA expression of target genes. RNA was extracted from cells utilizing TRI Reagent® (Sigma Aldrich, Bangalore, India), and the resultant RNA was quantified using a Nanodrop 2000 (ThermoFisher Scientific, Bangalore, India). cDNA synthesis was conducted utilizing the PrimeScript™ RT reagent Kit (DSS Takara Bio India Pvt. Ltd., Bangalore, India). RT-PCR was done using SYBR® Premix Ex Taq™ (DSS Takara Bio India Pvt. Ltd., Bangalore, India). Each real-time PCR utilized 100 ng of RNA. The quantitative RT-PCR was conducted utilizing the Light Cycler 2.0 (Applied Biosystems® StepOne RT-PCR equipment, Bangalore, India). A melting curve study was conducted post-amplification utilizing LightCycler software (A.B. Biosystems, India). Beta-actin served as an internal standard, and the results were presented as fold change over relative control. Primer list is added in Table 1.

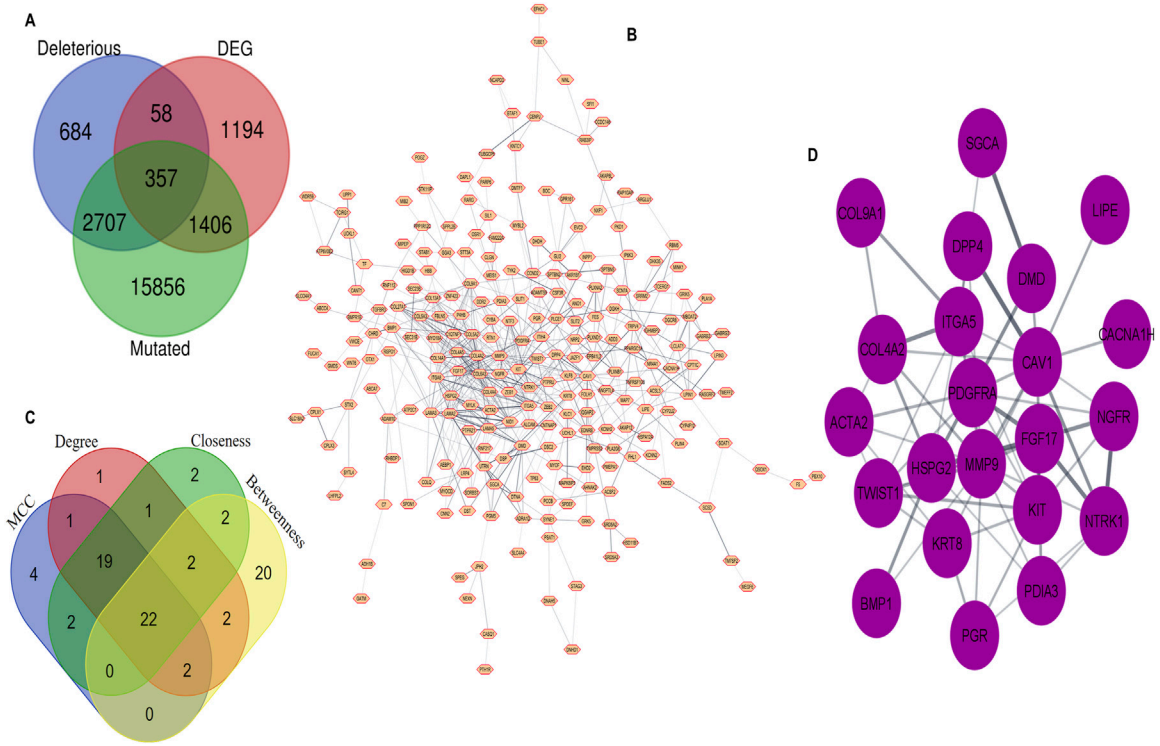

FIGURE 2
Integration of WGS and Trascriptomic data through PPI network analysis, **(A)** Common genes among Deleterious mutated genes, Differentially Expressed Genes and Mutated genes **(B)** Protein–Protein interaction of 357 common genes. **(C)** Hub genes identification by overlapping between the top 50 gene ranks based on four topological algorithms. **(D)** 22 hub genes.

2.2.9 DPP4 activity assay

DPP4 activity assay kit (MAK088) was obtained from Sigma-Aldrich, Bangalore, Karnataka, India. Cells were treated as previously described. DPP4 activity was performed based on the kit protocol.

2.2.10 Statistical analysis

GraphPad Prism 8.0 was used to do statistical analysis. The results are expressed as mean ± SD of three independent experiments. One-way ANOVA with Bonferroni's multiple comparisons was used to evaluate differences. $P < 0.05$ is considered significant.

2.2.11 Western blot analysis

Western blot analysis was performed using PC3 cells and DU145 cells, both treated with varying concentrations of Linagliptin (0, 20, and 40 μM for PC3 and 0, 20, and 60 μM for DU145) for 24 h. After treatment, total protein was extracted by resuspending the cells and lysing them for 1 h at 4°C in RIPA (radioimmunoprecipitation assay) buffer (Cat. No. R0278) with protease and phosphatase inhibitor cocktail. The cell lysates were then centrifuged at 12,000 rpm for 30 min at 4°C, and the Bradford assay was used to determine the protein concentration. An equal volume of 20 μg protein lysate from each sample was subjected to SDS-PAGE and subsequently transferred onto a nitrocellulose membrane (Bio-Rad, cat. no. 1620112). The membrane was blocked with 5% skimmed non-fat dry milk and incubated overnight at 4°C with various antibodies: anti-FGF17 (1:2000), anti-PI3K p-85α (1:1,000), anti-AKT (1:2000), anti-p-AKT (1:2000), anti-GAPDH (1:2000), and anti-Actin (1:1,000). Following this, the membranes were rinsed three times with TBS (Tris buffered saline), each for 10 minutes, and then incubated with HRP-conjugated secondary anti-mouse or anti-rabbit antibodies (diluted to 1:5000) for 1 h at room temperature. They were washed three more times with TBST (Tris buffered saline containing Tween-20, pH 7.5). Finally, the immunoblots were visualized using ECL substrate (Clarity™ western ECL substrate Cat# 170-5061) under the ChemiDoc MP Imaging System (Bio-Rad). All experiments were conducted in triplicates.

3 Results

3.1 *In-silico*

3.1.1 Variant calling

To obtain the full set of SNV data, we retrieved the whole genome sequence of a human adult male prostate tumor sample bearing the SRP250789 from ENA at https://www.ebi.ac.uk/ena/browser/view/SRP250789. We initially performed variant calling to identify the SNVs and the reads were aligned with the reference sequence. A total of reads with a quality score of <100 were retained and used for further analysis. These SNVs were mapped to the genes using BioMart (Kinsella et al., 2011), and we identified 20,326 mutated genes (MutG).

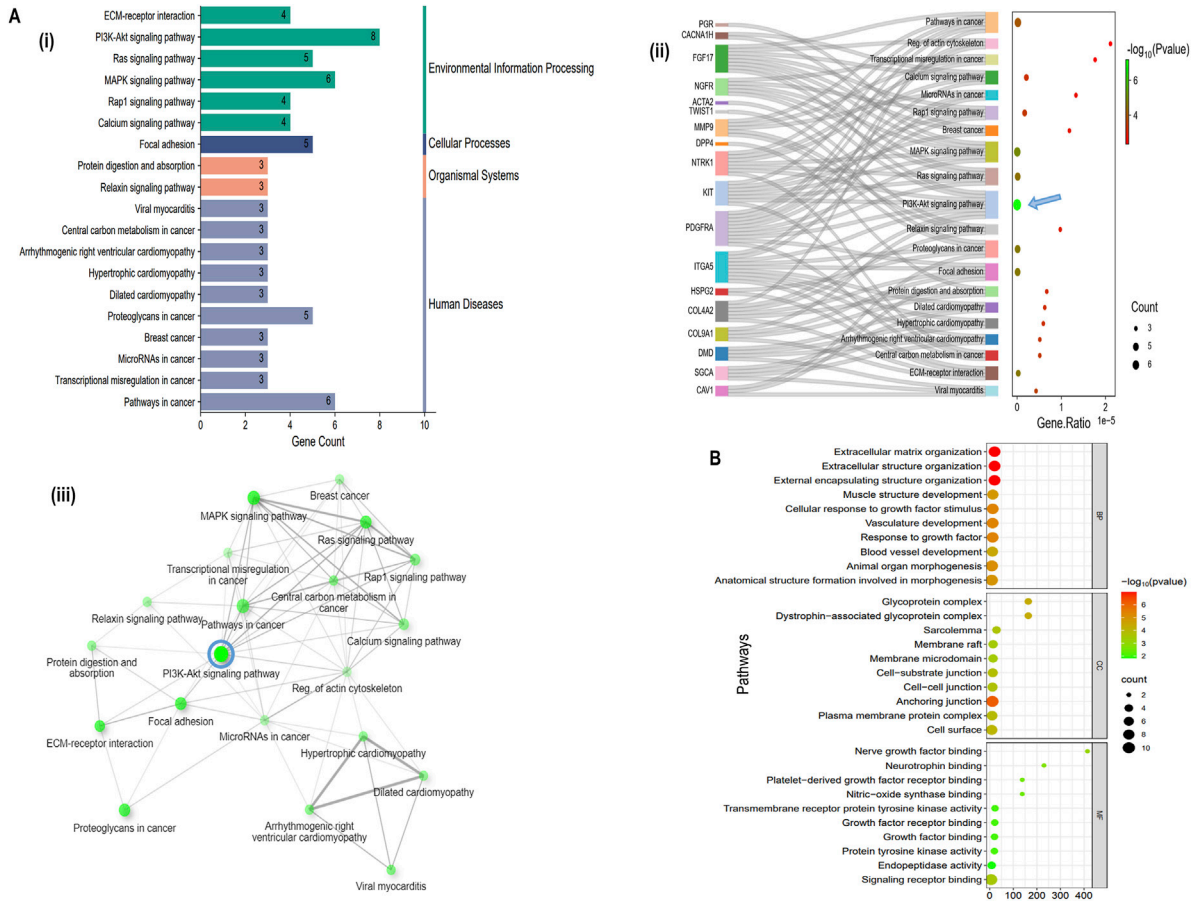

FIGURE 3
Functional enrichment of Hub genes, **(A (i)** Classification summary diagram of the top 30 KEGG pathways. **A (ii)** KEGG pathway enrichment for the identified 22 hub genes, **A (iii)** KEGG pathways network interaction (Edge cut-off = 0.2 and FDR p-value cut-off = 0.05), **(B)** Gene Ontology (GO) enrichment analysis of 22 hub genes.

3.1.2 Characterising the SNVs identified

To further investigate the SNVs identified in the whole genome sequence, we annotated them using PolyPhen2 based on chromosomal position and discarded multi-mutations SNVs. Only 2.88% of single-nucleotide variants (SNVs) were found in exons, which are dispersed in CDS and non-sense UTRs while a large portion was located in introns (52.09%) and intergenic regions (45.05%). These areas may contain mutations in regulatory elements, such as enhancers, silencers, and non-coding RNAs. Our main goal is to identify genes that change the protein sequence through missense, nonsense, or frameshift mutations, which can disrupt protein function and lead to cancer. Although mutations in non-coding regions (introns) can affect gene expression and may contribute to cancer, we further integrated exonic mutations with the differentially expressed genes (DEGs) from the TCGA-PRAD dataset. We identified that 39.54% (16,202) of the exonic mutations were missense mutations (Figure 1B), with C>G and G>C transitions being the most prevalent (Figure 1A). These missense mutations were annotated to 16,055 genes with at least one missense mutation. They were distributed across the chromosomes, with chromosome one having the most missense SNVs (Figure 1C). Out of these genes, we identified that 18.72%, 37.60%, and 46.68% were possibly damaging, benign, and probably damaging at the functional level, respectively. We observed that 61.48% of the mutated genes were affected by deleterious mutations that impaired protein functionality (Figure 1D). In this analysis, we focused on 3,806 unique genes that had mutations that deleteriously affected protein function (DMutGs), allowing us to gain insights into the potential genetic causes of PCa and identify potential therapeutic targets.

3.1.3 Common genes identification

To identify the most optimal key candidate gene with potential therapeutic implications, we obtained a list of 3,015 (PRAD) differentially expressed genes (DEGs) with tissue code: PRAD of GEPIA2 database using the limma differential method, with $\log_2$FC cut off >1 and q-value cut off <0.01. We combined the MutGs, DMutGs and DEGs and identified 357 genes (Supplementary Table S1) present in all three sets, as shown in Figure 2A.

3.1.4 PPI network construction and hub selection

We utilized the Cytoscape STRING (Shannon et al., 2003) plugin to construct a PPI network for the list of 357 genes, with an interaction score set to 0.4. The network includes proteins that physically interact with at least one other member consisting of 239 nodes and 575 edges, as shown in Figure 2B. We then used

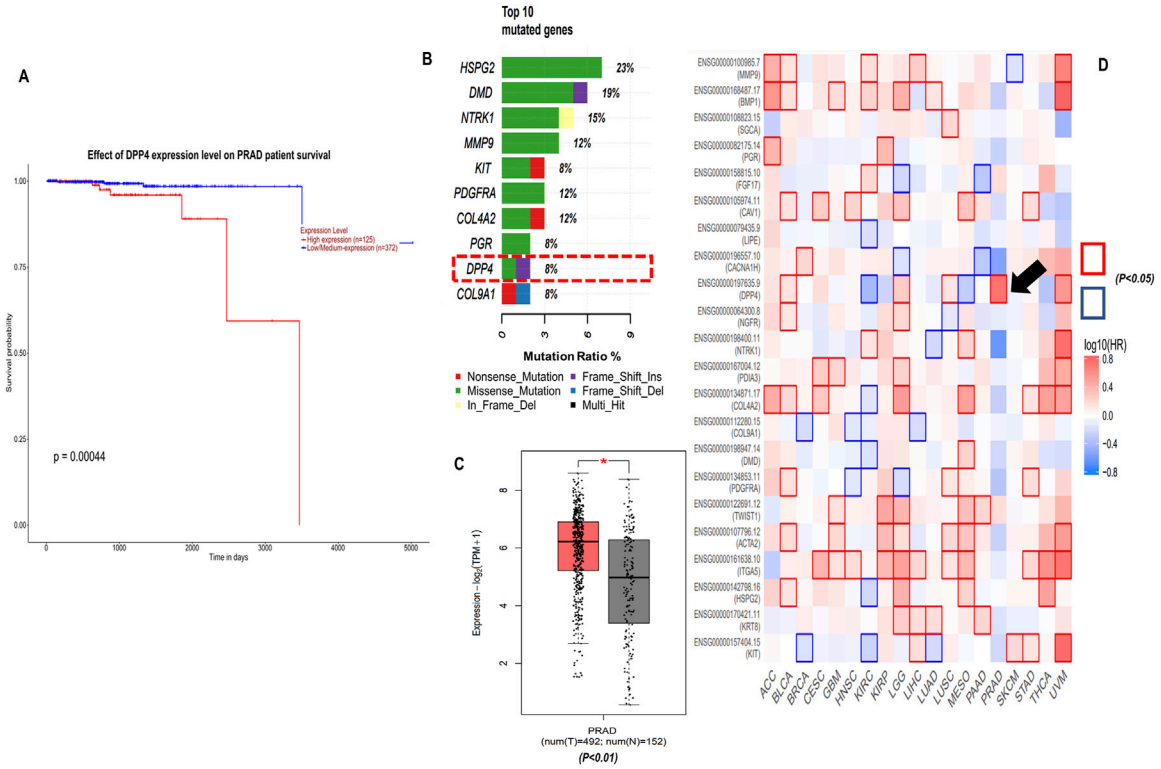

FIGURE 4
Clinical significance of DPP4, **(A)** Kaplan-Meier (KM) overall survival analysis of DPP4 using UALCAN database TCGA-PRAD cohort (log-rank p-value <0.001). **(B)** Top 10 mutated genes among 22 hub genes, **(C)** DPP4 gene expression TCGA-PRAD-GEPIA2 database, **(D)** Survival map of hazard ratio (HR) for the hub genes across cancers types with at least one significant HR (log_{10} (HR) $p < 0.05$).

cytoHubba to rank the top 50 genes based on four topological algorithms scoring values Supplementary Table S2 (i.e., MCC, degree, closeness, and betweenness) to identify the hub genes in the PPI network. We found that 22 hub genes overlapped within the four topological algorithms. This gene set was used for further analysis, as shown in Figure 2C. The identified hub genes are Collagen type IV alpha two chain *(COL4A2)*, Dystrophin *(DMD)*, Receptor tyrosine kinase *(KIT)*, Sarcoglycan alpha *(SGCA)*, Neurotrophic receptor tyrosine kinase 1 *(NTRK1)*, Actin alpha 2 smooth muscle *(ACTA2)*, Caveolin-1 *(CAV1)*, Lipase E *(LIPE)*, Integrin Subunit Alpha 5 *(ITGA5)*, Calcium channel, voltage-dependent, T type alpha 1H subunit *(CACNA1H)*, Twist-related protein 1 *(TWIST1)*, Progesterone receptor gene *(PGR)*, Fibroblast growth factor 17 *(FGF17)*, Nerve Growth Factor Receptor *(NGFR)*, Bone morphogenetic protein 1 *(BMP1)*, Keratin 8 *(KRT8)*, Heparansulfate proteoglycan 2 *(HSPG2)*, Platelet-derived growth factor receptor alpha *(PDGFRA)*, Collagen type IX alpha one chain *(COL9A1)*, Dipeptidyl peptidase 4 *(DPP4)*, Matrix metallopeptidase 9 *(MMP9)*, and Protein disulfideisomerase family A, member 3 *(PDIA3)* Figure 2D.

3.1.5 Enrichment analysis

The top 10 gene sets were enriched for biological process (BP), molecular function (MF), cellular component (CC) (log_{10}FDR p-value <0.05), and KEGG pathways were identified using the online tool ShinyGO and illustrated the signal pathway classification. The 22 hubs were found to be enriched for various processes, including extracellular matrix organization, extracellular structure organization, external encapsulating structure organization, muscle structure development, cellular response to growth factor stimulus, vasculature development, response to growth factor, blood vessel development, animal organ morphogenesis and anatomical structure formation involved in morphogenesis (BP). (CC) analysis revealed enrichment for anchoring junction, cell-cell junction, cell-substrate junction, membrane micro-domain, membrane raft, sarcolemma, dystrophin-associated glycoprotein complex, plasma membrane protein complex, cell surface and glycoprotein complex. (MF) analysis showed enrichment for signaling receptor binding, endopeptidase activity, protein tyrosine kinase activity, growth factor binding, growth factor receptor binding, transmembrane receptor protein tyrosine kinase activity, nitric-oxide synthase binding, Platelet-derived growth factor receptor binding, neurotrophin binding and nerve growth factor binding (Figure 3B). KEGG pathway analysis revealed that hubs gene enrichment majorly in *PI3K/Akt* pathway, pathways in cancer, focal adhesion, protein digestion and absorption, and ECM-receptor interaction (log_{10}FDR p-value <0.05) (Figure 3Aii). Interaction between the enriched KEGG pathways (Edge cut-off = 0.2 and FDR p-value cut-off <0.05) are depicted in Figure 3Aiii and predominantly involves human disease pathways such as the cancer pathways and proteoglycans in cancer (Figure 3Ai).

3.1.6 Overall Survival analysis of hub genes

To explore the prognostic value and clinical outcome of the hub genes, we used UALCAN (database) – to perform Kaplan-Meier

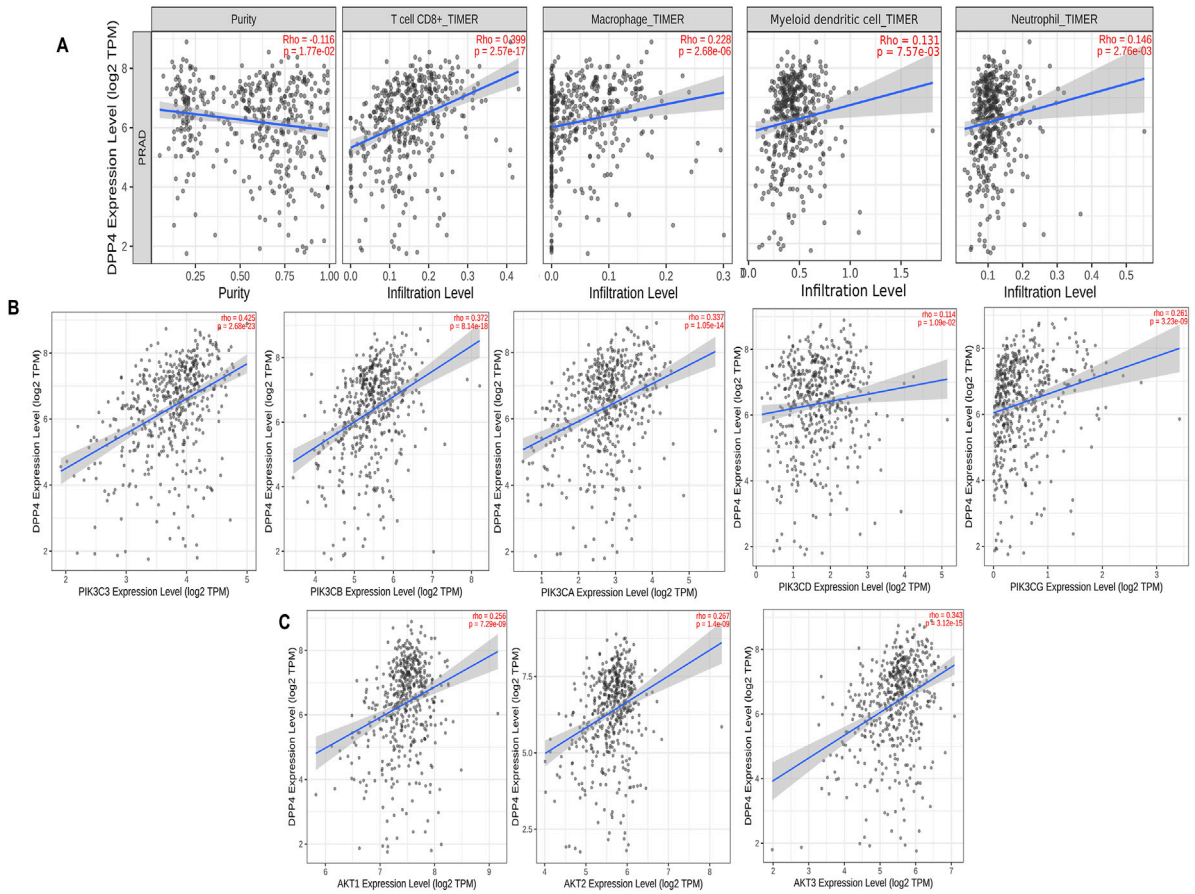

FIGURE 5
Tumor infiltration analysis of DPP4 using TIMER2.0 database, **(A)** Scatter plots that show significant positive correlations of DPP4 expression with the infiltrating levels of T cell CD8$^+$, macrophage, dendritic cell, and neutrophils. **(B)** Scatter plots that showing DPP4 expression significant positive correlations with class IA PIK3 expressions. **(C)** Scatter plots that showing DPP4 expression significant positive correlations with AKT. expressions. The Spearman's correlation value and the estimated statistical significance are displayed as the legends for each scatter plot (p-value< 0.05 (positive); p-value >0.05 (negative)).

overall survival analysis using TCGA–PRAD cohort, wherein the population was stratified into high–and low–expression groups based on the median hub genes expression level, ensuring an unbiased and biologically relevant comparison. The findings suggest that only DPP4 was significantly upregulated in PCa and affected patients' overall survival (log-rank p-value <0.001) while the other 21 hub genes did not show any significant association Figures 4A,C (Supplementary Figure S3) summarises these findings. Further heat map of survival hazard ratio $\log_{10}$ (HR) $p < 0.05$ of hub genes depicted using GEPIA2.0 found that only DPP4 was significant, depicting prognostic implication in PRAD (Figure 4D). It was also found that DPP4 was among the top 10 highly mutated hub genes as depicted in Figure 4B.

3.1.7 Tumor infiltration analysis

The tumor microenvironment (TME) is essential for cancer progression, supporting tumor growth and invasion. Our survival analysis showed that higher DPP4 levels correlate with worse outcomes. We analyzed tumor infiltration to determine if DPP4 promotes or suppresses tumor growth and affects the TME through immune cell activity, suggesting DPP4 as a potential therapeutic target in PCa. Using the TIMER2.0 database, we explored the relationship between DPP4 expression and tumor-infiltrating immune cells in the prostate adenocarcinoma cohort (PRAD). The results revealed a significant positive correlation between DPP4 expression and the levels of various immune cells: CD8$^+$ T cells (rho = 0.399, p-value = 2.57e-17), myeloid-derived dendritic cells (rho = 0.131, p-value = 7.57e-03), macrophages (rho = 0.228, p-value = 2.86e-04), and neutrophils (rho = 0.146, p-value = 2.76e-03), as shown in Figure 5A. Additionally, we performed a correlation analysis between DPP4 and the expression of class IA PIK3/Akt pathway components (PIK3C3, PIK3CA, PIK3CB, PIK3CD, PIK3CG) and the AKT family (AKT1, AKT2, AKT3), as revealed by pathway enrichment analysis. This analysis demonstrated a positive correlation with PIK3 (rho = 0.423, p-value = 2.68e-23), (rho = 0.337, p-value = 1.05e-14), (rho = 0.372, p-value = 8.14e-18), (rho = 0.114, p-value = 1.09e-02), and (rho = 0.261, p-value = 3.23e-09). Further, we observed positive correlations for AKT (rho = 0.256, p-value = 7.29e-09), (rho = 0.267, p-value = 1.4e-09), and (rho = 0.343, p-value = 3.12e-15), as shown in Figures 5B,C.

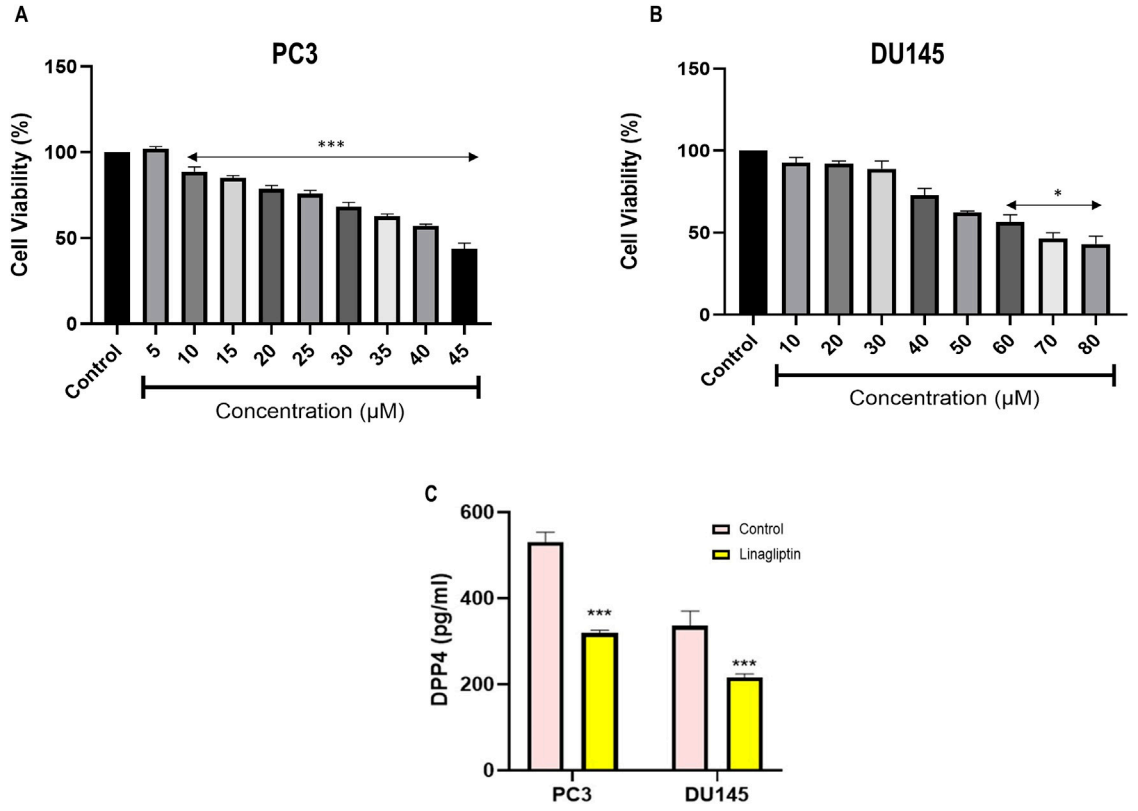

FIGURE 6
Cell cytotoxicity evaluation of Linagliptin against different cell lines, **(A)** PC3 and **(B)** DU145 prostate cancer cells. **(C)** DPP4 enzyme activity based in the Linagliptin treatment with respective IC50 values in PC3 and DU145. The results are expressed in mean ± SD of three independent experiments. ***P < 0.001 vs. Control, *P < 0.05 vs. Control.

3.2 *In-vitro*

3.2.1 *In-vitro* cytotoxicity and DPP4 activity

Typically, minimal cytotoxicity to noncancerous cells and targeted elimination of malignant cells are essential criteria for an optimal antineoplastic agent. Quantitatively assessing mitochondrial integrity with a 3-(4, 5-dimethylthiazol-2-yl)-2, 5-diphenyltetrazolium bromide (MTT) assay is an excellent method for detecting the cellular proliferation index in various cytotoxic compounds. Linagliptin treatment for 24 h in PC3 and DU145 effectively reduced cell viability in a dose-dependent manner with an IC50 value of 40 μM in PC3 (Figure 6A) and 60 μM in DU145 cells (Figure 6B) with less to moderate toxicity in normal human embryonic kidney cells. Further, we assess the morphological change induced by Linagliptin using an inverted microscope. As shown in Supplementary Figure S1, Linagliptin at IC50 concentration significantly altered cell morphology. Specifically, cells appeared to have a rounded shape with subsequent detachment from the surface. However, in normal untreated control, cells showed an intact morphology without cellular death, which suggests that Linagliptin at this particular concentration can induce cellular death and subsequently change the morphology of PCa cells. Further, we validated the effect of Linagliptin on cellular DPP4 activity in its IC50 values in PC3 and DU145. As depicted in Figure 6C, both the PCa cells exhibited a higher DPP4 activity; however, after Linagliptin treatment, the activity had reduced significantly as hypothesized ($P < 0.001$). Further studies have been performed to confirm Linagliptin's molecular mechanism of action to induce cellular death in cancer cells.

3.2.2 Linagliptin decreased *PI3K/Akt* gene expression in PCa cells

To further confirm our hypothesis, we checked the expression level of PI3K and AKT along with *PTEN* in Linagliptin-treated PC3 and DU145 cells. Linagliptin treatment at IC50 concentration significantly reduced the expression of *PI3KA* and *AKT* expression in PC3 and DU145 cells. We have also checked the PI3K negative regulator *PTEN* status, which acts as a tumour suppressor, and various studies have shown that the expression of PTEN influences the activation of the *PI3K/Akt* pathway. Our study revealed that the expression of *PTEN* after Linagliptin treatment significantly increased in both the cell lines, similar to Doxorubicin, suggesting *PI3K/Akt* inactivation, inhibition of cell proliferation and cell survival (Figure 7A).

3.2.3 Linagliptin induces cell cycle arrest in both PC3 and DU145 PCa

Due to inadequate DNA repair mechanisms, the administration of chemotherapeutic agents typically halts the cell cycle and induces apoptosis in cancer cells. To ascertain if Linagliptin influences any cell cycle phase of PC3 and DU145 cells, we monitored the cell cycle

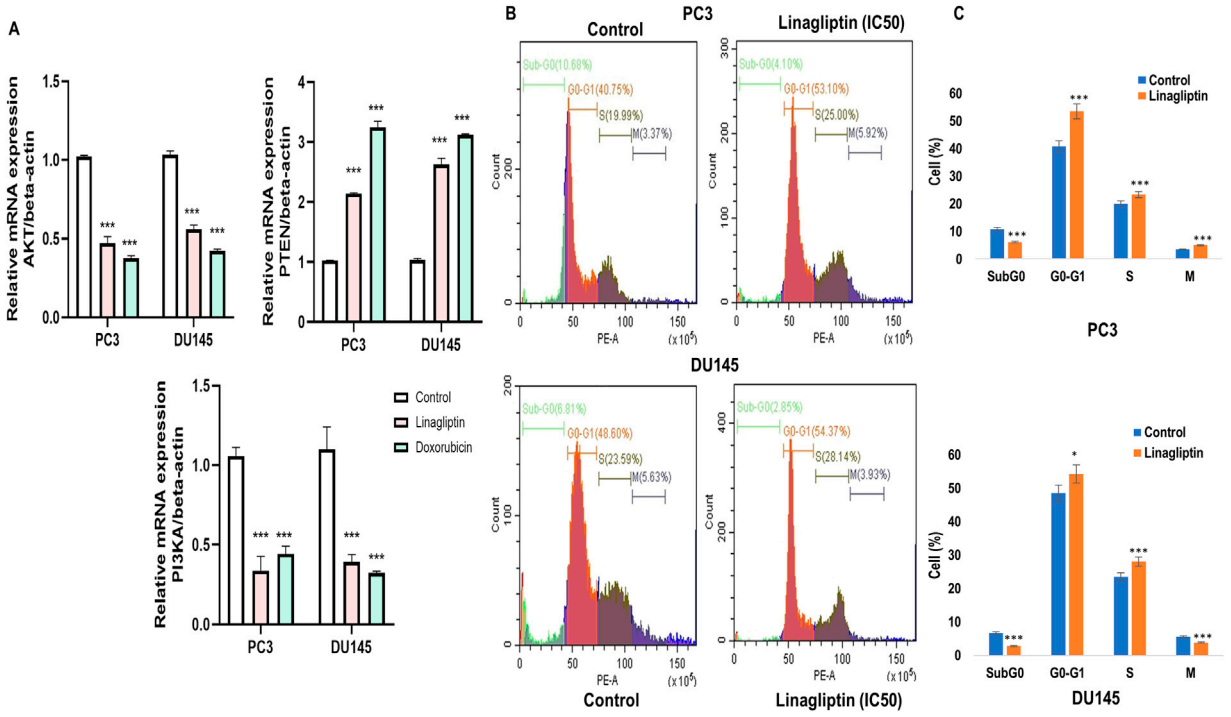

FIGURE 7
RT-PCR gene expression and cell cycle arrest. **(A)** *PI3K/AKT/PTEN* expression in PC3 and DU145 cell lines **(B)** DPP4 inhibition with Linagliptin induces of Cell cycle arrest in PC3 and DU145 cell lines. The results are expressed in mean ± SD of three independent experiments. ***P < 0.001 vs. Control, *P < 0.05 Vs. Control. **(C)** Bar graph representing the quantitative of the different cell cycle stages in both PC3 and DU145.

in four phases: Sub G0, G0/G1, S, and G2/M in the treated population using flow cytometry following propidium iodide (PI) staining.

Linagliptin influences cell cycle progression in PC3 and DU145 (Figures 7B,C). 24 h of Linagliptin treatment significantly increased cellular arrest in the G0/G1 phase by 13% and S phase by 4% for PC3 cells; whereas in DU145, Linagliptin induced cell cycle arrest in the G0-G0/G1 phase by 6% followed by the S phase by 5% compared to the control group. Further the doses of Linagliptin were given to PC3 and DU145 cells for 24 h. Apoptotic cell death was determined by flow cytometry using the annexin V-FITC/PI kit. Doses of Linagliptin-40 µM - PC3, 60 µM - DU145, had significantly increase percentages of apoptotic cells in PC3 and DU145 respectively (Figure 12).

3.2.4 Cellular migration after Linagliptin treatment

Metastasis entails disseminating cancer cells from the primary tumor to secondary locations, facilitated by cellular migration and invasion within circulatory systems and the tissue matrix. We examined the impact of Linagliptin on the migratory capacity of PC3 and DU145 cells *in vitro* by a wound healing migration test. Transwell migration assay illustrates that Linagliptin impeded the migratory capacity of PC3 and DU145 cells, as indicated by the *in vitro* cytotoxicity reduction in the rate of wound closure relative to the control cells Figures 8A,B. The transwell migration assay revealed a significant reduction in the number of migrated cells in those treated with Linagliptin compared to the untreated control. This suggests that Linagliptin can impede the cellular migration of PC3 and DU145 cells *in vitro*, hence altering the metastatic potential of this aggressive prostate cancer cell type Figures 9A,B.

3.2.5 DPP4 inhibition regulates hub genes in PC3 and DU145 cell line

Our study further confirms the status of hub genes, which regulate the *PI3K/Akt* pathway. Interestingly, Linagliptin regulates not all but most of the hub genes at the transcription level. Treatment with Linagliptin (DPP4i) for 24 h decreased the expression of *FGF17* and *PDGFRA* in transcription level. *FGF17* and PDGF are two major growth factors that regulate the *PI3K/Akt* pathway and are associated with its activation during cancer progression. A decrease in their expression inevitably decreased the activation of the *PI3K/Akt* pathway. Moreover, Linagliptin downregulated the expression of *COL4A1* and *COL4A2*, which encodes collagenase in the tissue (Figure 10A). However, Linagliptin was found to have no role in KIT expression, which encodes tyrosine kinase receptors. The possible interaction of DPP4 with *PDGF, FGF17, COL4A1* and *COL9A2* is depicted in Figure 10B.

3.2.6 Linagliptin induces apoptosis in PCa

To visually confirm cellular death induced by Linagliptin in PC3 and DU145 cells, we performed AO/EtBr dual staining. The principle behind dual staining is to distinguish between different stages of apoptosis. AO stains live cells green; however, loss in the cellular membrane integrity leads EtBr to enter and stain cells as red. Moreover, the stages can be divided into live cells in green color, early apoptotic cells in green with fragmented chromatin, late apoptotic cells in orange, and necrotic cells in bright red (Liu et al., 2015). As shown in Figure 11A, Linagliptin treatment has increased the number of early and late apoptotic cells in the field

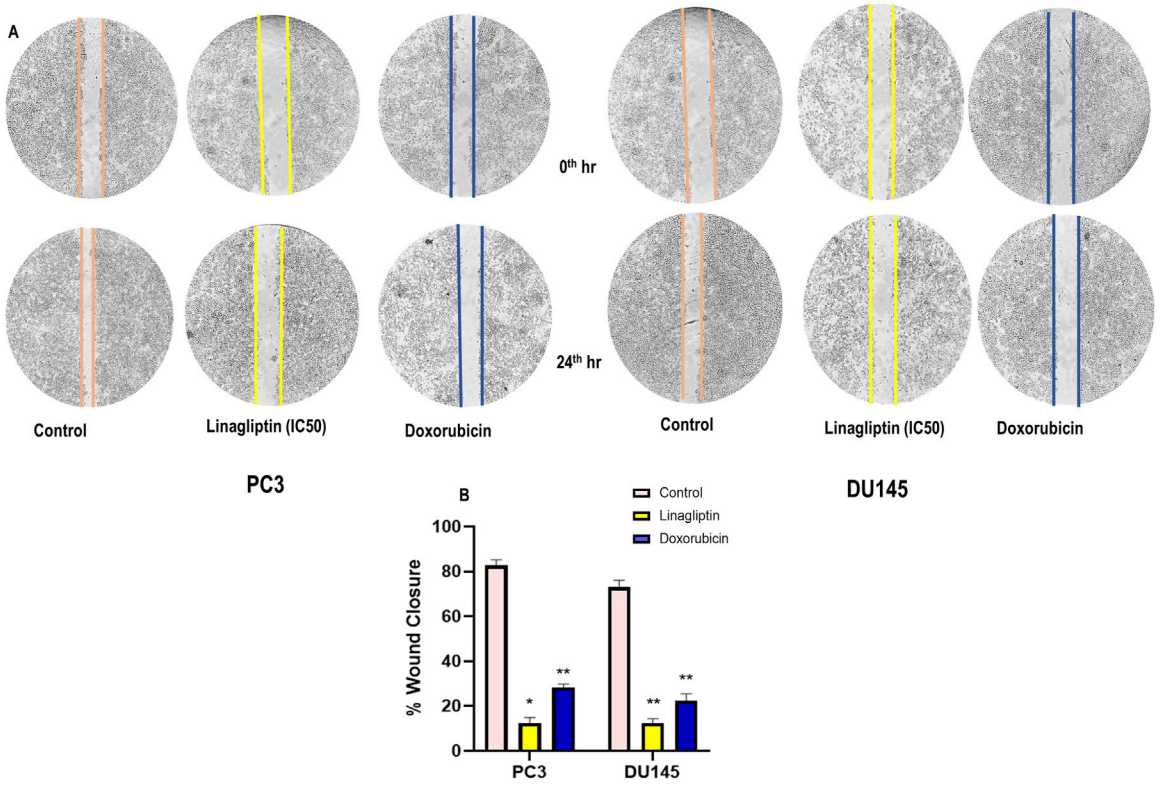

FIGURE 8
(A) Wound healing assay on prostate cancer cells (PC3 and DU145) treated with Linagliptin and Doxorubicin (Positive Control), **(B)** Bar graph representing the quantification of the wound healing. Results were presented graphically and the results are expressed in mean ± SD of three independent experiments. ***P < 0.001 vs. Control, **P < 0.01 Vs. Control, *P < 0.05 Vs. Control.

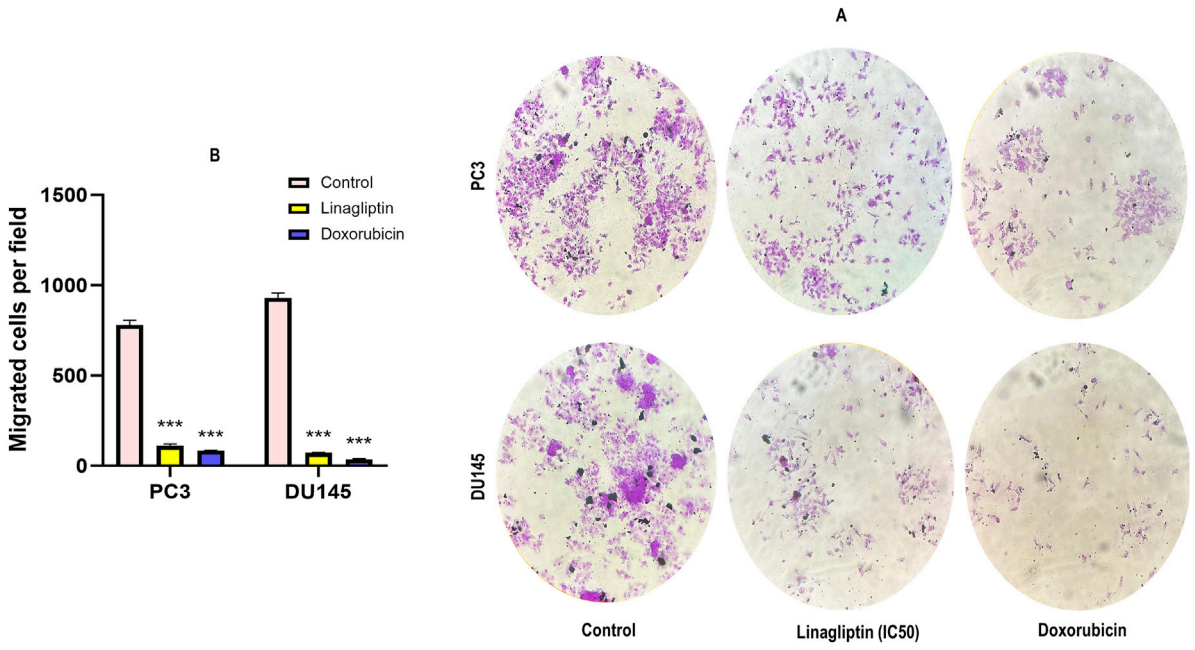

FIGURE 9
Transwell cell migration assay. **(A)** Representative photographs of migratory PC3 and DU145 treated with Linagliptin and Doxorubicin. **(B)** The results are expressed in mean ± SD of three independent experiments. ***P < 0.001 vs. Control.

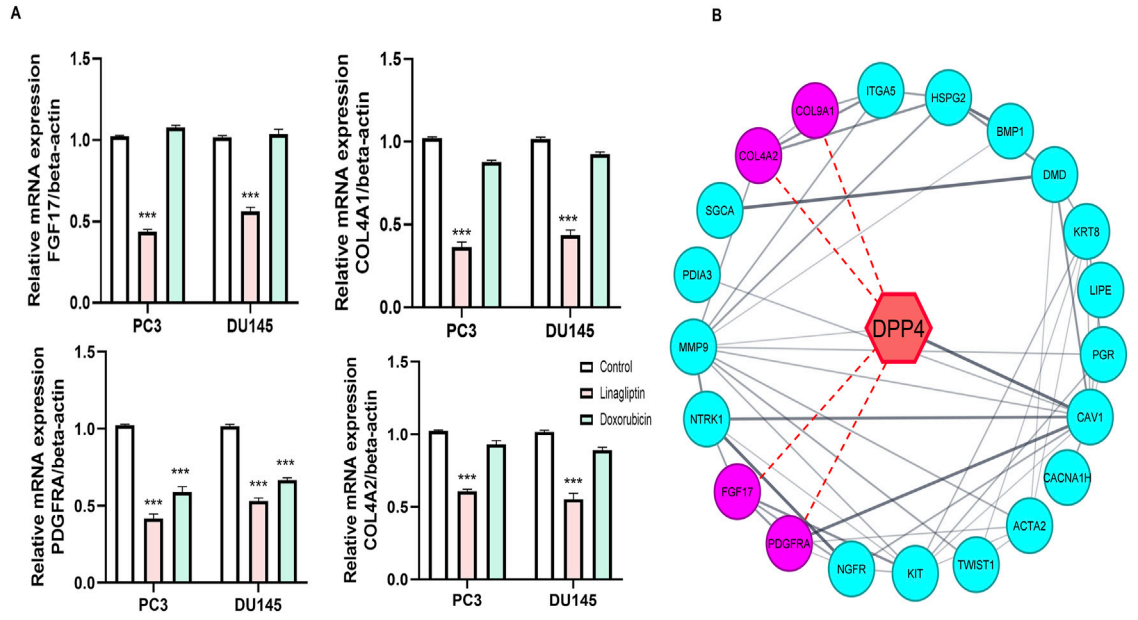

FIGURE 10
Effect of Linagliptin on Hub genes **(A)** Expression of *FGF17, COL4A1, PDGFRA, COL9A1* **(B)** Red dotted lines indicate possible interaction of DPP4 with *FGF17, COL4A1, PDGFRA, COL9A1*. The results are expressed in mean ± SD of three independent experiments. ***P < 0.001 vs. Control.

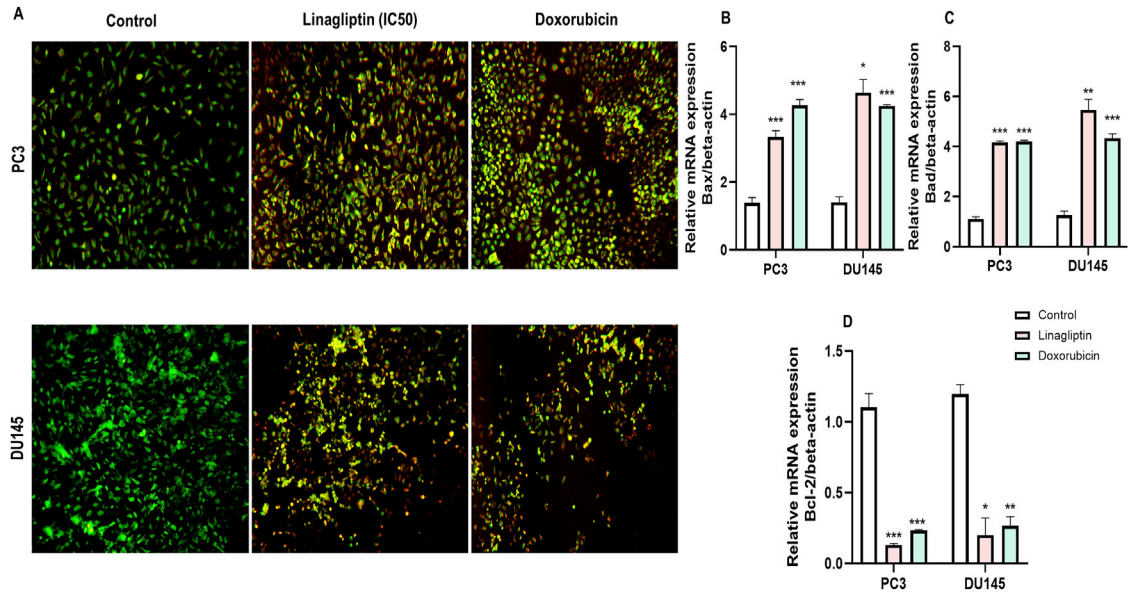

FIGURE 11
Linagliptin induces apoptosis in PC3 and DU145 prostate cancer cells. **(A)** AO/EtBr double staining assay–live cells and early apoptotic cells in green, with fragmented chromatin late apoptotic cells in orange and necrotic cells in bright red. **(B)** *Bax* expression **(C)** *Bad* expression **(D)** *Bcl-2* expression. The results are expressed in mean ± SD of three independent experiments. ***P < 0.001 vs. Control, **P < 0.01 vs. Control, *P < 0.05 Vs. Control.

compared to non-treated control cells. On the other hand, the positive control drug doxorubicin produced more necrotic cells than Linagliptin-treated cells, suggesting the probability of inducing future inflammation. To further confirm the initiation of apoptosis, we checked the expression level of pro and anti-apoptotic proteins. Linagliptin significantly reduced the expression of anti-apoptotic *BCL-2* compared to the untreated control group and significantly increased the pro-apoptotic *Bax* and *Bad expression*. Linagliptin showed a better apoptotic induction than Doxorubicin (Figures 11B–D). In addition to microscopy and protein expression analysis, Annexin V-FITC/PI flow cytometry was performed to quantitatively assess apoptosis induction by

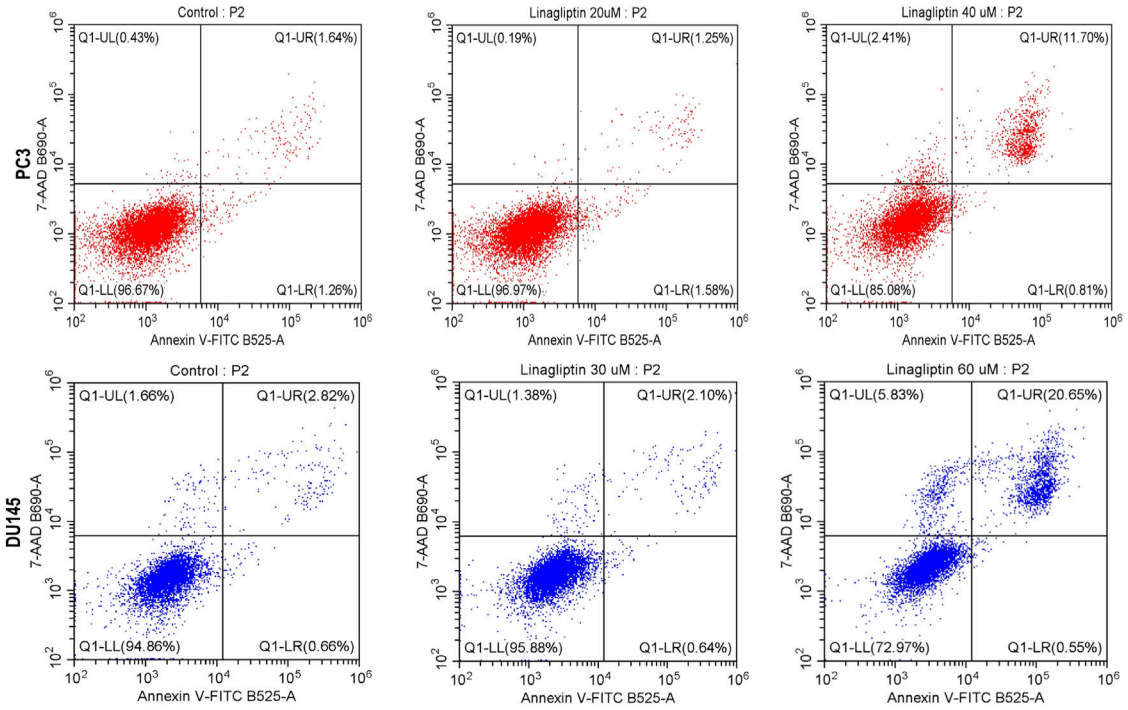

FIGURE 12
Apoptosis assay was performed with flow cytometry using PI and Annexin V-FITC double staining. Linagliptin induced apoptosis in PC3 and DU145 cells in a concentration-dependent manner.

Linagliptin. Flow cytometry data revealed a dose-dependent increase in apoptotic cell population, with the maximum apoptotic response up to 11.70% observed at 40 μM Linagliptin in PC3 cells, whereas 20.65% was observed in DU145 cells at 60 μM with early and late apoptotic cell populations significantly increased in both cell lines, confirming Linagliptin-induced apoptotic cell death (Figure 12).

3.2.7 DPP4 inhibition downregulates FGF17 expression, and suppresses PI3K/AKT signaling

To validate the transcriptomic data, suppression of PI3K/Akt signaling upon DPP4 inhibition, we performed Western blot analysis in PC3 and DU145 cells treated with Linagliptin. DPP4 inhibition led to a marked reduction in the levels of phosphorylated PI3K (p-PI3K) and phosphorylated Akt (p-Akt), indicating suppression of the *PI3K/Akt* signaling axis (Figures 13A,B). Total Akt protein levels remained unchanged, suggesting that the observed decrease was due to reduced pathway activation rather than total protein depletion. GAPDH and β-actin were used as loading controls and showed consistent expression across all samples. These results confirm that DPP4 inhibition attenuates *PI3K/Akt* signaling at the protein level, supporting a mechanistic link between DPP4 activity and oncogenic pathway activation in PCa (Figure 13).

This study clearly demonstrates that Linagliptin, a well-known DPP-4 inhibitor, can regulate the progression of prostate cancer cells by modulating the *PI3k/Akt* pathway and its key genes, as illustrated in the schematic presentation (Figure 14). Consequently, it induces apoptosis in prostate cancer cells *in vitro*. This highlights the *in vitro* molecular mechanism underlying Linagliptin's anti-proliferative efficacy in prostate cancer.

4 Discussion

Prostate cancer (PCa) remains a significant clinical challenge due to its complex molecular heterogeneity and variable treatment responses. Our integrated genomic-transcriptomic investigation has systematically identified DPP4 as a critical molecular regulator of PCa progression through modulation of the *PI3K/Akt* signaling pathway. These findings provide novel mechanistic insights that advance our understanding of PCa pathogenesis and potential therapeutic interventions. The central role of *PI3K/Akt* signaling in PCa development and progression has been extensively documented (Wise et al., 2017). Our study builds upon this foundation by employing a comprehensive systems biology approach to identify 22 hub genes (Figures 2A–D) of which 8 genes (*FGF17, NGFR, NTRK1, KIT, PDGFRA, ITGA5, COL4A2, COL9A1*) significantly enriched in this pathway (Figures 3A–D). The frequent loss of *PTEN*, a key negative regulator of *PI3K/Akt* signaling observed in 40%–60% of advanced PCa cases (Jamaspishvili et al., 2018), Cross talk pathway analysis for those hub genes further confirms their role in the Androgen receptor (AR) and Mitogen-Activated Protein Kinase (MAPK) signaling pathways Supplementary Figure S2. Previous studies have reported DPP4's involvement in AR signaling and MAPK pathways. For example, DPP4 has been shown to influence AR signaling and contribute to progression of castration-resistant PCa (Russo et al., 2018), as well as modulate MAPK-related FGF signaling (Wesley et al., 2005). According to Hashemi et al., 2023, *PI3k/Akt* pathway is frequently activated in advanced prostate cancer. Further DPP4 and *PI3k/Akt* pathway in prostate cancer is an area of ongoing research.

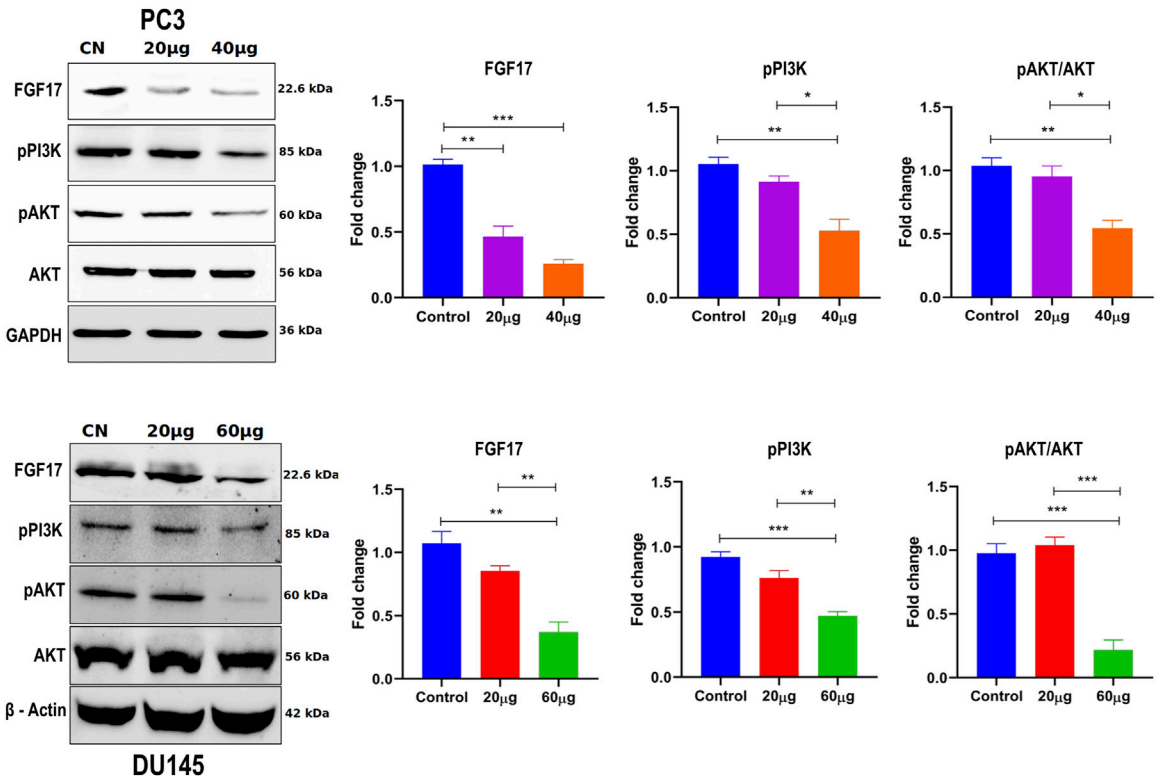

FIGURE 13
The effect of Linagliptin on *FGF17*, *PI3K/Akt* signaling pathway in PCa, A, B Expression of FGF17, PI3K/AKT in PCa, PC3 and DU145 both treated with varying concentrations of Linagliptin (0, 20, and 40 μM for PC3 and 0, 20, and 60 μM for DU145) for 24 h and cell lysates were subjected to western blot analysis with *FGF17*, PI3K, p-AKT and AKT anti-bodies, followed by sequential re-probing against GAPDH and beta-actin. The bar graph depicts densitometric expression analysis of FGF17, PTEN, PI3K, p-AKT and AKT. All the experiments were performed in triplicates and the data expressed as Mean ± SD. *P < 0.05, **P < 0.01, ***P < 0.001.

TCGA-PRAD cohort analysis revealed a strong association between elevated DPP4 expression and poor clinical outcomes was observed through overall survival analysis (Figures 4A–D), a finding that aligns with previous reports of DPP4 overexpression in metastatic PCa (Lu et al., 2022). However, our study significantly extends these observations by demonstrating that this prognostic association may be mechanistically linked to DPP4-mediated activation of *PI3K/Akt* signaling (Figures 5A–C). This connection provides a plausible explanation for the aggressive phenotype observed in DPP4-high tumors and suggests potential therapeutic vulnerabilities that could be exploited in clinical settings.

Treatment with the DPP4 inhibitor Linagliptin resulted in marked suppression of *PI3K/Akt* signaling pathway. The observed dose-dependent effects included: (i) significant downregulation of PI3K and AKT expression (Figure 7Aii associated upregulation of *PTEN*, (Figure 7Aiii) induction of G1/S cell cycle arrest (Figures 7B,C). This result strongly supports DPP4's role as a key upstream regulator of this oncogenic signaling cascade in PCa.

Linagliptin's anti-metastatic properties demonstrated superior efficacy compared to doxorubicin in both wound healing (Figures 8A,B) and transwell migration assays (Figures 9A,B), suggesting that DPP4 inhibition may represent a promising strategy for preventing or treating metastatic PCa. The molecular basis for this activity appears to involve DPP4's regulation of extracellular matrix components and growth factor signaling pathways, particularly through modulation of *FGF17* and *PDGFRA* expression. The downregulation of *FGF17* and *PDGFRA* (Figures 10A, 13A,B) following DPP4 inhibition provides important context to previous studies linking these growth factors to PCa progression (Teishima et al., 2019). From Figure 10A, DPP4 inhibition also affects collagen genes (*COL4A1, COL9A2*) offers new insights into potential mechanisms of tumor microenvironment remodeling in PCa, a process that has been increasingly recognized as critical for cancer progression (Zhang et al., 2023). The shift in apoptotic balance we observed (decreased *BCL2* with increased *BAX* expression Figures 11B,C) following DPP4 inhibition further supports the growing recognition of DPP4's role in cell survival pathways.

Our results strongly support the oncogenic function in primary PCa through *PI3K/Akt* activation, while some studies have suggested that the DPP4 role is influenced by tissue type, disease stage, and treatment context. DPP4 is found at higher levels in malignant prostate tissue compared to benign or normal prostate tissue. This increased expression is associated with PCa progression and correlates with factors such as prostate-specific antigen (PSA) levels, tumor size, and overall stage of the disease. The reasons behind these varying levels may be connected to the

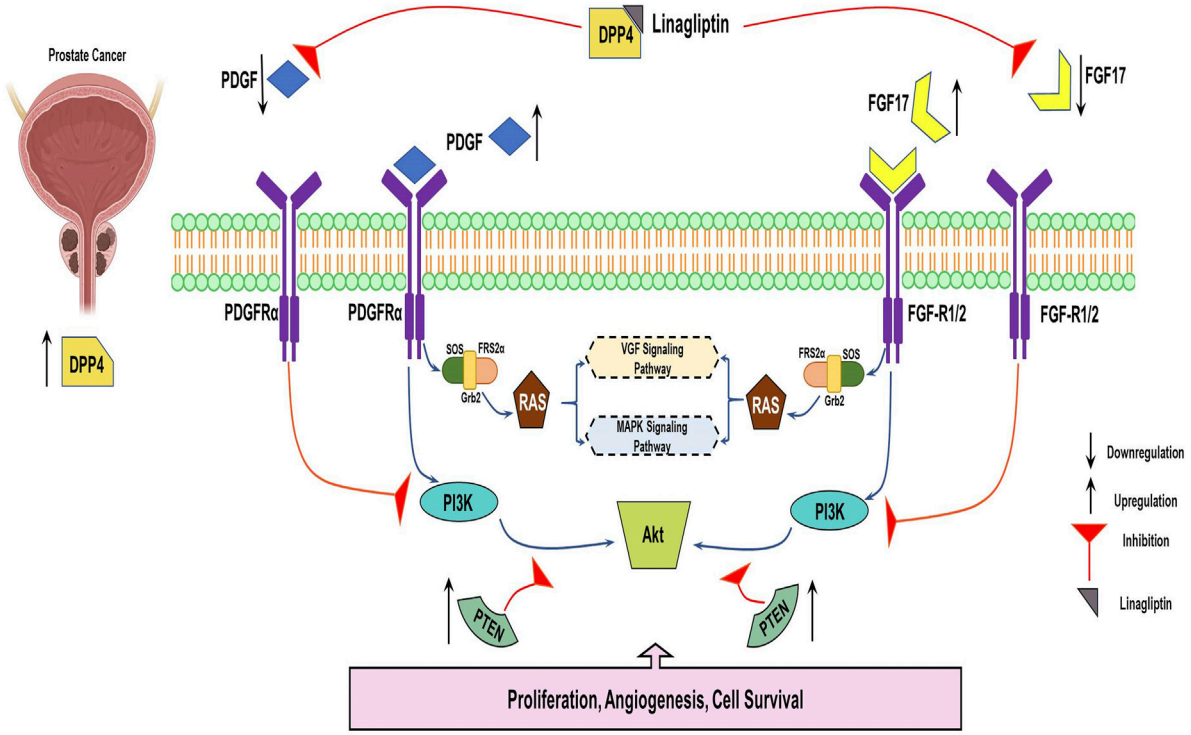

FIGURE 14
Systemic representation of DPP4 inhibitor downregulating FGF17and PDGF Prostate cancer progression via PI3K/AKT pathway.

tumor microenvironment and how the tumor interacts with different growth factors and signaling pathways.

In the localized stage of prostate cancer, DPP4 activity may be relatively high, while in advanced metastatic disease, its activity can be reduced. This reduction in activity in advanced disease may be due to a low-molecular-weight inhibitor, suggesting a potential difference in the role of DPP4 in different stages of the disease. Large population-based studies indicate that DPP4 inhibitors confer a survival advantage across various disease stages.

Particularly after treatments like androgen deprivation therapy, this emphasizes the need for a nuanced understanding of its biological context in different phases of PCa. Various treatments, including chemotherapy, androgen deprivation therapy, prostatectomy, and radiation therapy, suggesting that the benefit is not limited to a specific subgroup. DPP4 inhibitors, commonly used for type 2 diabetes, have shown potential in treating advanced prostate cancer in some contexts by improving overall survival. However, the enzyme's role can shift depending on the progression of the disease and the treatment. Furthermore, studies suggest that DPP4 may act as a tumor suppressor gene in the AR pathway, and its inhibition could potentially accelerate prostate cancer progression, particularly after androgen deprivation therapy.

These findings highlight the importance of considering tissue-specific expression, disease stage and treatment context when evaluating DPP4-targeted therapies in prostate cancer, as their efficacy appears closely tied to the unique biology of this tumor type (Russo et al., 2018; Shah et al., 2019; Mangoura et al., 2024). Such context-dependent behavior underscores the importance of careful patient selection in potential clinical applications of DPP4-targeted therapies. While Linagliptin was chosen for its relevance and specificity to DPP4, though we recognize the limitations of using a single agent and the possibility of off-target effects. Future studies will employ complementary methods, like DPP4-specific siRNA knockdown, and other DPP4 inhibitors, to better confirm DPP4's role in *PI3K/Akt* signaling and ensure the observed effects are due to DPP4 inhibition. The clinical implications of our findings are particularly significant given that DPP4 inhibitors are already FDA-approved for diabetes management. Our results provide a strong mechanistic rationale for re-purposing these agents in PCa treatment, building upon epidemiological studies suggesting improved outcomes in diabetic PCa patients taking DPP4 inhibitors (Pan et al., 2021). The multi-modal effects suggest that DPP4 inhibitors could offer comprehensive therapeutic benefits in PCa management.

5 Conclusion

To understand the PCa heterogeneity, we integrated whole genome SNV data with transcriptomic profiles from TCGA-PRAD. Although the majority of SNVs were located in non-coding regions, a subset of exonic mutations, primarily missense variants were functionally annotated, revealing 3.806 genes with deleterious effect on protein function. Integration of these deleterious mutation genes with differentially expressed genes identified 357 common genes, including 22 hub genes, with significant enrichment in *PI3K/Akt* pathway. Among these hubs,

DPP4 was found to modulate key regulators of this pathway, such as *FGF17, PDGFRA, COL4A1* and *COL9A2*. Our findings suggest that DPP4 inhibition via (Linagliptin) may suppress regulate *PI3K/Akt* signaling thereby impacting the cell survival and potentially suppressing PCa metastasis. These results highlight DPP4 as a promising therapeutic target for PCa, warranting further *in-vivo* validation and mechanistic studies.

Data availability statement

The original contributions presented in the study are included in the article/Supplementary Material, further inquiries can be directed to the corresponding author.

Author contributions

KC: Conceptualization, Data curation, Formal Analysis, Funding acquisition, Methodology, Validation, Visualization, Writing – original draft. EA: Funding acquisition, Investigation, Project administration, Resources, Software, Supervision, Writing – review and editing.

Funding

The author(s) declare that no financial support was received for the research and/or publication of this article.

Acknowledgments

The authors would like to acknowledge the School of Biosciences and Technology, Vellore Institute of Technology, for the resources and facilities. ICMR provided the Senior Research Fellowship to Chitluri Kiran Kumar vide BMI/11(54)/2022. The authors would like to acknowledge Dr. Tamizhselvi R and Tiasha Dasgupta for their support in shaping the manuscript. The authors would also like to thank Ritee Basu for providing the DPP IV activity assay kit.

Conflict of interest

The authors declare that the research was conducted in the absence of any commercial or financial relationships that could be construed as a potential conflict of interest.

Generative AI statement

The author(s) declare that no Generative AI was used in the creation of this manuscript.

Publisher's note

All claims expressed in this article are solely those of the authors and do not necessarily represent those of their affiliated organizations, or those of the publisher, the editors and the reviewers. Any product that may be evaluated in this article, or claim that may be made by its manufacturer, is not guaranteed or endorsed by the publisher.

Supplementary material

The Supplementary Material for this article can be found online at: https://www.frontiersin.org/articles/10.3389/fphar.2025.1606914/full#supplementary-material

References

Adzhubei, I., Jordan, D. M., and Sunyaev, S. R. (2013). Predicting functional effect of human missense mutations using PolyPhen-2. *Curr. Protoc. Hum. Genet.* 76, Unit7.20. doi:10.1002/0471142905.hg0720s76

Antonarakis, E. S., Gomella, L. G., and Petrylak, D. P. (2020). When and how to use PARP inhibitors in prostate cancer: a systematic review of the literature with an update on On-Going trials. *Eur. Urol. Oncol.* 3, 594–611. doi:10.1016/j.euo.2020.07.005

Berger, M. F., and Mardis, E. R. (2018). "The emerging clinical relevance of genomics in cancer medicine,", 15. England, 353–365. doi:10.1038/s41571-018-0002-6*Nat. Rev. Clin. Oncol.*

Bhargavi, R., Khilwani, B., Kour, B., Shukla, N., Aradhya, R., Sharma, D., et al. (2023). Prostate cancer in India: current perspectives and the way forward. *J. Reprod. Healthc. Med.* 4, 8. doi:10.25259/jrhm_17_2023

Chandrashekar, D. S., Bashel, B., Balasubramanya, S. A. H., Creighton, C. J., Ponce-Rodriguez, I., Chakravarthi, BVSK, et al. (2017). UALCAN: a portal for facilitating tumor subgroup gene expression and survival analyses. *Neoplasia* 19, 649–658. doi:10.1016/j.neo.2017.05.002

Chitluri, K. K., and Emerson, I. A. (2024). "The importance of protein domain mutations in cancer therapy," 10. doi:10.1016/j.heliyon.2024.e27655*Heliyone*27655

Creighton, C. J. (2023). Gene expression profiles in cancers and their therapeutic implications. *Cancer J. U. S.* 29, 9–14. doi:10.1097/PPO.0000000000000638

Crumbaker, M., Khoja, L., and Joshua, A. (2017). AR signaling and the PI3K pathway in prostate cancer. *Cancers (Basel)* 9, 34. doi:10.3390/cancers9040034

Ferroni, C., Del Rio, A., Martini, C., Manoni, E., and Varchi, G. (2019). Light-induced therapies for prostate cancer treatment. *Front. Chem.* 7, 719. doi:10.3389/fchem.2019.00719

Gatenby, R. A., and Brown, J. S. (2020). The evolution and ecology of resistance in cancer therapy. *Cold Spring Harb. Perspect. Med. U. S.* 10, a040972. doi:10.1101/cshperspect.a040972

Ge, S. X., Jung, D., and Yao, R. (2020). "ShinyGO: a graphical gene-set enrichment tool for animals and plants," Editor A. Valencia, 36, 2628–2629. doi:10.1093/bioinformatics/btz931

He, Y., Sun, M. M., Zhang, G. G., Yang, J., Chen, K. S., Xu, W. W., et al. (2021). "Targeting PI3K/Akt signal transduction for cancer therapy,", 6. *Signal Transduct. Target Ther.* 425. doi:10.1038/s41392-021-00828-5

Hoang, D. T., Iczkowski, K. A., Kilari, D., See, W., and Nevalainen, M. T. (2017). "Androgen receptor-dependent and -independent mechanisms driving prostate cancer progression: opportunities for therapeutic targeting from multiple angles,", 8. *Oncotarget*, 3724–3745. doi:10.18632/oncotarget.12554

Jamaspishvili, T., Berman, D. M., Ross, A. E., Scher, H. I., De Marzo, A. M., Squire, J. A., et al. (2018). Clinical implications of PTEN loss in prostate cancer. *Nat. Rev. Urol.* 15, 222–234. doi:10.1038/nrurol.2018.9

Jillson, L. K., Yette, G. A., Laajala, T. D., Tilley, W. D., Costello, J. C., and Cramer, S. D. (2021). Androgen receptor signaling in prostate cancer genomic subtypes. *Cancers (Basel). Switz.* 13, 3272. doi:10.3390/cancers13133272

Kinsella, R. J., Kahari, A., Haider, S., Zamora, J., Proctor, G., Spudich, G., et al. (2011). Ensembl BioMarts: a hub for data retrieval across taxonomic space. *Database* 2011, bar030. doi:10.1093/database/bar030

Li, C., Cheng, D., and Li, P. (2025). Androgen receptor dynamics in prostate cancer: from disease progression to treatment resistance. *Front. Oncol.* 15, 1542811. doi:10.3389/fonc.2025.1542811

Li, T., Fu, J., Zeng, Z., Cohen, D., Li, J., Chen, Q., et al. (2020). TIMER2.0 for analysis of tumor-infiltrating immune cells. *Nucleic Acids Res. Engl.* 48, W509–W514. doi:10.1093/nar/gkaa407

Liu, K., Liu, P., Liu, R., and Wu, X. (2015). Dual AO/EB staining to detect apoptosis in osteosarcoma cells compared with flow cytometry. *Med. Sci. Monit. Basic Res. U. S.* 21, 15–20. doi:10.12659/MSMBR.893327

Lu, S., Yin, H., Yu, O. H. Y., and Azoulay, L. (2022). Incretin-based drugs and the incidence of prostate cancer among patients with type 2 diabetes. *Epidemiology* 33, 563–571. doi:10.1097/EDE.0000000000001486

Ma, M., Zhu, Y., Xiao, C., Li, R., Cao, X., Kang, R., et al. (2024). "Novel insights into RB1 in prostate cancer lineage plasticity and drug resistance," in *Tumori J.* 03008916231225576: SAGE Publications Ltd STM. doi:10.1177/03008916231225576

Maitland, N. J. (2021). Resistance to antiandrogens in prostate cancer: is it inevitable, intrinsic or induced? *Cancers (Basel). Switz.* 13, 327. doi:10.3390/cancers13020327

Mangoura, S. A., Ahmed, M. A., and Zaka, A. Z. (2024). New insights into the pleiotropic actions of dipeptidyl Peptidase-4 inhibitors beyond glycaemic control. *touchREVIEWS Endocrinol.* 20, 19–29. doi:10.17925/EE.2024.20.2.5

Pan, K., Skelton, W. P., Elzeneini, M., Nguyen, T.-C., Franke, A. J., Ali, A., et al. (2021). A multi-center retrospective analysis examining the effect of dipeptidyl Peptidase-4 inhibitors on progression-free survival in patients with prostate cancer. *Cureus* 13, e14712. doi:10.7759/cureus.14712

Russo, J. W., Gao, C., Bhasin, S. S., Voznesensky, O. S., Calagua, C., Arai, S., et al. (2018). Downregulation of dipeptidyl peptidase 4 accelerates progression to castration-resistant prostate cancer. *Cancer Res. U. S.* 78, 6354–6362. doi:10.1158/0008-5472.CAN-18-0687

Sekhoacha, M., Riet, K., Motloung, P., Gumenku, L., Adegoke, A., and Mashele, S. (2022). "Prostate cancer review: Genetics, diagnosis, treatment options, and alternative approaches,", 27. *Molecules*. doi:10.3390/molecules27175730

Shah, C., Hong, Y.-R., Bishnoi, R., Ali, A., Skelton, W. P., Dang, L. H., et al. (2019). DPP4 inhibitors as novel agents in improving survival in patients with prostate cancer: a SEER-medicare study. *J. Clin. Oncol.* 37, e16532. doi:10.1200/JCO.2019.37.15_suppl.e16532

Shannon, P., Markiel, A., Ozier, O., Baliga, N. S., Wang, J. T., Ramage, D., et al. (2003). Cytoscape: a software environment for integrated models of biomolecular interaction networks. *Genome Res.* 13, 2498–2504. doi:10.1101/gr.1239303

Siegel, R. L., Miller, K. D., Wagle, N. S., and Jemal, A. (2023). Cancer statistics, 2023. *CA Cancer J. Clin.* 73, 17–48. doi:10.3322/caac.21763

Silberstein, J. L., Pal, S. K., Lewis, B., and Sartor, O. (2013). "Current clinical challenges in prostate cancer,", 2. *Transl. Androl. Urol.*, 122–136. doi:10.3978/j.issn.2223-4683.2013.09.03

Szklarczyk, D., Gable, A. L., Nastou, K. C., Lyon, D., Kirsch, R., Pyysalo, S., et al. (2021). The STRING database in 2021: customizable protein–protein networks, and functional characterization of user-uploaded gene/measurement sets. *Nucleic Acids Res.* 49, D605–D612. doi:10.1093/nar/gkaa1074

Tang, Z., Kang, B., Li, C., Chen, T., and Zhang, Z. (2019). GEPIA2: an enhanced web server for large-scale expression profiling and interactive analysis. *Nucleic Acids Res. Engl.* 47, W556–W560. doi:10.1093/nar/gkz430

Teishima, J., Hayashi, T., Nagamatsu, H., Shoji, K., Shikuma, H., Yamanaka, R., et al. (2019). Fibroblast growth factor family in the progression of prostate cancer. *J. Clin. Med.* 8, 183. doi:10.3390/jcm8020183

Waarts, M. R., Stonestrom, A. J., Park, Y. C., and Levine, R. L. (2022). "Targeting mutations in cancer,", 132(8):e154943. *J. Clin. Invest*. doi:10.1172/JCI154943

Wang, G., Wang, J., and Sadar, M. D. (2008). Crosstalk between the androgen receptor and β-Catenin in castrate-resistant prostate cancer. *Cancer Res.* 68, 9918–9927. doi:10.1158/0008-5472.CAN-08-1718

Wasim, S., Park, J., Nam, S., and Kim, J. (2023). Review of current treatment intensification strategies for prostate cancer patients. *Cancers* 15, 5615. doi:10.3390/cancers15235615

Wesley, U. V., McGroarty, M., and Homoyouni, A. (2005). Dipeptidyl peptidase inhibits malignant phenotype of prostate cancer cells by blocking basic fibroblast growth factor signaling pathway. *Cancer Res.* 65, 1325–1334. doi:10.1158/0008-5472.CAN-04-1852

Wise, H. M., Hermida, M. A., and Leslie, N. R. (2017). Prostate cancer, PI3K, PTEN and prognosis. *Clin. Sci.* 131, 197–210. doi:10.1042/CS20160026

Zhang, Q., An, Z.-Y., Jiang, W., Jin, W.-L., and He, X.-Y. (2023). Collagen code in tumor microenvironment: functions, molecular mechanisms, and therapeutic implications. *Biomed. Pharmacother.* 166, 115390. doi:10.1016/j.biopha.2023.115390

frontiers | Frontiers in Pharmacology

TYPE Original Research
PUBLISHED 04 August 2025
DOI 10.3389/fphar.2025.1634985

OPEN ACCESS

EDITED BY
Lei Yin,
Shanghai Jiaotong University School of Medicine, China

REVIEWED BY
Ronghao Wang,
Southwest Medical University, China
Shengfeng Zheng,
Fudan University, China

*CORRESPONDENCE
Gonghui Li,
3193119@zju.edu.cn
Lei Gao,
drgaolei0417@zju.edu.cn

RECEIVED 25 May 2025
ACCEPTED 21 July 2025
PUBLISHED 04 August 2025

CITATION
Zhou C, Ding L, Wang H, Li G and Gao L (2025) Integrative analysis of lactylation related genes in prostate cancer: unveiling heterogeneity through single-cell RNA-seq, bulk RNA-seq and machine learning.
Front. Pharmacol. 16:1634985.
doi: 10.3389/fphar.2025.1634985

Integrative analysis of lactylation related genes in prostate cancer: unveiling heterogeneity through single-cell RNA-seq, bulk RNA-seq and machine learning

Chenghao Zhou, Lifeng Ding, Huailan Wang, Gonghui Li* and Lei Gao*

Department of Urology, Sir Run Run Shaw Hospital, Zhejiang University School of Medicine, Hangzhou, China

Introduction: Lactylation, a post-translational modification characterized by the attachment of lactate to protein lysine residues on proteins, plays a pivotal role in cancer progression and immune evasion. However, its implications in immunity regulation and prostate cancer prognosis remains poorly understood. This study aims to systematically examine the impact of lactylation-related genes (LRGs) on prostate cancer.

Methods: Single-cell and bulk RNA sequencing data from patients with prostate cancer were analyzed. Data were sourced from TCGA-PRAD, GSE116918, and GSE54460, with batch effects mitigated using the ComBat method. LRGs were identified from exisiting literature, and unsupervised clustering was applied to assess their prognostic siginificance. The tumor microenvironment and functional enrichment of relevant pathways were also evaluated. A prognostic model was developed using integrative machine learning techniques, with drug sensitivy analysis included. The mRNA expression profiles of the top ten genes were validated in clinical samples.

Results: Single-cell RNA sequencing revealed distinct lactylation signatures across various cell types. Bulk RNA-seq analysis identified 56 prognostic LRGs, classifying patients into two distinct clusters with divergent prognoses. The high-risk cluster exhibited reduced immune cell infiltration and increased resistance to specific targeted therapies. A machine learning-based prognostic signature was developed, demonstrating robust predictive accuracy for treatment responses and disease outcomes.

Conclusion: This study offers a comprehensive analysis of lactylation in prostate cancer, identifying potential prognostic biomarkers. The proposed prognostic signature provides a novel approach to personalized treatment strategies, deepening our understanding of the molecular mechanisms driving prostate cancer and offering a tool for predicting therapeutic responses and clinical outcomes.

KEYWORDS

prostate cancer, lactylation, prognostic biomarker, machine learning, personalized treatment, immune microenvironment

Background

Prostate cancer (PCa) is a leading malignancy in men, is shaped by a complex interplay of genetic, metabolic, and immunological factors that drive its progression and therapeutic resistance (Chen et al., 2021). The disease's heterogeneity is reflected in its diverse genetic landscape, with notable genomic alterations, including TMPRSS2-ERG fusions and SPOP mutations, emerging in the early stages (He et al., 2022). Next-generation sequencing has revolutionized our understanding of PCa's genomic landscape, uncovering a range of genetic abnormalities that are linked to disease progression and resistance to treatment (Fujita and Nonomura, 2019; Guo et al., 2024). Recent studies highlight the importance of metabolic shifts within the tumor microenvironment (TME), particularly the roles of lactic acid and lactylation in promoting cancer advancement and immune evasion (Zha et al., 2024).

Lactylation, the covalent attachment of lactate to protein lysine residues, is gaining recognition as a critical post-translational modification (PTM) that bridges metabolism and epigenetics, with profound implications for cancer biology (Brown and Ganapathy, 2020; Lv et al., 2023). In PCa cells, metabolic reprogramming in prostate cancer cells, characterized by the Warburg effect, leads to a shift towards aerobic glycolysis, resulting in lactate production even in the presence of oxygen (Luo et al., 2022). While previously considered a metabolic anomaly; lactate is now understood to function as a signaling molecule and a regulator of gene expression through lactylation. Once regarded solely as a byproduct of anaerobic metabolism, lactate is now recognized for its roles in systemic metabolism, cellular signaling, and as a substrate for oxidative metabolism in other tissues (Li et al., 2022). In PCa, lactate metabolism and lactylation contribute to immune evasion, angiogenesis, and the modulation of tumor microenvironment (TME).

The TME in PCa is characterized by hypoxia and acidosis, conditions that foster promote lactate accumulation (Liang et al., 2024). Through its receptor GPR81, lactate exerts a significant impact on cellular metabolism and tumor growth, independent of monocarboxylate transporters, protons, and glucose metabolism (He et al., 2024). Lactate also stabilizes hypoxia-inducible factor-1α (HIF-1α), a key regulator of the hypoxic response, which in turn activates the transcription of genes involved in tumorigenesis (Berglund et al., 2018). Additionally, lactate influences the immunological landscape of PCa by modulating immune cell function, facilitating immunosuppression and immune evasion. Lactate accumulation in the TME acidifies the environment, impairing T lymphocyte activity and inducing tumor-associated macrophages (TAMs) to adopt a pro-tumorigenic M2 phenotype (Luo et al., 2022).

This study provides a comprehensive analysis of lactylation-associated data derived from single-cell and bulk RNA sequencing, utilizing multiple databases to explore gene expression patterns. A novel prognostic biomarker was developed based on lactylation-related genes (LRGs). This biomarker evaluated the relationship between the LRG signature and various clinical and pathological features, as well as its correlation with PCa progression. Additionally, this study investigated the signature's association with the TME, genetic mutations, and the effectiveness of immuno- and chemotherapy with PCa. Lastly, the mRNA expression profiles of top ten genes were valdated using ten paired prostate cancer clinical samples.

Materials and methods

Data collection and processing

RNA-seq data and corresponding clinical information for TCGA-PRAD were obtained from UCSC-XENA (https://xenabrowser.net/datapages/). Gene microarray data and clinical details from 248 patients with PRAD in the GSE116918 cohort and 106 patients in the GSE54460 cohort were retrieved from the Gene Expression Omnibus (GEO) database. The ComBat method from the sva package was applied to integrate and adjust for batch effects across the GSE116918, GSE54460, and TCGA-PRAD datasets. Public cancer databases, including GSCA (Liu et al., 2022), Tumor Immune Dysfunction and Exclusion (TIDE) (Jiang et al., 2018), and TISCH2 (Han et al., 2022), were also utilized in the study. As the datasets were publicly available, approval from an Ethical Review Committee and informed consent were not necessary. Patients without prognostic information or expression profiles were excluded from the analysis. The single-cell sequencing dataset of GSE176031 was downloaded from TISCH2, which included 19,969 genes and 15,339 cells. The filtered dataset was further analyzed using the Seurat package, with PCA and t-SNE applied for effective cell sample clustering. The COSG package was utilized for detailed cell type annotation and key gene selection in single-cell data (Dai et al., 2022). To identify genes linked to lactylation-related genes (LRGs), 327 genes were compiled from previously published studies (PMID37242427, PMID35761067. Supplementary Table S1).

We also employed the Single-Cell Identification of Subpopulations by Correlating with bulk Sample phenotypes (SCISSOR) method to investigate, at single-cell resolution, how LRGS relates to prognostic phenotypes, by jointly analyzing survival outcomes and transcriptomic data from the combined cohort (Sun et al., 2022).

Unsupervised clustering of lactylation-related genes

For unsupervised clustering of the LRGs, we utilized the "ConsensusClusterPlus" R package (Wilkerson and Hayes, 2010). Agglomerative clustering was conducted using a spearman correlation distance metric was performed, with 80% of the samples resampled for 10 repetitions. The optimal number of clusters was determined using an empirical cumulative distribution function plot. Kaplan-Meier analysis was performed to assess the RFS (Recurrence Free Survival) of patients with PRAD across different clusters.

Evaluation of the cell tumor microenvironment and functional enrichment of pathways

An immune landscape specific to patients with PRAD was developed to explore the regulatory influence of the LRG score

model on the TME. The immune gene signature encompasses the expression of key immune checkpoints and the infiltration characteristics of diverse immune cells. Gene signatures of immune cells were sourced from seven different platforms using the IOBR package: TIMER, CIBERSORT, CIBERSORT-ABS, QUANTISEQ, MCPCOUNTER, XCELL, and EPIC (Zeng et al., 2024). GO and KEGG pathway analyses were conducted using the clusterProfiler package (v4.6.2) (Wu et al., 2021). Further, gene set variation analysis (GSVA) and gene set enrichment analysis (GSEA) were conducted using the GSVA package (v1.46.0) to assess the various gene signatures (Hänzelmann et al., 2013).

Development of a prognostic model using integrated machine learning techniques

To ensure a reliable identification of LRGs, 10 machine-learning algorithms were integrated to enhance accuracy and stability. These algorithms included various techniques such as random survival forest (RSF), elastic network (Enet), Lasso, Ridge, stepwise Cox, CoxBoost, partial least squares regression for Cox (plsRcox), supervised principal components (SuperPC), generalized boosted regression modeling (GBM), and survival support vector machine (survival-SVM). The signature generation process involved: (a) applying these algorithm combinations to the 56 identified prognostic LRGs to build predictive models in the combined cohort, and (b) cross-validating all models using separate datasets (GSE116918, GSE54460, and TCGA-PRAD). The Harrell's concordance index (C-index) was computed for each model across all validation datasets, and the model with the highest average C-index was deemed as optimal.

Potential drug sensitivity analysis

The oncoPredict R package (Maeser et al., 2021) was used to predict the chemosensitivity of patients with PRAD based on their LRG Risk Score (LRGRS). This approach correlates patients' tissue gene expression profiles with those of cancer cell lines to estimate the half-maximal inhibitory concentration (IC50). The Wilcoxon test was employed to compare differences in drug IC50 value between high- and low-risk groups, with statistical significance set at $p < 0.05$.

Collection of patient samples, RNA extraction, and quantitative real-time PCR

The study was approved by the Ethics Committee of Sir Run Shaw Hospital, Zhejiang University, with all patients providing written informed consent. All procedures were performed in accordance with the Declaration of Helsinki. Expression of LRGs was assessed in 20 tissue samples collected from randomly selected patients. The specimen collection process involved the following steps: patient selection and consent, tissue collection, fixation, embedding, sectioning, histopathological analysis, sample storage, and RNA extraction. Tissue RNA was extracted using TRIzol reagent (Invitrogen, CA, United States). First-strand cDNA synthesis was performed using the HiFiScript cDNA Synthesis Kit (CWBio), and real-time quantitative PCR (RT-qPCR) was conducted using the SYBR Green method on a Roche LightCycler® 480 System. Primer sequences used in this study are listed in Table 1.

Statistical analysis

All statistical analyses were conducted using R software (version 4.4.1). A chi-squared test was used to compare clinical characteristics between the training and internal validation sets. The Wilcoxon test, a non-parametric method, was used to assess differences between variables that did not follow a normal distribution. Differentially expressed genes (DEGs) were evaluated for statistical significance using FDR-corrected p-values. Biochemical recurrence-free survival (BCR) among subgroups was compared using Kaplan-Meier survival analysis and the log-rank test with the "survival" package in R. Independent prognostic factors were analyzed using univariate and multivariate Cox regression models. Model performance was evaluated using ROC curve analysis and AUC calculation with the "timeROC" package in R. Spearman's correlation analysis was conducted to assess the relationship between risk scores and immune cell infiltration. A Student's t-test was used to analyze qRT-PCR results. Statistical significance was defined as $p < 0.05$, unless otherwise stated.

Results

Lactylation characteristic in single-cell transcriptome

Single-cell RNA sequencing data from 34,155 PCa cellsusing were anlyzed using the TISCH2 dataset. Dimensionality reduction was performed on the top 2,000 variant genes via principal component analysis (PCA) and t-distributed stochastic neighbor embedding (t-SNE). Cells were clustered into 40 groups with a resolution of 0.8. Ten primary cell clusters were identified based on marker genes specific to various cell types: CD8T, epithelial, fibroblasts, malignant, mast, mono. macro, plasma, progenitor, and Treg cells (Figure 1A). Differential gene expression is illustrated in the volcano plot (Figure 1B), while the heatmap highlights the top five marker genes for each cell population (Figure 1C). Functional enrichment analysis of these cell types were analyzed based on Hallmark, KEGG and Reactome pathways (Figures 1D–F).

Lactylation activity was assessed using the "AddModuleScore" function from the Seurat package to evaluate the expression levels of a 257-gene set across various cell types (Figure 2A). Cells were categorized into high- and low-lactylation groups based on their lactylation activity (Figure 2B). Among the 9 cell types, CD8T and malignant cells exhibited significantly higher lactylation activity (Figures 2C–F).

Identification of lactylation patterns in bulk RNA-seq

To enhance statistical power and diversity, the GSE116918, GSE54460 and TCGA-PRAD datasets were integrated using the

10.3389/fphar.2025.1634985

TABLE 1 Primers of top ten LRGs.

Gene symbol	Primer F	Primer R
RBM17	AGTGGAGACCAGTGACTCAAA	CTGGGGCGAGGACTGTACT
MTA1	ACGCAACCCTGTCAGTCTG	GGGCAGGTCCACCATTTCC
PRAM1	GCAGCCTGAGTTGAGTACCTT	GGCACGGACTTCTTAGGGAG
RACGAP1	ATGATGCTGAATGTGCGGAAT	CGCCAACTGGATAAATTGGACTT
VIM	GACGCCATCAACACCGAGTT	CTTTGTCGTTGGTTAGCTGGT
MKI67	ACGCCTGGTTACTATCAAAAGG	CAGACCCATTTACTTGTGTTGGA
MNDA	AACTGACATCGGAAGCAAGAG	CCTGATTCGGAGTAAACGAAGTG
CCNA2	CGCTGGCGGTACTGAAGTC	GAGGAACGGTGACATGCTCAT
RBM10	ATGGAGTATGAAAGACGTGGTGG	TCCCGGTAGTCGTGGTCTC
KIF2C	CTGTTTCCCGGTCTCGCTATC	AGAAGCTGTAAGAGTTCTGGGT

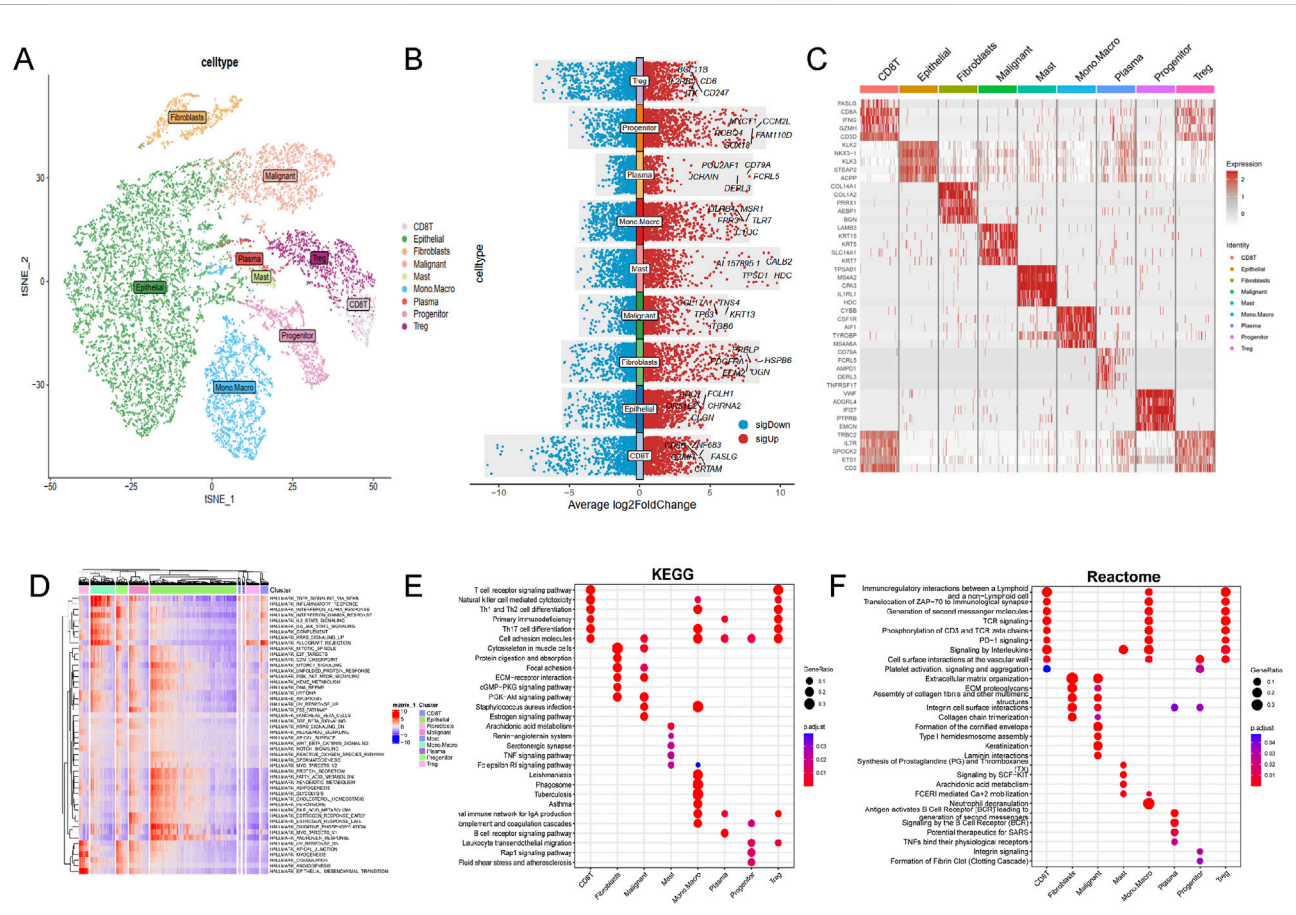

FIGURE 1
Single-cell RNA sequencing data analysis in PRAD cohort. **(A)** The results of the dimension reduction cluster analysis are shown in the t-SNE diagram. **(B)** Violin plots showing the distribution of average log2 fold change in gene expression for significant genes across different cell types. **(C)** Heatmap representation of gene expression profiles across various cell types. **(D)** Hallmark pathways, **(E)** KEGG pathways and **(F)** Reactome enrichment analysis among different cell types.

ComBat method. Resulting in a merged cohort consisting of 15,245 genes and 822 patients. Univariate Cox regression analysis was conducted to investigate the prognostic significance of 327 LRGs. Fifty-six genes were found to be significantly associated with RFS (P value <0.01, Figure 3A). Unsupervised cluster analysis based on the 56 prognostic genes

10.3389/fphar.2025.1634985

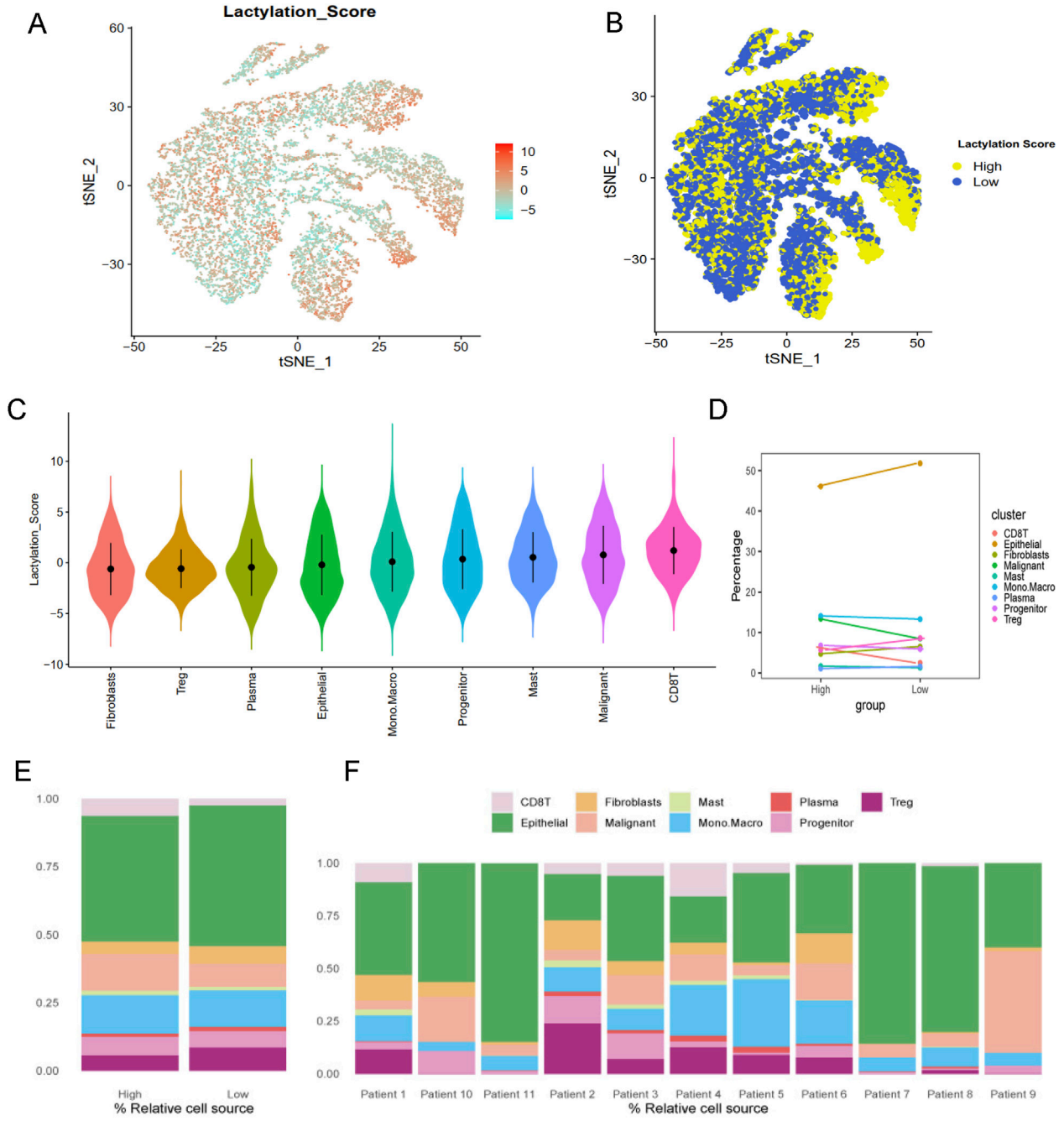

FIGURE 2
Lactylation characteristic in the single-cell transcriptome. **(A)** The activity score of lactylation in each cell types with t-SNE plot. **(B)** The high- and low-lactylation score group with t-SNE plot. **(C)** The distribution of the lactylation score in different cell types. **(D)** The dotplot and **(E)** barplot of different cell type percentage between high- and low-lactylation score. **(F)** The barplot of cell type percentage among different patients.

categorized samples from the combined cohort into two distinct groups, Cluster A and Cluster B (Figure 3B). Survival analysis revealed that Cluster B was associated with a worse prognosis that Cluster A ($P < 0.05$, Figure 3C). Figure 3D presents a boxplot illustrating the variations in prognostic genes between Cluster A and Cluster B. The heatmap demonstrated the association of prognostic genes expressions among age, survival status and T stage in different clusters (Figure 3E), suggesting a worse clinical outcome.

Differences in biological characteristics between lactylation subtypes

Enrichment analysis for Cluster A and Cluster B was conducted using the GSVA method, with five types of analyses performed. Pathway enrichment analysis revealed that Cluster B was significantly enriched in cancer-related pathways, including base excision repair, DNA replication, DNA mismatch repair, cell cycle, and integrated cancer pathways (Figure 4A). These results were

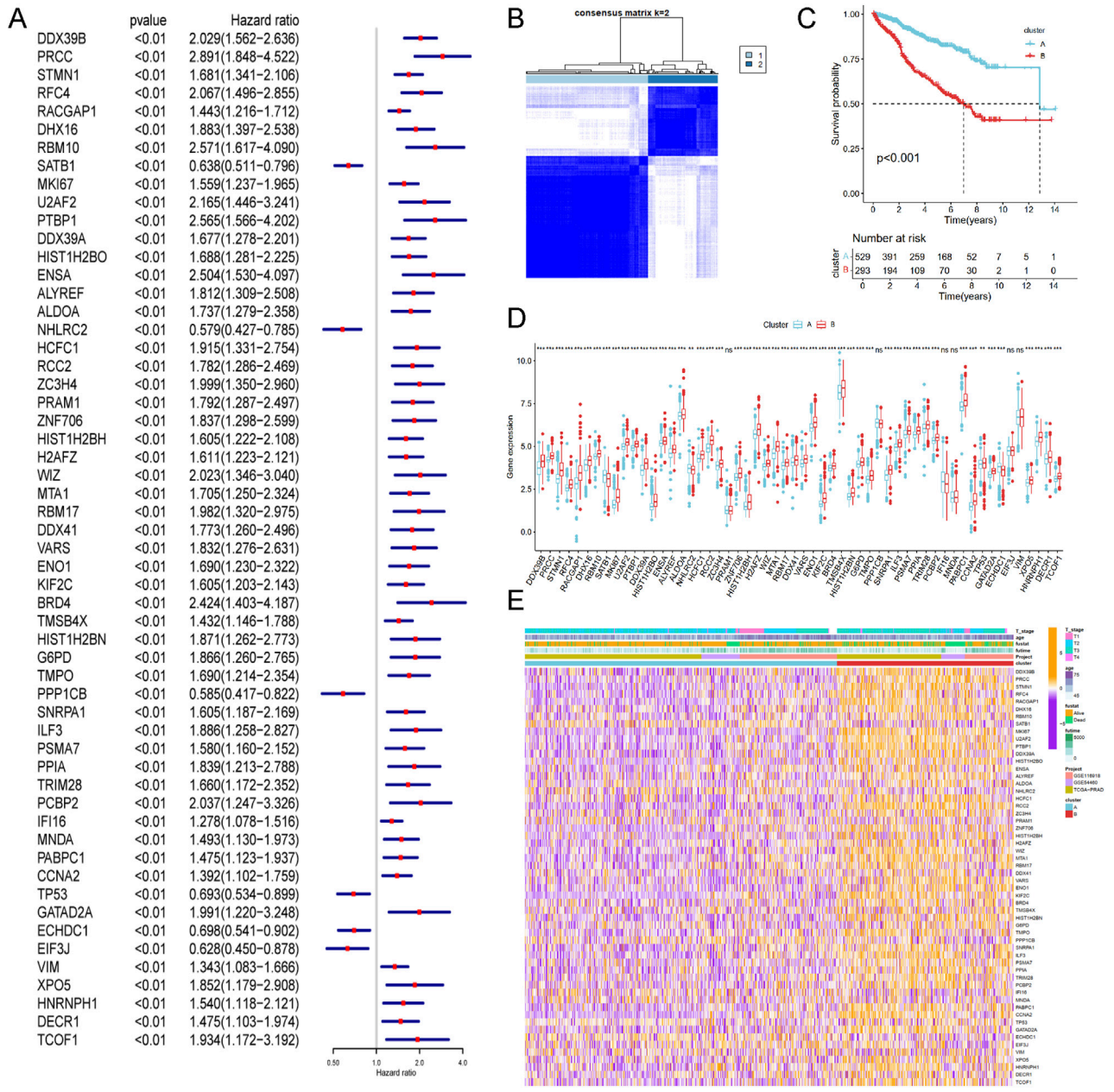

FIGURE 3
Identification of lactylation related molecular subtypes and comprehensive pathway enrichment analysis in combined cohorts. **(A)** Forest plot displaying the results of cox analysis shows 56 genes with prognostic value (Pvalue <0.01). **(B)** Consensus clustering matrixes was generated for values as k = 2. **(C)** Kaplan-Meier survival curves for these two distinct clusters ($p < 0.001$). **(D)** Gene set enrichment analysis (GSEA) plot showing the enrichment of gene sets in two clusters. **(E)** Heatmap of gene expression levels among different clinical characteristics (age, t stage, survival status).

consistent with the findings from Reactome and Biocart enrichment analyses (Figures 4B–E). In contrast, Cluster A exhibited significant enrichment in hallmark pathways such as estrogen response early, apical surface, myogenesis, and androgen response (Figure 4D). KEGG pathway analysis also indicated that Cluster A was enriched in several metabolic pathways, including beta-alanine metabolism, fatty acid metabolism, propanoate metabolism, tryptophan metabolism, and drug metabolism via cytochrome P450 (Figure 4E).

Based on the principal component analysis (PCA) of prognostic genes, the samples in merged cohort could be divided into two cluster A and B (Figure 5A), aligning with the results from Figure 3B. Immune cell analysis revealed that Cluster B exhibited higher levels of activated B cells, activated $CD4^+$ T cells, activated $CD8^+$ T cells, MDSCs, natural killer T cells, natural killer cells, T follicular helper cells, Type 1 helper cells, and Type 2 helper cells (Figure 5B), consistent with immune infiltration results from eight different methods (Figure 5C). These biological characteristics of function enrichment indcated that Cluster B was activated in cancer related pathways, while Cluster A was characterized by distinct metabolic states. Despite the activated immune cells in Cluster B, the presence of immunosuppressive cells was also notable.

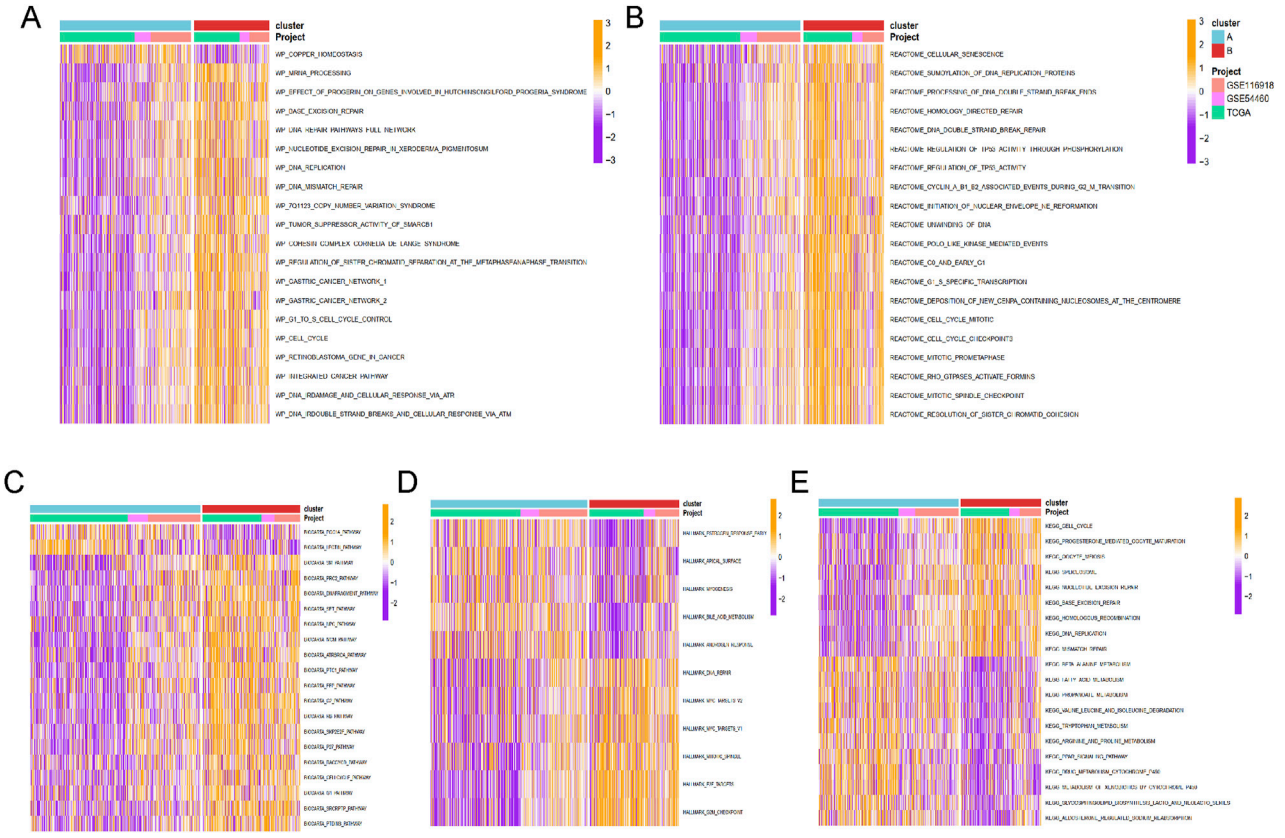

FIGURE 4
The functional enrichment analysis results of GSVA methods between different clusters. The **(A)** wikipathway, **(B)** Reactome, **(C)** Biocarta, **(D)** HALLMARK, and **(E)** KEGG pathways enrichment of cluster A and B groups.

Construction of a prognosis signature based on integrative machine learning

To develop a consensus LRG signature (LRGS), ten machine-learning algorithms were employed to analyze 56 prognostic genes identified via univariate Cox regression. A total of 101 prediction models were applied to the merged dataset using tenfold cross-validation, and C-index values were calculated for all training and validation sets (Figure 6A). After extensive screening, the RSF model was identified as the most accurate and clinically relevant predictive model (Figure 6B). In the combined cohort, patients classified as high-risk had significantly poorer RFS compared to those in the low-risk category ($p < 0.001$, log-rank test). The GSE116918, GSE54460, and TCGA-PRAD datasets further confirmed that RFS was significantly improved in the low-risk group ($p < 0.001$, log-rank test; Figure 6C). ROC curve analysis showed that the LRGS achieved AUC values of 0.876, 0.853, and 0.793 for 1-, 3-, and 5-year intervals, respectively (Figure 6D). The correlation between the prognostic signature's risk score and clinical characteristics revealed that higher death rates and higher T stages were associated with higher risk scores (Figures 7A,B). Univariate and multivariate Cox regression analyses on the prognostic risk scores (PRS) within the combined cohort identified LRGS as an independent prognostic factor for patients with PRAD, with a hazard ratio of 1.108 (95% CI: 1.095–1.120, $p < 0.001$) (Figures 7C,D).

Molecular mechanisms underlying LRGS in bulk transcriptomics

To further elucidate the molecular mechanisms linking the LRGS with prognosis in PRAD, genes positively and negatively correlated with risk scores were identified. Several genes, such as TACC3, CDC20, TROAP, UBE2C, MYBL2 are positive associated with risk score (Figure 7E), while genes such as RDH11, ACPP, CTBS, RNF185, CPE are negative with risk score (Figure 7F). Functional enrichment analysis was performed using the GSEA method, revealing that the GO gene set was enriched in pathways related to chromosome segregation regulation, mitotic spindle checkpoint signaling, and spindle assembly checkpoint signaling (Figure 7G). KEGG pathway analysis indicated gene enrichment in pathways associated with the cell cycle (including cell cycle and DNA replication) and immune processes (such as neutrophil extracellular trap formation, NK cell-mediated cytotoxicity, and Th17, Th1, and Th2 cell differentiation) (Figure 7H). Reactome pathway enrichment analysis (Figure 7I) further confirmed these

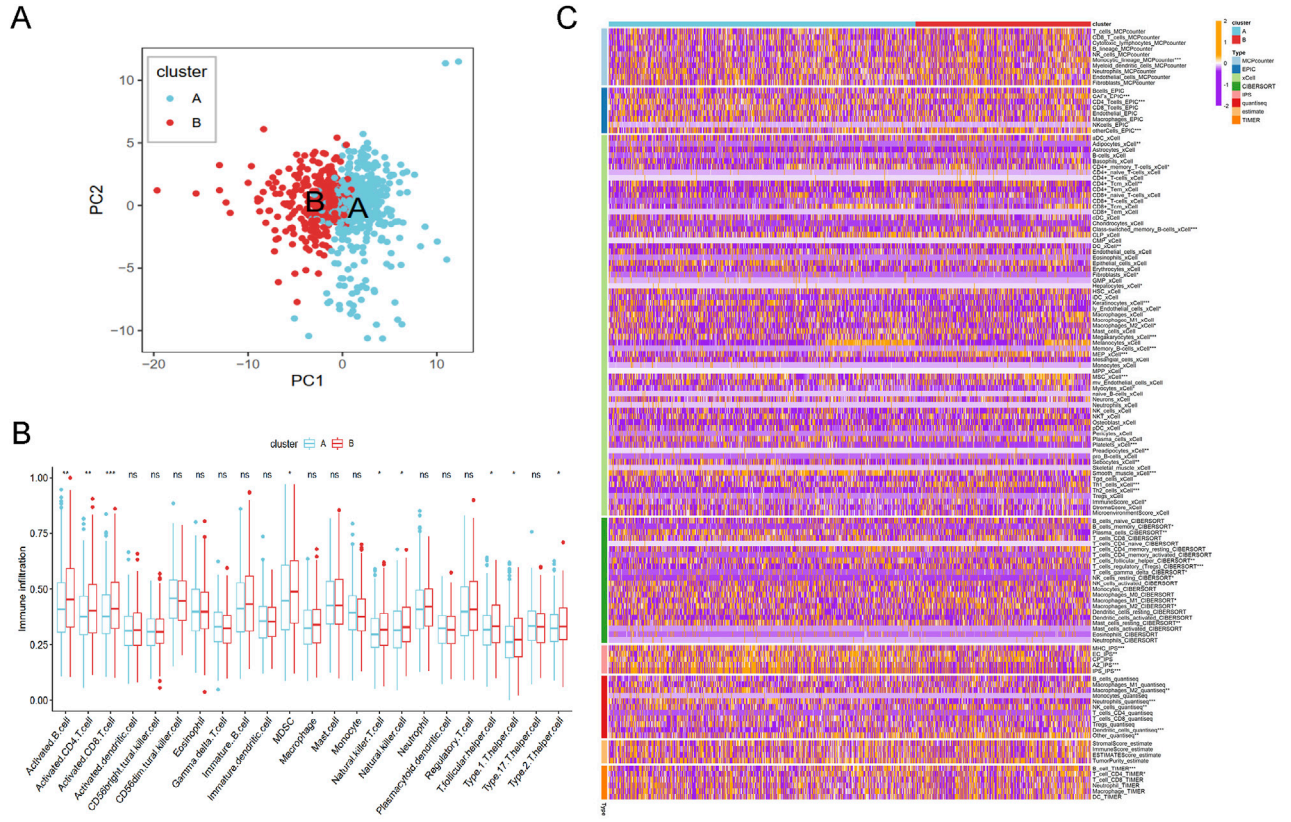

FIGURE 5
The immune analysis results between different cluster. **(A)** The PCA plot of cluster A and B. **(B)** The immune cells distribution based on ssGSEA algorithm. **(C)** Heatmap of tumor-related infiltrating immune cells based on TIMER, CIBERSORT, CIBERSORT-ABS, QUANTISEQ, MCPCOUNTER, XCELL, and EPIC methods.

results, showing strong association with cancer-related biological processes and immune-related pathways.

The correlation of immune microenvironment and immune characteristics with the LRGS

A series of algorithms were used to investigate the TME across different risk score groups. The high-risk group exhibited reduced levels of T cells, CD8T cells, cytotoxic lymphocytes, NK cells, monocytes, and other immune cell types compared to the low-risk group (Figure 8A). Additionally, expression levels of chemokines (such as CCL5, CCL8, CCL16-18, CCL20-22), interleukins (such as IL10, IL11, IL12A-B, IL17, IL23A, IL24, IL27, IL31), interferons (such as IFNA1, IFNB1), and receptors were significantly different between the high- and low-risk groups (Figure 8B). TIDE and dysfunction scores were calculated using the TIDE dataset, indicating that the high-risk group exhibited elevated dysfunction and TIDE scores, suggesting immune effector cell exhaustion in high-risk samples (Figure 8C).

To address the malignant potential of PCa, this study explored various drug databases to identify therapeutic agents tailored to specific subtypes, focusing on the different risk score groups. The high-risk group demontrated resistance to targeted therapies such as erlotinib and gefitinib, but exhibited increased sensitivity to axitinib (Figure 8D). This highlights potential therapeutic strategies for PCa based on varying lactylation risk scores.

The correlation of the top ten hub genes with single-cell characteristics

Given their cirtical roles in PCa, then we selected the top ten genes, RBM17, MTA1, PRAM1, RACGAP1, MKI67, MNDA, CCNA2,VIM,MNDA and RBM10 for further analysis. In TISCH2 datasets, MNDA information is not found. Then we only included other nine genes. The results showed that RMB17, RBM10, MTA1, VIM and RACGAP1 were enriched in endothelial, fibroblasts, epithelial and malignant (Figures 9A,B,D,E,I). As for CCNA2, KIF2C, MKI67 and PRAM1 were enriched in monocytes, macrophage and progenitor cells (Figures 9C,F–H). These findings aligned with immune cell infiltration patterns identified through various TME methodologies (Figure 8A).

To assess the prognostic relevance of LRGS, we performed Scissor analysis, an integrative method that links single-cell transcriptomic data with bulk-level phenotypes. By incorporating bulk RNA-seq expression profiles and corresponding survival information from the merged cohort, the Scissor algorithm classified single cells into three distinct groups: Scissor + cells, associated with poorer prognosis; Scissor− cells, linked to better survival outcomes; and background cells with no

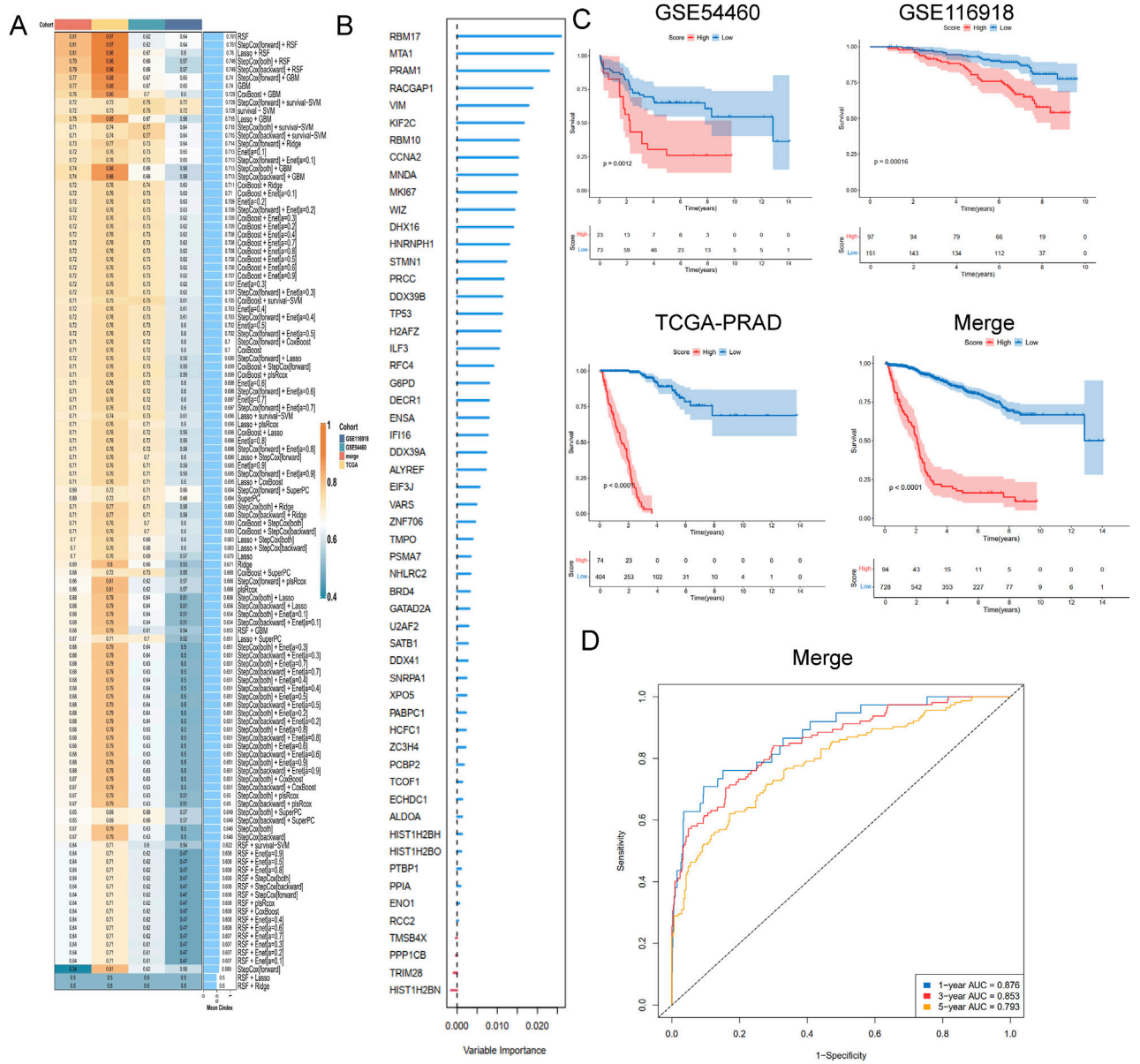

FIGURE 6
A consensus LRGRS was developed and validated via the machine learning-based combined procedure. **(A)** A total of 10 kinds of machine learning via a tenfold cross-validation framework and further calculated the C-index of each model across all validation datasets. **(B)** The barplot of hub genes based on forest trees methods. **(C)** Kaplan–Meier curves of OS according to the LRGRS in the GSE54460, GSE116918, TCGA-PRAD and combined cohorts, based on the log-rank test. **(D)** The ROC curves in combined cohorts.

significant phenotype association (Supplementary Figure S1). Notably, macrophage/monocyte and fibroblast populations exhibited consistent associations across different Scissor analysis iterations, underscoring their potential roles in modulating prognostic phenotypes.

Analysis of the multi-omics characteristics of the hub genes and validation of gene expression in PRAD

Using the GSCA dataset, gene expressions levels of hub top genes and associated with SNV percentage, CNV percentage, methylation. The results demonstrated that MKI67 and KIF2C had 5%, 2% SNV percentage. PRAM1, MNDA and RBM10 had higher methylation levels (Figure 10A). The homozygous CNV showed that MNDA, MKI67, RBM17, MTA1, VIM, RBM10 and RACGAP1 had high homozygous amplication, CCNA2, MNDA, MKI67, RBM17, MTA1, VIM and KIF2C had high homozygous deletion. As for heterozygous CNV, these ten hub genes had high heterozygous CNV (Figure 10B). Subsequently, the correlation between mRNA expression of ten hub genes and methylation, CNV levels were explored. These ten hub genes, expect MKI67, had significant difference with methylation (Figure 10C). As for the correlation with CNV levels, only RBM17, KIF2C and RBM10 had

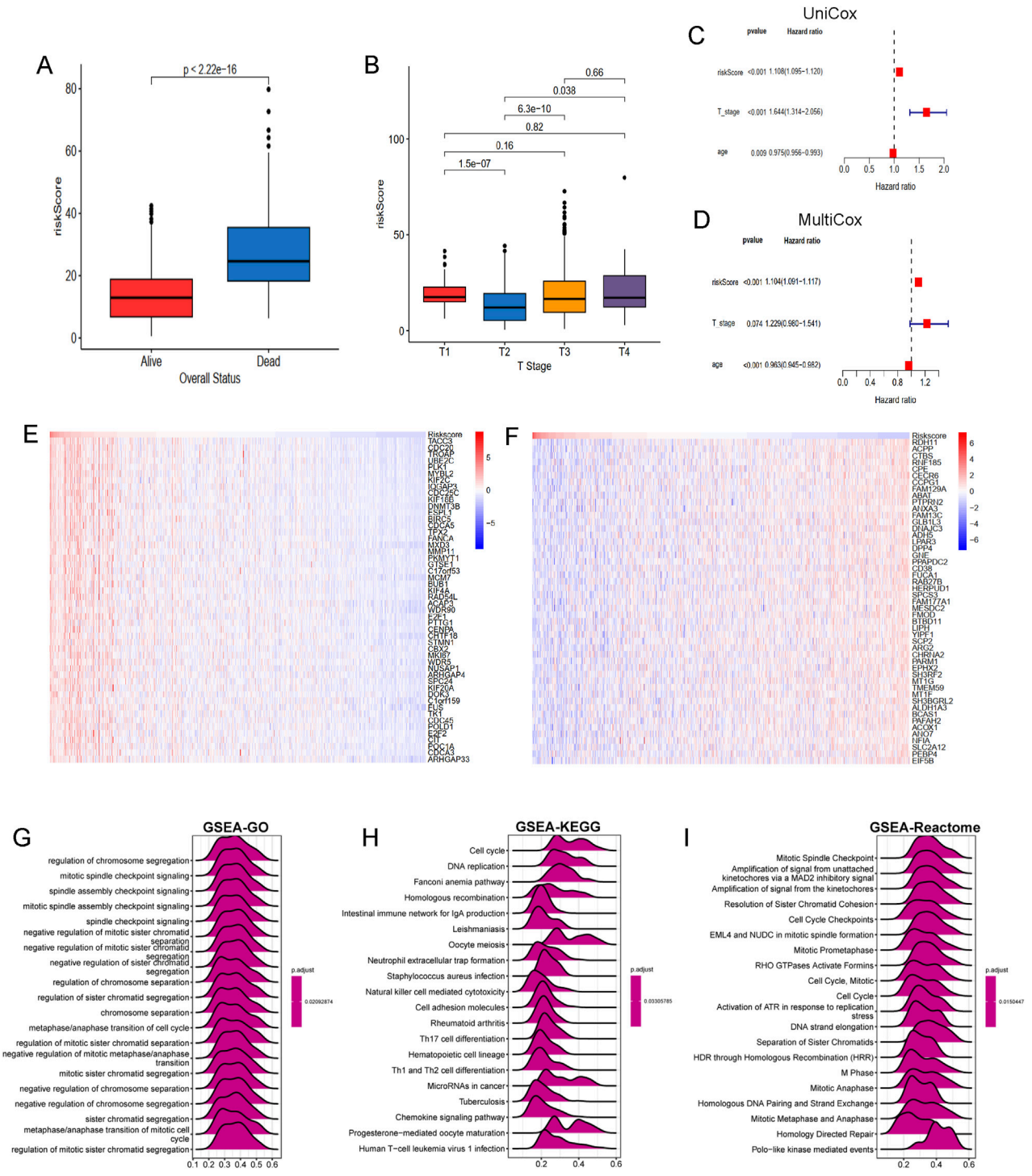

FIGURE 7
The association of LRGRS and clinical features, functional enrichments between different risk groups. **(A)** The boxplot of overall status and riskScore. **(B)** The boxplot of T stage and riskScore. The results of **(C)** univariate and **(D)** multivariate cox regression analysis. The mRNA expression profiles of positive genes **(E)** and negative genes **(F)** correlation with risk score. The GSEA results of GO **(G)**, KEGG **(H)** and Reactome **(I)** signal pathways.

significant difference (Figure 10D). The analysis revealed that the majority of hub genes exhibited a positive correlation with macrophages, Th1, Tr1, CD4 T cells, iTreg, DC, Tfh cells, as well as CD4 naïve, Th17, and neutrophil cells (Figure 10E).

RT-qPCR was performed to assess the mRNA expression levels of the ten hub genes in clinical samples using RT-qPCR.The results indicated that the majority of signature genes (RBM17, MTA1, RACGAP1, MKI67, CCNA2, RBM10 and KIF2C) were expressed at

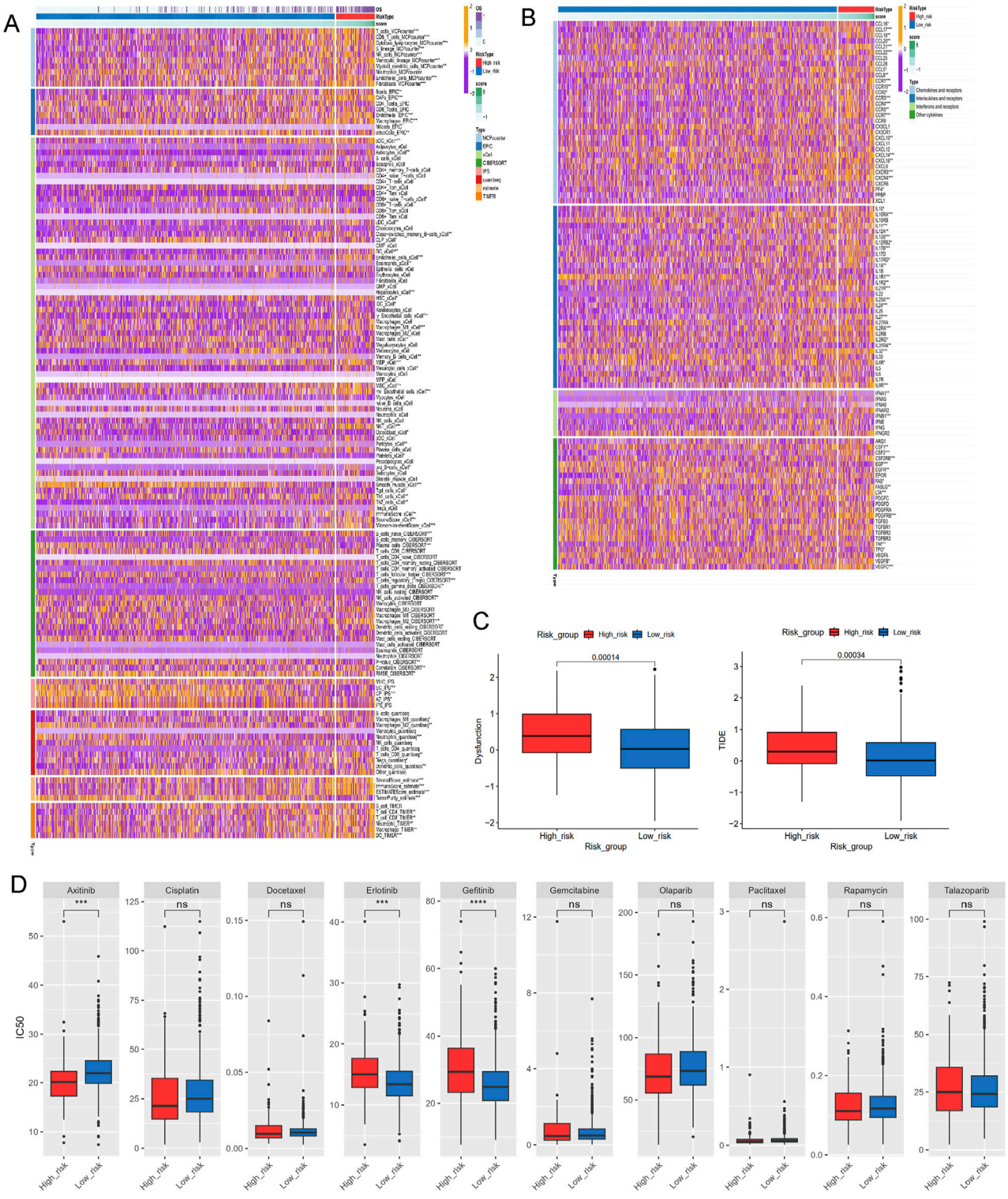

FIGURE 8
Investigations of immune profiling, immune score and drug sensitivity. **(A)** Heatmap of tumor-related infiltrating immune cells based on TIMER, CIBERSORT, CIBERSORT-ABS, QUANTISEQ, MCPCOUNTER, XCELL, and EPIC algorithms. **(B)** Heatmap of immune-related genes. **(C)** The immune function scores based on TIDE dataset. **(D)** Estimated IC50 of the indicated molecular-targeted drugs. ns > 0.05, $p < 0.05$, **$p < 0.01$, ***$p < 0.001$, ****$p < 0.0001$. ns, no significance.

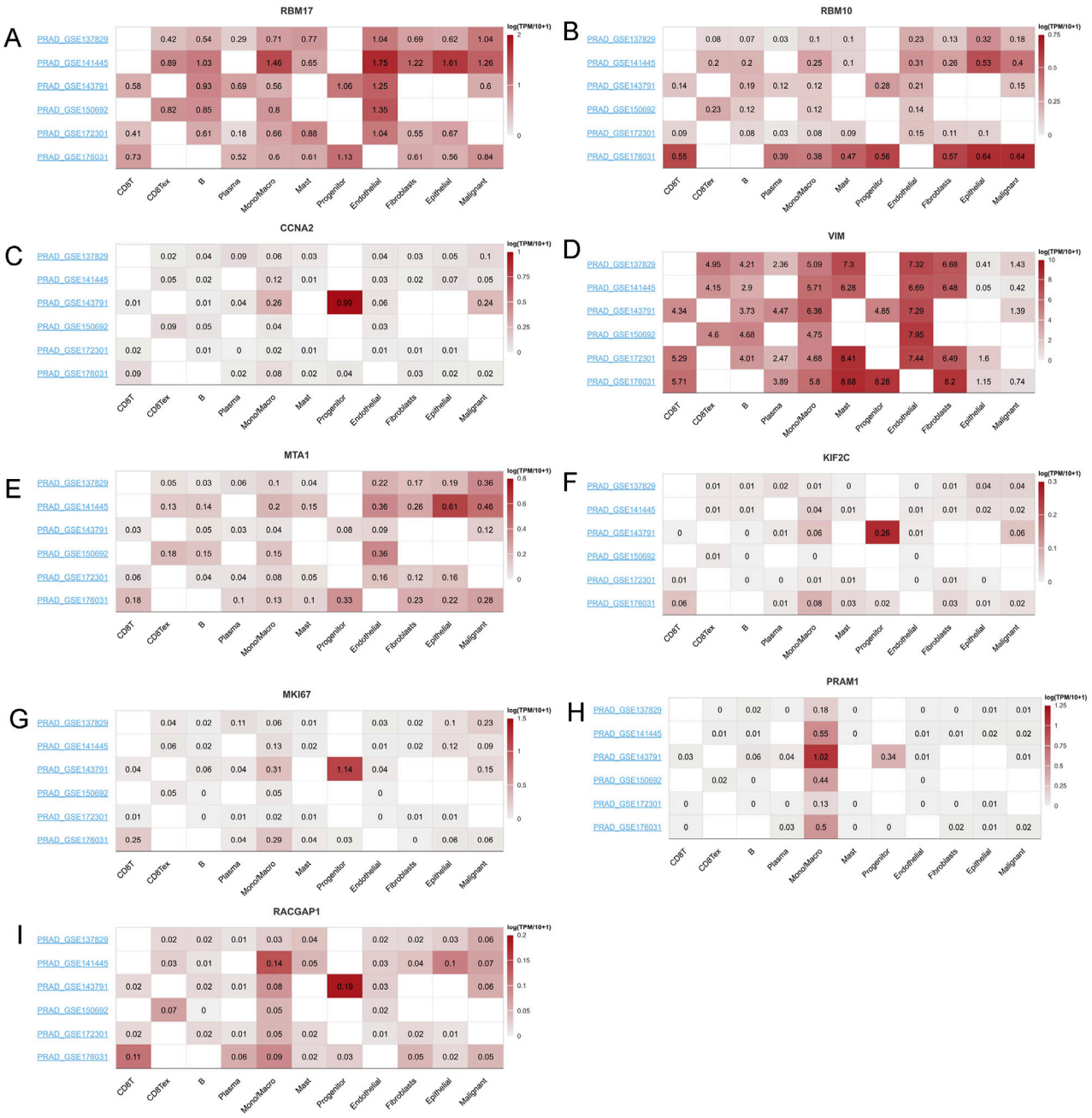

FIGURE 9
The mRNA expression profiles top ten genes in single cell sequencing levels based on TISCH2 dataset. The mRNA expression profiles of **(A)** RBM17, **(B)** RBM10, **(C)** CCNA2, **(D)** VIM, **(E)** MTA1, **(F)** KIF2C, **(G)** MKI67, **(H)** PRAM1 and **(I)** RACGAP1 in different PRAD datasets.

higher levels in PCa tissues compared to adjacent normal samples (Figure 10F).

Discussion

Recent estimates from GLOBOCAN 2024 indicate that PCa remains a leading cause of cancer incidence and mortality, with significant variations across different continents and among various ethnic groups (Bray et al., 2024; Gizzi et al., 2024). This disparity highlights the urgent need for a personalized approach to understanding, diagnosing, and treating PCa. A thorough understanding of its complexity is vital for developing individualized treatment strategies. This study advances the understanding of lactylation, a crucial PTM that influences gene expression and cellular metabolism in cancer cells (Li et al., 2024; Zhang Q. et al., 2024; Zhou et al., 2023).

Our single-cell RNA sequencing analysis reveals significant cellular heterogeneity within PCa, identifying distinct cell types exhibiting diverse lactylation profiles. This cellular diversity mirrors the broader genetic and metabolic heterogeneity of PCa, which is characterized by numerous genomic alterations and extensive metabolic reprogramming (Baca et al., 2013; Barbieri et al., 2012). The identification of LRGs as potential

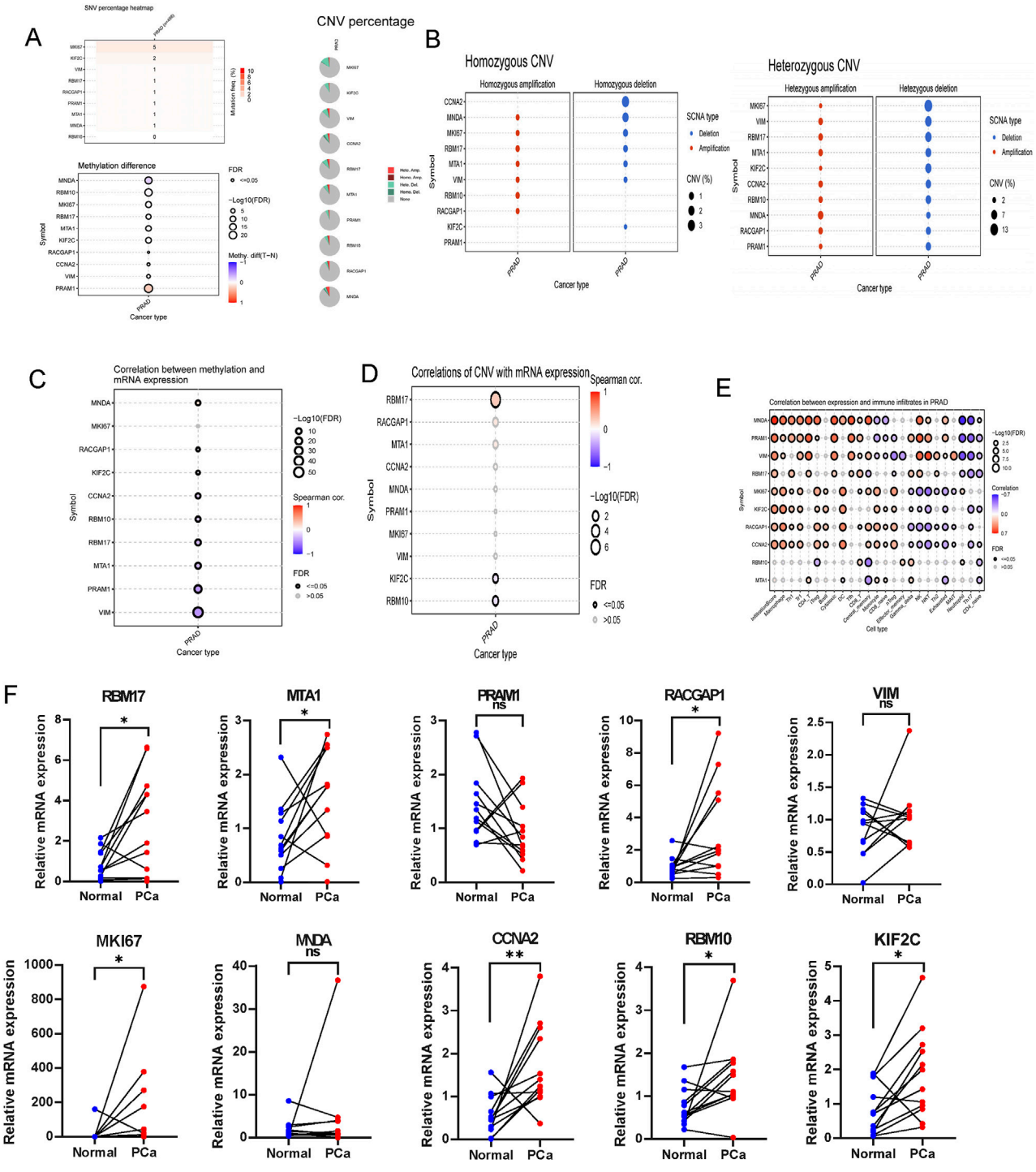

FIGURE 10
The association of gene mutations, CNV, methylation, immune infiltration and mRNA expression profiles in TCGA-PRAD, and validation in ten paired clinical samples. **(A)** The summary of SNV percentage, CNV percentage and methylation difference. **(B)** The homozygous and heterozygous CNV of TCGA-PRAD. The correlations between of top ten genes mRNA expression with methylation **(C)**, CNV **(D)** and immune infiltration **(E)**. **(F)** qRT-PCR analysis of hub genes expression in prostate cancer and paired adjacent normal tissues based on patient samples from Sir Run Run Shaw Hospital. ns > 0.05, p < 0.05, **p < 0.01, ***p < 0.001, ****p < 0.0001. ns, no significance.

prognostic biomarkers marks a key step toward personalized medicine, enabling the stratification of patients based on LRG expression profiles.

Metabolic reprogramming, particularly the shift toward aerobic glycolysis, is a hallmark of PCa cells. This shift, characteristic of the Warburg effect, results in lactate accumulation, which, through lactylation, can modulate gene expression and promote tumor growt (Zhang X. et al., 2024; Pan et al., 2024). These insights into the immunomodulatory effects of lactate provide a rationale

for targeting lactylation as part of immunotherapeutic strategies for PCa.

The TME plays a pivotal role in cancer progression, and our study demonstrates that lactate can profoundly influence the immune landscape within this environment. Lactate-induced acidification of the TME impairs T lymphocyte function and promotes the polarization of TAMs toward the protumorigenic M2 phenotype (Loeb et al., 2014).

These insights into the immunomodulatory effects of lactate provide a rationale for targeting lactylation as part of immunotherapeutic strategies for PCa.

The prognostic biomarker developed in this study, based on LRGs, offers a novel method for predicting treatment response and disease-free survival in patients with PCa. The use of machine learning algorithms to identify this biomarker emphasizes the potential of integrating computational methods with biological data to propel personalized medicine (Zeng et al., 2024). The identification of key genes such as TACC3, CDC20, and UBE2C, which are positively correlated with risk scores, lays the groundwork for further investigation into the molecular mechanisms underlying lactylation's role in PCa.

The correlation between lactylation status and the immune microenvironment indicates that high-risk groups may exhibit a reduced presence of immune cells, potentially contributing to treatment resistance. This observation, coupled with the finding that high-risk groups may be more resistant to certain targeted therapies but show sensitivity to others, such as axitinib, underscores the critical need for personalized treatment strategies (Barbieri et al., 2012; Bray et al., 2018).

In summary, this study provides an in-depth analysis of lactylation in PCa, emphasizing its roles in tumor biology, immune evasion, and prognosis. The identification of LRGs as a prognostic biomarker, along with insights into their molecular mechanisms, forms the basis for the development of novel therapeutic strategies (Pan et al., 2024). Future research should aim to validate these findings in larger patient cohorts and explore lactylation as a potential therapeutic target. Personalized treatment strategies based on lactylation profiles have the potential to revolutionize PCa management, ultimately improving patient outcomes.

Conclusion

This study comprehensively analyzed LRGs in PCa through single-cell and bulk RNA sequencing data. This multifaceted approach enabled the identification and characterization of LRG expression patterns across various cell types within the TME. The prognostic significance of these genes was confirmed by classifying clinical samples into two distinct subtypes, each associated with different tumor-related pathways, metabolic processes, and immune profiles. A machine learning-based prognostic signature model was developed, demonstrating high accuracy and offering new insights into personalized treatment strategies for PCa. This innovative model enhances our understanding of the molecular mechanisms driving PCa and provides a valuable tool for predicting treatment response and disease outcomes, ultimately facilitating more effective clinical management.

Data availability statement

The raw data supporting the conclusions of this article will be made available by the authors, without undue reservation.

Ethics statement

The studies involving humans were approved by the Ethics Committee of Sir Run Run Shaw Hospital. The studies were conducted in accordance with the local legislation and institutional requirements. The human samples used in this study were acquired from primarily isolated as part of your previous study for which ethical approval was obtained. Written informed consent for participation was not required from the participants or the participants'; legal guardians/next of kin in accordance with the national legislation and institutional requirements.

Author contributions

CZ: Writing – original draft, Writing – review and editing. LD: Writing – review and editing. HW: Writing – review and editing. GL: Writing – review and editing. LG: Writing – review and editing, Writing – original draft.

Funding

The author(s) declare that no financial support was received for the research and/or publication of this article.

Conflict of interest

The authors declare that the research was conducted in the absence of any commercial or financial relationships that could be construed as a potential conflict of interest.

Generative AI statement

The author(s) declare that no Generative AI was used in the creation of this manuscript.

Publisher's note

Supplementary material

The Supplementary Material for this article can be found online at: https://www.frontiersin.org/articles/10.3389/fphar.2025.1634985/full#supplementary-material

SUPPLEMNTARY FIGURE S1
Correlation of LRGS with survival phenotype at single cell scale identified by the Scissor methods. **(A)** tSNE plots showcasing the survival phenotypes. **(B)**

Balloonplot shows the proportation of cells based on cox methods. **(C)** tSNE plot shows the LRGS high and low phenotypes. **(D)** Balloonplot shows the proportation of cells based on logistic methods. **(E)** The proportation of cells among survival and LRGS phenotypes.

References

Baca, S. C., Prandi, D., Lawrence, M. S., Mosquera, J. M., Romanel, A., Drier, Y., et al. (2013). Punctuated evolution of prostate cancer genomes. *Cell* 153 (3), 666–77. doi:10.1016/j.cell.2013.03.021

Barbieri, C. E., Baca, S. C., Lawrence, M. S., Demichelis, F., Blattner, M., Theurillat, J. P., et al. (2012). Exome sequencing identifies recurrent SPOP, FOXA1 and MED12 mutations in prostate cancer. *Nat. Genet.* 44 (6), 685–689. doi:10.1038/ng.2279

Berglund, E., Maaskola, J., Schultz, N., Friedrich, S., Marklund, M., Bergenstråhle, J., et al. (2018). Spatial maps of prostate cancer transcriptomes reveal an unexplored landscape of heterogeneity. *Nat. Commun.* 9 (1), 2419. doi:10.1038/s41467-018-04724-5

Bray, F., Ferlay, J., Soerjomataram, I., Siegel, R. L., Torre, L. A., and Jemal, A. (2018). Global cancer statistics 2018: GLOBOCAN estimates of incidence and mortality worldwide for 36 cancers in 185 countries. *CA Cancer J. Clin.* 68 (6), 394–424. doi:10.3322/caac.21492

Bray, F., Laversanne, M., Sung, H., Ferlay, J., Siegel, R. L., Soerjomataram, I., et al. (2024). Global cancer statistics 2022: GLOBOCAN estimates of incidence and mortality worldwide for 36 cancers in 185 countries. *CA Cancer J. Clin.* 74 (3), 229–263. doi:10.3322/caac.21834

Brown, T. P., and Ganapathy, V. (2020). Lactate/GPR81 signaling and proton motive force in cancer: role in angiogenesis, immune escape, nutrition, and warburg phenomenon. *Pharmacol. Ther.* 206, 107451. doi:10.1016/j.pharmthera.2019.107451

Chen, S., Zhu, G., Yang, Y., Wang, F., Xiao, Y. T., Zhang, N., et al. (2021). Single-cell analysis reveals transcriptomic remodellings in distinct cell types that contribute to human prostate cancer progression. *Nat. Cell Biol.* 23 (1), 87–98. doi:10.1038/s41556-020-00613-6

Dai, M., Pei, X., and Wang, X.-J. (2022). Accurate and fast cell marker gene identification with COSG. *Briefings Bioinforma.* 23 (2), bbab579. doi:10.1093/bib/bbab579

Fujita, K., and Nonomura, N. (2019). Role of androgen receptor in prostate cancer: a review. *World J. Mens. Health* 37 (3), 288–295. doi:10.5534/wjmh.180040

Gizzi, M., Seront, E., Tombal, B., and Van Damme, J. (2024). Systemic treatments for metastatic prostate cancer in 2024. *Eur. Urol. Focus* 10 (4), 522–524. doi:10.1016/j.euf.2024.07.013

Guo, S., Cao, Y., Cheng, B., Zhou, Y., Li, X., Zhang, M., et al. (2024). A nanoprodrug derived from branched poly (ethylene glycol) recognizes prostate-specific membrane antigen to precisely suppress prostate cancer progression. *Int. J. Biol. Macromol.* 282 (Pt 2), 136831. doi:10.1016/j.ijbiomac.2024.136831

Han, Y., Wang, Y., Dong, X., Sun, D., Liu, Z., Yue, J., et al. (2022). TISCH2: expanded datasets and new tools for single-cell transcriptome analyses of the tumor microenvironment. *Nucleic Acids Res.* 51 (D1), D1425–D1431. doi:10.1093/nar/gkac959

Hänzelmann, S., Castelo, R., and Guinney, J. (2013). GSVA: gene set variation analysis for microarray and RNA-seq data. *BMC Bioinforma.* 14 (1), 7. doi:10.1186/1471-2105-14-7

He, Y., Song, T., Ning, J., Wang, Z., Yin, Z., Jiang, P., et al. (2024). Lactylation in cancer: mechanisms in tumour biology and therapeutic potentials. *Clin. Transl. Med.* 14 (11), e70070. doi:10.1002/ctm2.70070

He, Y., Xu, W., Xiao, Y. T., Huang, H., Gu, D., and Ren, S. (2022). Targeting signaling pathways in prostate cancer: mechanisms and clinical trials. *Signal Transduct. Target Ther.* 7 (1), 198. doi:10.1038/s41392-022-01042-7

Jiang, P., Gu, S., Pan, D., Fu, J., Sahu, A., Hu, X., et al. (2018). Signatures of T cell dysfunction and exclusion predict cancer immunotherapy response. *Nat. Med.* 24 (10), 1550–1558. doi:10.1038/s41591-018-0136-1

Li, H., Sun, L., Gao, P., and Hu, H. (2024). Lactylation in cancer: current understanding and challenges. *Cancer Cell* 42 (11), 1803–1807. doi:10.1016/j.ccell.2024.09.006

Li, X., Yang, Y., Zhang, B., Lin, X., Fu, X., An, Y., et al. (2022). Lactate metabolism in human health and disease. *Signal Transduct. Target Ther.* 7 (1), 305. doi:10.1038/s41392-022-01151-3

Liang, X. H., Chen, X. Y., Yan, Y., Cheng, A. Y., Lin, J. Y., Jiang, Y. X., et al. (2024). Targeting metabolism to enhance immunotherapy within tumor microenvironment. *Acta Pharmacol. Sin.* 45 (10), 2011–2022. doi:10.1038/s41401-024-01304-w

Liu, C.-J., Hu, F. F., Xie, G. Y., Miao, Y. R., Li, X. W., Zeng, Y., et al. (2022). GSCA: an integrated platform for gene set cancer analysis at genomic, pharmacogenomic and immunogenomic levels. *Briefings Bioinforma.* 24 (1), bbac558. doi:10.1093/bib/bbac558

Loeb, S., Bjurlin, M. A., Nicholson, J., Tammela, T. L., Penson, D. F., Carter, H. B., et al. (2014). Overdiagnosis and overtreatment of prostate cancer. *Eur. Urol.* 65 (6), 1046–1055. doi:10.1016/j.eururo.2013.12.062

Luo, Y., Yang, Z., Yu, Y., and Zhang, P. (2022). HIF1α lactylation enhances KIAA1199 transcription to promote angiogenesis and vasculogenic mimicry in prostate cancer. *Int. J. Biol. Macromol.* 222 (Pt B), 2225–2243. doi:10.1016/j.ijbiomac.2022.10.014

Lv, X., Lv, Y., and Dai, X. (2023). Lactate, histone lactylation and cancer hallmarks. *Expert Rev. Mol. Med.* 25, e7. doi:10.1017/erm.2022.42

Maeser, D., Gruener, R. F., and Huang, R. S. (2021). oncoPredict: an R package for predicting in vivo or cancer patient drug response and biomarkers from cell line screening data. *Brief. Bioinform* 22 (6), bbab260. doi:10.1093/bib/bbab260

Pan, J., Zhang, J., Lin, J., Cai, Y., and Zhao, Z. (2024). Constructing lactylation-related genes prognostic model to effectively predict the disease-free survival and treatment responsiveness in prostate cancer based on machine learning. *Front. Genet.* 15, 1343140. doi:10.3389/fgene.2024.1343140

Sun, D., Guan, X., Moran, A. E., Wu, L. Y., Qian, D. Z., Schedin, P., et al. (2022). Identifying phenotype-associated subpopulations by integrating bulk and single-cell sequencing data. *Nat. Biotechnol.* 40 (4), 527–538. doi:10.1038/s41587-021-01091-3

Wilkerson, M. D., and Hayes, D. N. (2010). ConsensusClusterPlus: a class discovery tool with confidence assessments and item tracking. *Bioinformatics* 26 (12), 1572–1573. doi:10.1093/bioinformatics/btq170

Wu, T., Hu, E., Xu, S., Chen, M., Guo, P., Dai, Z., et al. (2021). clusterProfiler 4.0: a universal enrichment tool for interpreting omics data. *Innov. (Camb)* 2 (3), 100141. doi:10.1016/j.xinn.2021.100141

Zeng, D., Fang, Y., Qiu, W., Luo, P., Wang, S., Shen, R., et al. (2024). Enhancing immuno-oncology investigations through multidimensional decoding of tumor microenvironment with IOBR 2.0. *Cell Rep. Methods* 4, 100910. doi:10.1016/j.crmeth.2024.100910

Zha, J., Zhang, J., Lu, J., Zhang, G., Hua, M., Guo, W., et al. (2024). A review of lactate-lactylation in malignancy: its potential in immunotherapy. *Front. Immunol.* 15, 1384948. doi:10.3389/fimmu.2024.1384948

Zhang, Q., Cao, L., and Xu, K. (2024a). Role and mechanism of lactylation in cancer. *Zhongguo Fei Ai Za Zhi* 27 (6), 471–479. doi:10.3779/j.issn.1009-3419.2024.102.20

Zhang, X., Liang, C., Wu, C., Wan, S., Xu, L., Wang, S., et al. (2024b). A rising star involved in tumour immunity: lactylation. *J. Cell Mol. Med.* 28 (20), e70146. doi:10.1111/jcmm.70146

Zhou, Y., Li, T., Jia, M., Dai, R., and Wang, R. (2023). The molecular biology of prostate cancer stem cells: from the past to the future. *Int. J. Mol. Sci.* 24 (8), 7482. doi:10.3390/ijms24087482

frontiers | Frontiers in Oncology

TYPE Case Report
PUBLISHED 18 November 2025
DOI 10.3389/fonc.2025.1604933

OPEN ACCESS

EDITED BY
Lei Yin,
Shanghai Jiaotong University School of Medicine, China

REVIEWED BY
Ahmad Khajeh-Mehrizi,
Tehran University of Medical Sciences, Iran
Makarand Khochikar,
KIMS -UAIMS Hospital, Sangli, India

*CORRESPONDENCE
Jianguo Wei
mickmouse88@163.com

RECEIVED 02 April 2025
ACCEPTED 27 October 2025
PUBLISHED 18 November 2025

CITATION
Zheng Z, Liu E, Yang M, Liu X and Wei J (2025) A case report and literature review: an intra-abdominal epithelioid neoplasm with EWSR1::CREB fusions originating from the kidney.
Front. Oncol. 15:1604933.
doi: 10.3389/fonc.2025.1604933

A case report and literature review: an intra-abdominal epithelioid neoplasm with EWSR1::CREB fusions originating from the kidney

Zhen Zheng[1], Enjie Liu[2], Minglei Yang[2], Xiu Liu[2] and Jianguo Wei[2]*

[1]Department of Pathology, Zhejiang Hospital, Hangzhou, China, [2]Department of Pathology, The First Affiliated Hospital of Zhengzhou University, Zhengzhou, China

Background: EWSR1::CREB fusion is a newly identified group of aggressive tumors with epithelioid morphology and multiple growth patterns. These tumors are often located in the abdominal cavity and frequently show cytokeratin expression immunohistochemically. This invasive epithelioid soft tissue tumor has a remarkable preference for mesothelial-lined cavities, with rare extension into intra-abdominal organs such as the kidney. Given its rarity, early diagnosis and treatment are crucial. Currently, the diagnosis and treatment of this disease pose significant challenges.

Case demonstration: A 36-year-old male patient with no significant past medical history was admitted with a mass in the left kidney. Computed tomography showed a mass in the lower left kidney near the renal portal, and chromophobe carcinoma was suspected. The patient subsequently underwent a partial nephrectomy. The case was initially diagnosed as a malignant tumor with epithelial and mesenchymal components. RNA sequencing and FISH of the kidney mass confirmed the diagnosis of intra-abdominal epithelioid neoplasms with EWSR1::CREB fusions originating from the kidney. The patient did not undergo any adjuvant therapy and has been followed up for 14 months. He is currently in good condition.

Conclusion: Intra-abdominal epithelioid neoplasm with EWSR1::CREB fusions originating from the kidney is rare. The remarkable morphological features of the case presented here further confirm the significant morphological heterogeneity of tumors characterized by EWSR1::CREB fusion and expand the morphological spectrum of malignant epithelioid tumors with EWSR1::CREM rearrangements originating from the kidney. Additionally, neoplastic cells encircled native renal tubules, demonstrating an infiltrating growth pattern, and the renal tubules proliferated significantly, which may lead to misdiagnosis as other tumors that exhibit biphasic morphology.

KEYWORDS

EWSR1::CREB fusion, intra-abdominal, epithelioid neoplasm, kidney, clinicopathological features

Background

The EWSR1 gene encodes the RNA-binding protein EWSR1, which is a member of the TET family of transcription factors. These factors regulate various cellular processes like gene expression and RNA processing (1). There is increasing evidence that this gene is rearranged in various mesenchymal and epithelial tumors and can merge with many distinct genes (2). The fusion between EWSR1 and the CREB transcription factor family was particularly significant (3). CREB1, ATF1, and CREM form a subfamily of the alkaline leucine zipper (bZIP) superfamily of transcription factors, collectively known as the CREB family of transcription factors, that have multiple biological functions and regulate the expression of other genes (4). EWSR1 is a common fusion gene that fuses with CREB transcription factors, particularly ATF1 and CREB1, as 3′-partners (5). Furthermore, the fusion of the CREB gene family with EWSR1 or FUS gene partners leads to a wide variety of tumor pathogenesis. The EWSR1::CREB gene fusion was first described in a melanoma cell line (6). Later, EWSR1::CREB gene fusion was also reported in various mesenchymal tumors, including clear cell sarcoma of soft tissue, malignant gastrointestinal neuroectodermal tumor, hemangiomatoid fibrohistiocytoma, clear cell carcinoma of the salivary gland, clear cell odontogenic tumor, myoepithelial tumor, primary pulmonary myxoid sarcoma and primary intracranial myxoid sarcoma, paraganglioma, malignant mesothelioma in young adults, and intra-abdominal epithelioid malignancies. Masato et al. (5) statistically found that EWSR1/FUS::CREB rearranged tumors could occur in diverse anatomical locations, including the brain, soft tissue, head and neck, lung, internal organs, and abdominal cavity. Currently, EWSR1/FUS::CREB rearranged epithelioid malignancies have been documented in various intra-abdominal locations, such as the adrenal glands, colon, kidneys, liver, pancreas, stomach, and uterine adnexa (7).

Case demonstration

A 36-year-old male patient was referred in 2024 to the Department of Urology with a finding of a mass on the left kidney for 7 days. He had been diagnosed with a cyst in the left renal parenchyma area 1 year earlier during physical examination, but he had no further tests performed at that time. During physical examination in July 2024, ultrasound revealed once more a hypoechoic area in the left kidney, and further examination was recommended. The patient underwent computed tomography (CT) imaging at another unit, and a mass in the lower pole of the left kidney was found. The possibility of chromophobe renal cell carcinoma was considered.

The patient had no past medical history of hypertension or heart disease. He had no family history of cancer or hereditary diseases that were known. Moreover, he was a non-smoker and a non-drinker.

The patient subsequently underwent a partial nephrectomy at the First Affiliated Hospital of Zhengzhou University. Grossly, the tumor measured 5.5 cm × 5.0 cm × 2.3 cm. On microscopic examination, the tumor was well circumscribed, surrounded by a fibrous capsule (Figure 1A). The neoplastic cells were arranged in nests and sheets (Figure 1B) around the blood vessels, forming a hemangiopericytomatoid growth pattern (Figure 1C) in concordance with what was reported by Zhao et al. (1): a pseudochrysanthemum-like structure (Figure 1D), with local cystic or microcystic changes (Figure 1E). Round or short fusiform tumor cells displayed monomorphic nuclei with smooth nuclear contours and open chromatin. Tumor cells showed a slightly eosinophilic or transparent cytoplasm, with variably prominent nucleoli. The tumor showed relatively low mitotic activity (1 to 2/10 HPFs) and lacked nuclear pleomorphism (Figure 1F). The interstitial fibrocollagen was not prominent, and there were no signs of inflammatory cell infiltration or necrosis. Foam-like histiocyte aggregation, multinucleated giant cell responses, and cholesterol crystallization deposits were focally seen. In particular, neoplasms encircled a higher number of native renal tubules, which were especially pronounced around the tumor. The markedly hyperplastic renal tubules (Figure 2A) exhibited tubular and annular shapes (Figure 2B), with certain areas characterized by the presence of nipples, micronipples, and complex cribriform structures (Figure 2C). Some lumens were either dilated or slit-like, containing eosinophilic secretions (Figure 2D). The renal tubular epithelial cells were arranged in a single row, closely aligned focally, with overlapping nuclei. The epithelium cells showed mild morphological features, such as round nuclei, clear nuclear membranes, fine chromatin, and detectable nucleoli, while showing no mitoses (Figure 2E). The cytoplasm was eosinophilic and partially transparent (Figure 2F).

Immunohistochemical studies revealed that the neoplastic cells were diffusely positive for CD99 (Figure 3A), CD56 (Figure 3B), and CD57, while the involved renal tubules were not immunoreactive. Cyclin D1 showed a moderately positive result. SMA and CD34 were focally positive (Figure 3C). AE1/AE3 (Figure 3D), CK7, and PAX8 were negative in the tumor cells, whereas the adjacent tubular epithelial cells showed diffuse and strong positivity. Additionally, CK20, P504s, WT-1, P63, GATA 3, and renin were negative in the tumor cells. ALK (5A4) and syn showed partial positivity, and the Ki-67 proliferation index was approximately 10%. RNA sequencing revealed EWSR1::CREM gene fusion (Figure 3E). FISH analysis confirmed the EWSR1 break (Figure 3F) and EWSR1::CREM fusion (Figure 3G), whereas no BRAF V600E gene alteration was detected by fluorescence PCR.

Based on the clinical history, imaging features, histological morphology, immunohistochemical results, and molecular results, the patient was pathologically diagnosed with intra-abdominal epithelioid neoplasm with EWSR1::CREB fusions originating from the kidney. No local recurrence or metastatic lesions were detected 14 months after the surgery without adjuvant therapy, and he is currently in good condition.

Discussion

With the widespread use of RNA sequencing technology, the EWSR1/FUS::CREB fusion mesenchymal tumor family has

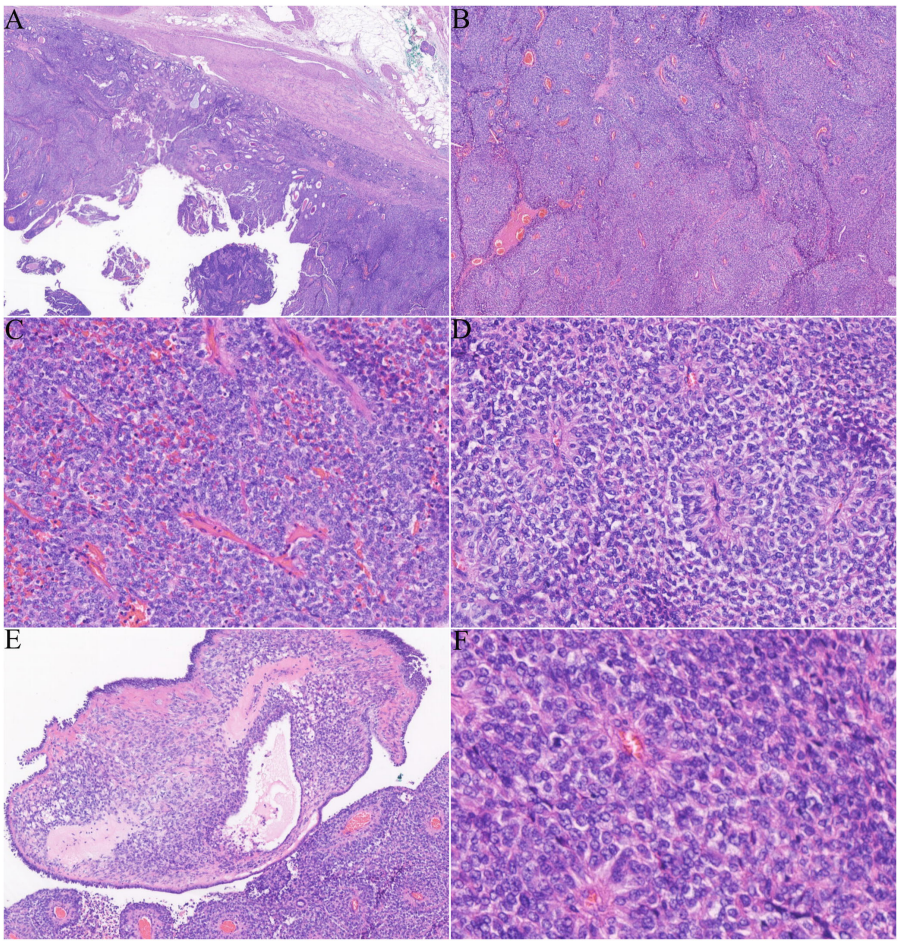

FIGURE 1
Histological features of the tumor: **(A)** a tumor with clearly defined edges and a fibrous envelope. **(B, C)** The solid and nested tumor cells displayed a hemangiopericytomatoid growth pattern. **(D)** Dense tumor cells formed clusters resembling pseudochrysanthemums around blood vessels. **(E)** Localized microcapsules contained pink liquid. **(F)** The cell boundaries were unclear, with round or oval nuclei and low mitotic activity (1–2/10 HPFs).

expanded rapidly to include potentially aggressive tumors rather than any well-established WHO entity. EWSR1/FUS::CREB fusion has been considered to define a group of aggressive tumors with epithelioid morphology. Primary tumors presenting as intraperitoneal internal organs are rare and involve the mesothelial space, often forming a mass in the abdominal cavity (8).

Including our case, there has been a total of nine cases (4, 8–11) of intraperitoneal malignant epithelioid tumors with EWSR1/FUS::CREM rearrangement that originated in the kidney described in the literature. Clinical and pathologic characteristics are summarized in Table 1. Of the nine tumors, five were found in female patients and four in male patients; these patients had a median age of 34 years (range, 17 to 61 years) at diagnosis, whose tumors ranged from 4.0 to 30.0 cm (median: 7.5). All patients presented with a mass in the kidney, with four and three tumors affecting the left and right kidney, respectively. The locations of the other two tumors were not specified. Seven patients underwent radical nephrectomy, one patient had a left renal tumor resection, while the procedure for the rest of the patients was unknown. Six patients had no adjuvant therapy performed after surgery, while two patients underwent adjuvant chemotherapy (10, 11).

Histologically, three tumors were not encapsulated and displayed irregular borders, while the other six tumors displayed clear boundaries with surrounding renal tissue, four of which had a visible fibrous pseudocapsule. Argani et al. (8) and Wu et al. (12) have outlined the key morphological features of intraperitoneal malignant epithelioid tumors with EWSR1/FUS::CREM rearrangement as follows: i) the presence of epithelioid cells, which can be mixed with epithelial/spindle cells or epithelial/round cells; ii) cystic or microcystic changes; and iii) varying amounts of chronic inflammatory cell infiltration. Among the nine patients, seven tumors exhibited round epithelioid cells, while one tumor was composed of round cells alongside scattered epithelioid cells. The current renal neoplasm, characterized by round and short fusiform shapes, showed cytoplasmic transparent epithelioid cells in the focal area, which is reported for the first time in the kidney. Cystic or microcystic changes were noted in four tumors. Three tumors showed prominent intratumoral inflammation, not including the current tumor. The mitotic activity ranged from 1 to 20/10 HPFs

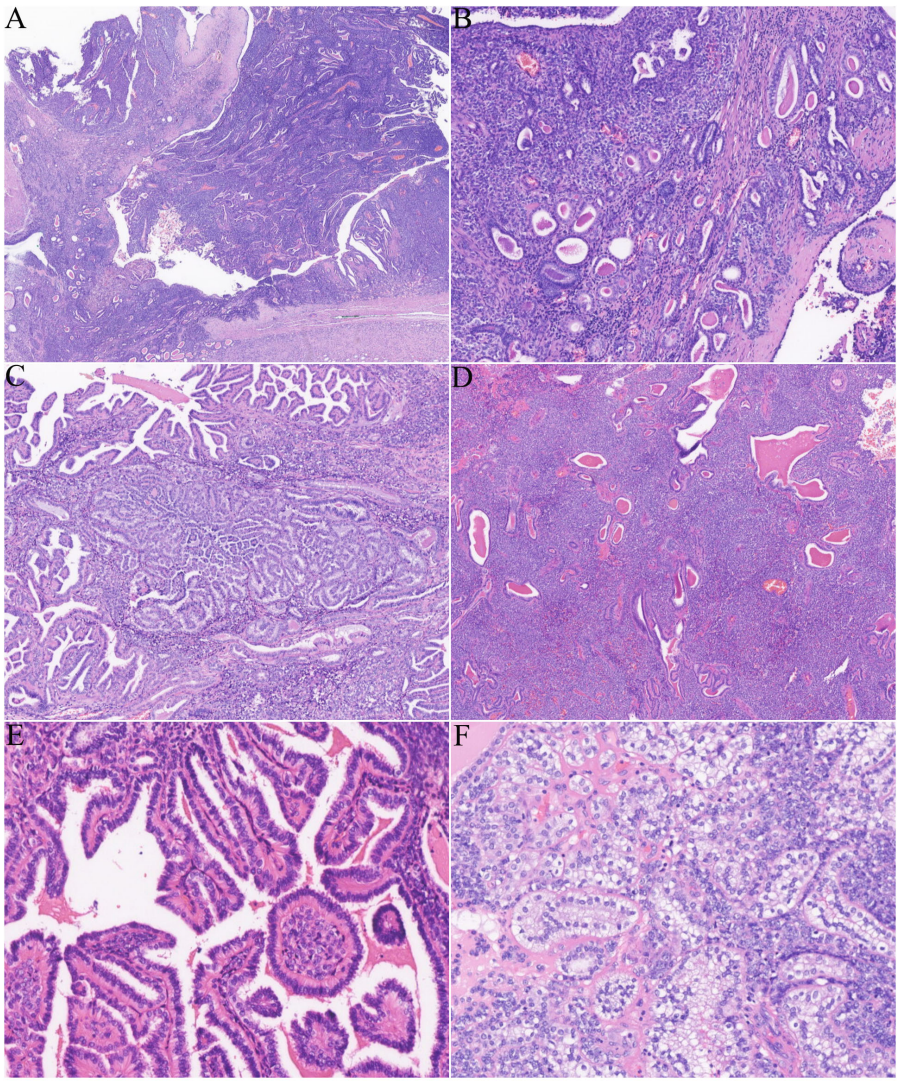

FIGURE 2
The tumor involved abundant renal tubules, particularly in the surrounding areas. **(A)** Low magnification revealed numerous renal tubules involved both around and within the tumor. **(B)** Small tubular and annular structures. **(C)** The affected renal tubules showed significant proliferation, resulting in the formation of micropapillae, papillae, and cribriform structures. **(D)** Some renal tubules displayed either slit-like or cystic dilatation, accompanied by eosinophilic secretions found in the lumen. **(E)** Renal tubular epithelial cells are mild, unilinear, featuring rounded nuclei and eosinophilic cytoplasm. **(F)** Certain areas of proliferative tubular epithelial cells contain a clear cytoplasm.

(mean, 4), and necrosis was present in four cases. Notably, neoplasms encircled native renal tubules, and/or a glomeruli growth pattern was commonly seen in four cases, especially in our case, where the involved renal tubular tissue showed prominent hyperplasia displaying a variety of morphological structures, which had not previously been emphasized in EWSR1::CREB fusion neoplasms involving the kidney. Other patterns that were noted in most cases included hemangiopericytoma-like structures, pseudochrysanthemum cluster structures, collagenous sclerotic interstitium, rhabdomyoid cells, and pseudoalveolar-like structures. Additionally, we also observed local histiocytic aggregation, cholesterol crystallization, and a multinucleated giant cell reaction. Immunohistochemically, the reported eight neoplasms showed variable expression of epithelial markers (AE1/AE3, EMA), six tumors showed MUC4 expression, and four cases were immunoreactive for CD99. Our case showed CD56 and CD57 positivity, while AE1/AE3 was negative. This is the second case of an AE1/AE3-negative condition. In the other case of AE1/AE3 negativity, EMA was focally positive (11). Seven neoplasms showed EWSR1::CREM fusion by RNA-seq, and four tumors were confirmed by FISH. Additionally, one neoplasm exhibited EWSR1::ATF1 fusion (4), and another one exhibited EWSR1::CREB1 fusion (11).

According to previous literature, intra-abdominal epithelioid neoplasms with EWSR1::CREB fusions originating from the kidney should be considered in the differential diagnosis of sclerosing epithelioid fibrosarcoma (SEF), angiomatoid fibrous histiocytoma (AFH), epithelioid mesothelioma (EM), clear cell sarcoma of the kidney (KCCS), synovial sarcoma (SS), solitary fibrous tumors (SFT), or metanephric stromal tumor (MST) (4). The key points

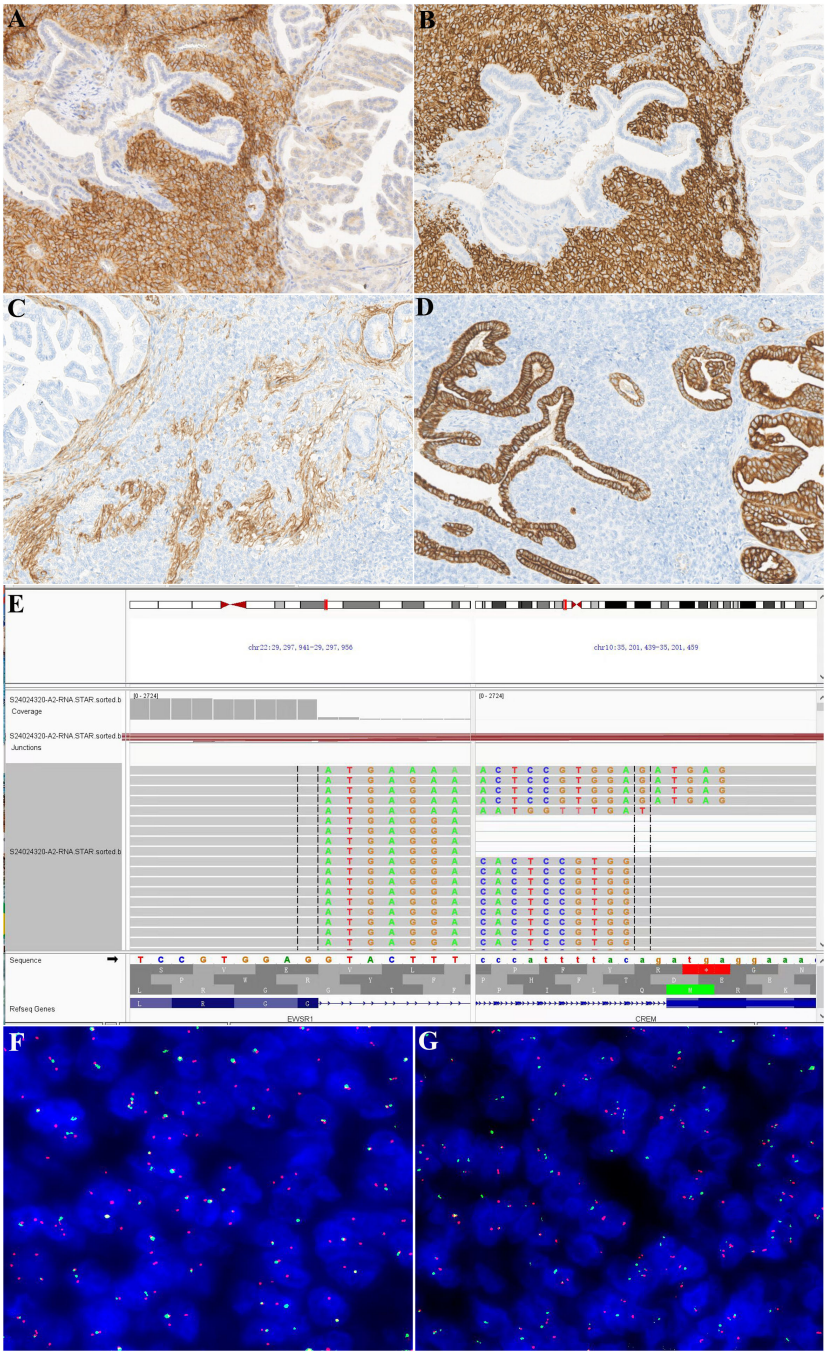

FIGURE 3
Immunohistochemical and molecular findings. This neoplasm was diffusely positive for CD99 **(A)** and CD56 **(B)**, and the affected tubular epithelium was negative. The tumor cells showed focal positivity for CD34 **(C)** but were negative for AE1/AE3 **(D)**. In contrast, the affected tubular epithelium was negative for CD34 and diffusely positive for AE1/AE3. RNA sequencing showed EWSR1::CREM fusions **(E)**. FISH confirmed the results of RNA sequencing [**(F)** EWSR1 broken signals; **(G)** EWSR1 and CREM fusion signals].

for identification are listed in Table 2. From a morphologic perspective, the most important distinction to be made in our case is bidirectional synovial sarcoma (BSS). The cases presented here showed a large amount of normal renal tubular tissue wrapped by tumor tissue, with tubular, annular, papillary, micropapillary, or complex cribriform structures forming biphasic morphology with short spindle tumor cells, mimicking SS. SS occurs mainly in the deep soft tissues of the extremities and is rarely seen in the kidney. Biphasic SS comprises different proportions of epithelioid cells and spindle cells. Epithelioid cells may contain glandular secretion or mucus, and they may form papillary, beam, and solid nest mass patterns. More than 95% of SS has the characteristic t(X; 18) (p11.2; q11.2) chromosomal translocations resulting in the generation of SS18::SSX gene fusion, subsequently resulting in diffuse, positive

TABLE 1 Clinicopathological and molecular characteristics of intraperitoneal malignant epithelioid tumors with EWSR1::CREB rearrangement originating from the kidney.

Case	Age/sex	Size (cm)	Site	Therapy	Histology	RNA sequencing	FISH	Clinical follow-up
Zhao et al. (4)	18/F	7.8	Left	Radical nephrectomy, NDT	SEF-like, with hyaline stroma	EWSR1(ex4)::CREM(ex7) fusion	EWSR1::CREM fusion	5 months, multiple bone and spinal metastases
	17/M	30.0	Right	Radical nephrectomy, NDT	SEF-like, with hyaline stroma	EWSR1(ex16)::CREM(ex5) fusion	EWSR1::CREM fusion	9 months, NED
	61/F	5.6	Left	Radical nephrectomy, NDT	SEF-like, with hyaline stroma	EWSR1(ex4)::ATF1(ex4) fusion	EWSR1::ATF1 fusion	120 months, NED
Agaimy et al. (9)	55/M	7.5	Unknown	Radical nephrectomy, NDT	Epithelioid cells and fibrous stroma	EWSR1::CREM fusion	EWSR1::CREM fusion	23 months, pelvic metastases
Agaimy et al. (10)	34/F	7.5	Right	Radical nephrectomy, Seven cycles of adjuvant chemotherapy	Epithelioid or round cell composition	EWSR1(ex 16)::CREM (ex 6) fusion	Not done	50 months, NED
Argani et al. (8)	29/M	10.0	Unknown	Unknown	Cystic solid; tumor cells were round and epithelioid	EWSR1::CREM fusion	Not done	Peritoneum, para-aortic metastasis
Li et al. (11)	31/F	5.4	Left	Radical nephrectomy, adjuvant chemotherapy	Round and epithelioid present	EWSR1::CREM	Not done	21 months, NED
	38/F	4.0	Right	Radical nephrectomy, NDT	Round and epithelioid	Not done	EWSR1 isolation and EWSR1::CREB1 fusion	33 months, NED
This case	36/M	5.5	Left	Partial nephrectomy, NDT	Tumor cells were round or short fusiform, showing renal tubular involvement and significant proliferation	EWSR1::CREM fusion	EWSR1::CREM fusion	14 months, NED

F, female; male; SEF, sclerosing epithelioid fibrosarcomatoid; NDT, no adjuvant therapy was performed; NED, no evidence of disease.

10.3389/fonc.2025.1604933

TABLE 2 Differential diagnosis of intraperitoneal malignant epithelioid tumors with EWSR1::CREB rearrangement originating from the kidney.

Tumor	Key morphological features	Core immunohistochemical markers	Genetic alteration
Intra-abdominal epithelioid neoplasm with EWSR1::CREB fusions	Epithelioid cells are dominant, with rare true spindle cell components and mucoid or collagenous stroma.	AE1/AE3 and EMA were focal or dot-like or had diffuse positivity, whereas PAX8 and WT1 were negative.	EWSR1::CREM/ATF1, EWSR1::CREB1 (common)
BSS	The tumor exhibits a distinct biphasic pattern composed of spindle and epithelioid cells, with the formation of glandular lumina and potential stromal calcification.	EMA and CK (AE1/AE3) showed strong positivity in the epithelial area. TLE1 was nuclear positive (sensitive but not specific). Simultaneous positivity for S100 and CD99 is helpful for diagnosis. The positivity of SS18-SSX antibodies is related to specificity.	t(X;18), resulting in the SS18::SSX1/2/4 fusion gene
RC	For the vast majority of carcinosarcomas, if sufficient tissue samples are obtained, different proportions/types of renal cell carcinomas can be observed.	The cancerous area expresses markers such as PAX8, PAX2, and CK. The sarcoma area expresses corresponding mesenchymal or epithelial markers to varying degrees (such as SMA, desmin, S100).	The molecular genetics of different types of renal cell carcinomas vary considerably. For instance, clear cell carcinomas may have a 3-chromosome deletion or be associated with VHL syndrome, while papillary renal cell carcinomas may have trisomy of chromosomes 7 and 17 and deletion of the Y chromosome.
MST	The cells are mainly in a spindle shape, forming a "sock-like" structure that surrounds the renal tubules. The background is composed of collagen. This condition is more common in children.	CD34+, WT1−, S100−, PAX8−	The BRAF V600E gene mutation is a key molecular alteration
SEF	Epithelioid and spindle cells are embedded in dense sclerotic collagen, with a low cell density.	MUC4 showed a strong positive reaction (highly sensitive and specific), and almost all markers mentioned in this article were negative.	The most common gene rearrangement is EWSR1::CREB3L1, with a few being EWSR1::CREB3L2 fusion
AFH	Multiple nodular formations, pseudo-vascular tumor-like cavities, and lymphocytic cuffs. The tumor cells can be spindle-shaped, histiocyte-like, or epithelioid.	Desmin+ (50%), EMA+ (40%), and CD99 may be positive.	EWSR1::CREB fusion, or there can also be FUS::ATF1 fusion.
EM	The epithelioid cells are arranged in sheet-like, tubular, and papillary patterns, and the cytoplasm is often eosinophilic and basophilic.	CK5/6+, calretinin+, WT1+ (nuclear+), D2-40+, PAX8−	BAP1 deficiency (common), CDKN2A homozygous deletion
CCSK	The morphology is diverse, the nucleolus is not prominent, the cytoplasm is lightly stained, and the interstitium is rich in branched vascular networks. This is commonly seen in children.	BCOR+, cyclin D1+, WT1−, PAX8−	BCOR : CCNB3 fusion, BCOR ITD or YWHAE::NUTM2
SFT	"Unstructured" pattern, spindle-shaped cells, antler-shaped blood vessels, and collagenization.	STAT6+ (nuclear), CD34+	NAB2::STAT6 fusion

BSS, bidirectional synovial sarcoma; RC, renal carcinosarcoma; MST, metanephric stromal tumor; SEF, sclerosing epithelioid fibrosarcoma; AFH, angiomatoid fibrous histiocytoma; EM, epithelioid mesothelioma; CCSK, clear cell sarcoma of the kidney; SFT, solitary fibrous tumor.

nuclear expression of SS18-SSX (13). The other tumor to be differentiated from our case is renal carcinosarcoma (RC). Renal carcinosarcoma is a highly malignant tumor that occurs in the kidney and has both epithelial and mesenchymal differentiation (14). The malignant epithelial component originates from the renal tubular epithelium or renal pelvis epithelium, and the pathological manifestations are renal cell carcinoma and transitional cell carcinoma. The sarcomatous components are derived from the renal interstitium, and the pathological manifestations are fibrosarcoma, leiomyosarcoma, and other mesenchymal tissue sarcomas. Finally, given the characteristic features of extensive infiltrating growth pattern that result from its interaction with entrapped native renal elements, as well as the marked hyperplasia of renal tubules, the differential diagnoses should also include an MST, which is an extremely rare benign tumor of the kidney. The tumor cells are spindle-shaped or stellate, and they are arranged characteristically in a "concentric circle" pattern around the invaginated blood vessels or renal tubules, resembling an "onion skin-like change," with dysplasia of the invaginated blood vessels. Immunohistochemistry reveals that the tumor cells exhibit varying degrees of positive CD34 expression. The BRAF V600E mutation is frequently present (15). In this case, the BRAF V600E gene alteration was not detected by fluorescence PCR, thereby ruling out MST. For a renal epithelial-like tumor, the following diagnostic process is recommended: First, morphological screening should be conducted to determine whether the tumor is mainly composed of

epithelial-like cells or contains other components (such as spindle cells, glands, and heterologous components). Second, immunohistochemical screening can be performed using a set of immunohistochemical markers such as PAX8, CK, CD99, CD34, ERG, STAT6, MUC4, SS18-SSX, BCOR, and WT1. If all the above markers are negative or only CK is positive (including diffuse positivity or focal positivity), EWSR1::CREB fusion epithelioid tumors, angiomatoid fibrous histiocytomas, and other conditions should be suspected. The final diagnosis must rely on molecular testing, such as FISH detection (EWSR1 break probe) or next-generation sequencing, to determine whether there is EWSR1::CREB family fusion and to pay attention to the final distinction from a morphologically similar angiomatoid fibrous histiocytoma. In summary, an EWSR1::CREB fusion epithelial-like tumor originating from the kidney is an "exclusively" diagnosable condition. A systematic morphological, immunohistochemical, and molecular pathological analysis is required to rule out all the above similar tumors before making an accurate diagnosis.

Currently, no standard treatment exists for neoplasms with EWSR1::CREB fusions (6), while complete surgical resection with negative margins is recommended as the main treatment strategy for these genetically defined tumor types (16). According to the reports in earlier literature, most patients underwent radical nephrectomy (seven of nine) (4, 8–11), while our case underwent partial nephrectomy but with negative margins. In addition, only two patients (10, 11) received adjuvant chemotherapy after surgery. One patient (10) underwent seven consecutive cycles of chemotherapy. Most patients (six of nine) had a good prognosis with no signs of disease for 5 to 120 months after the initial diagnosis, while three patients experienced metastases during follow-up, including multiple bone and spinal lesions (4), pelvic (9), and peritoneal and para-aortic (8) metastases. Overall, three of nine tumors were progressive at the last follow-up, indicating an overall progressive course in 33.3% of patients, indicating the highly aggressive nature of the tumor. Therefore, such tumors may require long-term follow-up to monitor the possibility of late recurrence or metastasis. In addition, large-scale reports of tumors with EWSR1/FUS::CREB fusion features, whether intrarenal or extrarenal, are rare in the literature. A relatively large number of cases were reported by Argani et al. (8) and Shibayama et al. (17), with 13 and 8 cases of tumors with EWSR1/FUS::CREB fusion, respectively. A total of 21 cases were included, comprising 8 with EWSR1::CREM fusion, 8 with FUS::CREM fusion, 4 with EWSR1::ATF1 fusion, and 1 with EWSR1::CREB1 fusion. Among patients with EWSR1::CREM fusion, the maximum follow-up duration was 204 months. Of these, five cases (5 of 8) experienced recurrence or metastasis, one case succumbed to the disease, and one case remained free of recurrence or metastasis during follow-up. Four patients with FUS::CREM fusion were lost to follow-up, while the remaining four patients had the longest follow-up period of 58 months. Three patients experienced recurrence or metastasis (3 of 4), among whom two died of tumors, and one had no recurrence or metastasis during the follow-up period. Two patients with EWSR1::ATF1 fusion experienced recurrence or metastasis during the follow-up period, of which one died of the tumor, and two had no recurrence or metastasis during the follow-up period. The longest follow-up period was 25 months. There was only one patient with EWSR1::CREB1 fusion. The follow-up duration for this patient was 122 months; however, there were two recurrences. The recurrence or metastasis rates of the four different fusion genes were 62.5%, 75.0%, 50.0%, and 100%, respectively, and the mortality rates were 12.5%, 50.0%, 25.0%, and 0%, respectively. Based on these data, the EWSR1::CREB1 fusion had the highest recurrence or metastasis rate, followed by the FUS::CREM fusion. The FUS::CREM fusion had the highest mortality rate, followed by the EWSR1::ATF1 fusion. However, these data are limited by the small number of cases and require more data support.

Conclusion

In summary, we describe a new case of intra-abdominal epithelioid neoplasm with recurrent EWSR1::CREB gene fusions involving the kidney, which exhibited notable native renal tubular hyperplasia and were immunonegative for keratin AE1/AE3. The unusual histological morphology and immunophenotype have not been previously reported in the literature, which could lead to misdiagnosis as tumors with bidirectional morphology, such as synovial sarcoma and carcinosarcoma. Molecular detection, along with morphological and immunohistochemical observations, is essential for accurately diagnosing this type of tumor.

Data availability statement

The original contributions presented in the study are included in the article, further inquiries can be directed to the corresponding author.

Ethics statement

The studies involving humans were approved by the Ethics Committee of the First Affiliated Hospital of Zhengzhou University. The studies were conducted in accordance with the local legislation and institutional requirements. The human samples used in this study were acquired from pathological tissue sections after surgery. Written informed consent for participation was not required from the participants or the participants' legal guardians/next of kin in accordance with the national legislation and institutional requirements. Written informed consent was obtained from the individual(s) for the publication of any potentially identifiable images or data included in this article.

Author contributions

ZZ: Conceptualization, Writing – original draft, Writing – review & editing. EL: Conceptualization, Data curation,

Methodology, Writing – review & editing. MY: Conceptualization, Data curation, Methodology, Writing – review & editing. XL: Data curation, Methodology, Writing – review & editing. JW: Conceptualization, Data curation, Formal Analysis, Methodology, Writing – review & editing.

Funding

The author(s) declare that no financial support was received for the research and/or publication of this article.

Conflict of interest

The authors declare that the research was conducted in the absence of any commercial or financial relationships that could be construed as a potential conflict of interest.

Generative AI statement

The author(s) declare that no Generative AI was used in the creation of this manuscript.

Any alternative text (alt text) provided alongside figures in this article has been generated by Frontiers with the support of artificial intelligence and reasonable efforts have been made to ensure accuracy, including review by the authors wherever possible. If you identify any issues, please contact us.

Publisher's note

References

1. Kaprio H, Heuser VD, Orte K, Tukiainen M, Leivo I, Gardberg M. Expression of transcription factor CREM in human tissues. *J Histochem Cytochem*. (2021) 69:495–509. doi: 10.1369/00221554211032008

2. Flucke U, van Noesel MM, Siozopoulou V, Creytens D, Tops BBJ, van Gorp JM, et al. EWSR1—the most common rearranged gene in soft tissue lesions, which also occurs in different bone lesions: an updated review. *Diagnostics (Basel)*. (2021) 11:1093. doi: 10.3390/DIAGNOSTICS11061093

3. Breik O, Higginson J, Al-Ajami AK, Mohamed A, Martin T, Amel-Kashipaz R. Clear cell odontogenic carcinoma: first report of novel EWSR1-CREM fusion gene in case of long-term misdiagnosis. *Head Neck Pathol*. (2021) 15:1391–8. doi: 10.1007/s12105-021-01302-y

4. Zhao M, Gan H, Zhong S, Xia Q, Bai Y, Xu J, et al. Intra-abdominal epithelioid neoplasm with EWSR1::CREB fusions involving the kidney: A clinicopathologic and molecular characterization with an emphasis on differential diagnosis. *Mod Pathol*. (2024) 37:100468. doi: 10.1016/j.modpat.2024.100468

5. Komatsu M, Sakai Y, Nishikubo M, Tane S, Nishio W, Kajimoto K, et al. EWSR1-CREM fusion in pulmonary mesenchymal neoplasm showing distinctive clear cell morphology. *Pathol Int*. (2020) 70:1020–6. doi: 10.1111/pin.13030

6. Javaid S, Patton A, Tinoco G, Oghumu S, Iwenofu OH. Metastatic sporadic paraganglioma with EWSR1::CREM gene fusion: A unique molecular profile that expands the phenotypic diversity of the molecular landscape of the EWSR1::CREM gene fusion positive tumors. *Genes Chromosomes Cancer*. (2023) 62:85–92. doi: 10.1002/gcc.23094

7. Trecourt A, Macagno N, Ngo C, Philip CA, Lopez J, Ferreira J, et al. CREB fusion-associated epithelioid mesenchymal neoplasms of the female adnexa: three cases documenting a novel location of an emerging entity and further highlighting an ambiguous misleading immunophenotype. *Virchows Arch*. (2023) 482:967–74. doi: 10.1007/s00428-023-03546-1

8. Argani P, Harvey I, Nielsen GP, Takano A, Suurmeijer AJH, Voltaggio L, et al. EWSR1/FUS-CREB fusions define a distinctive Malignant epithelioid neoplasm with predilection for mesothelial-lined cavities. *Mod Pathol*. (2020) 33:2233–43. doi: 10.1038/s41379-020-0646-5

9. Agaimy A, Stoehr R, Otto M, Bräsen JH, Pfarr N, Konukiewitz B, et al. Intra-abdominal EWSR1/FUS-CREM-rearranged Malignant epithelioid neoplasms: two cases of an emerging aggressive entity with emphasis on misleading immunophenotype. *Virchows Arch*. (2022) 480:481–6. doi: 10.1007/s00428-021-03140-3

10. Agaimy A, Blakely M, Breimer GE, Hölsken A, Koppes SA, Meidenbauer N, et al. Extra-abdominal and intra-abdominal FET::CREM fusion mesenchymal neoplasms: comparative clinicopathological study of 9 new cases further supporting a distinct potentially aggressive sarcoma and report of novel sites. *Virchows Arch*. (2025) 485 (6):1007–19. doi: 10.1007/s00428-024-03917-2

11. Li J, Zeng Q, Chen X, Huang H. Malignant epithelioid tumors with EWSR1::CREB fusion involving the kidney: a report of two cases. *Virchows Arch*. (2025) 487 (4):901–8. doi: 10.1007/s00428-024-03989-0

12. Wu JH, Xu SX, Xu M, Shen P, Chen JF, Jin XT, et al. Intra-abdominal EWSR1/FUS-CREM rearranged Malignant epithelioid neoplasms: report of a case. *Zhonghua Bing Li Xue Za Zhi*. (2024) 53:299–302. doi: 10.3760/cma.j.cn112151-20231023-00286

13. Raquib AR, Hofvander J, Ta M, Nielsen TO. Expanding the use of an SS18-SSX antibody for molecular assays in synovial sarcoma. *Appl Immunohistochem Mol Morphol*. (2022) 30:531–9. doi: 10.1097/PAI.0000000000001049

14. Hacıosmanoğlu T, Baloğlu İH, Türk S, Demirel HC, Özağarı AA. Carcinosarcoma arising from the renal pelvis: A rare case report. *Cureus*. (2023) 15: e45610. doi: 10.7759/cureus.45610

15. Fan Y, Yu J, Zhao M. Metanephric stromal tumor with *BRAF* V600E mutation in an adult patient: Case report and literature review. *Front Oncol*. (2022) 12:993414. doi: 10.3389/fonc.2022.993414

16. Sun Y, Liu D, Chen X, Zhang J, Yang S. Epithelioid mesenchymal neoplasm with FUS::CREM gene fusion in the tongue: Report of a rare and challenging diagnosis. *Oral Surg Oral Med Oral Pathol Oral Radiol*. (2023) 135:e108–13. doi: 10.1016/j.oooo.2022.12.003

17. Shibayama T, Shimoi T, Mori T, Noguchi E, Honma Y, Hijioka S, et al. Cytokeratin-positive Malignant tumor in the abdomen with EWSR1/FUS-CREB fusion: A clinicopathologic study of 8 cases. *Am J Surg Pathol*. (2022) 46:134–46. doi: 10.1097/PAS.0000000000001742

Frontiers in Pharmacology

Explores the interactions between chemicals and living beings

The most cited journal in its field, which advances access to pharmacological discoveries to prevent and treat human disease.

Discover the latest Research Topics

See more →

Frontiers

Avenue du Tribunal-Fédéral 34
1005 Lausanne, Switzerland
frontiersin.org

Contact us

+41 (0)21 510 17 00
frontiersin.org/about/contact